

Sheffield Hallam University

Effect of cellular factors on the generation of beta-amyloid.

ANDERSON, David.

Available from the Sheffield Hallam University Research Archive (SHURA) at:

<http://shura.shu.ac.uk/19274/>

A Sheffield Hallam University thesis

This thesis is protected by copyright which belongs to the author.

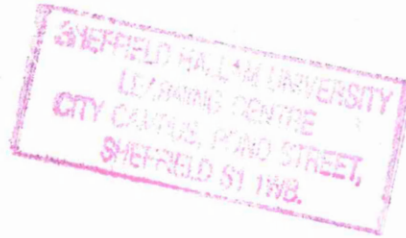
The content must not be changed in any way or sold commercially in any format or medium without the formal permission of the author.

When referring to this work, full bibliographic details including the author, title, awarding institution and date of the thesis must be given.

Please visit <http://shura.shu.ac.uk/19274/> and <http://shura.shu.ac.uk/information.html> for further details about copyright and re-use permissions.

LEARNING CENTRE
CITY CAMPUS, HOWARD STREET
SHEFFIELD S1 1WB

101 768 444 8



Fines are charged at 50p per hour

27 JUL 2007 5.00pm

28 JUL 2007

18 AUG 07 5pm

23 AUG 2007 5pm

ProQuest Number: 10694154

All rights reserved

INFORMATION TO ALL USERS

The quality of this reproduction is dependent upon the quality of the copy submitted.

In the unlikely event that the author did not send a complete manuscript and there are missing pages, these will be noted. Also, if material had to be removed, a note will indicate the deletion.



ProQuest 10694154

Published by ProQuest LLC (2017). Copyright of the Dissertation is held by the Author.

All rights reserved.

This work is protected against unauthorized copying under Title 17, United States Code
Microform Edition © ProQuest LLC.

ProQuest LLC.
789 East Eisenhower Parkway
P.O. Box 1346
Ann Arbor, MI 48106 – 1346

Effect of cellular factors on the generation of β -amyloid

David Anderson

A thesis submitted in partial fulfilment of the requirements of Sheffield
Hallam University for the degree of Doctor of Philosophy

November 2003



Acknowledgements

This study was performed in the Biomedical Research Centre, Sheffield Hallam University during the years 2000-2003.

I wish to thank my supervisor Professor David Parkinson for giving me the opportunity to undertake this PhD and for his co-operation, guidance and encouragement during these years.

I also wish to thank all my colleagues at the BMRC who have made my studies all the more bearable for their sense of humour.

I should like to thank both John Proctor at Sheffield University for his invaluable TEM skills and Aviva Tolkovsky at Cambridge University for her comments regarding the TEM images.

Lastly, I am indebted to my wife Mariam who has never lost faith in my abilities and who has been a constant source of encouragement to me.

And Allah has created you, and then He will cause you to die, and of you there are some who are sent back to senility, so after having much knowledge, they know nothing. Truly! Allah is All-Knowing, All-Powerful.

Sura An-Nahl (The Bee). Quran, 16:70.

Contents

Abstract	1
List of abbreviations	2
Chapter 1	
1.0 Relevance of Alzheimer's disease	4
1.1 Introduction to AD	4
1.2 Pathophysiological features of AD	5
(i) Neurological and transmitter alterations	5
(ii) Micro-histopathological features of AD	7
(iii) NFTs contain aggregates of hyperphosphorylated tau	7
(iv) Amyloid peptide deposits in the AD brain	9
(v) Neuritic plaques	10
(vi) Diffuse plaques	11
1.3 Biology of amyloid precursor protein	
(i) Proteolytic processing of APP	12
(ii) α -secretase pathway	13
(iii) β -secretase pathway	14
(iv) γ -secretase pathway	15
(v) APP trafficking and A β generation within the cell compartment	15
(vi) Function of APP	19
1.4 A β associated toxicity in AD	
(i) A β structure and toxicity	20
(ii) Oxidative stress and AD	22
(iii) Inflammatory Reactions and AD	23
1.5 Theories proposed to account for AD	
(i) Amyloid cascade hypothesis	24
(ii) Amyloidosis and tauopathy	25
(iii) Competing hypotheses in AD	25
1.6 Genetics of AD	28
(i) APP mutations and FAD	30
(ii) Presenilin mutations and FAD	32
(iii) Apolipoprotein E polymorphism and AD	34
(iv) α -macroglobulin polymorphism and AD	35
(v) AD risk locus on chromosome 10	36
1.7 Biology of presenilins	
(i) Presenilin structure and biochemistry	38
(ii) Presenilin and development	40

(iii)	Apoptosis and presenilin in AD	42
(iv)	Presenilin complex formation	43
(v)	Presenilin and β -catenin interaction	44
(vi)	Active γ -secretase requires several components	45
1.8	Project rationale	47

Chapter 2 Materials and Methods

2.0	Cell Culture	48
2.1	Cell fixation, antibody staining and imaging	48
2.2	Antibody staining	48
2.3	Reduction and alkylation of disulphide bonds	49
2.4	Preparation of soluble and membrane bound cell fractions for SDS-PAGE analysis	50
2.5	SDS PAGE/Urea Bicine gel preparation	50
2.6	Immunoprecipitation of conditioned media	50
2.7	Detection of β -amyloid peptides	51
2.8	SDS-PAGE running conditions	53
2.9	Polymerisation chain reaction conditions	53
2.10	Restriction digestion and preparation of cDNAs	54
2.11	Preparation of electrocompetent DH5 α <i>E.coli</i>	54
2.12	Transformation of DH5 α <i>E.coli</i>	54
2.13	Transfection of Mammalian Cells	55
2.14	Transmission electron microscopy	55

Results

Chapter 3 Characterisation of PS1-CTF and PS1–NTF fragments in Cos-7 cells by immunocytochemistry

3.1	Introduction	57
3.2	Criteria for assessing reporter molecule localisation within the cell compartment	57
3.3	1039 antibody staining of PS1 in Cos-7 cells	58
3.4	923 antibody staining of PS1 in Cos-7 cells	58
3.5	923 staining of Brefeldin-A treated Cos-7 cells is largely vesicular and co-localises with ERGIC53	58
3.6	Western blot analysis of endogenous PS1 expressed in Cos-7 cells	61
3.7	The 923 antibody does not recognize the PS1 N-terminus	62

Chapter 4 Construction of NTPS1-EGFP plasmid and expression by transfected Cos-7 cells

4.1	Introduction	66
4.2	Amplification of N-terminal PS1 cDNA by PCR	67
4.3	Optimisation of conditions for PCR	67
4.4	Subcloning of N-terminal PS1 cDNA into N2-pEGFP	70
4.5	Restriction digestion analysis of putative N-terminal PS1 cDNA	71
4.6	Cos-7 cells transfected with pNTPS1-EGFP display several phenotypes	73
4.7	Western blot analysis of NTPS1-EGFP fusion protein locates to the cell membrane	74
4.8	The NTPS1 fusion protein localises to the ER and Golgi compartments	76
4.9	The NTPS1 fusion protein does not co-localise with 923 staining and returns to the ER following BFA treatment and in Cos-7 cells	80
4.10	Chapter summary	81

Chapter 5 Construction of mutant PS1 cDNA and expression in cells

5.1	Introduction	88
5.2	The phenotypes exhibited by the fusion protein are not an artefact of the cell fixation process	88
5.3	The phenotypes displayed by the fusion protein are found within other cell types	89
5.4	Construction of wild type and FAD mutant PS1 plasmids	92
	(i) Alteration of PS1 cDNA base sequences by site directed mutagenesis	92
	(ii) Site directed mutagenesis by PCR	93
	(iii) Optimisation of PCR conditions	94
	(iv) Restriction analysis of PCR products	98
5.5	Expression of NTMPS1-EGFP by Cos-7 cells	98
5.6	Expression of Full length PS1-EGFP and Full length mutant PS1 by Cos-7 cells	99
5.7	Endoproteolysis of the full-length fusion protein generates separate pools of NTF and CTF in a proportion of cells expressing the transgene	99
5.8	BFA treatment of Cos-7 cells expressing the full-length fusion protein	100

5.9	Western analysis of Cos-7 cells expressing FLPS1-EGFP, FLMPS1-EGFP and NTMPS1-EGFP fusion proteins	104
5.10	Chapter summary	105

Chapter 6 Biological properties of the fusion protein

6.0	Introduction.	111
6.1	Reduction in antibody staining of the ER resident proteins Colligin and PDI.	111
6.2	Reduction in antibody staining of Golgi-associated proteins Mannosidase II and GalNac.	112
6.3	β -Catenin does not associate with NTMPS1-EGFP in Cos-7 and HEK293 cells.	112
6.4	The fusion protein shows limited localisation with the anti-APP antibodies 874, 993 and DE2.	113
6.5	Detection and separation of synthetic $A\beta_{40}$ / $A\beta_{42}$ by bicine SDS PAGE.	118
6.6	Immunoprecipitation of APP ₇₇₀ from conditioned and complete. Media.	119
6.7	Selection of HEK293 cells stably expressing full length and truncated PS1-EGFP.	127
6.8	Western analysis of stable HEK293 cells expressing the fusion Proteins.	128
6.9	Mannosidase staining in control cells	133
6.10	The NTMPS1-EGFP sensitizes Cos-7 cells to staurosporine-induced apoptosis.	134
6.11	Staurosporine induced apoptosis in NTMPS1-EGFP NRK cells show increased Grasp65 cleavage compared to untransfected cells.	135
6.12	Chapter summary.	137

Chapter 7 Functional and morphological characteristics of the blob phenotype

7.0	Introduction.	144
7.1	Introduction of an in-frame STOP codon between PS1 and EGFP cDNA	144
7.2	Removal of the EFGP moiety does not alter the phenotypes displayed by cells expressing truncated or full-length PS1.	146
7.3	Western analysis of soluble and membrane fractions prepared from cells expressing full-length and truncated PS1-STOP proteins.	146
7.4	Analysis of the cell compartment in which the fusion protein resides.	147

7.5	The blob phenotype does not co-localise with antibodies to the ER, Golgi or the ERGIC compartment.	152
7.6	Altered COP II staining in Cos-7 cells exhibiting the blob phenotype.	152
7.7	The blob-like aggregates do not associate with the Lysosomal compartment.	153
7.8	Proteasome 20S antibody staining of the fusion protein.	153
7.9	The blob-like aggregates show ubiquitination.	161
7.10	The NTMPS-EGFP fusion protein accumulates as a distinct perinuclear structure following inhibition of the proteasome.	162
7.11	Higher weight fusion protein aggregates show increased ubiquitin immunoreactivity in cells treated with proteasome inhibitors.	163
7.12	MG132 concentrations in the nanomolar range are sufficient to cause the collapse of vimentin around the aggresome.	164
7.13	MTOC staining is altered in Cos-7 cells expressing high levels of the fusion protein.	164
7.14	Formation of the blob-like phenotypes do not require intact microtubules.	165
7.15	The PS1 fusion protein phenotypes do not alter over time.	177
7.16	TEM examination of the cells expressing the fusion protein reveals laminar structures and phagosomes.	178
7.17	Chapter summary.	179

Chapter 8 Discussion

8.0	The putative PS1NTF 923 antibody staining is distinct from 1039 PS1CTF antibody staining	186
8.1	Construction and expression of N-terminal truncated PS1-EGFP	187
8.2	Immunoanalysis of the NTF fusion protein	189
8.3	Expression of mutant full-length and truncated PS1 fusion proteins	190
8.4	Endoproteolysis of the full-length PS1	191
8.5	Expression and sub cellular distribution of EGFP-tagged presenilin in this and previous studies	193
8.6	Functional aspects of PS fusion proteins	196
8.7	Detection of β -Amyloid	197
8.8	Alterations in the ER and Golgi compartments	198
8.9	The N-terminal fusion protein sensitises cells to apoptosis	200
8.10	Identity of the blob-like aggregates	203
8.11	The fusion protein, aggresomes and the ubiquitin-proteasome system	205

8.12	TEM analysis of Cos-7 cells expressing the fusion protein	208
8.13	Autophagosomes and multilaminar bodies in transfected cells	209
8.14	Consequence of fusion protein over expression	212
8.15	Impairment of the ubiquitin-proteasome system	213
8.16	Formation of the blob-like aggregate phenotype	215
8.17	Blobs- insoluble aggregates, inclusion bodies or membrane bound compartments?	217
8.18	Apoptosis and autophagy	219
8.19	Summary of main findings	221
8.20	Concluding remarks	223
	References	225

1.0	Simplified time line of AD research from first discovery in 1906 to present day.	6
1.1	β -Amyloid plaque surrounded by dystrophic neurites.	8
1.2	Secretase cleavage of APP splice forms.	16
1.3	Primary and secondary structure of A β 42.	21
1.4	Amyloid cascade hypothesis.	27
1.5	Biofloculant hypothesis of AD.	29
1.6	AD as a disorder of brain self-organisation and dysmorphoregulation.	30
1.7	Topological representation of PS1 showing the eight transmembrane model.	40
2.0	Dimensions used for Bis-acrylamide gel.	52
3.1	Endogenous staining of PS1 in Cos-7 cells.	59
3.2	PS1, Colligin and Golgin antibody staining of Cos-7 cells.	60
3.3	BFA treatment of Cos-7 cells.	63
3.4	923 and ERGIC53 antibody staining of BFA treated Cos-7 cells.	64
3.5	923 and 1039 antibody staining of Cos-7 whole cell lysate.	65
4.0	Generation of N-terminal PS1 fusion protein by PCR and subcloning.	68
4.1	Amplification of N-terminal PS1 fragment by PCR.	69
4.2	Restriction digest of cDNA recovered from transformed DH5 α <i>E.coli</i> .	72
4.3	Restriction digest of pNTPS1-EGFP recovered from transformed DH5 α <i>E.coli</i> .	75
4.4	Transfection of Cos-7 cells with the N-terminal PS1 fusion construct generates distinct phenotypes.	77
4.5	Phenotypes expressed by Cos-7 cells transfected with the fusion construct.	78
4.6	Western analysis of Cos-7 cells expressing the fusion protein	79
4.7	Anti-EGFP antibody staining of Cos-7 cells expressing the NTPS1 fusion protein.	82
4.8	ER antibody staining of Cos-7 cells expressing the NTPS1 fusion protein.	83
4.9	The fusion protein overlaps to varying degrees with markers to the Golgi.	84
4.10	923 antibody staining and BFA treatment of transfected Cos-7 cells.	85
4.11	ERGIC 53 antibody staining of BFA-treated Cos-7 cells expressing the NTPS1 fusion protein.	86
4.12	1039 antibody staining of Cos-7 expressing the NTPS1 fusion protein.	87
5.0	Cell fixation method.	90
5.1	Transfection of different cell types with pNTPS1-EGFP.	91
5.2	Schematic representation of the PCR required to generate PS1 cDNAs.	95
5.3	Amino acid sequence of PS1.	96
5.4	Amplification by PCR of pCLneoPS1.	97
5.5	Analysis of PCR product.	97
5.6	Restriction digestion of putative FLMPS1 and NTMPS1 cDNAs.	101
5.7	Single restriction digest of pEGFP, and putative pEGFP-containing FLMPS1 and NTMPS1 plasmids.	102
5.8	NTMPS1 and NTPS1 exhibit identical phenotypes.	103
5.9	Phenotypes displayed by full-length proteins.	107
5.10	Transfection of Cos-7 cells with the full-length fusion constructs.	108
5.11	NT7 staining of the blob-like aggregate phenotype.	109
5.12	Western analysis of NTMPS1, FLPS1, and FLMPS1 fusion proteins.	110

6.0	Altered ER antibody staining.	114
6.1	Altered Golgi antibody staining.	115
6.2	β -Catenin antibody staining.	116
6.3	APP 993-antibody staining.	120
6.4	APP 874-antibody staining.	121
6.5	APP DE2-antibody staining.	122
6.6	Detection and separation of synthetic $A\beta_{40}$ and $A\beta_{42}$ peptides	125
6.7	Immunoprecipitation of $A\beta_{40}/A\beta_{42}$	126
6.8	Modifications to immunoprecipitation protocol.	127
6.9	HEK293 cells stably expressing FLPS1-EGFP or NTMPS1-EGFP fusion proteins.	130
6.10	Western analysis of stable NTMPS1-EGFP HEK 293 cells.	131
6.11	Western analysis of stable full-length-EGFP HEK 293 cells.	132
6.12	Effect of varying staurosporine concentrations on Cos-7 morphology over time.	138
6.13	Staurosporine treatment of Cos-7 cells expressing the truncated fusion protein over time.	139
6.14	GRASP65 staining of pNTMPS1-EGFP transfected NRK cells treated for 4 hours with 1 μ M staurosporine.	140
6.15	Quantitation of Grasp65 staining of pNTMPS1-EGFP transfected and untransfected NRK cells treated with 1 μ M staurosporine over 4 hours.	141
6.16	Polyclonal Grasp65 immunoblotting of whole cell lysate taken from NRK cells expressing the NTMPS1-EGFP fusion protein following treatment with 1 μ M staurosporine over 4 hours.	142
7.0	Oligo linker sequence.	145
7.1	NT7 and 1039 staining of Cos-7 cells transfected with PS1-STOP-EGFP constructs.	148
7.2	Western analysis of full-length and truncated PS1-STOP proteins.	150
7.3	Colligin and Mannosidase II antibody staining of Cos-7 and HEK293 cells.	154
7.4	ERGIC53 antibody staining of Cos-7 and HEK293 cells expressing the NTMPS1-EGFP fusion protein.	155
7.5	Membrin antibody staining of Cos-7 and HEK293 cells displaying the blob phenotype.	156
7.6	β -COP staining of Cos-7 and HeK293 cells expressing NTMPS1-EGFP.	157
7.7	COP II staining in HEK 293 cells displays a peri-nuclear and punctate phenotype.	158
7.8	COP II staining of Cos-7 cells expressing moderate levels of the fusion protein exhibits a peri-nuclear phenotype.	159
7.9	LAMP-1 staining of Cos-7 expressing the NTPS1-EGFP fusion protein.	160
7.10	Ubiquitin antibody staining of cells expressing the NTMPS1-EGFP fusion protein.	166
7.11	Aggresome formation causes a redistribution of the IF vimentin following proteasome inhibition.	167
7.12	Vimentin staining of Cos-7 cells treated for 12 hours with the proteasomal inhibitors MG132 and Lactacystin.	168
7.13	Vimentin staining of HEK293 cells treated for 12 hours with the proteasomal inhibitors MG132 and Lactacystin.	169
7.14	Proteasome inhibition of NTMPS1 HEK 293 cells.	170
7.15	Overnight treatment of NTMPS1 HEK 293 cells with MG132.	171
7.16	Effect of varying MG132 concentration on the distribution of vimentin in HEK 293 NTMPS1 cells.	172

7.17	MTOC and Mitochondria antibody staining in HEK293 and Cos-7 cells.	173
7.18	Cos-7 cells were treated for 12 hrs with MG132 alone or in combination with the microtubule disrupting agent nocodazole.	174
7.19	Analysis of transfected cells over time.	175
7.20	Origin of the blob phenotype.	176
7.21	Transmission electron microscopy of Cos-7 cells expressing the fusion protein (A).	181
7.21	TEM images (B & C).	182
7.21	TEM images (D, E, F & G).	183
7.21	TEM images (H, I, J & K).	184
7.21	TEM images (L, M, N & O).	185
8.0	Schematic outline of events proposed to account for the presence of the blob phenotype	224

1.0	Genetic factors predisposing to AD.	31
1.1	Examples of missense mutations in human PS1 and age of FAD onset.	33
1.2	Genetic loci associated with AD.	37
1.2	Oxidative stress and inflammation in AD.	16
1.3	Primer sequences used to amplify by PCR truncated (NTPS1) and full length (FLPS1) PS1 mutant and wild-type cDNAs from pCLneoPS1.	21
1.4	Primer sequences used to amplify by PCR truncated (NTPS1) and full length (FLPS1) PS1 mutant and wild-type cDNAs from pCLneoPS1.	30
2.0	Antibodies used within this study.	49
2.1	Composition and stock solutions used for Bicine gels	52
2.2	Final gel volumes.	52
4.0	Primer sequences used for the amplification by PCR truncated and full length PS1 mutant and wild-type cDNAs from pCLneoPS1.	70
4.1	Predicted versus observed fragment sizes generated following restriction enzyme digestion of plasmid DNA.	75
5.0	Fragment sizes of PCR products following single site restriction digest	101
5.1	Comparison of fragment sizes.	102
6.0	Data for staurosporine treatment of NTMPS1-EGFP transfected Cos-7 cells.	134
6.1	Summary of data for Grasp65 staining of pNTMPS1-EGFP transfected NRK cells treated with 1 μ M staurosporine.	141

Abstract

There is considerable interest in the role of aggregated protein in the underlying pathology of human neurodegenerative conditions including Alzheimer's disease (AD), light chain amyloidosis, spongiform encephalopathies, Huntingdon's disease, Parkinson's disease, etc. AD is a progressive neurodegenerative condition responsible for dementia in the elderly. An early onset, familial genetic basis (FAD) for the disease has been established in kindreds, where mutations in the amyloid precursor protein (APP) and the presenilin proteins (PS) cause cerebral deposition and aggregation of the β -amyloid ($A\beta$) peptide responsible for the clinical and pathological features of the disease.

In order to investigate the cell biology of presenilin1 and the effect of AD-causing mutations on intracellular dynamics, constructs of enhanced green fluorescent protein fused to wild type or mutant N-terminal fragment and full-length PS1 were prepared. Immunocytochemical analysis reveals that the fusion proteins display four distinct phenotypes: ER, Golgi, vesicular and 'blob-like aggregates'. Furthermore, removal of the EGFP moiety had no effect on the phenotype. The 'blob-like aggregates', are high copy number, ubiquitinated structures that originate from the nuclear/ER interface, and are not dependent on microtubules for their formation nor are they contained by the intermediate filament vimentin, indicating that they are neither aggresomes nor inclusion bodies.

Moderate to high levels of the fusion protein disrupt the endoplasmic reticulum and Golgi compartments, suggesting that the normal trafficking of materials within the cell may be disturbed. Additionally, the N-terminal construct sensitises cells to staurosporine-induced apoptosis. TEM images from cells expressing the fusion protein reveals numerous phagosomes and multilaminar bodies that fit the profile seen for the blob-like aggregates in terms of dimension, number and general morphology. These data suggest that the blob-like aggregates might be novel membrane-bound structures. These fusion proteins provide a convenient means for studying the consequences of protein aggregation on the ubiquitin-proteasome system (UPS), apoptosis and phagocytosis within the cell.

List of abbreviations

A2M	α -2 macroglobulin
A β	Beta Amyloid
AD	Alzheimer's Disease
ADAM	'a disintegrin and metalloprotease'
AICD	APP intracellular domain
ALS	Amylo
Aph-1	Anterior pharynx defective-1
APS	Ammonium Peroxydisulphate
AP	Alkaline Phosphatase
ApoE	Apolipoprotein E
APP	Amyloid Precursor Protein
BACE	Beta-site APP-cleaving enzyme
BCIP	5-Bromo-4-chloro-3-Indoyle phosphate
BFA	Brefeldin-A
CAT	Choline acetyltransferase
CAPS	Cyclohexylamino-1-propanesulfonic acid
CFTR	Cystic fibrosis transmembrane conductance regulator
CHO	Chinese Hamster Ovary
COP	Coatmer proteins
CPP	Common Population Polymorphism
CSF	Cerebrospinal fluid
CTF	C-terminal fragment
DAPI	Diaminobezamide
DMEM	Dulbecco's modified Eagles medium
DNA	Deoxyribonucleic acid
DTT	Ditheothreitol
DS	Down Syndrome
ECS	Extracellular space
EGFP	Enhanced Green Fluorescent Protein
ERGIC	ER intermediate compartment
ER	Endoplasmic Reticulum
FAD	Familial Alzheimer's Disease
FALS	Familial amyotrophic lateral sclerosis
FNDI	Familial Neurohypophyseal Diabetes Insipidus
FLCPS1	Full length conserved (wild type) presenilin
FLMPS1	Full length mutant presenilin
gadd45	Growth arrest and DNA damage-inducible gene
GalNac	N-acetylgalactosaminyltransferase
HEK	Human Embryonic Kidney
HRP	Horse Radish Peroxidase
IC —	Intermediate compartment
ICD	Intracellular domain
IDS	Insulin degrading enzyme

(continued)	
iNct	Immature nicastrin
IPTG	Isopropyl-beta-D-thiogalactopyranoside
LAMP	Lysosomal Associated Membrane Protein
LOAD	Late onset Alzheimer's Disease
LTP	Long term potentiation
LDL	Low density lipoprotein receptor
LB	Luria-Bertani Broth
LRP	LDL receptor-related protein
mNct	Mature nicastrin
MRSI	Magnetic resonance spectroscopic imaging
MTOC	Microtubule Organising Centre
Nct	Nicastrin
NBT	Nitroblue Tetrazolium
NICD	Notch intercellular domain
NRK	Normal Rat Kidney cells
PAG	Proliferation-associated gene product
PAGE	Polyacrylamide Gel Electrophoresis
Pen-2	Presenilin enhancer-2
PBS	Phosphate Buffered Saline
PCR	Polymerase Chain Reaction
PenStrep	Penicillin-Streptomycin
PMSF	Phenylmethylsulfonylfluoride
PS	Presenilin
PVDF	Polyvinylidene fluoride
RAGE	Receptor for advanced glycation end products
RIPA	Radioimmunoprecipitation
ROS	Reactive oxygen species
SDS	Sodium Dodecyl Sulphate
SDM	Site directed mutagenesis
SOD	Superoxide dismutase
STS	Staurosporine
TACE	Tumor necrosis factor- α converting enzyme
TBS	Tris Buffered Saline
TEMED	Tetramethylethylenediamine
TGN	Trans Golgi Network
TGF- β 1	Transforming growth factor beta 1
TM	Transmembrane domain
UPR	Unfolded protein response
UPS	Ubiquitin proteasome system
WGA	Wheat Germ Agglutinin
X-Gal	5-bromo-4-chloro-3-indolyl-beta-D-galactopyranoside

Chapter 1

1.0 Relevance of Alzheimer's disease

For the majority of individuals living in the West, the advent of modern medicine, particularly the development of antibiotics in the previous century, has effectively extended the average life expectancy. Mortality commonly associated with microbial infection has now been supplanted by maladies arising as a consequence of the normal ageing process. As the population ages the health cost associated with increased longevity threatens to undermine Western health care systems. Of increasing concern is the rise in the number of cases of dementia, particularly Alzheimer's disease (AD) now thought to affect 15 million individuals world-wide. Beside the emotional burden placed on patients, their families and carers, society will have to reckon with the long-term economic costs of a population affected by AD. The annual economic costs of AD to the USA alone were estimated at US\$ 80-100 billion (National Institute on Aging). Thus efforts to find an effective therapy to this most debilitating disease are crucial if a future social healthcare crisis is to be avoided.

1.1 Introduction to Alzheimer's Disease

In 1906 at a scientific meeting in Munich a Bavarian psychiatrist, Alois Alzheimer (1864-1915) described the neuropathology of a 51-year-old Frankfurt woman referred to as Auguste D, who had died following a period of progressive dementia. Using recently developed silver staining techniques, Alzheimer described a host of pathological abnormalities including amyloid plaques and neurofibrillary tangles, now considered the major hallmarks of the disease. AD is the commonest form of dementia accounting for 50-70% of typical late onset cases, and is characterised by progressive loss of memory and orientation. It is an age-related condition affecting approximately 11% of the population over 65 years of age and 50% over 85 years of age (Hof et al, 1995). Globally, AD is thought to affect 1 in 20 people. Though the aetiology of the disease process is currently unknown, AD can manifest itself in two ways. Firstly, a familial basis for AD (FAD) has been

established whereby specific gene mutations cause the early onset of the disease. Secondly, whereas FAD accounts for less than 1% of all AD cases, the majority of patients who exhibit AD characteristics do so sporadically. This late-onset AD (LOAD) is likely due to genetic as well as epigenetic (environmental) factors. In general terms, AD can be thought of as a multifactorial syndrome resulting from impaired processing of proteins, oxidative stress and inflammation events rather than as a disease attributable to a single cause (Selkoe, 1999). Much of the earlier research in AD consisted of anatomical investigations of the brain coupled with improved silver staining protocols. The development of biochemical and immunological techniques since the 1970s have provided a wealth of data on AD pathology, that when taken together with current molecular and genetic technologies has brought the prospect of an effective therapeutic treatment ever closer. A simplified schema outlining the history of AD research from its initial descriptions back in 1906 to the present day is shown in figure 1.0.

1.2 Pathophysiological features of AD

(i) Neurological and transmitter alterations

In the early stages of the disease, neurodegeneration occurs primarily within cholinergic regions such as the hippocampus, entorhinal cortex and amygdala, suggesting early-stage AD to be a corticolimbic neurodegenerative disorder (Pearson and Powell, 1989; Schneider et al, 1999). Even in mild cases of AD there is already a 50% loss of neurons in the entorhinal cortex, a neural bridge that connects the hippocampus with the neocortex.

Initially, an AD patients motor, sensory, and linguistic abilities are preserved, however eventually the disease evolves into a global impairment affecting multiple cognitive domains, leading to dementia and ultimately death. Behaviourally, affected individuals are no longer able to perform learned perceptuo-motor tasks such as dressing, washing, eating etc, and invariably patients show impaired social skills and are given over to bouts of jealousy, and in some instances, violent rage. In advanced stages of the disease affected individuals show significant memory

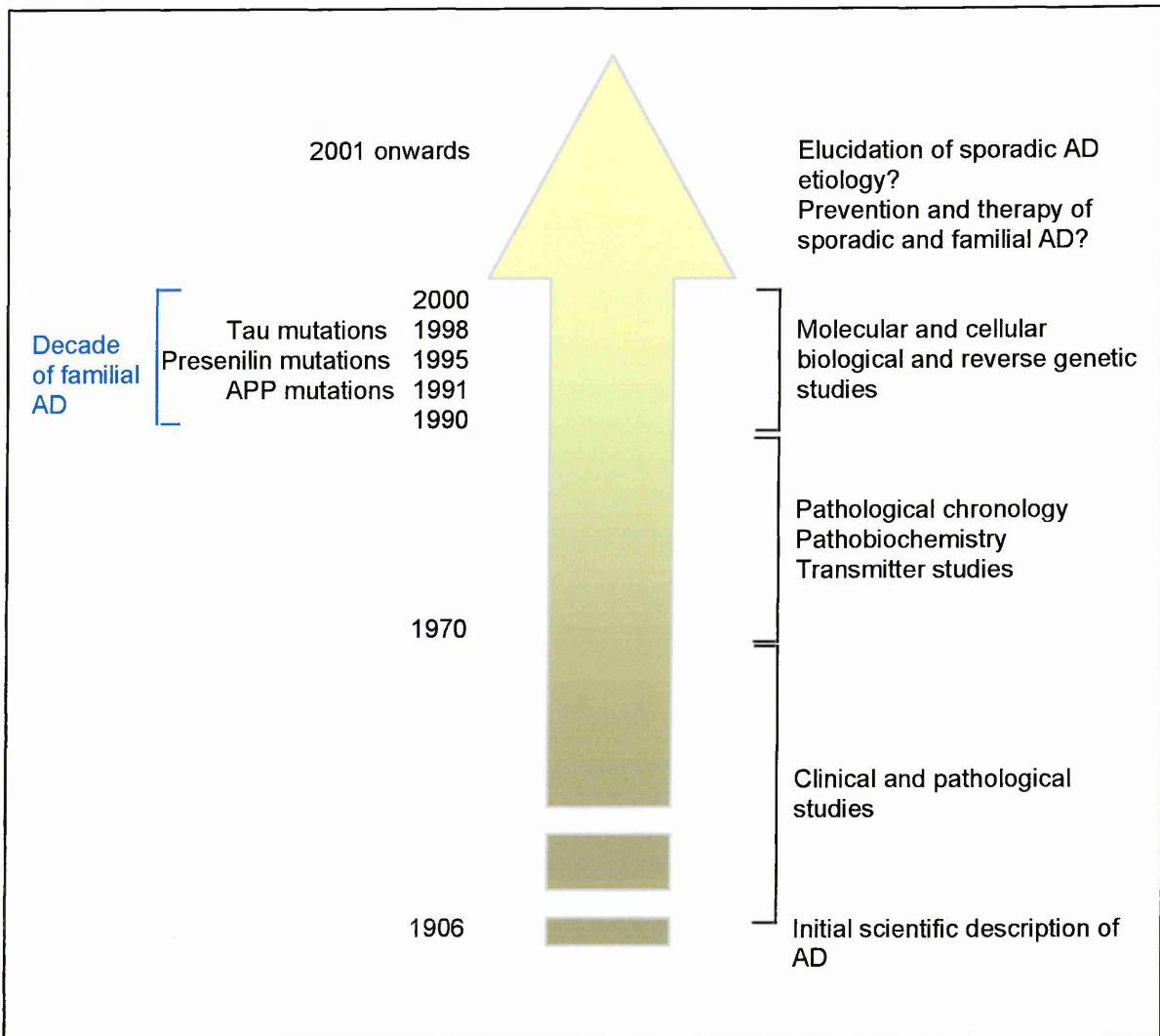


Figure 1.0. Simplified time line of AD research from first discovery in 1906 to present day. Modified from Saido, (2003).

loss, aphasia (loss of language), apraxia (impairment of purposeful movement) and agnosia (inability to recognise objects) (Strange, 1992).

Many of these behavioural changes can be explained by the loss of various neurotransmitters and their associated markers. These include losses of noradrenergic neurones in the locus ceruleus (structures associated with an individual's level of attention and vigilance) and decreases in the serotonergic system responsible for overall cortical activity. Most striking is the loss of markers from cholinergic neurons in the basal forebrain and ventral striatum (Perry et al, 1973).

The loss of cortical choline acetyl transferase (CAT) and decline in acetylcholine synthesis in biopsy specimens has been found to correlate strongly with cognitive impairment (Felician and Sandson, 1999; Vickers et al, 2000; Law et al, 2001). In terms of therapeutics, the selected loss in cholinergic neurotransmission as a consequence of AD has been addressed through the use of drugs that either sustain the action of acetylcholine within the synaptic cleft or mimic its action at cholinergic receptors. Overall though, cholinergic enhancement provides at best only mild symptomatic relief for patients with AD, thus current research into new therapies is focused on non-cholinergic aspects of AD metabolism.

(ii) Micro-histopathological features of AD

As well as gross anatomical changes in the AD brain such as gyral atrophy typified by sulci widening, ventricular dilation and frontal, parietal and temporal lobe shrinkage, post mortem microscopic examination reveals the presence of two distinct micro-pathological lesions. The first of these lesions, originally noted by Alzheimer himself, consist of interneuronal, aggregated fibrils referred to as neurofibrillary tangles (NFTs). The second type of lesion consists of aggregated β -amyloid ($A\beta$) peptides that form extracellular inclusions referred to as senile plaques.

(iii) NFTs contain aggregates of hyperphosphorylated tau

In AD brains tau deposits occur as abnormally phosphorylated intracellular threads within neurites (dendrites and axonal terminals that have degenerated), or as NFTs composed of pairs of ~10 nm filaments wound into paired helical filaments (PHF) located within the neuronal cell body (figure 1.1). The normally soluble tau present in tangles resists the actions of most detergents such as SDS or guanidine hydrochloride but can be partially solubilized by boiling in SDS. In fact, long after neurons have undergone apoptosis NFTs remains as so-called 'tombstone' markers (Selkoe et al, 1982). Tau is one of several microtubule-associated proteins (MAPs) that function to stabilise microtubules responsible for maintaining cell polarity, intracellular transport and the development of cellular processes.

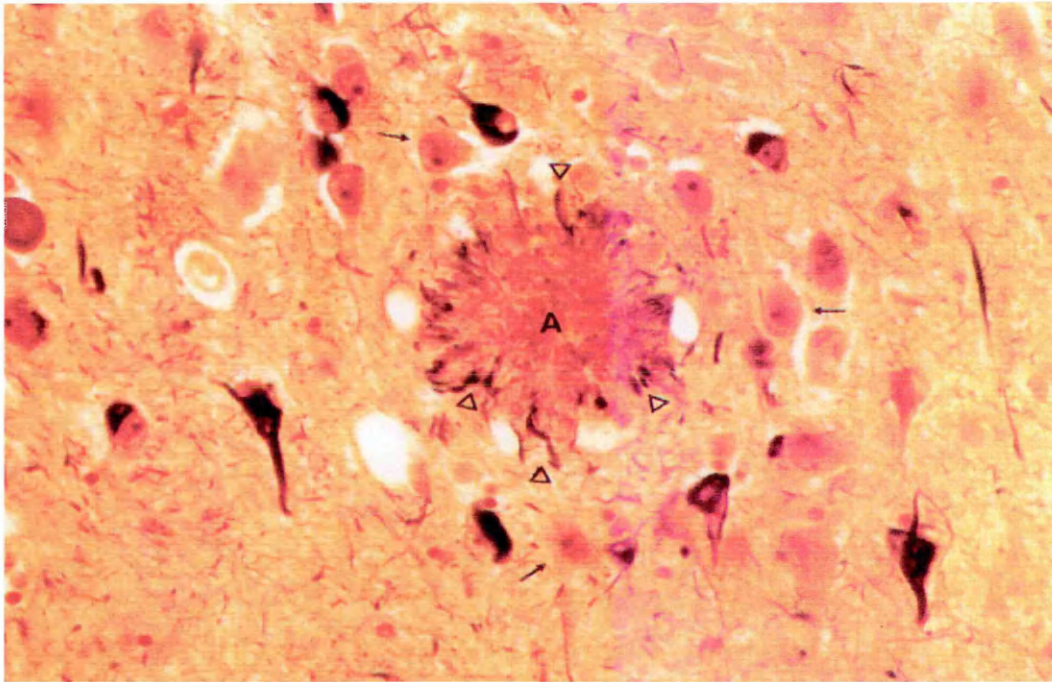


Figure 1.1. β -Amyloid plaque 'A' present within amygdala of a 69 year old AD male (plaque diameter $\sim 75\mu\text{M}$). Pyramidal neurons show neurofibrillary tangles (darkly staining bodies). Arrowheads indicate dystrophic neurites containing PHF. Specimen shows Bielchowsky silver staining (Selkoe, 1991).

The spatial-temporal development of AD and the attendant clinical manifestations of the disease correlate well with tau pathology and synaptic loss. Tau deposits spread from the transentorhinal region to the hippocampus and the neocortex in a series of observable stages, six in all, the first two being pre-clinical (Braak and Braak, 1991). The majority of AD cases are sporadic, i.e. there is no underlying, overt genetic cause, and thus tau PHFs have been proposed as the best correlate for clinical progression/pathological indicator of AD. Tau proteins undergo phosphorylation at multiple sites as a means of regulating its microtubule binding properties. Learning and memory formation requires that neurons and their synapses be labile so as to allow new memories to be hard wired into new or pre-existing neural networks. This requires flexibility of the underlying cytoskeletal architecture, thus de novo microtubule assembly and stabilisation requires the presence of proteins such as tau and other MAPs at axonal locations and synaptic junctions (Arendt, 2001).

Tau has multiple phosphorylation sites accessible to a variety of different kinases such as glycogen synthase kinase-3 (GSK-3), MAP kinase, cyclin dependent kinase 5, microtubule affinity-regulating kinase (MARK), etc (Mandelkow and Mandelkow, 1998). It is the combined actions of kinases and phosphatases that are responsible for the constant remodelling of the cell interior, for example during mitosis. In the AD brain tau undergoes aberrant phosphorylation at sites only seen during foetal development. Following hyperphosphorylation the ability to bind to microtubules is lost leaving tau free to associate with sulphated glycosaminoglycans or nucleic acids, leading to the formation of PHF within neurons (Goedert, 1996; Hasegawa et al, 1997), which consequently disturb axonal transport, ultimately affecting neurite outgrowth. Destabilization may decrease axoplasmic flow, so generating dystrophic neurites that contribute to synaptic loss.

Several questions concerning the formation of tangles remains unanswered, in particular the nature of the trigger and the identity of the kinase responsible for the hyperphosphorylation of tau. Whilst PHF can be generated in vitro, attempts at generating them in cell models has so far failed. Moreover, over expression of human tau isoforms in transgenic mice has not resulted in an AD-like pathology (Mandelkow and Mandelkow, 1998). Ultimately NFTs within neurites of the AD brain may be seen to be the pathological consequence of A β amyloidosis rather than as a first cause.

(iv) Amyloid peptide deposits in the AD brain

The second pathological lesion found in the AD brain is the presence of extracellular plaques that fall broadly into two morphologically distinct types, so called *neuritic* and *diffuse* plaques. Following purification and sequencing in the 1980s plaques were found to contain aggregated fibrils of A β peptide (Glennner and Wong, 1984; Masters et al, 1985). Under normal metabolic conditions A β is proteolytically derived from its amyloid precursor protein (APP) by the sequential action of two secretases, referred to as β - and γ -secretase, to yield a 4 kDa peptide composed of 39-43 amino acids (Kang et al, 1987). In the case of γ -secretase, cleavage is mediated either directly by a group of transmembrane proteins referred

to as the presenilins (PS1 and PS2), or else the presenilins are a crucial cofactor intimately involved in the γ -cleavage of APP (Selkoe, 1999).

(v) Neuritic plaques

Neuritic plaques are spheroid structures 10 to 120 μm diameter found in large numbers in the limbic and association cortices that vary in the degree of compaction of the amyloid core (Dickson, 1997). Analysis of the core reveals $\text{A}\beta$ fibrils (7-10 nm) intermixed with non-fibrillar forms, surrounded by activated microglia, fibrillary astrocytes and dystrophic neurites from many neurotransmitter classes, both within the amyloid deposit and immediately surrounding it. Ultrastructural analysis of the neurites reveals the presence of PHF as well as abnormally enlarged lysosomes and numerous mitochondria (Selkoe, 1996). Activated microglial cells expressing CD45 markers are often found within and adjacent to the central core of the plaque whereas astrocytes tend to form a ring around the plaque body (Selkoe, 2001).

The time scale in which these changes take place is currently unknown but likely involves many months or years. The deposition of $\text{A}\beta$ appears to be the earliest morphological change in the formation of neuritic plaques (Mann and Esiri, 1989). The C-terminus of $\text{A}\beta$ affects the solubility of the peptide such that the $\text{A}\beta_{40}$ variety is extremely soluble compared to $\text{A}\beta_{42}$, which readily forms highly insoluble fibrils in vitro (Jarret et al, 1993). In fact the latter isoform makes up the bulk of $\text{A}\beta$ within neuritic plaques along with $\text{A}\beta_{40}$ even though it is produced in very small amounts. Overall $\text{A}\beta_{40}$ makes up 90% of secreted amyloid, whilst $\text{A}\beta_{42}$ is produced in fractional amounts, however, co-incubation of $\text{A}\beta_{42/43}$ with $\text{A}\beta_{40}$ readily forms aggregates suggesting that the longer amyloid isoform may act a seeding agent in the formation of plaques (Tomita et al, 2001).

(vi) Diffuse plaques

Diffuse plaques are composed of amorphous A β and are found throughout the brain particularly within the cerebral vasculature and without the surrounding neuritic degeneration. At the time the presence of the soluble nonfibrillary peptide and the absence of neurites had been interpreted as representing an early stage in the development of senile plaques (Bugiani et al, 1995). However, with the development of specific A β antibodies it became clear that the A β_{42} constituted the major component of diffuse plaques with no, or little A β_{40} immunoreactivity in contrast to the heterogeneity of mixed neuritic plaques (Dickson, 1997; Selkoe, 2001). This would suggest that specific alterations in A β underlie the variations in A β deposition, arguing against diffuse to neuritic plaque staging (Vickers et al, 2001). However, evidence supporting a temporal staging of plaque development comes from observations that in normal aged, non-AD brains diffuse plaques are often found within the limbic and association cortices without any cognitive behavioural impairment. Additionally, immunohistochemical analysis of the teenage Down Syndrome (DS) brain in which APP is over expressed, reveal the presence of diffuse plaques composed solely of A β_{42} , yet NFT and neuritic degeneration is not observed until the third decade, when A β_{40} deposits begin to associate with plaques, along with microgliosis, astrocytosis (Lemere, 1996).

The aggregation and deposition of A β in both diffuse deposits and within amyloid cores is seen as the defining lesion of AD, yet in some kindreds there exist large plaques lacking the classical core of amyloid fibrils (Crook et al, 1998; Yanker, 1998). Those regions of the brain not associated with the clinical aspects of the disease, such as the thalamus and cerebellum, as well as the brains of equal aged matched individuals still show the presence of A β , albeit in very diffuse deposits not associated with plaques or tangles.

Diagnosis during disease onset has proven problematic in the past, however the level of A β_{42} may be informative as a diagnostic marker in some early onset AD families bearing missense mutations (De Jonghe et al, 1999a). Differences in the levels of insoluble A β found in AD, normal and pathologic ageing brains suggest that pathologic ageing is a transition state between normal ageing and AD (Wang

et al, 1999). Current attempts at diagnosing the early stages of AD in living brains has been attempted using advances in magnetic resonance imaging techniques (Fox and Rossor, 2000). Ultimately, it is the presence of plaques and tangles representing classical end-stage lesions that allow a definitive diagnosis of AD to be made post mortem.

1.3 Biology of the amyloid precursor protein

(i) Proteolytic processing of APP

APP is a glycosylated, single pass type I transmembrane protein (110-140 kDa) constitutively expressed in many different cell types and has many alternate transcripts produced from one gene, giving rise to many different APP isoforms (Selkoe, 1998). APP belongs to the APP-family, which contains the APP-like proteins 1 and 2 (APLP1 and APLP2). Three main APP species have been recognised: a 751 and a 770 amino acid protein commonly found in both neurons and non-neuronal cells; and a 695 amino acid protein found almost exclusively in neurons (Goldgaber et al, 1987; Kang et al, 1987). APP₆₉₅ is expressed both intracellularly and at the cell surface, and can be converted at both these sites to different secreted forms (Kang et al, 1999). The metabolic fate of APP (half-life of ~45-60 mins) is thought to be regulated by many factors including first messengers such as cholinergic agonists, and second messengers such as phospholipase-C and protein kinase-C, which appear to enhance α -secretase activity. This in part may be down to alteration in the phosphorylation status of the secretase or enhanced trafficking of Golgi-derived APP-containing vesicles to the cell surface (Selkoe, 1996).

Like many other proteins passing through the secretory pathway, APP undergoes post-translational modifications including *N*- and *O*-linked glycosylation, phosphorylation and sulphation. APP is co-translationally translocated into the endoplasmic reticulum (ER) via its signal peptide and then undergoes maturation as it passes through the Golgi (Cook et al, 1997; Hartmann et al, 1997). A hydrophobic stretch of amino acids situated at the carboxy terminal of APP helps anchor the molecule within the cell membrane compartment. Three main

secretase enzymes responsible for the cleavage of APP have been identified; the α -, β - and γ -secretases.

(ii) α -secretase pathway

The α -secretase has not been identified as any single proteinase, but two members of the ADAM (a disintegrin and metalloprotease) metalloprotease family, ADAM-10 or Kuzbanian and ADAM-17 are candidate α -secretases. ADAM family proteases typically possess several domains including an endothelial growth factor-like domain, a transmembrane domain, a cytoplasmic domain and an autoinhibitory domain that must be removed for activity. Additionally, these proteases are characterised by the presence of a disintegrin domain able to bind integrins or other receptors and a metalloproteinase domain that contains a consensus active-site sequence for a zinc-dependent metalloprotease (Primkoff and Myles, 2000).

ADAM 10 activity releases a soluble form of Delta, a ligand for the cell surface receptor molecule Notch responsible for cell fate during development and neurogenesis. Cells carrying mutant forms of the *KUZ* (ADAM10 gene) do not receive inhibitory signals from neighbouring cells leading to an excessive neuronal cell proliferation (Primkoff and Myles, 2000). The role of ADAM 10 α -secretase activity in basal and stimulated ectodomain shedding of APP has been demonstrated by studies investigating ADAM 10 overexpression in cells that lead to a severalfold increase of α APP_s and the p10 fragment that is further cleaved by the γ -secretase to yield soluble p3 (Lammich et al, 1999).

ADAM 17 or tumor necrosis factor- α converting enzyme (TACE) is thought to be a membrane-anchored enzyme that shows poor sequence specificity when cutting single-pass proteins and is responsible for the release of a 17 kDa tumor necrosis factor (α -TNF) fragment involved in inflammation. In the cleavage of APP, the α -secretase cuts at a specific distance from the outer membrane surface (Sisodia et al, 1992). APP proteolysis occurs between lysine 687 and leucine 688 (residues 16 & 17 of A β) to release a large soluble ectodomain molecule referred to as α -APP, whereas α -secretase activity in combination with γ -secretase releases a

p3 fragment containing part of the A β sequence and a larger C-terminal membrane-bound fragment called C83 (figure 1.2). Thus the α -secretase pathway is non-amyloidogenic and from the perspective of AD, any shift towards increased α -secretase activity might conceivably have beneficial effects. In most cell cultures, 10-30% of all APP undergoes α -cleavage thus alteration in TACE activity in the aged brain may contribute to amyloid formation. TACE is thought to be involved in regulated α -secretion since disruption of the TACE gene abolishes regulated α -cleavage in cultured cells, whereas APP_s is unaffected in cells derived from knockout mice (Bauxbaum et al, 1998).

(iii) β -secretase pathway

A second enzyme termed β -secretase (beta-site APP-cleaving enzyme, BACE) is a type 1 transmembrane protein that exists as a preproenzyme of 501 amino acids that displays several features including a 21-residue signal peptide, a prosegment of about 39 residues, a catalytic unit with active site aspartyl residues at positions 93 and 289, a 27-residue transmembrane region, and a 21-residue C-terminal domain (Walter et al, 2001). Studies examining the overexpression of BACE reveal the presence of the enzyme within the ER-intermediate compartment (ERGIC), Golgi vesicles and lysosome/endosome compartment of neurons (Vassar et al, 1999). The majority of A β appears to be generated within the trans Golgi network (TGN), presumably the same location as β - and γ -secretase activity, whereas radioiodination experiments and cell surface biotinylation (Lammich et al, 1999) show α -secretase cleavage of APP at the plasma membrane. BACE is highly expressed in brain and other tissues as demonstrated by the production of A β .

Evidence for the role of BACE in APP processing comes from the use of antisense oligonucleotides that block BACE expression greatly diminishing the production of A β , whereas, overexpression of BACE in a number of cell lines leads to enhances A β production. Significantly, BACE knock-out mice show no adverse phenotype but have dramatically reduced levels of A β demonstrating that

elimination does not pose serious consequences for the animal, a factor of great importance in targeting BACE for inhibition in AD therapy (Walter et al, 2001).

BACE is a novel transmembrane aspartyl protease that initiates A β generation by cleaving APP after met 671, producing a ~12 kDa C-terminal fragment some 99 amino acids in length (Vassar et al, 1999). The C-terminal is retained within the membrane whilst the N-terminal is the first amino acid (Asp) of the A β peptide (figure 1.2). The released fragment is referred to as β APP (Seubert et al, 1992). The C99 peptide serves as the substrate for the generation of A β by the γ -secretase and therefore constitutes the amyloidogenic pathway responsible for the accumulation of A β . Uniquely APP appears to be the only protein substrate that is cleaved by BACE.

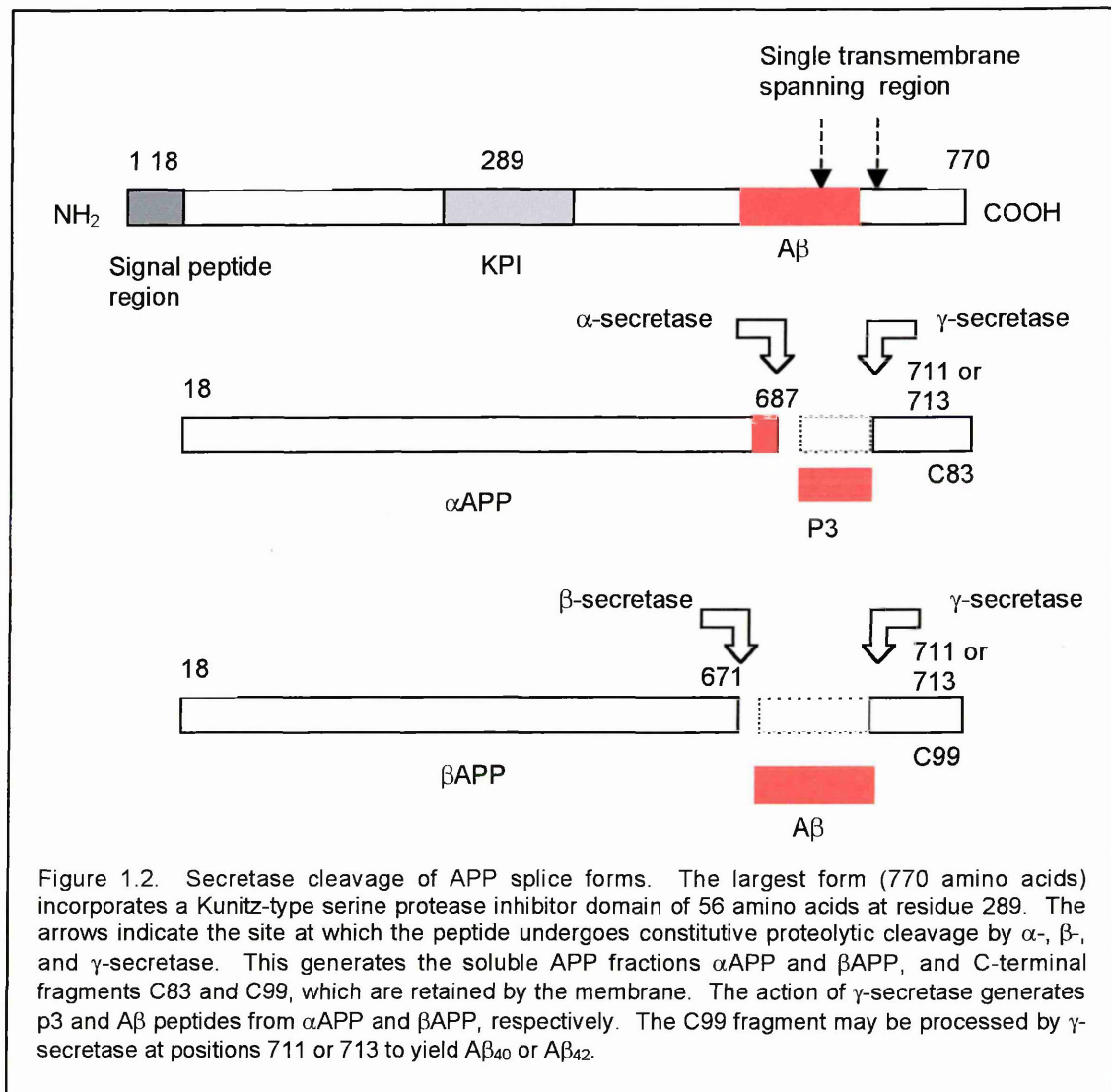
(iv) γ -secretase pathway

The third protease involved in the proteolysis of APP termed γ -secretase, acts on both APP transcripts within the hydrophobic transmembrane domain. γ -secretase is equated as being presenilin, or at the least, intimately associated with γ -secretase activity (Selkoe, 1999; Wolfe et al, 1999b). In the case of the α -APP C-terminal fragment, γ -secretase generates a peptide fragment called p3, whilst its action on the β APP C-terminal fragment generates A β proper. A β 40 is the predominant isoform produced during normal metabolism of β APP (Haass et al, 1992; Jarett and Lansbury, 1993) and is detected in the CSF and plasma of normal healthy individuals throughout life. γ -secretase cleavage of APP at valine 711 generates A β ₄₀ or the toxic A β ₄₂ species following cleavage at isoleucine 713 (figure 1.2). A more detailed appraisal of γ -secretase is discussed in the section dealing with the biology of presenilin in AD.

(v) APP trafficking and A β generation within the cell compartment

The majority of α APP is derived by the action α -secretase processing APP at the plasma membrane (Sisodia et al, 1992) or during secretory intracellular trafficking of the peptide, whereas BACE activity occurs during the late secretory trafficking of

APP (Haass et al, 1993). The generation of the $A\beta_{42}$ peptide appears to occur within the ERGIC, while the production of the $A\beta_{40}$ is thought to occur more distally within the secretory pathway, predominantly within the TGN/endosomal-lysosomal systems (Golde et al 1992; Haass et al, 1994). Those APP peptides untouched by enzymic action at the plasma membrane are endocytosed by clathrin coated vesicles and trafficked to late endosomal compartments for recycling or lysosomal degradation (Walter et al, 2001).



Investigations into the subcellular compartments from which amyloid variants are generated and secreted, have demonstrated that $A\beta_{40}$ and $A\beta_{x-40}$ (x being a NH₂-terminal truncated 'ragged' form) are generated exclusively within the TGN where they are packaged into secretory vesicles (Cook et al, 1997; Hartmann et al, 1997;

Greenfield et al, 1999). These peptides formed in the TGN consist of two pools, a soluble population extractable with detergents and a detergent-insoluble form (Greenfield et al, 1999). The majority of A β is destined for secretion into the CSF and the blood plasma, however, A β generated from APP whilst still within the ERGIC, may not be destined for secretion but may instead be retained and catabolised inside cells, where it could confer pathogenic properties distinct from those mediated by extracellular plaque formation (Cook et al, 1997).

Much of the data on the location of APP and A β is complex and difficult to interpret. In particular there appears to be a discrepancy between the site at which A β_{42} is generated and the ER/IC location of the β - and γ -secretases needed to generate it, a finding referred to as the so-called spatial paradox (De Strooper et al, 1997; Annaert et al, 1999). Brefeldin-A (BFA) treatment of NTera 2 cells prevents A β secretion, in particular A β_{40} whereas BFA-treatment of cells has little effect on A β_{42} secretion suggesting that the toxic species is generated in the ERGIC (Cook et al, 1997; Chen et al, 2000). Additionally, cleavage of β -APP by BACE takes place predominantly within acidic compartments i.e. within the TGN and endosomes (Haass et al, 1993). Similarly, pulse chase experiments show that the majority of the C83 and C99 fragments derived from APP are glycosylated, i.e. their cleavage by γ -secretase must occur post-Golgi. Whether other intracellular sites beyond the ERGIC contribute to the generation of secreted A β_{42} remains to be determined. Biochemical and immunocytochemical experiments have detected β APP in the ER and post-Golgi secretory vesicles; A β_{42} in the ER; and A β in glycolipid membranes (Selkoe, 1999), indicating that A β can be generated and/or accumulate at various points along the secretory pathway.

Other studies indicate that intracellular A β_{42} also forms insoluble aggregates within lysosomes that resist degradation. The addition of A β_{42} to cultured cells likewise, leads to the accumulation of newly synthesized A β , particularly the ragged forms, indicating that intracellular A β may derive from a 'solid phase', cellular pathway. This pathway, which preferentially generates ragged A β_{42} , contrasts to the pathway that primarily produces secreted A β (Yang et al, 1999). Other findings imply that the progressive shift of A β_{40} /A β_{42} , from soluble to insoluble pools, plays a mechanistic role in the onset and/or progression of AD

(Wang et al, 1999). Although the majority of studies indicate that the secretion of A β ₄₂ into the extracellular space is the likely route by which it forms insoluble fibrils, other studies suggest that a portion may enter through the blood brain barrier, via a receptor-mediated transport system similar to the uptake of insulin (Poduslo et al, 1999). Furthermore, the majority of peripheral as well as centrally located cells such as astrocytes, microglia, endothelial and smooth muscle cells all produce APP and generate A β in variable amounts, possibly contributing to the secreted pool of A β from within the brain or via the blood brain barrier (Selkoe, 2001).

Previous studies indicate that APP is rapidly transported anterogradely within neurons along axons out to axon terminals where they are present within vesicles (Koo et al, 1990). Similarly, retrograde transport of APP from the terminals back to the cell body has also been observed. Here, some APP may be translocated to the somatodendritic surface or may recycle via the endosome system, possibly generating A β in the presence of β - and γ -secretase (Yamazaki et al, 1995). More recently, APP has been demonstrated to bind to Kinesin-1, a microtubule motor protein, where it functions as a kinesin-1 receptor and assists in the transport of vesicles containing BACE and PS1 along the axons of peripheral neurones (Kamal et al, 2001). Analysis of the compartment in which these proteins reside shows APP is cleaved by γ -secretase, generating A β and an APP-C-terminal fragment (CTF) and liberates kinesin-1 from the membrane. The significance for AD is that cleavage of APP due to axonal damage or blockage could lead to A β deposition. If substantial, this may interfere with other transport processes or neurotrophic signalling, leading to possible neuronal death.

Damage to neurones in AD as evidenced by dystrophic neurites indicate axonal reaction to trauma. In preclinical AD these changes are typified by abnormal phosphorylation and accumulation of neurofilaments. Morphologically such regions are identical to distal and proximal segments of physically damaged axons. A simple view of the disease process states that A β accumulated within the extracellular space inflicts physical and mechanical stress onto nearby axons through constriction, triggering a neurological reaction to injury. Over a number of years the maturation of plaques only serve to exacerbates matters (Vickers et al, 2000).

(vi) Function of APP

Little is known about the precise physiological role played by APP, though it appears to be closely involved in synaptic plasticity and the morphoregulation of neurite outgrowth. Functions proposed for β APP include a role as a mediator of cell-cell and cell-substrate interactions, and as a trophic or neuroprotective molecule (Arendt, 2001). Localisation studies show that APP is heavily involved in synaptic formation and cell adhesion where it co-localises at the cell surface of neurons with cell-cell adhesion molecules such as β -1 integrin. In mammals, transmembrane APP is associated with elongating axons, whereas secreted APP is implicated in synaptogenesis. The expression of APP appears to be developmentally regulated and is released during long-term potentiation (LTP) where it increases memory retention in rats. Removal of APP either in transgenic knockouts or following anti-APP antibody treatment results in decreased LTP and impaired cognitive performance (Arendt, 2001). The alternate proteolytic processing of APP suggests that it may have several functions apart from development, since APP knockout mice show neither early mortality nor significant morbidity in vivo. Possibly the APP-like proteins lacking the A β sequence function in a similar fashion to APP (Selkoe, 1999).

The β APP molecule is known to bring about mitosis in cultured cells by stimulating a mitogen-activated protein kinase. The Kunitz serine protease inhibitor sequence within the longer APP isoforms inhibits a serine protease called Factor XIa of the coagulation cascade in human platelets (Smith et al, 1990). Additionally, during conditions normally associated with neuronal injury such as inflammation, ischemia, excitotoxicity etc, KPI-APP expression in astrocytes is stimulated whereas expression of the shorter 695 isoform, which lacks the inhibitory domain, is decreased (Robinson and Bishop, 2002).

More recently, a cytoplasmic fragment of β -APP, the APP intracellular domain (AICD), has been implicated in signal transduction and is generated in an analogous fashion to Notch cleavage following the action of β - and γ -secretase activity. The AICD is thought to form a transcriptionally active complex along with other known proteins such as Fe65 and Tip60 a histone acetyltransferase (Cao

and Südhof, 2001) and is potentially important in the pathogenesis of AD since due to aberrant processing of APP may severely curtail the decrease levels of AICD.

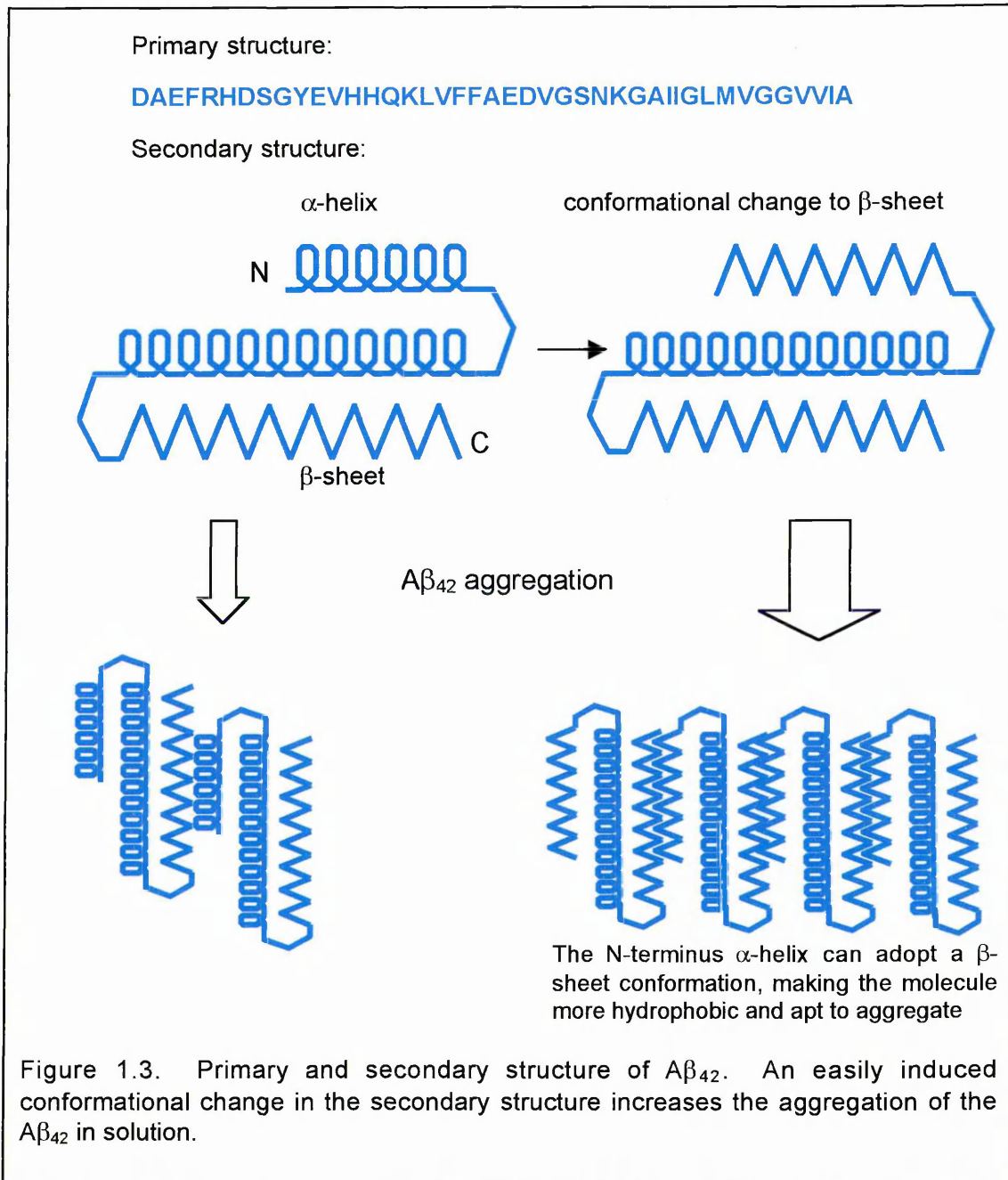
1.4 A β associated toxicity in AD

(i) β -Amyloid structure and toxicity

A central question concerning the role of A β in AD is the extent to which this peptide is toxic in vivo. Chemically, the additional of the two hydrophobic residues on the A β_{42} peptide are responsible for its aggregation into insoluble fibrils. The secondary structure of A β_{42} as predicted by the Chou-Fasman algorithm shows two α -helices and one β -sheet (figure 1.3). The N-terminal α -helix is able to adopt an alternate β -sheet configuration that markedly increases aggregation in solution (Saido, 2003). The adoption of the β -sheet conformation following a nucleation-mediated process has also been demonstrated following the release of A β into the cytoplasm (Jarrett and Lansbury, 1993). More recently, using sensitive immunoprecipitation and SDS PAGE analysis, A β oligomers from conditioned media, in the absence of monomers and amyloid fibrils, disrupted synaptic plasticity and inhibited LTP in vivo at physiological concentrations found inside the human brain (Walsh et al, 2002). Additionally, pre-treatment of the complete media with insulin degrading enzyme (IDE), which degrades monomeric but not oligomeric A β , had no affect on LTP indicating that the synaptotoxicity is associated specifically with oligomeric form of A β .

Long before A β_{42} containing plaques (diffuse) form, structural changes in the synapse as well as electrophysiological alterations have been observed in mutant APP transgenic mice (Hsia et al, 1999). Moreover, cultured cortical and hippocampal neurons treated with high concentrations of neurotoxic fibrillar A β (Loo et al, 1993) exhibit changes characteristic of apoptosis, including nuclear chromatin condensation, plasma membrane blebbing, and internucleosomal DNA fragmentation. Though these and other data showing toxic effects of synthetic A β in neuronal cultures, the role of A β_{42} oligomers in initiating cellular dysfunction in AD remains unproven (Selkoe, 2001). Moreover, data from experiments in which

fibrillar A β is injected directly into the brain of rodents and monkeys are inconclusive, since A β can be neuroprotective in the brains of young animals but toxic to older brains (Robinson and Bishop, 2002). In general the concentration of A β used in toxicity studies is often much greater than physiological concentrations.



Another difficulty with A β concerns its acute toxicity. AD pathology typically develops over several decades whereas the biochemical action of A β can be measured rapidly, in the case of LTP, effects can be seen within 1 hour of adding

A β to hippocampal neurons. Though in this case, it has been pointed out that A β may contribute to mild cognitive impairment in early AD via a novel mechanism independent of neuronal death (Klein et al, 2001). Additionally, whereas aged human neurons may be unduly susceptible to the effects of A β because of years of various insults, neurons used for in vitro studies are obtained from embryonic or postnatal animals, thus making a direct comparison of A β toxicity between the two cell populations difficult to interpret (Vickers et al, 2000).

(ii) Oxidative stress and AD

A β toxicity may be mediated via binding to the RAGE receptor (receptor for advanced glycation end products) a member of the immunoglobulin superfamily of cell surface receptors (Yan et al, 1996). This receptor is highly expressed by cortical neurons, especially in the hippocampus and cerebellum during rat brain development, and in a variety of other cell types, including endothelial cells and phagocytes. RAGE activation is believed to trigger cellular oxidative reactions and has been shown to mediate the interaction of A β with glial cells, leading to the first steps in the inflammatory cascade as seen by glial cell activation, cytokine production, chemotaxis, and haptotaxis. However, antioxidants appear not to protect neurons from A β in toxicity assays, nor is there any evidence showing oxidative damage of genomic DNA specific to AD or DS (Vickers et al, 2000).

Oxidative stress is believed to be a critical factor in normal aging brain and in other neurodegenerative diseases besides AD, such as Parkinson's disease and amyotrophic lateral sclerosis (ALS). Comparisons of AD brains with age matched controls show an increase in oxidative damage, whilst plaques and tangles display immunoreactivity to antioxidant enzymes (Pappolla et al, 1992). The presence of reactive oxygen species (ROS) within the brain results in lipid peroxidation of the cell membranes impairing the function of various membrane proteins involved in ion homeostasis, such as N-methyl-D-aspartate receptor channels or ion-motive adenosine triphosphatases. Consequently, the increased intracellular calcium and ROS levels leads to protein, DNA, and lipid damage that may be the trigger for apoptosis. Additionally, the exposure of PC12 cells to A β_{25-35} and A β_{1-40} has been

shown to induce a concentration-dependent accumulation of ROS that impair energy metabolism, so leading to a reduction in ATP levels that compromise cellular viability (Pereira et al, 1999). Other studies suggest that A β exerts its toxic effect via the activation and inhibition of several transcription factors (Santiard-Baron et al, 1999). Exposure of Ntera 2 cells, for example, to A β_{25-35} induces the expression of several genes including the 'growth arrest and DNA damage-inducible gene' (gadd45) implicated in the DNA excision/repair process, whereas A β represses, amongst others, a gene encoding a 'hinge protein' subunit of the mitochondrial cytochrome-c reductase enzyme. The up-regulation of gadd45 in response to DNA strand breaks in cells exposed to A β may therefore be a critical event in AD pathology. Additionally, increased intracellular calcium may also alter calcium-dependent enzyme activity such as the implication of protein kinase-C in amyloid protein metabolism and the phosphorylation of tau. The apoptotic pattern of cellular death seen in oxidative stress is similar to that produced by A β exposure (Felician and Sandson, 1999).

(iii) Inflammatory Reactions and AD

The inflammatory and immune aspect of AD is becoming increasingly important for researchers. A typical hallmark associated with inflammation in AD is the presence of reactive microglia densely embedded within the senile plaques (Selkoe, 2001). Increased cytokines levels are seen in the serum, plaques and neurons of patients with AD compared with aged-matched controls. Furthermore, the anti-inflammatory cytokine-transforming growth factor beta1 (TGF- β 1) is able to promote or accelerates the deposition of A β (Wyss-Coray et al, 1997). Classical complement pathway fragments are also found in the brains of AD patients, and A β may directly activate the classical complement pathway in an antibody-independent manner perhaps by interacting with some aspect of the immune system.

Whether these markers are a consequence of the disease or a cause remains to be seen. Brain specimens from elderly patients with arthritis treated with non-steroidal anti-inflammatory drugs have similar numbers of senile plaques, as do control brains. However, less microglial activation is seen in the arthritis patients'

brains, suggesting that anti-inflammatory agents may delay or prevent clinical symptoms of AD by limiting the associated inflammation (Felician and Sandson, 1999).

As well as the increase in RAGE expression in neurons, vasculature, and microglia in affected regions of AD brains in response to A β (Yan et al, 1996), A β fibrils also bind to an unrelated 'class A scavenger receptor' expressed by large numbers of microglial associated with senile plaques (El Khoury et al, 1996). This receptor as well as RAGE may therefore represent novel pharmacological targets for reducing the inflammatory and oxidative reactions associated with AD.

1.5 Theories proposed to account for AD

(i) The amyloid cascade hypothesis

A controversial issue in the pathogenesis of AD is the relationship between amyloid deposition and NFT formation. A substantial body of evidence supports the idea that the aggregation of insoluble A β fibrils is behind the pathology of AD. The fibrillar form of A β has also shown to alter the phosphorylation status of the tau protein. It appears that aggregated but not monomeric A β peptides *in vitro* can induce toxicity on cells by presumably related processes such as oxidative stress, disruption of calcium homeostasis and cytoskeletal reorganisation. However, It remains to be demonstrated whether the absence of β APP function in AD patients, even those harbouring β APP missense mutations is responsible for the effects observed in the disease state (De Jonghe et al, 1998). The opposite may in fact be true that APP mutations work by a gain-of-function i.e. increased A β production. The identification of several point mutations within the APP gene in some patients with early-onset FAD and the development of transgenic mice exhibiting cognitive changes and neuritic plaques also incriminate A β in AD. Additional evidence comes from data supporting the role of presenilins in A β metabolism as well as findings of abnormal production of A β protein in mutant PS1 FAD kindreds (Selkoe, 1996).

The above data and others have been formulated as the 'amyloid cascade

hypothesis', which places the aberrant processing of APP and the subsequent deposition of A β as central events in AD pathology (Hardy and Selkoe, 2002). A hypothetical scheme to explain the temporal unfolding of dementia in FAD begins with FAD mutations that lead to A β isoform accumulation that then triggers inflammatory responses in glial and astrocytes. Downstream consequences involve perturbed homeostasis, oxidative injury, and PHF formation. Eventually these pathologies result in cortical then global dysfunction best characterised as dementia (Selkoe, 2001). Figures 1.4 outline the main features of the amyloid cascade hypothesis.

(ii) Amyloidosis and Tauopathy

The amyloid hypothesis is not uniformly accepted especially since dementia severity correlates better with the number of neocortical NFTs than with neuritic plaques. The normal function of tau is to stabilise neuronal microtubules. Apo ϵ 3 may protect tau against hyperphosphorylation by bindings to those sites on tau involved in the assembly of PHFs (Felician and Sandson, 1999). The hyperphosphorylation of tau disrupts the Golgi apparatus by destabilization of the microtubular system, leading to abnormal protein processing and increased A β production (Terry, 1996).

Another difficulty with the amyloid hypothesis is the lack of evidence showing nerve cell body degeneration in the vicinity immediately surrounding the plaque. In fact cortical nerve cell bodies have been demonstrated within the plaque core. Similarly, nerve cell degeneration has not been demonstrated in transgenic mice that develop A β plaques, nor do A β deposits that occur throughout the AD brain, such as in the cerebellum, show signs of surrounding degeneration (Vickers et al, 2000).

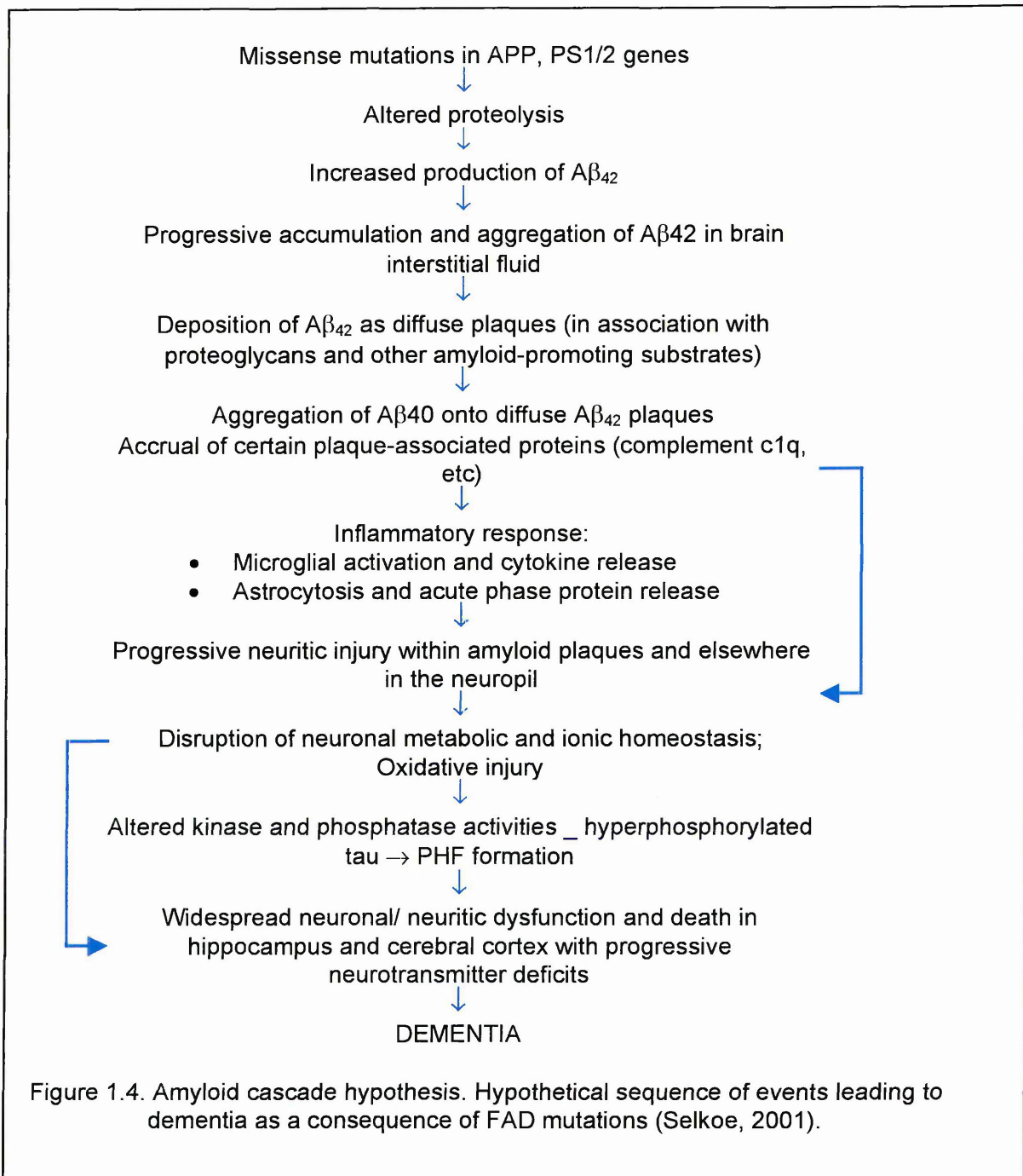
(iii) Competing hypotheses in AD

The evidence provided by studies examining A β used for justifying the amyloid hypothesis has similarly been re-interpreted to support the notion of A β as a

biofloculant. Whereas the amyloid hypothesis implicates A β as the neurotoxic substrate in AD, the biofloculant hypothesis concludes the opposite; that A β is *neuroprotective* (Robinson and Bishop, 2002). In this proposal A β generated from APP functions by binding neurotoxic solutes, such as metal ions, which could otherwise mediate cell damage.

According to the biofloculant hypothesis, plaque formation is a consequence of A β binding toxic agents resulting in the precipitation of the A β complex within the extracellular space (ECS). The precipitate either affects neurons directly or physically displaces neurites or impairs the traffic of metabolites in the extracellular space. Ordinarily, macrophages stimulated by a local inflammatory response clear the A β -toxin complex. In AD the biofloculant hypothesis explains this event as a neuroprotective response that is compromised when A β clearance is outstripped by deposition and the capacity of macrophages to phagocytose these deposits is exceeded. This hypothesis maintains that increases in A β deposition in LOAD are particularly damaging within the ECS. The trigger for this is believed to be previous trauma such as stroke/ischaemia, head injuries, etc. Data investigating the effect these traumas have on narrowing the ECS following inflammatory reactions, shows that the passage of large macromolecules through the ECS are hampered, leading to their deposition with bound A β (Robinson and Bishop, 2002).

An obvious difficulty with this hypothesis is the role A β plays in FAD. Both plaques and A β aggregates are thought to occur in FAD brains over a period of decades. If A β acts as a biofloculant it is reasonable to assume that there would be sufficient time for the clearance of A β -toxic complexes, barring a precipitous event occurring over a short space of time. Moreover, it is difficult to reconcile A β as a neuroprotective agent when clearly individuals with APP or PS mutations develop AD. If anything it would be expected that such individuals would be protected from developing AD by the misprocessing of APP. The role of A β as a biofloculant is outlined in figure 1.5.



Yet another hypothesis characterises AD as a developmental disease that recapitulates early development resulting in morphoregulatory dysfunction associated primarily with the synapse (Arendt, 2001). The main thrust of this argument states that in AD it is the ability of the brain to modify its own structural organization and functioning, as an adaptive response to functional demands that is impaired, as opposed to the brain reacting to some unspecified, age-related disorder. Much of the evidence presented in favour of this hypothesis includes data from studies demonstrating aberrant neuroplasticity at the synapse. In this

hypothesis AD is an unavoidable consequence of the ageing process. Cumulative damage over a lifetime caused by 'wear and tear' in the brain is exacerbated in vulnerable regions, such as the hippocampus whose role in memory demands significant neuroplastic remodeling. The vulnerability of these regions in combination with the individual's polymorphic genotype, as well as other epigenetic pressures is postulated to be the cause of AD. A β accumulation in this context has been shown to disrupt cell adhesion mechanisms in vivo leading to impaired synaptogenesis, reduction in LTP, cytoskeletal changes, disturbances in axonal transport, impaired neurotransmitter release, etc (Arendt, 2001). Figure 1. 6 illustrates the main features of this hypothesis.

1.6 Genetics of AD

Many epidemiological studies investigating AD show a clear association between dementia and age. The prevalence rates for dementia and AD double approximately every 5 years from rates of 2%–3% (65 to 74 years) in the case of dementia, to over 30% in subjects 85 years and over. The prevalence of AD, initially 1%–2% in 65 to 74 year olds increases to 25-50% in subjects aged 85 years or older. This relationship with age is seen even in studies reporting different prevalence rates (Hendrie, 1999).

To date five genetic loci have been identified with respect to AD. These include three fully penetrant, autosomal dominant mutations in genes for PS1, PS2, and APP as well as two at-risk common-population-polymorphisms (CPP) associated with LOAD, such as the ApoE4 and α -macroglobulin-2 (A2M-2) polymorphisms. Differences in the onset of the disease range from the early thirties in Down's Syndrome patients (DS), the mid-thirties to fifties in early onset FAD and individuals greater than 50 years of age in LOAD. Table 1.0 summarises some of the main genetic factors associated with AD and the phenotypic consequences of the gene defect.

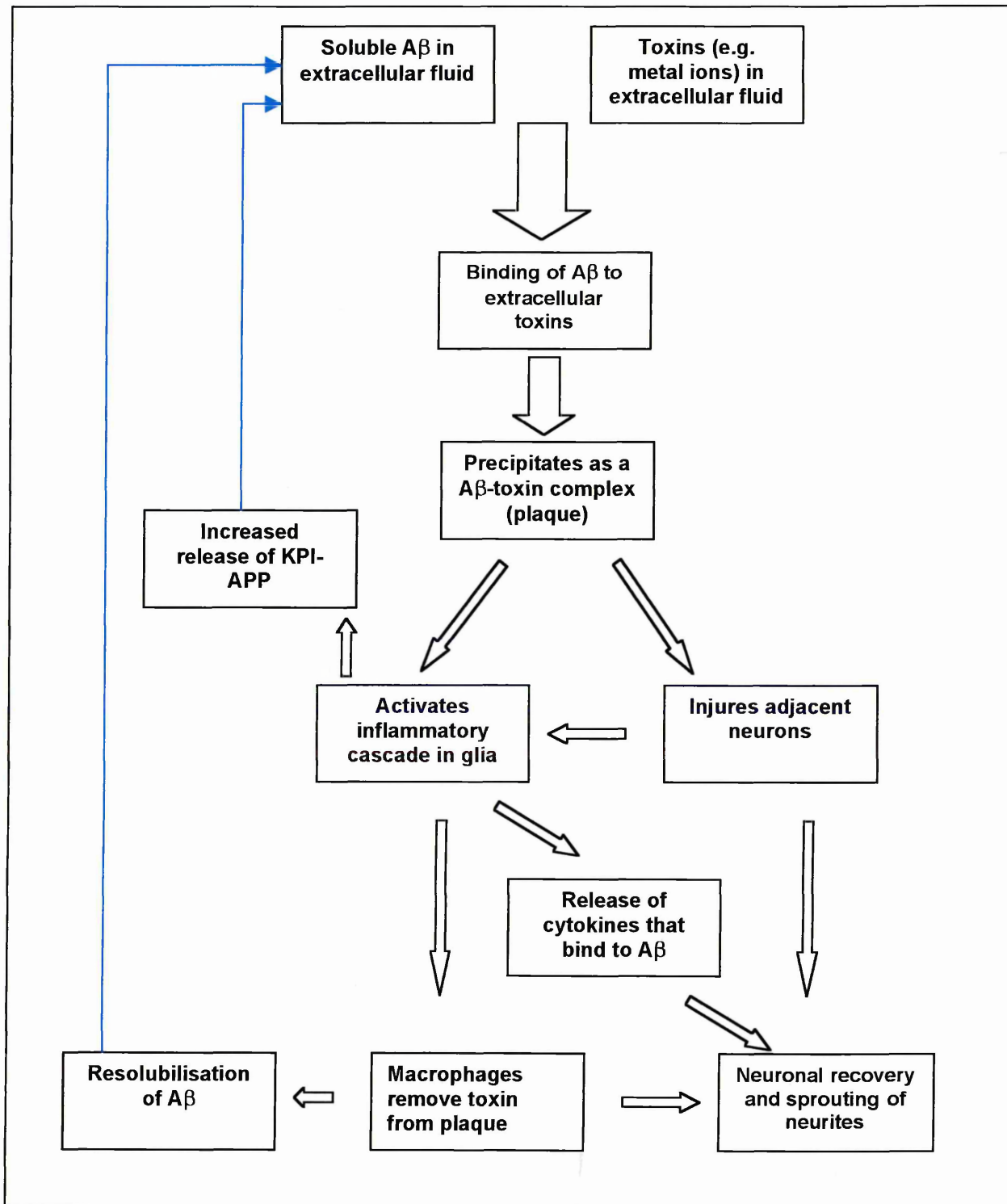


Figure 1.5. Biofloculant hypothesis of AD. Unlike the amyloid cascade hypothesis which implicates A β as the toxic substrate, the biofloculant hypothesis maintains that A β is a neuroprotective agent whose function is compromised in AD (Robinson and Bishop, 2002).

sequence of APP. In all cases each mutation increase A β production, though by slightly different mechanisms. One such mutation at position E693Q of the A β sequence within APP results in A β deposition within the cerebral vasculature, leading to the diseased state in some cases, and cerebral haemorrhage and angiopathy in others (Levy et al, 1990). The adjacent mutation at position A692G, again within the A β sequence of APP, is associated with plaque and tangle formation and results in dementia and severe microvascular β -amyloidosis with occasional cerebral haemorrhages (Hendriks et al, 1992).

Table 1.0. Genetic factors predisposing to Alzheimer's disease (modified after Hardy, 1997)

Genotype	Biochemical result	Phenotype
Down's Syndrome	more APP production	more A β_{42} / A β_{40}
APP _{670/671} (Swedish)	potentiation of β -secretase	more A β_{42} / A β_{40}
APP ₆₉₂ (Flemish)	inhibition of site of α -secretase	more A β_{42}
APP ₇₁₆ (Florida)	alteration of site of γ -secretase cut	more A β_{42}
APP ₇₁₇ (London)	alteration of site of γ -secretase cut	more A β_{42}
PS1/PS2 mutations	subtle alteration of APP processing	more A β_{42}
ApoE4	unclear	increase plaque density and vascular deposits.
α -macroglobulin-2	unclear	increase A β deposits

Families harbouring APP mutations have onsets before 65 years, often in their 50s. In DS the situation is quite different. Though the pathology parallels that of AD (neuritic plaques and NFT), here trisomy caused by non-disjunction of the 21st chromosome leads to an extra APP gene. The gene dosage effect results in over expression of APP and therefore the build up of A β_{40} and A β_{42} peptides from birth (Takuda et al, 1997). Diffuse plaques containing A β_{42} have been detected in the brain of DS patients as young as 12 years old, but neuritic plaques containing A β_{40} are not detected until the third decade (Lemere et al., 1996). Dementia onset in

DS appears to be influenced by the *ApoE* allele and occurs between 40 and 70 years of age.

The observation that the majority of APP mutations increase $A\beta_{42}$ production has led to the conclusion that $A\beta$ precipitates AD. However, APP has several functions in the developing and adult brain quite distinct from $A\beta$ generation, such as neuroprotection, synaptogenesis, and memory formation and consolidation. This has led to the notion that APP dysfunction as a result of mutations in AD brains may produce more APP to correct the deficit and as a by-product excess $A\beta$ is produced which then aggregates (Robinson and Bishop, 2002).

(ii) Presenilin mutations and FAD

Three loci have been associated with early onset aetiology; the APP gene on chromosome 21 (Goate et al, 1991); the PS1 gene on chromosome 14 (Sherrington et al, 1995); and the PS2 gene on chromosome 1 (Levy-Lahad et al, 1995; Rogaev et al, 1995). The most common cause of FAD are mutations found within the presenilin genes, which account for 40 percent of all early onset FAD cases and roughly one to two percent of all AD case (Tanzi et al, 1998). How these mutations cause the form of AD with the earliest age of onset is as yet unknown. To date ~130 mutations in PS1 alone are have been reported and are the primary cause of AD with onset below the age of 55 (table 1.1). Studies utilising cell cultures and transgenic mice have shown that these mutations alter APP processing so favouring the production of the highly amyloidogenic $A\beta_{42}$ species, as opposed to $A\beta_{40}$ (Younkin et al, 1994; Selkoe, 1999). Mutations in PS2 have been described in two families that exhibit a more variable onset ranging between 40 and 80 years (Rogaev et al, 1995) as compared to the PS1 mutations, which vary between 25 to 55 years.

All presenilin mutations are missense mutations, with the exception of a splice acceptor site mutation, that results in the deletion of exon 9 (Δ -exon 9). Under physiological conditions PS are cleaved into NH_2 -terminal (NTF) and $COOH$ -terminal fragments (CTF). The PS1 Δ -exon 9 transcript lack a series of

charged residues present on the loop domain leading to an increase in uncleaved holoprotein.

Table 1. 1. Examples of missense mutations found in human PS1 and the approximate age of onset in FAD patients (Czech et al, 2000).

Codon	Mutation	Age of onset (years)
82	Val_Leu	55
96	Tyr_His	37
115	Glu_Asp	48
139	Met_Thr	49
143	Ile_Thr	35
146	Met_Val	38
163	His_Arg	50
171	Leu_Pro	40
231	Ala_Thr	52
233	Met_Thr	35
235	Leu_Pro	32
246	Ala_Glu	55
263	Cys_Arg	47
267	Pro_Ser	35
280	Glu_Ala	47
280	Glu_Gly	42
286	Leu_Val	50
384	Gly_Ala	35
392	Leu_Val	25-40
410	Cys_Tyr	48

A second splice mutation arises from the deletion of a guanine residue from a splice donor site leading to the production of three unique transcripts (De Jonghe et al, 1999b). The majority of mutations are primarily localised to highly conserved transmembrane domains and the large hydrophilic loop domain and are found in both PS1 and PS2 (figure 1.7). The sensitivity of the protein to mutations suggests that a specific topology is required to bring about the normal physiological processing of APP.

(iii) Apolipoprotein E polymorphisms and AD

A gene encoding Apolipoprotein E (ApoE), a serum lipoprotein involved in tryglyceride and cholesterol metabolism during neurodevelopment as well as after neural injury, has been linked to late-onset familial and sporadic AD. ApoE is produced by hepatocytes and is found within the general circulation, whereas astrocytes are thought to contribute to ApoE within cerebrospinal fluid (CSF). Three common isoforms are encoded by alleles $\epsilon 2$, $\epsilon 3$, and $\epsilon 4$ on chromosome 19 (Mahley, 1988; Roses, 1994). Each isoform show differences in amino acids at two positions thus: $\epsilon 4$ 112_{Arg}/158_{Arg}; $\epsilon 3$ 112_{Cys}/158_{Arg}; $\epsilon 2$ 112_{Cys}/158_{Cys}.

Earlier research demonstrated an association between the $\epsilon 4$ allele of APOE and AD (Strittmatter et al, 1993), that is both age and gender related. This association has been reported for the most common forms of LOAD, both sporadic and familial (Felician et al, 1999). Statistically, individuals homozygous for $\epsilon 4$ have a 15% greater risk of developing the disease before the age of 70 than heterozygous individuals (Blacker et al, 1997). Case-control studies indicate that the $\epsilon 4$ allele association and AD may account for 30%–40% or more of all cases of AD (Lorenzo et al, 1994). Several studies have suggested that the $\epsilon 2$ allele may, in some cases have a protective effect.

One difficulty with ApoE as a risk factor is that many $\epsilon 4$ carriers never develop AD. Furthermore, many patients with AD do not possess the $\epsilon 4$ allele, therefore its presence cannot be used for the diagnosis of AD. Instead possession of the $\epsilon 4$ allele predisposes an individual towards developing the disease. Reported frequencies of $\epsilon 4$ vary widely among populations, ranging from 5% or less in the Amish community of North America to over 40% in some aboriginal populations in Australia, though it is not clear yet what effect these population-frequency variations have on the association between $\epsilon 4$ and AD. What is clear is that the number and density of cerebral and cerebrovascular A β deposits is statistically higher in AD cases bearing the Apo $\epsilon 4$ phenotype. The Apo $\epsilon 4$ alleles may differentially affect the generation, secretion or clearance of A β from the extracellular fluid (Rebeck et al, 1995). The $\epsilon 4$ allele may enhance aggregation of A β or alternatively, it may lack a biological function performed by the other alleles,

such as supporting neurite outgrowth or stabilising tau protein on microtubules (Strittmatter et al, 1993).

Apo ϵ 4 is produced centrally by astrocytes though neurones may contain it either because they internalise it or express it. Apo ϵ 4 can be internalised via certain receptors, including the low-density lipoprotein receptor (LDL) for the LDL receptor-related protein (LRP) (Rebeck et al, 1995). In this instance Apo ϵ 4 may influence β APP processing or $A\beta$ secretion or re-uptake either via a receptor-mediated mechanism or a receptor-independent mechanism such as a direct interaction with α -secretase at the cell surface or with an extracellular protease that normally degrades $A\beta$ (Biere et al, 1995). Investigation into Apo ϵ 4 effects on β APP processing in neural and non-neural cell lines do not show increased processing of β APP in contrast to findings in AD linked to APP and PS1 mutations (Biere et al, 1995).

Biochemical experiments have shown that ApoE can bind to tau and MAP2, particularly the ϵ 2 and ϵ 3, whereas the ϵ 4 isoform performs poorly in comparison (Strittmatter et al, 1994). This has led to the suggestion that the former isoforms are therefore neuroprotective by reducing the ability of tau to bind to microtubules, become hyperphosphorylated, and form PHF (St George-Hyslop, 2000). ApoE also appears to be involved in synaptic plasticity during regeneration and repair and that the ϵ 4 allele is less efficient in this role. Mice deficient in ApoE exhibit a loss in MAP2 immunoreactivity in dendrites and synaptophysin in nerve terminals (Arendt, 2001).

(iv) α -macroglobulin polymorphism and AD

Another AD risk locus has been identified on chromosome 12 and involves polymorphic variants of α -2 macroglobulin (A2M) (Blacker et al, 1998). A2M plays an important role in the brain during development and following neuronal injury by regulating the activity of several proteases. Immunoanalysis reveals that A2M binds the neurotoxic $A\beta_{42}$ peptide with high affinity and antibodies to A2M stain senile plaques in AD brains. In case control studies a CPP at amino acid position 1000 (V/I) of A2M was found to be associated with AD as well as increased $A\beta$

deposition (Liao et al, 1998). Moreover, database searches have revealed that one polymorphic variant of the *A2M* gene had five fewer bases than the standard version, and that this variant is carried by 30% of the population (Tanzi, 1999). In terms of risk, individuals harbouring a single polymorphism (*A2M-2*) are three times more likely to develop AD compared to the standard polymorphism. In comparison a single copy of *A2M-2* has the same risk as a homozygous Apo $\epsilon 4$ carriers, suggesting that *A2M-2* may be an even more powerful LOAD risk factor than Apo $\epsilon 4$.

A2M functions by inhibiting all classes of proteases by a steric trapping mechanism following a conformational change. *A2M* first binds a serine protease then $A\beta$ to form a complex that then binds to the LRP receptor, which it shares with Apo E and APP. Thus *A2M* potentially impacts both APP and Apo E metabolism in the brain via a single biochemical cascade (St George Hyslop, 2000). Data suggest that a serine protease-*A2M* complex can degrade $A\beta$ and that trypsin-activated *A2M* can efficiently degrade $A\beta$, preventing fibril formation of the peptide in cultured human cortical neurons thus reducing toxicity (Zhang et al, 1996). Tanzi (1999) has been proposed that the ability of *A2M-2* to clear $A\beta$ is reduced leading to the extracellular accumulation of $A\beta$, leading to plaque formation. Apo E may hasten the disease process by competing with *A2M-2* for LRP and $A\beta$.

(v) AD risk locus on chromosome 10

Most AD cases have ages of onset above 65 years and exhibit no clear pattern of inheritance. The APO E4 allele is the only known genetic risk factor for LOAD. However, 50% of LOAD patients do not carry an APO E4 allele suggesting additional risk factors. For instance using genetic linkage analysis a susceptibility locus has been mapped to a region on chromosome 10 in families with LOAD (Myers et al, 2000). Furthermore, plasma $A\beta$ has been used as a quantitative trait for identifying novel LOAD loci. In this study evidence links a region of chromosome 10 to high levels of the $A\beta_{42}$ peptide in LOAD families (Ertekin-Taner et al, 2000). Moreover, recent data suggest an important role for the insulin-degrading enzyme (IDE) in the degradation and clearance of soluble $A\beta$ secreted

by neurones and glial cells. Using linkage analysis an additional putative LOAD associated loci has been mapped to the long arm of chromosome 10q, within 195 kilobases of the *IDE* gene (Bertram et al, 2000).

Other forms of LOAD have been linked to chromosome 12 and to possible mutations on maternally transmitted mitochondrial cytochrome-C oxidase genes (Felician et al, 1999), and a gene encoding for the major histocompatibility complex, located on chromosome 6. More recently a CPP has been found in the interleukin-1 (IL-1) genes *IL-1A* and *IL-1B*. Homozygosity for both IL-1 alleles confers a tenfold risk of AD (Chapman et al, 2001). Doubtlessly more at-risk loci associated with AD will emerge as research continues. Known genetic loci linked with AD are summarized in table 1.2.

Table 1.2. Genetic loci associated with AD. Data collated from information available at www.ncbi.nlm.nih.gov/entrez/dispomim.cgi?id=104300

Gene product	Chromosome locus	OMIM entry number
APP	21q21	104760
PS1	14q24.3	104311
PS2	1q31-q32	600759
ApoE	19q13.2	107741
A2M-2	12p13.3-p12.3	103950
Transcription factor CP2 (TCFP2)	12p11.23-q13.12	189889
Unknown-maps close to insulin degrading enzyme gene (<i>IDE</i>)	10q24	605526
Unknown	10p13	606187
Unknown-maps close to Cystatin C protease inhibitor gene	20p	607116
Originally thought to be cytochrome C oxidase. Possible mitochondrion-specific polypeptide involved in respiration	Mitochondrial DNA	502500

1.7 Biology of Presenilins

(i) Presenilin structure and biochemistry

Central to the processing of APP is the role-played by the presenilin proteins, particularly in those families harbouring PS1 FAD mutations that lead to the early onset disease phenotype. PS proteins are widely expressed in most cell types both human and murine, embryonically and centrally (Kovacs et al, 1996; Lee et al 1996). High concentrations of PS are found within the hippocampal formation and entorhinal cortex, whereas low levels are detectable within white matter glial cells. In situ hybridisation studies have shown that the expression patterns of PS1 and PS2 in the brain are very similar, if not identical (Rogaev et al, 1995). Moreover, PS1 and PS2 share substantial amino acid and structural similarities with each other suggesting that they may be functionally related. PS1 and PS2 also exhibit strong homology with sel-12 found in the nematode *Caenorhabditis elegans*, and is involved in the intracellular trafficking and recycling of proteins (Levitan & Greenwald, 1995).

The PS genes code for transmembrane spanning proteins approximately ~44 kDa in size and in its longest form is 467 (PS1) and 448 (PS2) amino acids long. Structurally the presenilins are putative eight helical transmembrane proteins (figure 1.5) located principally within the ER, Golgi apparatus, and nuclear membrane. In FAD PS1 mutations lie predominantly within the helical TM domains and the cytoplasmic loop suggesting that the disruption of the alignment of these domains is responsible for the disease state (Hardy and Crook, 2001). Once correctly folded, PS undergoes constitutive endoproteolysis. In PS1 endoproteolysis occurs within the exon 9 region of the cytosolic loop between TM6 (Thr 291) and TM7 (Ala 299) via autocatalytic aspartate residues at positions 257 and 385 to generate a 17~ kDa CTF and a ~28 kDa NTF, which are maintained in a 1:1 stoichiometry (Podlisney et al, 1997; Li & Greenwald, 1998; Wolfe et al, 1999b). Uncleaved full-length presenilin (holoprotein) remains within the ER whereas the NTF and CTF traffic to the Golgi where they are re-incorporated as a heterodimer along with other factors, such as β -catenin into a functional complex (Yu et al, 1998; Zhang et al, 1998).

Restricted incorporation of the NTF and CTF along with other co-factors into a multimeric complex in the ER and Golgi apparatus may provide an explanation for the regulated accumulation of the NTF and CTF (Yu et al, 1998). PS1 within cells is quickly turned over ($T_{1/2}$ ~60 min), in part to the two major fragments (Podlisny et al, 1997). Steady state levels of the PS fragments appear to be tightly regulated since transgene overexpression does not increase the overall level of fragments (Thinakaran et al, 1997). The AD-associated Δ exon9 splice error mutation results in the accumulation of the uncleaved full-length protein. The pathological activity of PS1 Δ exon9 is independent of its inability to undergo proteolytic processing, but is due instead to a point mutation (S290C) occurring at the aberrant exon 8/10 splice junction (Steiner et al, 1999).

Two hypotheses have been advanced to explain the role of PS1 in APP cleavage. Either PS1 regulates the transport of γ -secretase to APP without any physical interaction with the latter (Thinakaran et al, 1998), or PS1 is the γ -secretase/or is physically involved in the cleavage of APP, as indicated by PS1/APP co-immunoprecipitation from whole cell lysates, ER and Golgi vesicles (Xia et al, 1997b; Selkoe, 1999; Chen et al, 2000). Strong support for the latter hypothesis comes from data showing residues 1 to 87 of PS2 to interact with the last 45 amino acids of APP. The close homology of PS1 and PS2 would indicate that they share similar determinants of binding to APP (Pradier et al, 1999). Other evidence supporting a direct involvement of presenilin in the cleavage of APP by γ -secretase is seen in PS1 knockout mice and cell lines. Levels of the γ -secretase C83 and C99 substrate increase substantially whilst $A\beta$ levels decreases. What little processing does occur is likely to be carried out by PS2 (De Strooper et al, 1998). The alternate hypothesis holds that PS1 plays a crucial role as a facilitator of γ -secretase function by bringing together, through membrane trafficking, the various co-factors needed to bring about APP cleavage (Thinakaran et al, 1998).

More recently, evidence for PS1 as the putative γ -secretase has been provided by studies utilizing peptidomimetic transition state analogs to inhibit γ -secretase. These drugs contain the $A\beta_{40-45}$ region and their action results in a decrease in the levels of C83 and C99 (Wolfe et al, 1999a). Furthermore, selective mutation of the aspartate residues on TM6 and TM7 (figure 1.7) prevents the

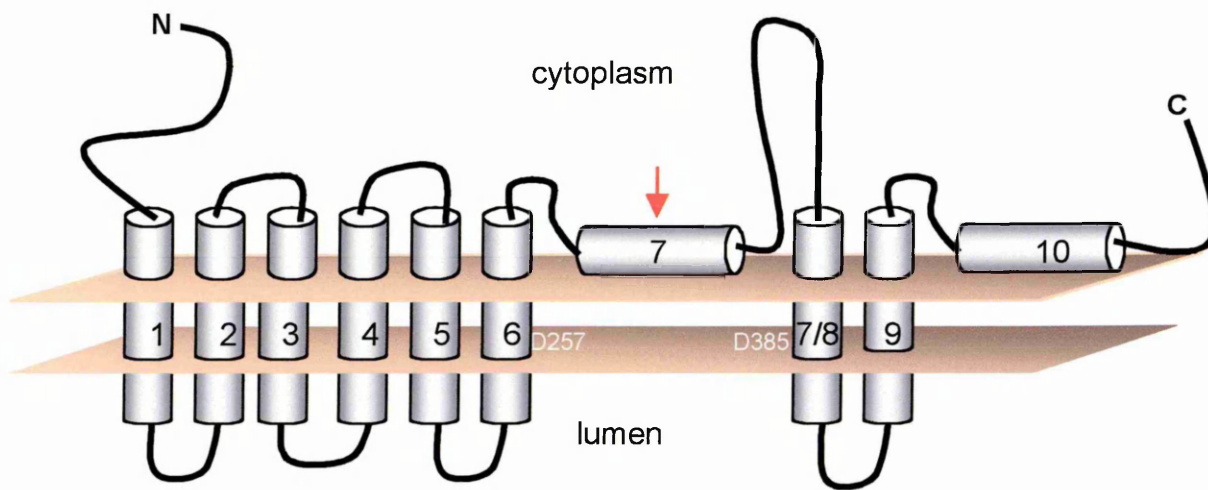


Figure 1.7. Topological representation of PS1 showing the eight transmembrane model. Shown are transmembrane domains 7 and 10, which associate with the cytoplasmic face of the membrane (Li and Greenwald, 1998). Alternatively, transmembrane 7 align within the lipid bilayer. PS1 mutations are primarily localised to the transmembrane domains and the large hydrophilic loop. The arrow indicates the site at which the molecule is cleaved into N- and C-terminal fragments. The two evolutionary conserved aspartate residues (D257/D385) are thought to be autocatalytic (Wolfe et al, 1999).

endoproteolysis within the cytosolic loop of the holoprotein (Wolfe et al, 1999b) leading to its accumulation, as well as increasing the C83 and C99 APP fragments whilst markedly reducing A β 40/A β 42 levels (De strooper et al, 1998). Disruption to the aspartate residues (D385A) similarly prevents the maturation of PS1 into a complex containing β -catenin (Yu et al, 1998; Nishimura et al, 1999a). In other studies also using transition state analogues, γ -secretase inhibitors were observed binding covalently to the aspartate residues in both PS fragments, but not the holoprotein, suggesting uncleaved PS to be novel aspartyl protease zymogen (Li et al, 2000).

(ii) Presenilin and development

The presenilins appear to function as unique aspartyl proteases that cleave a series of type 1 transmembrane proteins including APP, the APLP, Notch and Ire 1, a 'stress sensor' involved in the unfolded protein response (Selkoe, 2001). In addition to their location within the ER/Golgi cell compartment, the PS are localised to the synapse and at cell-cell contact sites where they form adhesion complexes

with cadherins, a family of cell surface single-pass transmembrane proteins (Arendt 2001). Additionally, PS1 forms complexes in vivo with the actin binding protein filament at the cell surface in lymphocytes. This binding protein is known to form bridges between cell surface receptors and the cytoskeleton and to mediate cell adhesion and cell motility (Schwarzman et al, 1999). Furthermore, the CTFs of PS1 accumulate along with PHF tau, suggesting a close relationship between PS1 and the cytoskeletal abnormalities seen in AD brains (Tomidokoro, et al, 1999).

Another important function of PS is their role in developmental signalling in the Notch/Delta pathway (Levitan and Greenwald, 1995). Notch and Delta are single pass cell surface receptors located within the developing embryo that are regulated by presenilins. It has been proposed that signal transduction involves cleavage and transport of the Notch intracellular domain (NICD) to the nucleus. Here, the NICD interacts with a DNA-bound protein and activates transcription of a number of genes that regulate a number of cellular decisions during development and in the adult brain (Kopan, 2002). Experiments involving *Drosophila* and mammalian cells support this idea, indicating that cleavage occurs in or near the transmembrane domain. The absence of PS or null mutations generated within *Drosophila* presenilin prevents this signaling, suggesting that PS may process Notch in an analogous fashion to the processing of β APP (Struhl & Greenwald, 1999). The PS-notch interaction in development is exemplified in mice, *Drosophila* and *C. elegans* harbouring PS loss of function mutations that result in notch-like phenotypes.

Although FAD mutations of PS1 rescue PS1 knockout mice, mutation of the transmembrane aspartates destroys the ability of PS1 to rescue *C.elegans* carrying the *sel-12* mutation, and therefore establishes the functional homology between PS1 and *sel-12*. The importance of presenilins in development is seen in experiments where targeted disruption of the PS1 gene in mice results in severe developmental abnormalities due to defects in somite differentiation and segmentation. PS1 knockout mice display impaired neurogenesis deformation of the axial skeleton and massive neuronal loss, which culminate in premature death shortly after birth (Shen et al, 1997). In vitro, the FAD M146V PS1 mutation prevents the differentiation of retinoic acid treated NTera 2 cells into neurons

(Tokuhiro et al, 1998), as does antisense-oriented PS1 constructs transfected into stable Ntera 2 cells (Hong et al, 1999).

(iii) Apoptosis and presenilin in AD

The extent to which programmed cell death or apoptosis is involved in AD is unknown. If not causative, apoptosis is at least associated with the late stage of AD neuropathology (Alves da Costa et al, 2002). Involvement of both PS in apoptosis was first suggested from data showing increased sensitivity to different apoptotic stimuli, including $A\beta_{42}$, in cells overexpressing PS2 and reduced sensitivity in the presence of anti-sense PS2 construct (Vito et al, 1996; Wolozin et al, 1998). The data on presenilins show PS2 to be pro-apoptotic, in particular the N-terminus bearing the N141I mutation. Mutant PS however, predispose the cells of individuals with FAD to apoptosis, suggesting that PS may be anti-apoptotic, since p53 and p21-induced-apoptosis quickly switches off PS1 gene expression (Roperch et al, 1998; Alves da Costa et al, 2002).

By contrast, PS2 and mutant PS2N141I drastically increase p53 expression and transcriptional activity in various cell systems (Alves da Costa et al, 2002), whereas the C-terminal 103 amino acids of mouse PS2, referred to as ALG3, was able to rescue a T-cell hybridoma from Fas-induced apoptosis (Vito et al, 1997). One of the final steps taken before a cell is committed to die by apoptosis is the cleavage of PS by caspase-3. Recently it has been demonstrated that overexpression of CTF-PS2 increases caspase-3 activity and immunoreactivity in staurosporine (STS) treated cells, and PS knockout cells. The latter observation demonstrates that CTF-PS2 may function independently of the N-terminal, γ -secretase-derived counterpart (Alves da Costa et al, 2003).

Using the yeast two-hybrid system to identify proteins interacting with PS1, the 'armadillo' protein p0071 has been demonstrated to bind specifically to the hydrophilic loop of presenilin-1 (Stahl et al, 1999), whilst Bcl-XL, an anti-apoptotic member of the Bcl-2 family, interacts with CTFs of both PS1 and PS2. The over expression of Bcl-2 in antisense-PS1 cell clones reduces cell death by apoptosis and allows the recovery of neuronal differentiation whereas, stable Ntera 2 cells transfected with antisense-oriented PS1 constructs fail to differentiate. Conversely,

antisense-oriented PS2 does not interfere with cell differentiation suggesting different roles for PS1 and PS2 (Hong et al, 1999). Both PS2 and its naturally occurring carboxyl-terminal products, PS2short and PS2Ccas, associate with Bcl-XL in vivo, whereas the caspase-3-generated amino-terminal PS2Ncas fragment does not (Passer et al, 1999). Moreover, the phosphorylation of serine residues adjacent to the caspase site in PS2, prevents cleavage and by doing so enhances its anti-apoptotic properties. Such alterations in the phosphorylation status of PS2 may increase the susceptibility of neurons to apoptotic stimuli (Tomidokoro et al, 1999).

Precisely how PS cause apoptosis is unknown, though recently a proliferation-associated gene product (PAG) belonging to the thioredoxin peroxidase family has been described that appears to mediate apoptosis in sympathetic neurons by interacting with PS1. Overexpression of PAG alone sensitises cells to apoptosis following trophic factor withdrawal, however co-injection of PAG with wild type but not mutant PS1 cDNA prevented apoptosis (Zhou et al, 2002). PS mutations found in FAD appear to sensitise neurons to apoptosis by disrupting calcium homeostasis. A pro-apoptotic calcium binding protein called calsenilin interacts with both presenilins in vitro by binding to the C-terminus ALG3 sequence (Buxbaum et al, 1998). Overexpression of calsenilin in neuroglioma cells somehow alters the processing of PS2, similar to that observed after caspase activation during apoptosis. Caspase-3 specifically cleaves PS2 rendering it inoperable during apoptosis by generating an amino-terminal PS2Ncas fragment (Tanzi et al, 1998). Recently it has been shown that calsenilin-mediated apoptosis is reduced in PS1 knockout mouse fibroblasts and neuronal cells, whereas cells expressing FAD gain of function mutants increased calsenilin-induced apoptosis (Jo et al, 2003).

(iv) Presenilin complex formation

Presenilins do not undergo glycosylation sulphation, acylation or glycosaminoglycan addition (De Strooper et al, 1997), however, they do show phosphorylation on serine residues, though what physiological role this plays ordinarily or in the disease state is unknown. Curiously, the majority of newly

synthesised presenilins are rapidly degraded and only small amounts of the holoprotein are detected in cells or transfected cells (Thinakaran et al, 1996; Podlisney et al, 1997). Processing of the presenilins is tightly regulated by competition for limiting factors that presumably are rate limiting in the maturation of PS into a functional complex. Over expression of transgene PS do not increase CTF or NTF but instead displace endogenous PS levels. Functional PS is thought to consist of several sub units that constitute a mature complex ~150 to ~2000 kDa.

(v) Presenilin and β -catenin interactions

Proteins known to interact with the PS heterodimeric complex include members of the armadillo family such as neuron specific δ -catenin, and β -catenin. The latter protein plays a key role in the 'Wingless pathway' (Wnt) in *Drosophila* and is responsible for the regulation of cell-cell adhesion between the cytoskeleton and adheren junctions (Czech et al, 2000). β -catenin is regulated by GSK-3 β , which phosphorylates its N-terminal and by doing so targets the molecule for degradation via the ubiquitin-proteosome pathway. GSK-3 β appears to associate with β -catenin via 'axin', which is suspected of negatively regulating the phosphorylation of β -catenin (Kang et al, 1999). Activation of the Wnt pathway inhibits GSK-3 β activity resulting in an increase in cytoplasmic β -catenin, which is then free to bind to transcription factors, following transportation to the nucleus. The interaction of PS1 with β -catenin is thought to modulate the Wnt pathway. Both wild type or mutant full length and CTFs have been shown to bind to β -catenin in transgenic mice and transfected cell lines.

Overexpression of PS1, but not mutant forms (Δ X9, M146IL), increase the association of GSK-3 β and promotes the turnover of β -catenin. The association of β -catenin with PS1 occurs at the CTF of PS1, whilst GSK-3 β interacts with the NTF of PS1 (Takashima et al, 1998; Kang et al, 1999). The finding that mutant PS1 exert a dominant-negative activity on β -catenin turnover, perhaps by delaying phosphorylation by GSK-3 β may underscore some aspect of the pathology of AD (Kang et al, 1999). Signalling errors due to faulty β -catenin/PS1 interaction might

explain why PS1 knockout mice embryos fail to develop in utero. Additionally, PS1 FAD mutations alter the trafficking of β -catenin arising from a dominant 'gain of aberrant function'. Lithium induced Wnt activation in FAD human fibroblasts decreases the nuclear trafficking of β -catenin compared to wild type fibroblasts (Nishimura et al, 1999a). Besides regulating the distribution of β -catenin, GSK-3 β is thought to be the kinase responsible for the hyperphosphorylation of tau. PS1 binds directly both tau and GSK-3 β and mutations in PS1 increase this interaction (Takashima et al, 1998). The ability of PS1 to bring tau and GSK-3 β into close proximity suggests that PS1 may participate in the regulation of tau phosphorylation thereby contributing to tau aggregation and the development of PHF and NFTs (Czech et al, 2000).

(vi) Active γ -secretase requires several components

Currently evidence suggests that PS1 is involved in transmitting extracellular signals to the cell interior via the intramembrane cleavage of type 1 transmembrane proteins. This 'regulated intramembrane proteolysis' (RIP) is a generic function of PS, which so far is responsible for the cleavage of nine known substrates including APP, Notch, LRP, ErbB4, E-cadherin, CD44, Ire1 α , APLP-1 and Nectin-1 α , all thought to be involved to some extent in regulating transcriptional activity (Kim et al, 2002; Medina and Dotti, 2003). All of these substrates share similar γ -secretase consensus motifs and reside at or near the cell surface, where ectodomain shedding prior to γ -secretase-like cleavage releases the intracellular domain (ICD).

According to recent studies core γ -secretase activity requires three additional transmembrane proteins besides PS: Nicastrin (Nct), APH-1 and PEN2. Together with PS these subunits constitute the active γ -secretase complex known as a 'secretosome', which when expressed in yeast constitutes γ -secretase activity (Marlow et al, 2003). Nicastrin, a 709 amino acid-long, type 1 transmembrane protein was the first member of the secretosome to be discovered (Yu et al, 2000). Nascent unglycosylated Nct (~80 kD) undergoes glycosylation to form immature Nct (iNCT ~110 kD) and mature Nct (mNct ~150 kD) after entering the Golgi. The

latter Nct species associates with active γ -secretase and requires PS for its maturation. Removal of Nct from *C.elegans* generates an embryonic lethal phenotype similar to that when PS and Notch gene activity is reduced. Furthermore, Nct binds to the γ -secretase substrates C99 (α CTF) and C83 (β CTF) derived from APP (Yu et al, 2000). Subsequent studies revealed the presence of Nct in *Drosophila* and in MDCK cells where nicastrin and PS1 co-localise within the ER and Golgi (Yu et al, 2003).

Genetic screening of *C.elegans* led to the detection of two novel genes, *Aph-1* (anterior pharynx defective), known to interact with the notch signalling pathway, and *pen-2* (presenilin enhancer) (Francis et al, 2002). *Aph-1* has seven transmembrane domains and is found as two highly homologous forms in mammal cells (*aph-1a* and *aph-1b*), and both are functionally equivalent in *C.elegans* rescue experiments. Using small interfering RNA experiments in human cell lines leads to the accumulation of α CTF and β CTF, and a decrease in $A\beta$ as well as the inhibiting NICD production, thereby implicating itself directly in the function of the γ -secretase complex (Lee et al, 2002). *Pen-2* codes for a small protein of 101 amino acids that contains two predicted transmembrane domains. Human *Pen-2* is an essential co-factor in the γ -secretase complex as demonstrated by data showing co-immunoprecipitation of *Pen-2* with both the uncleaved PS holoprotein and Nct (Steiner et al, 2002).

More recently *Aph-1* has been shown to bind preferentially within the ER to iNct in the early stages of γ -secretase assembly (Steiner et al, 2002), whereas cleaved PS and *Pen-2* bind preferentially to the mNct species (La Voie et al, 2003). The formation of a stable intermediate complex of *Aph-1* with iNct appears to be independent of PS, *Pen-2* and PS endoproteolysis. The glycosylation status of the *Aph-1*-iNct complex and its additional glycosylation to the mature sub-complex appears to regulate its interaction with PS and *Pen-2*. Stabilisation of the PS holoprotein is thought to occur through interaction with the *Aph-1*-iNct complex to form a trimeric intermediate complex that then binds to *Pen-2*, allowing for PS endoproteolysis and the final glycosylation of Nct (Takasugi et al, 2003; La Voie et al, 2003).

1.8 Project rationale

The work undertaken herein aims to extend the previous research carried out by this laboratory, specifically the characterisation of PS1 within the cell compartment using fluorescent anti-PS1 antibody staining and immunoblotting techniques. To achieve these aims, a functional approach was adopted whereby a PS1-EGFP transgene was constructed for the purpose of confirming the previous antibody staining data, but also to investigate what effect introducing FAD mutations into the PS1 construct would have on the location PS1 within the cell. Additionally, a functional PS1-EGFP fusion protein would provide a convenient means for studying the biochemistry of APP and A β generation (see chapter 3).

Chapter 2

Materials and Methods

2.0 Cell Culture

CHO, Cos-7, HEK 293, HeLa, NRK and PS1 mouse knock-out cells used within this project were cultured in DMEM with Glutamax and 4.5 g/l glucose supplemented with 10% foetal calf serum and PenStrep (100 μ /ml and 0.1 mg/ml) (Life Technologies). Cells were cultured at 37°C in the presence of 5% CO₂. Cells were passaged 1:10 using trypsin (Life technologies) once cells had become sub-confluent.

2.1 Cell fixation

Cells grown on 13 mm glass coverslips were fixed in -20°C methanol for 10 minutes, followed by three 5 minute washes in TBS. Alternatively, cells were fixed for 10 minutes in 3-4% paraformaldehyde (Aldrich-Sigma), followed by neutralization with 1xTBS. Paraformaldehyde was prepared by heating a 4% solution for 20 min at 65°C. 2M NaOH was added drop wise to dissolve the resultant pellet. The final solution was kept in 1xPBS at 4°C for one week. Para formaldehyde treated cells were permeabilised with Triton X-100 (Sigma) for 5 minutes at room temperature. Cell nuclei were stained for 5 minutes with 1 μ g/ml DAPI and affixed to slides with Fluoromount-G (Southern Biotechnology Associates, Inc, AI, USA). Images were captured using a JVC 3-CCD digital camera mounted on an Olympus BX80 microscope. Images were optimised (level equalization) using Corel Photo-Paint 8.

2.2 Antibody staining

A list of antibodies used for immunoanalysis is shown in table 2.0 below. Antibodies to PS1 (NT7, 1039, 923), Ubiquitin, anti-EGFP, the APP antibody AB10 and GRASP65 were used for both immunofluorescence microscopy and Western blotting. All other antibodies were used solely for immunofluorescence microscopy.

Table 2. Antibodies used within present study

Primary Antibodies	Source	Antigen or Catalogue N ^o (where relevant)
rabbit α APP/A $\beta_{40/42}$ (AB10)	This laboratory	DAEFRHDSGYEVHHQK
mouse Colligin	Stressgen	SPA-470
mouse β -Catenin	Sigma	C-2206
mouse β -COP	Sigma	G 2206
rabbit APP (DE2)	This laboratory	DAEFRHDSGYEVHHQK
mouse ERGIC53	H.P. Hauri	GI/93
mouse GalNac-T2	H. Clausen	UH4
rabbit Golgin 245	M. Feiszler	-
mouse Grasp65	M. Lowe	-
rabbit EGFP	Clontech	8367-1
mouse LAMP1	Sigma	H4A3
mouse α -Mitochondria	This laboratory	unknown
rabbit Mannosidase II	This laboratory	PGTQNISEINLSPMEISTFRIQLR
mouse Membrin	Stressgen	VAM-PT046
mouse MTOC (EG3)	This laboratory	unknown
rabbit NT7 N-terminal PS1	This laboratory	MTELPAPLSYFQNAQMSEDNHLNNT
rabbit PDI	T. Wileman	-
mouse α 20S Proteasome	Zymed	20973498
rabbit γ -Tubulin	Sigma	T-3559
rabbit Ubiquitin	Sigma	U-5379
mouse Vimentin	Sigma	V-6630
rabbit 923 N-terminal PS1	This laboratory	FQNAQMSEDNHLNNTVRSQN
rabbit APP KPI (993)	This laboratory	REVCSEQAETGPCRAMISRWYFD
rabbit PS1C-terminus/loop (1039)	This laboratory	PS1 298-367 fused to C-terminus of maltose binding protein
rabbit APP (1151)	This laboratory	PVTIQNWCKR GRKQCKTHPH
rabbit DP23 OX2 domain of APP	This laboratory	SQSLKTTQEPLARD
rabbit COPII	T. Wileman	-
Secondary antibodies	Source	Catalogue N ^o
rabbit Alexa 594	Molecular Probes	A11012
rabbit Alexa 488	Molecular Probes	A11008
mouse Alexa 594	Molecular Probes	A11005
mouse Alexa 488	Molecular Probes	A11001
rabbit Alkaline Phosphatase	Cell Signaling	7054
rabbit HRP	Cell Signaling	7074

2.3 Reduction and alkylation of disulphide bonds

To facilitate antibody detection of APP, Cos-7 cells expressing the fusion protein were fixed and reduced for 3 hours at room temperature by 10 mM DTT in 0.5 ml of 0.1 M Tris HCl (pH 8) and 1 mM EDTA treatment. Following three 5 minute TBS washes, each well was alkylated for 1 hour in 25 μ l 250mg/ml (0.06 μ M) sodium Iodoacetate, and then washed twice for 5 minutes in TBS.

2.4 Preparation of soluble and membrane bound cell fractions for SDS-PAGE analysis

Where cell fractions were required for Western analysis, either control, non-transfected or Cos-7 cells transiently transfected (24 hours) with the fusion constructs were scraped using a Falcon cell scraper from 6 well plates (27 sq cm) and homogenised in 10 mM phenylmethylsulfonylfluoride (PMSF) (Sigma) and 1 ml ice-cold 10 mM Tris HCl pH 8. Samples were prepared in a Dounce homogeniser (1 ml capacity) following 30 strokes of the piston. Samples were centrifuged at 13,000 rpm for 30 minutes. The resultant supernatant was kept and constituted the soluble fraction. Pellets were washed in 10 mM Tris HCl pH 8 and centrifuged at 13,000 rpm for a further 30 minutes. The supernatant was discarded and resultant pellet constituted the membrane fraction. Samples were heated at 50°C for 10 minutes in the presence of equal volumes of 2 X DTT. Samples were stored at -20°C until time of use.

2.5 SDS PAGE/Urea Bicine gel preparation

Synthetic peptides corresponding to A β 1-40 and A β 1-42 were obtained from Sigma. Bicine and BisTris were obtained from Lancaster synthesis. Urea, SDS, APS, TEMED, Glycine and CAPS used for electrotransfer were purchased from Sigma chemicals. Bis-acrylamide was obtained from Biorad. Immobilon-P PVDF membrane was purchased from Millipore and Nitrocellulose membrane from Amersham Life Sciences. SDS-PAGE molecular weight standards 7 Blue and 1 Blue (Sigma) or Benchmark protein ladder (Invitrogen) were used to assess protein size. SDS-PAGE was carried out using the Bio-Rad Mini protean II Electrophoresis gel system. For separation of Presenilin fusion proteins, 10% Urea gels were used in an attempt to resolve higher molecular weight species.

2.6 Immunoprecipitation of conditioned media

Conditioned cell culture media was removed after 24 hours incubation and analysed by immunoprecipitation for A β peptides. Immunoprecipitation was carried out using

either 50 mM TRIS.HCl pH 7.4, or radioimmunoprecipitation buffer (RIPA) (0.5% Nonidet P-40 (BDH), 0.25% sodium deoxycholate, 0.05% SDS, 150 mM NaCl, 50 mM HEPES, and 1 tablet of protease inhibitor mixture Complete Mini (Roche Molecular Biochemicals) per 2 ml of 5X RIPA, pH adjusted to 7.4 with NaOH). For immunoprecipitation 1.0 ml of conditioned media was added to 250 μ l anti-A β AB10 (mouse monoclonal supernatant), 50 μ l 50% slurry Anti-Mouse IgG (Sigma) and 100 μ l TRIS.HCl pH 7.4. Samples were rocked for 2 hours at room temperature. Where RIPA buffer was used 1.0 ml of conditioned media was added to 250 μ l AB10 plus 50 μ l 50% Protein-A beads (Pierce, Rockford, Ill, USA). Samples were rotated overnight at 4°C. Samples were centrifuged briefly at 2000 rpm for 2 minutes, washed with TBS, and repeated for a second time. Where RIPA buffer was used, beads were washed four times in PBS/0.1% BSA and once in 10 mM Tris.HCl, pH 7.4. To elute the beads incubated in Tris buffer, samples were aspirated followed by addition of 100 μ l 1xDTT/urea and heating at 60°C for 10 minutes. Samples incubated with RIPA buffer were eluted by heating the samples to 95°C for 5 minutes with 25 μ l sample buffer.

2.7 Detection of β -amyloid peptides

The urea version of the Bicine/Tris SDS-PAGE system was used for the detection of the β -Amyloid 40 and 42 peptides (Wiltfang, et al 1998). This gel system utilises three phases; a comb, stack and resolving gel components. The approximate dimensions are shown in figure 2.0 below. Cell pellets were resuspended in 25 ml of sample buffer (0.72 M bistris 0.32 M bicine, 2% SDS, 30% (w/v) sucrose, 5% 2-mercaptoethanol, 0.008% (w/v) bromophenol blue, heated to 95°C for 10 minutes and separated by bicine/Tris/urea SDS-PAGE. Table 2.1 below shows the buffer composition and stock solutions used for Bicine/Tris SDS-PAGE. Table 2.2 lists the final comb, stacking and resolving gel volumes needed for Bicine/Tris SDS-PAGE. For Coomassie staining, gels were fixed in 10% acetic acid and 50% methanol for 10 minutes, followed by overnight staining with 0.05% w/v CBB R-250 in 10% acetic acid. Gels were de-stained overnight with rocking in 2% acetic acid.

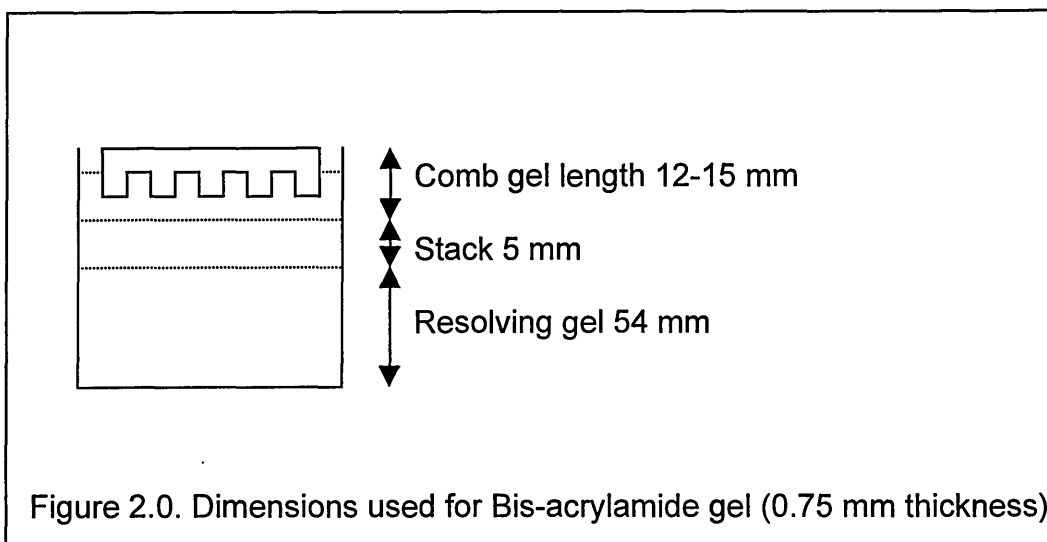


Table 2.1 Composition and stock solutions used for Bicine gels

	Composition
Resolving buffer	1.6 M Tris, 0.4 M H ₂ SO ₄ .
Stacking buffer	0.8 M BisTris, 0.2 M H ₂ SO ₄ .
Comb buffer	0.72 M BisTris, 0.32 M Bicine.
Cathode buffer	0.2 M Bicine, 0.1 M NaOH, 0.25 M w/v SDS.
Anode buffer	0.2 M Tris, 0.05 M H ₂ SO ₄ .

Table 2.2. Final gel volumes

Comb Gel (9%T /5% C)	1.5 mls comb gel buffer 900 µl Acrylamide/Bis (30% T/ 5% C) 30 µl 10% w/v SDS 514 µl dH ₂ O 36µl APS (5%) 20µl TEMED
Stacking gel (6% T/ 5%C)	1.0 ml Stacking gel buffer 400 µl Acrylamide/Bis (30% T/ 5% C) 20 µl 10% w/v SDS 540 µl dH ₂ O 20 µl APS (5%) 20µl TEMED
Resolving Gel (10% T/5% C/ 8M Urea)	2.5 mls resolving gel buffer 3.34 mls Acrylamide/Bis 4.8 g Urea 100 µl 10% SDS 40 µl APS (5%) 5 µl TEMED

2.8 SDS-PAGE running conditions

The SDS-PAGE urea gels were run at room temperature at 100 V for 30 min followed by 150 V for 1 hour. The Bicine/Tris SDS-PAGE urea gels were run at room temperature at 60 V for 15 min followed by 100 V for 1 hour. PVDF membranes were wetted in methanol prior to transfer in Towbin buffer (0.025 M Tris, 0.192 M Glycine, 20% Methanol), whereas nitrocellulose membranes were transferred in CAPS buffer (10 mM CAPS, 10% methanol, pH 11.0). Both membranes were transferred at 200 amps for 1 hour.

For immunostaining, Immobilon-P PVDF membranes were boiled for 3 minutes in PBS. Membranes were blocked in 2.5% nonfat dry milk in TBS-T for 1 hour (0.05% v/v Tween-20, 5% w/v nonfat dried milk). Following primary antibody incubation for 90 minutes, membranes were washed three times for 10 minutes in TBS-T, followed by secondary incubation with alkaline phosphatase (AP) (1:1000) or horseradish peroxidase (HRP-linked) (1:2000) secondary antibody (Cell Signalling Technologies) for 45 minutes at room temperature.

Membranes were washed twice for 10 minutes in TBS-T, and then once for 5 minutes in TBS. AP membranes were developed in 4 mls AP-buffer (100mM TRIS.HCl, 100mM NaCl, 5 mM MgCl₂ pH 9.5) containing 40µl bromo-chloro-indolyl phosphate (BCIP, 15mg/ml in DMSO/MeOH) and 40µl nitroblue tetrazolium (NBT, 30mg/ml in MeOH) (Sigma). Membranes exposed to HRP were developed using Biowest ECL detection kit according to the manufacturers instruction and imaged on an Epi Chemi II Darkroom (UVP BioImaging Systems).

2.9 Polymerisation chain reaction conditions

Following the optimization of reaction conditions, PCRs were performed using 1 unit of Taq polymerase (NE biolabs), 0.2 mM dNTPs (Bioline) and 2.0 mM Mg²⁺. Reactions were carried out on a Primus PCR machine (MWG-Biotech) programmed to heat the PCR mixtures to 95°C for 10 minutes, followed by 30 cycles of denaturing at 95°C for 1 minute, annealing at 65°C for 1 minute and extension at 72°C for 1 minute. Finally, samples were heated to 72°C for 10 minutes.

2.10 Restriction digestion and preparation of cDNAs

Double and single restriction digestion of pGEMT (Promega), pN2-EGFP (Clontech) and amplified cDNA was carried out with 0.1 units of enzyme/ μg DNA at 37°C for 2 hours. Ligation of inserts into linearised plasmid was carried out using T4 DNA ligase/ligation buffer (1.0 Weiss unit/ μg DNA - NE Biolabs) at 4°C overnight. DNA samples containing loading buffer were analysed by gel electrophoresis on a 1% TAE agarose gel stained with ethidium bromide. All cDNAs used for restriction digest and ligation reactions were purified using a Qiagen QIAquick Gel extraction kit according to the manufacturers instructions. The DNA band size was estimated by comparison with a 1 kb ladder (NE Biolabs) and by performing linear regression analysis. DNA concentration was measured using a Cecil CE9500 spectrophotometer.

2.11 Preparation of electrocompetent DH5 α *E.coli*

Electrocompetent bacteria were prepared by diluting 5-10mls of an overnight culture to 100 mls in LB broth in a sterile 250 ml flask. Cells were shaken at 37 °C for 2-3 hours until the OD₆₀₀ read 0.5. The culture was decanted into pre-cooled 50 ml Falcon tubes and left on ice for 30 minutes, followed by centrifugation at 4000 rpm for 15 minutes at 4°C. The pellet was re-suspended in 50 ml of sterile water. This procedure was repeated a second time. The pellet was then re-suspended in 25 mls of sterile water, and centrifuged at 4000 rpm for 15 minutes at 4°C. This procedure was repeated a second time. The pellet was re-suspended in 4 mls 10% glycerol and centrifuged at 8000 rpm for 15 minutes at 4°C. The final pellet was re-suspended in 0.4 ml 10% glycerol and divided into 40 μl aliquots. Cells were stored at -70°C until needed.

2.12 Transformation of DH5 α *E.coli*

Electrocompetent DH5 α *E.coli* (40 μl) were prepared and transformed using the Invitrogen electroporator II, according to the Invitrogen Electroporator II Instruction Manual. Briefly, 1-5 μl volumes of 1mg/ml pGEM-T or pEGFP containing PS1 cDNAs

were incubated along with the electrocompetent bacteria and electroporated using the following input values: Input voltage 1500 volts; capacitance V max 1800; load resistance 15 amps. Transformants were incubated for 1 hour with shaking in the presence of 1ml Luria-Bertani broth (LB) containing 0.1 mM MgCl and 0.4 mg/ml glucose. 150µl of the suspension was plated-out onto LB agar containing an appropriate selection antibiotic – 100 µg/ml ampicillin or 30 µg/ml kanamycin (Gibco). pGEM-T containing cDNAs were plated-out in the presence of 80 µg/ml 5-bromo-4-chloro-3-indolyl-beta-D-galactopyranoside (X-gal) and 0.5 mM Isopropyl-beta-D-thiogalactopyranoside (IPTG). Plates were incubated at 37°C overnight. Transformant colonies were picked and cultured overnight with shaking in LB/antibiotic broth at 37°C. Plasmid preparations were prepared by the alkaline-lysis method (Sambrook et al, 1989).

2.13 Transfection of Mammalian Cells

Cells used for immunomicroscopy were grown on 13 mm coverslips and transfected at 50-80% confluency. Cells were transfected with pEGFP or pEGFP containing PS1 cDNAs, in the ratio 0.7-0.8 µg DNA/ 1.75 µl Lipofectamine or 0.8 µg DNA/ 2.0 µl Lipofectamine-2000, per well of a 24 well plate, as per the manufacturers instructions (Gibco). For larger transfections in 6 well plates (27 cm²) materials were scaled-up 10 fold.

2.14 Transmission electron microscopy

Cos-7 cells expressing the NTMPS1-EGFP fusion protein were grown on 25 mm coverslips in a six well plate. Twenty four hours post transfection, cells were fixed in Karnovsky's fixative (2% paraformaldehyde, 2.5% glutaraldehyde in 0.1M phosphate buffer) for 3 hours at 4°C. Fixed specimens were then handed over to John Proctor at Sheffield University for further fixation and imaging by TEM. Cells were post-fixed in osmium tetroxide for 1 hour at room temp. Specimens were dehydrated by a series of 15 min graded ethanol washes (75, 95, and 100%) at room temp and dried over anhydrous copper sulphate for 15 min. Specimens were then placed in propylene oxide for two changes of 15 min duration.

Specimens were infiltrated using a 50/50 mixture of propylene oxide/Araldite resin and left overnight at room temp. Specimens were left in full-strength Araldite resin for 6-8 hours at room temp after which time they were embedded in fresh Araldite resin for 48 hours at 60°C. Ultrathin 70-90 nm sections were cut on a Reichert Ultracut E ultramicrotome and stained for 15 min with 3% uranyl acetate in 50% ethanol followed by Reynold's lead citrate staining for 2 min.

Sections were examined using a Philips CM10 mono transmission electron microscope at an accelerating voltage of 80 Kv. Electron micrographs were recorded on Kodak 4489 electron microscope film.

3.1 Introduction

Functional PS1 is thought to result from the endoproteolysis of the immature holoprotein within the ER compartment to yield stable NH₂- and COOH-terminal fragments (NTF and CTF, respectively), (Thinakaran et al, 1996; Yu et al, 1998), which are subsequently transported to the Golgi (Zhang et al, 1998), where they re-associate (Thinakaran et al, 1998; Capell et al, 1998) within a functional complex containing other proteins such as β -catenin, nicastrin, etc. Whether PS1 NTFs and CTFs have different functions either separately, or within a functional complex, and where within the cell compartment these fragments have their biological effect is currently unclear. However, in addition to the PS1 localisation to the ER, ERGIC and Golgi (Cook et al, 1996; Kovacs et al, 1996), PS1 has been reported at the cell surface of T-cells (Schwarzman et al, 1999), NT2N and DAMI cells (Dewji & Singer, 1997), and the cell-cell contacts in Cos-7 cells (Takashima et al, 1996).

To investigate the biology of PS1 fragments, rabbit polyclonal antisera raised against the C-terminus loop domain (296-367) and N-terminus of human PS1 (10-24) designated 1039 and 923 respectively, were used to stain endogenously expressed wild-type PS1 in Cos-7 cells and imaged by immunofluorescence microscopy.

3.2 Criteria for assessing reporter molecule localisation within the cell compartment

Where antibodies/proteins are said to *co-localise* within the same compartment, this should be taken to mean that the merged yellow image is more or less identical to the two separate images shown in the red and green figures. A more strict definition of co-localisation would be when two separate reporters, say antibodies recognizing different epitopes on the *same* molecule appear merged. A good example would be an anti-EGFP antibody staining EGFP (see figure 4.7). Where staining is said to be *co-incident*, *co-distributed* or *overlapping*, this means that although the merged image appears to show co-localisation, this is only coincidental since in the separate channels the reporter molecules occupy very different compartments. A good example of overlapping staining is shown in figure 3.2 d below.

3.3 1039 antibody staining of PS1 in Cos-7 cells

Endogenous staining of PS1 in Cos-7 cells with the C-terminal PS1 antibody 1039, results in a predominantly reticular staining pattern throughout the cell and around the nucleus (figure 3.1, upper panel and figure 3.2, panel a). The distribution observed for the 1039 antibody is consistent with the reticular network characteristic for the ER. A comparison of 1039 staining with endogenous staining of the ER specific marker Colligin (Hsp 47) show the same general morphological features (figure 3.2, panel a and d).

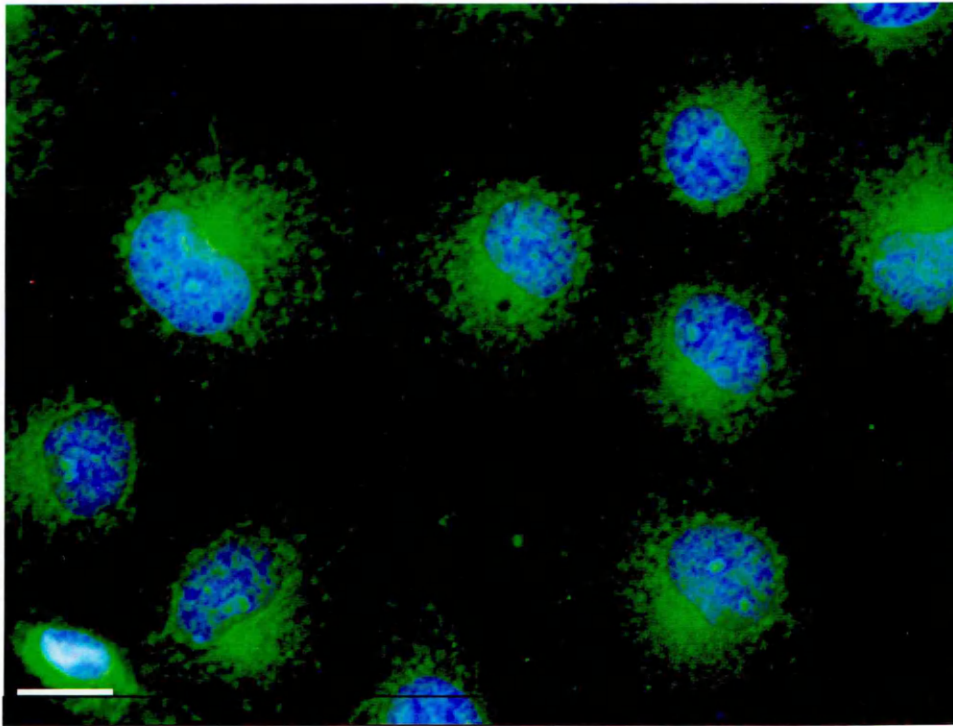
3.4 923 antibody staining of PS1 in Cos-7 cells

Whereas staining with the anti-C-terminus PS1 antibody 1039 is ER-like, antibody staining of Cos-7 cells with the anti-N-terminal PS1 antibody 923 is predominantly perinuclear with some tubulo-vesicular staining (figure 3.1, lower panel and figure 3.2, panel b). Similarly, staining of Cos-7 cells with the trans Golgi marker antibody Golgin 245 is distinctly peri-nuclear and not unlike that of 923 staining pattern (figure 3.2, panel c). Similarly, double staining of Cos-7 cells with the ER marker Colligin and the 923 antibody reveals that the N-terminus PS1 fragment does not localise with Colligin (figure 3.2, lower panels). Challenge with the peptide immunogen used to generate 923 completely or significantly reduces 923 antibody staining (D.Parkinson unpublished observations).

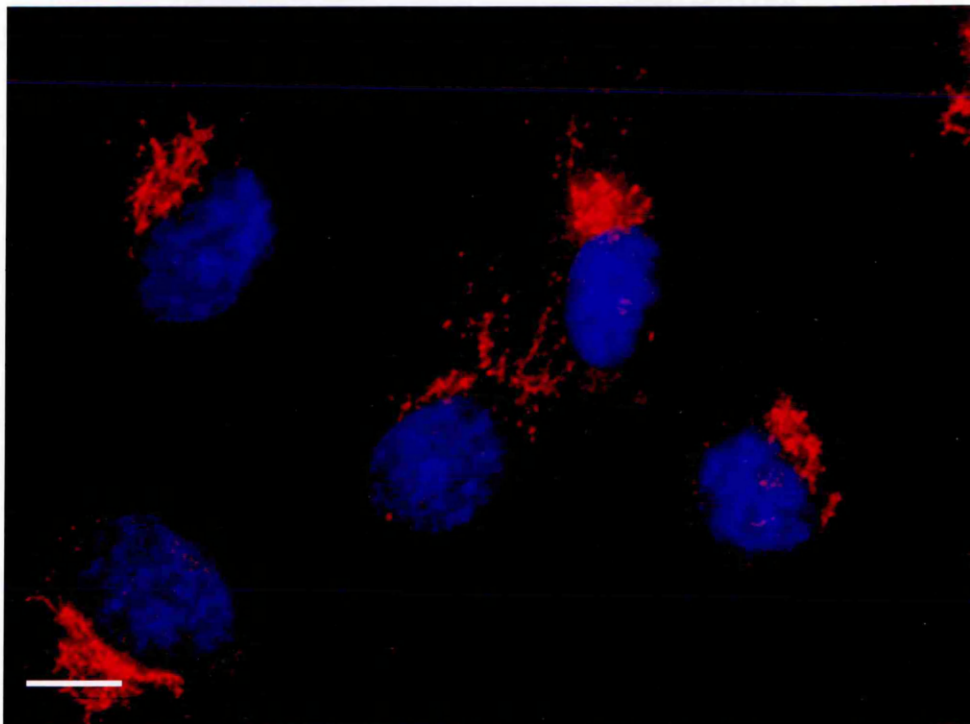
3.5 923 staining of Brefeldin-A treated Cos-7 cells is largely vesicular and co-localises with ERGIC53

To further characterise the cell compartments in which endogenous PS1 resides, Cos-7 cells were treated with the fungal metabolite Brefeldin-A (BFA) which reversibly blocks protein transport from the ER to the Golgi apparatus by preventing membrane recruitment of COPI proteins, resulting in distinct morphological changes, including collapse of the Golgi stacks (Klausner, 1992). Pharmacologically, BFA prevents the retrograde transport of proteins normally resident in the Golgi into the ER, though in the case of the trans Golgi network (TGN), BFA causes it to reassemble into extensive tubular processes without redistributing into the ER (Wood et al, 1991). Antibody staining of BFA-treated Cos-7 cells should reveal if any of the PS1 fragments resides within the cis, medial, trans Golgi, or the TGN. BFA treatment of Cos-7 cells resulted in differential staining patterns for the 923 and 1039 PS1 antibodies (figure 3.3). Both Colligin and 1039 antibody staining is largely unaffected by BFA treatment since both

PS1 antibodies stain separate compartments in Cos-7 cells



The CTPS1 antibody 1039 displays a reticular staining pattern



The NTPS1 antibody 923 displays a perinuclear staining pattern

Figure 3.1. Endogenous staining of PS1 in Cos-7 cells. Methanol treated Cos-7 cells affixed to coverslips were stained with the PS1 C-terminal antibody 1039 (upper panel) and the PS1 N-terminal antibody 923 (lower panel). DAPI stain in blue. Bar, 20 μ m.

PS1 N-terminus 923 antibody and PS1 C-terminus antibody differentially stain PS1 in Cos-7 cells

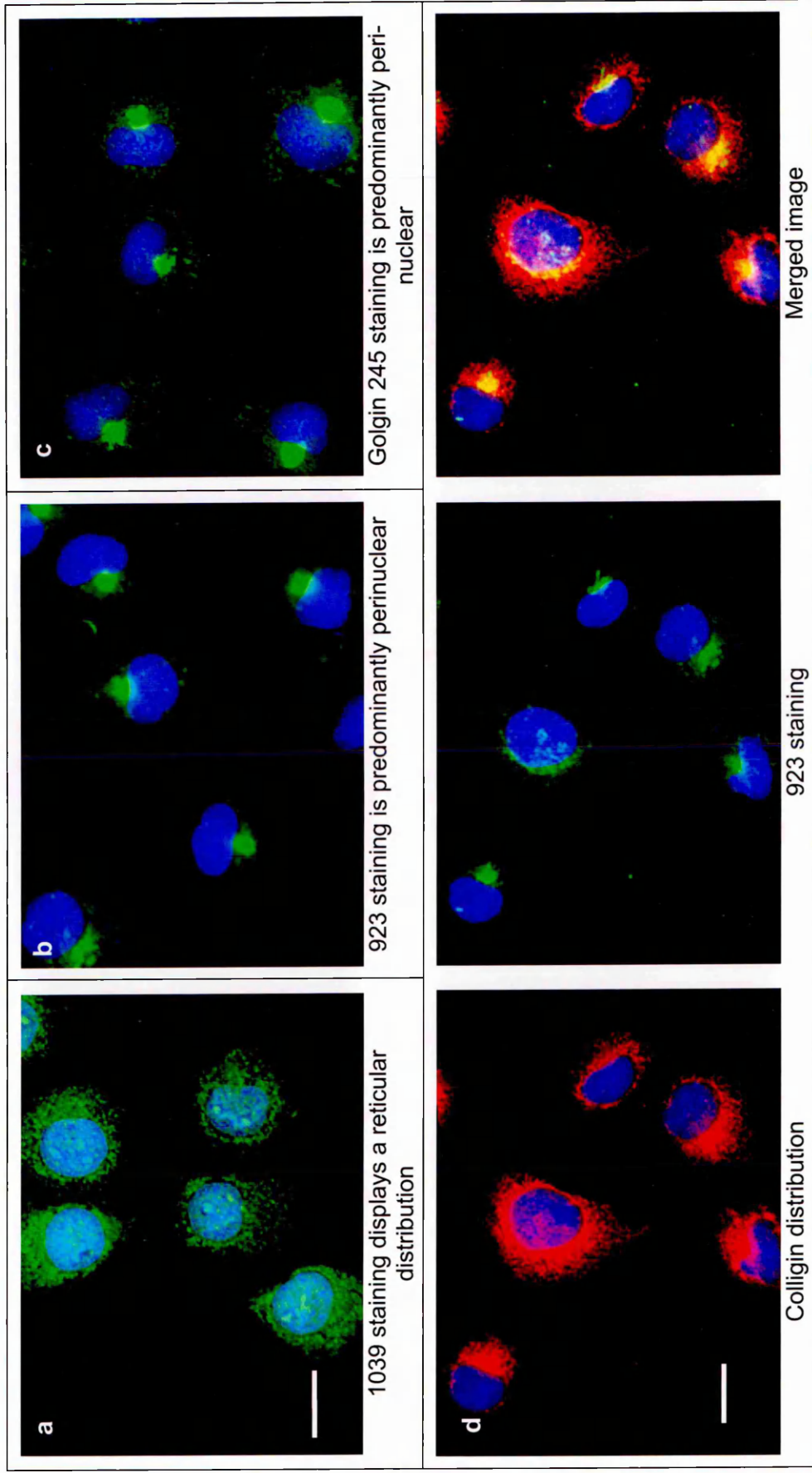


Figure 3.2. PS1, Colligin and Golgin antibody staining of Cos-7 cells. Cos-7 cells fixed in methanol were stained with antibodies to both PS1 and the cell compartment. The anti NTPS1 antibody 923 displays a distinctly perinuclear distribution within Cos-7 cells (b) similar to that of the Golgi marker Golgin 245 (c). In contrast the CTPS1 antibody 1039 displays a reticular pattern of staining (a) similar to that seen for the ER marker Colligin (d). DAPI stain in blue. Bars, 20 μm .

maintain a uniform reticular distribution pattern throughout the cell cytoplasm and around the nucleus (figure 3.3, panels a and c, respectively), as was the case for the control, non-BFA treated cells shown in figure 3.2, panels a and d. Following BFA treatment of Cos-7 cells the distinct perinuclear-staining pattern displayed by Golgin-245 (figure 3.1) is lost and instead redistributes to the ER forming a reticular pattern (figure 3.3, panel a). Interestingly, 923 antibody staining of BFA treated cells shifts from a Golgi-like distribution pattern to one that is predominantly vesicular, possibly indicative of the ER-intermediate compartment (ERGIC) (fig 3.2, upper middle panel). To investigate this possibility, BFA treated Cos-7 cells were double stained with the 923 antibody and the ERGIC specific marker antibody ERGIC53. Figure 3.4 shows that the 923 staining strongly co-localises with the ERGIC53 marker, initially within the Golgi compartment (top row) and then within the ERGIC following BFA treatment (bottom row). In conclusion, the above results show that immunostaining of endogenous PS1 in Cos-7 cells displays differential localization of the CTF and NTF PS1 fragments. Furthermore, upon BFA treatment of Cos-7 cells endogenous PS1NTF 923 staining locates to the ERGIC unlike that of the CTFPS1, which returns to the ER.

3.6 Western blot analysis of endogenous PS1 expressed in Cos-7 cells

Cos-7 cells were lysed in DTT/Urea to give whole cell lysate and analysed by SDS PAGE and immunoblotting with 1039 and 923 antibodies (figure 3.5). The anti-CTFPS1 antibody stains immunoreactive bands at approximately 22 kD (lane 2) consistent with previous reports, whereas the 923 anti-NTFPS1 antibody unexpectedly shows very poor staining (lane 4). The 1039 doublet suggests alternate CTFPS1 transcripts, whereas the higher band at ~60 kD may represent the uncleaved holoprotein (Dewji and Singer, 1997). In addition to this band, 1039 stains a double immunoreactive band at ~90 kD that may represent PS1 dimerisation and/or aggregation. Caution is advised in interpreting PS1 immunoblot data since crude preparation for a range of different tissues and cells leads to proteolytic events that result in PS1 artifacts (Dewji et al, 1997).

The absence of 923 immunoblot staining of PS1 may be explained by proposing that the antibody only recognises specific epitope conformers, such that denaturation and linearisation of the protein, as a prerequisite to immunoblotting, effectively abolishes 923 antibody recognition of PS1. Indirect evidence for this is provided by the immunocytochemistry results where the 923 antibody recognizes the

putative PS1 epitope. Alternatively, cleavage of the N-terminus amino acid sequence of PS1 to which the 923 antibody was directed against could likewise explain its failure to immunoblot. However, it has been demonstrated by peptide competition studies that 923 staining is significantly reduced. Furthermore, the 923 antibody failed to immunoprecipitate PS1 from Cos-7 cells, arguing against an N-terminus cleavage event (D. Parkinson - unpublished observations). Similarly, the immediate addition of DTT directly to cultured Cos-7 cells during the preparation of whole cell lysate is sufficient to prevent major proteolytic activity and as such is unlikely to account for the absence of 923 immunoblot staining of PS1. In any event, had proteolysis of the whole cell lysate occurred, it might be expected that immunoblotting of the sample would show protein laddering, however 1039 staining (figure 3.5) suggests that this was not the case.

3.7 The 923 antibody does not recognize the PS1 N-terminus

To validate the 923 antibody data a PS1 N-terminus EGFP chimera was constructed (chapter 4), and a second antibody, NT7, that recognizes the N-terminus of PS1 was utilised since this both western blots and immunostains transgene and endogenous PS1 (see chapter 5.5 and figures 5.8 lower panels, and figures 7.1 and 7.2a). Subsequently data from these investigations (chapters 4 and 5) show that the 923 antibody does not recognize either endogenous or transgene PS1 (see chapter 4.9 and figure 4.10). Consequently the data showing a difference in the PS1 CTF and NTF distributions, as measured by 923 and 1039 antibody staining, is only valid for the PS1-CTF but not for the 923 antibody, which appears to recognize an unknown epitope distinct from PS1.

3.8 Chapter summary

In summary, the above results are consistent with the PS1 holoprotein undergoing proteolysis as part of the maturation process that gives rise to functional PS1. However, the novel observation that the two PS1 fragments appear to reside in separate compartments suggest, if correct, that C- and N-terminal PS1 fragments may function separately to that of the mature PS1 complex and/or that the two fragments may be degraded by separate pathways. Later analysis of the 923 antibody data suggests that it does not in fact recognize N-terminal PS1.

923 antibody staining of BFA-treated Cos-7 cells is distinctly vesicular

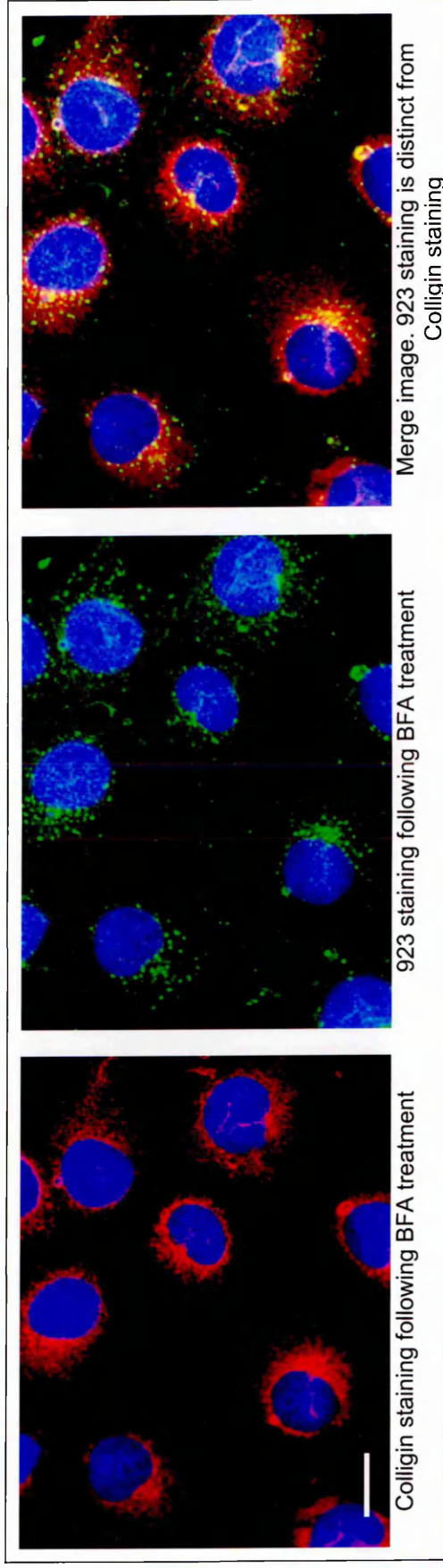
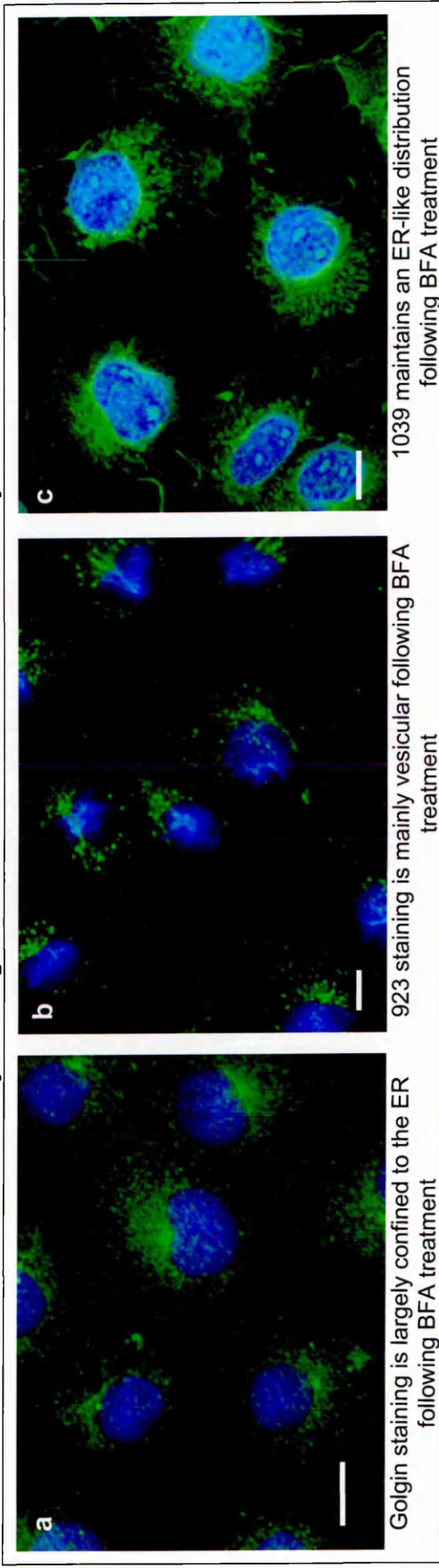


Figure 3.3. BFA treatment of Cos-7 cells. The anti-N-terminus PS1 antibody 923 shows a distinctly peri-nuclear pattern of staining (see figure 3.1). Following 10 μ g BFA treatment for 20 min this staining becomes largely vesicular (panel b) whereas Golgin and 1039 staining is reticular (panels a and c, respectively). Following BFA treatment 923 staining remains distinct from that seen for the Colligin antibody (lower panels). DAPI stain in blue. Bars, 20 μ m.

923 antibody staining co-localises with ERGIC53 in Cos-7 cells

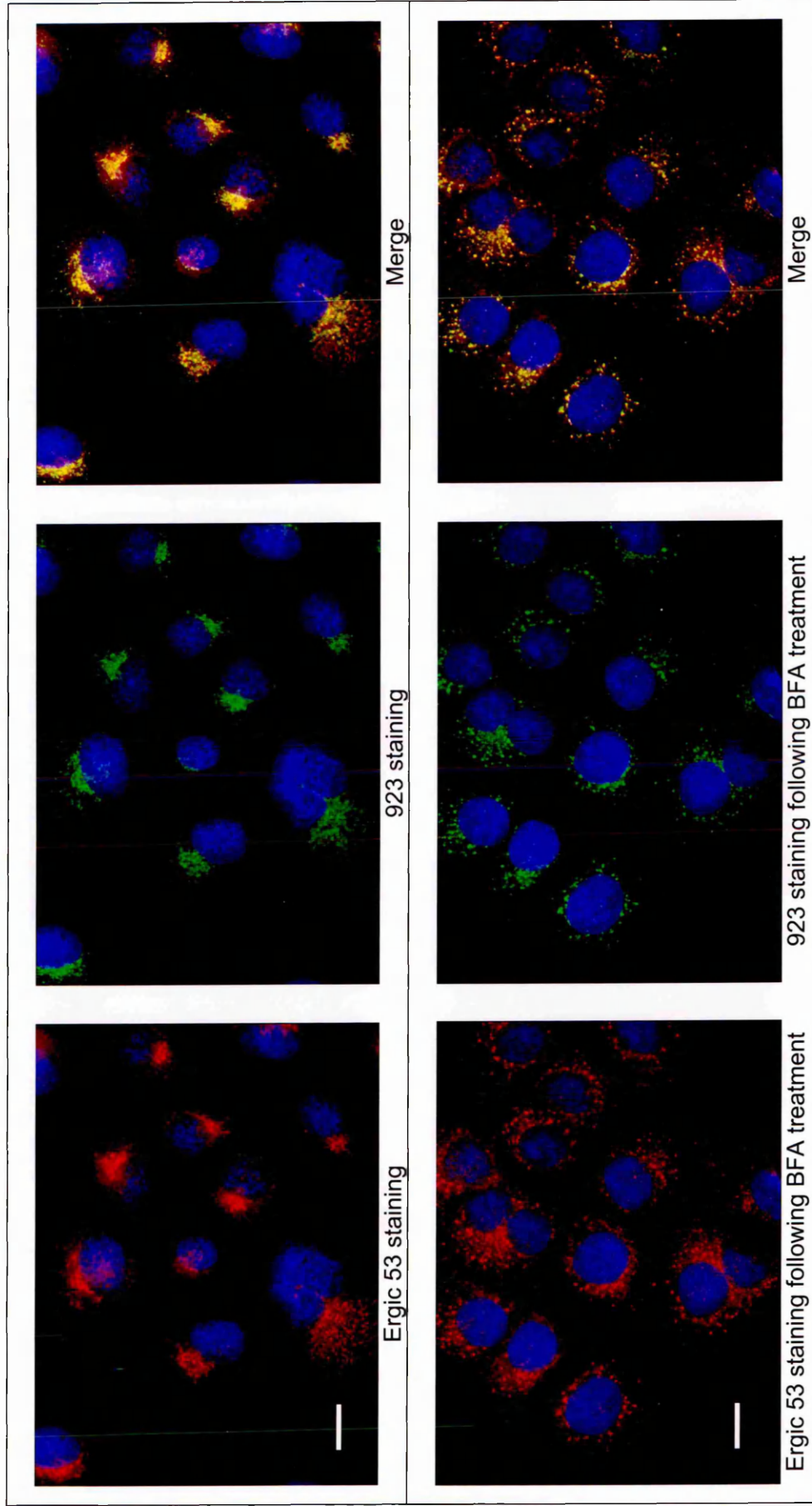
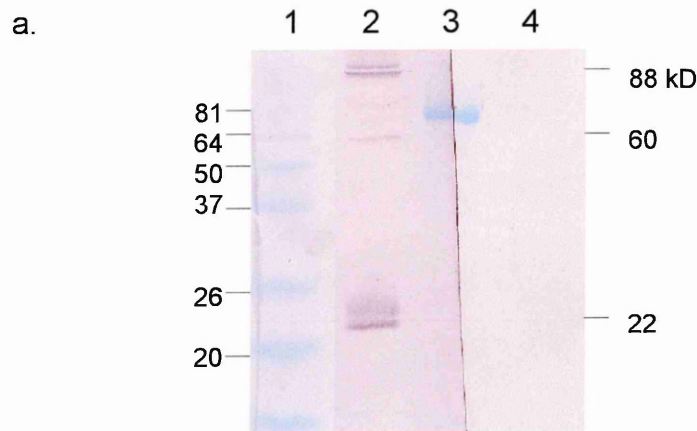
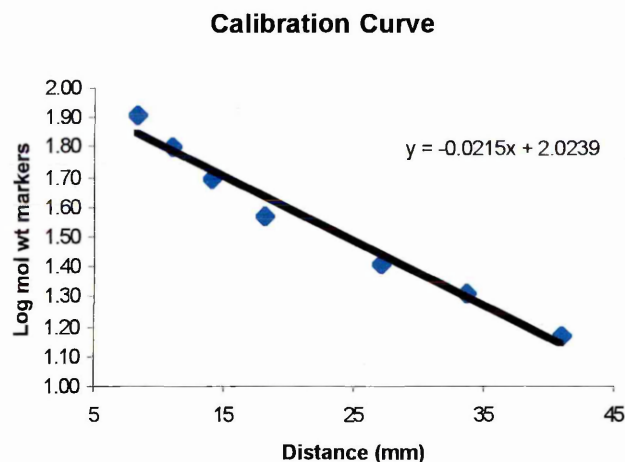


Figure 3.4. 923 and Ergic53 antibody staining of BFA treated Cos7 cells. Top row: control non-BFA-treated cells. Ergic53 staining (red) localises with 923 antibody staining (green), which is maintained following 5 μg/ml BFA treatment for 30 minutes (bottom row). DAPI stain in blue. Bars, 20 μm.



Lanes: 1 Ladder
 2 CTPS1 1039 staining
 3 I blue marker
 4 NTPS1 923 staining

b.



Linear regression analysis of immunoreactive bands

Molecular weights for PS1 fragments (kDa):

Holoprotein	~55	kDa
C-terminal PS1	~14-29	kDa
N-terminal PS1	~30	kDa

Figure 3.5. a. 923 and 1039 antibody staining of Cos-7 whole cell lysate. (Lane 2) Immunoblotting of CTPS1 by 1039 detected bands at approximately 88 kD, 60 kD and 22 kD. (Lane 4) The NTPS1 antibody 293 failed to immunoblot endogenous PS1. Samples analysed by 10% Urea SDS PAGE. b. The size of the immunoreactive bands was calculated using linear regression.

4.1 Introduction

The observation that the NTFPS1 923 antibody does not react in Western blot analysis raises doubts about the identity and utility of this antibody in characterising the biology of PS1 for this project. In order to clarify this issue and effectively extend the previous findings that PS1-NTF and PS1-CTFs reside within different cellular compartments, and that upon BFA treatment these fragments follow different retrograde pathways, a course of action was taken to construct a PS1NTF-EGFP (Enhanced Green Fluorescent Protein) fusion protein. This scheme has the advantage over immunostaining in that living cells transfected with the fusion construct can be imaged without relying on antibody detection as the primary reporter molecule.

The expression of fusion proteins tagged with EGFP is routinely used to study the function and localisation of proteins in a wide variety of cells. EGFP is an optimised variant of the GFP expressed by the jellyfish *Aequorea Victoria* (Chalfie et al, 1994;Cubitt et al, 1995), that allows detection by fluorescence microscopy of living or fixed cells, or by Western blot analysis with EGFP antibodies. Within the jellyfish, light is produced when energy is transferred from the Ca^{2+} -activated photoprotein, aequorin to GFP. When expressed in cells and illuminated by either UV or blue light (absorbance at 395 nm), GFP generates a bright green fluorescence emission at 509 nm independent of co-factors or substrates. The GFP chromophore consists of a cyclic tripeptide derived from Ser-Tyr-Gly in the primary protein sequence and is only fluorescent when embedded within the complete GFP protein. Nascent GFP is not fluorescent and requires that the chromophore undergo cyclisation and oxidation in the presence of oxygen. Thus cells expressing the protein will only fluoresce within an aerobic environment.

GFP fusion proteins have been shown to maintain their fluorescence in living cells as well as retaining the normal biological function of the fusion partner. Such tagged proteins provided increased sensitivity and resolution when compared to conventional antibody staining techniques (Wang & Hazelrigg, 1994). The use of

the fluorescent tag does not require fixation or permeabilisation steps thus making this reporter system suitable for kinetic studies concerned with protein localisation and trafficking.

To construct the NTPS1-EGFP plasmid involved the use of molecular biology techniques such as PCR and the sub-cloning of the NTPS1 cDNA into the target vector. Briefly, suitable primers incorporating restriction sites were designed to anneal with the N-terminus region of PS1 cDNA during PCR. The amplified product was double digested and ligated into the target EGFP vector. The steps taken in the construction of the NTPS1-EGFP fusion plasmid are summarised in figure 4.0. By subcloning the PS1 NTF cDNA into the EGFP vector upstream from the EGFP tag, translation of the mRNA and the subsequent protein synthesis should generate a fusion protein consisting of the first half of human PS1 with the EGFP moiety attached at the C-terminus.

4.2 Amplification of N-terminal PS1 cDNA by PCR

The primer design incorporated both an Xho I and an EcoR1 restriction site to help facilitate subcloning of the cDNAs into the target vectors. Using appropriate primers the N-terminal region transmembrane domains 1-6 (codon 1 - codon 282) were amplified by PCR from the pCIneo plasmid containing full-length human PS1. To facilitate subsequent sub-cloning steps, forward and reverse primers were designed to incorporate Xho I and an EcoR1 restriction sites, respectively. Table 4.0 below shows the primer sequences used to generate truncated and full-length wild type and FAD PS1 constructs (see later).

4.3 Optimisation of conditions for PCR

An initial approach taken towards PCR is to first optimise the reaction conditions that yield sufficient cDNA of the required size whilst minimising the generation of non-specific bands. To this end PCR was carried out in the presence of five varying magnesium concentrations and three annealing temperatures. Figure 4.1 shows the effect of magnesium concentration on the yield of PCR product. As

Generation of N-terminal PS1 fusion protein by PCR and subcloning

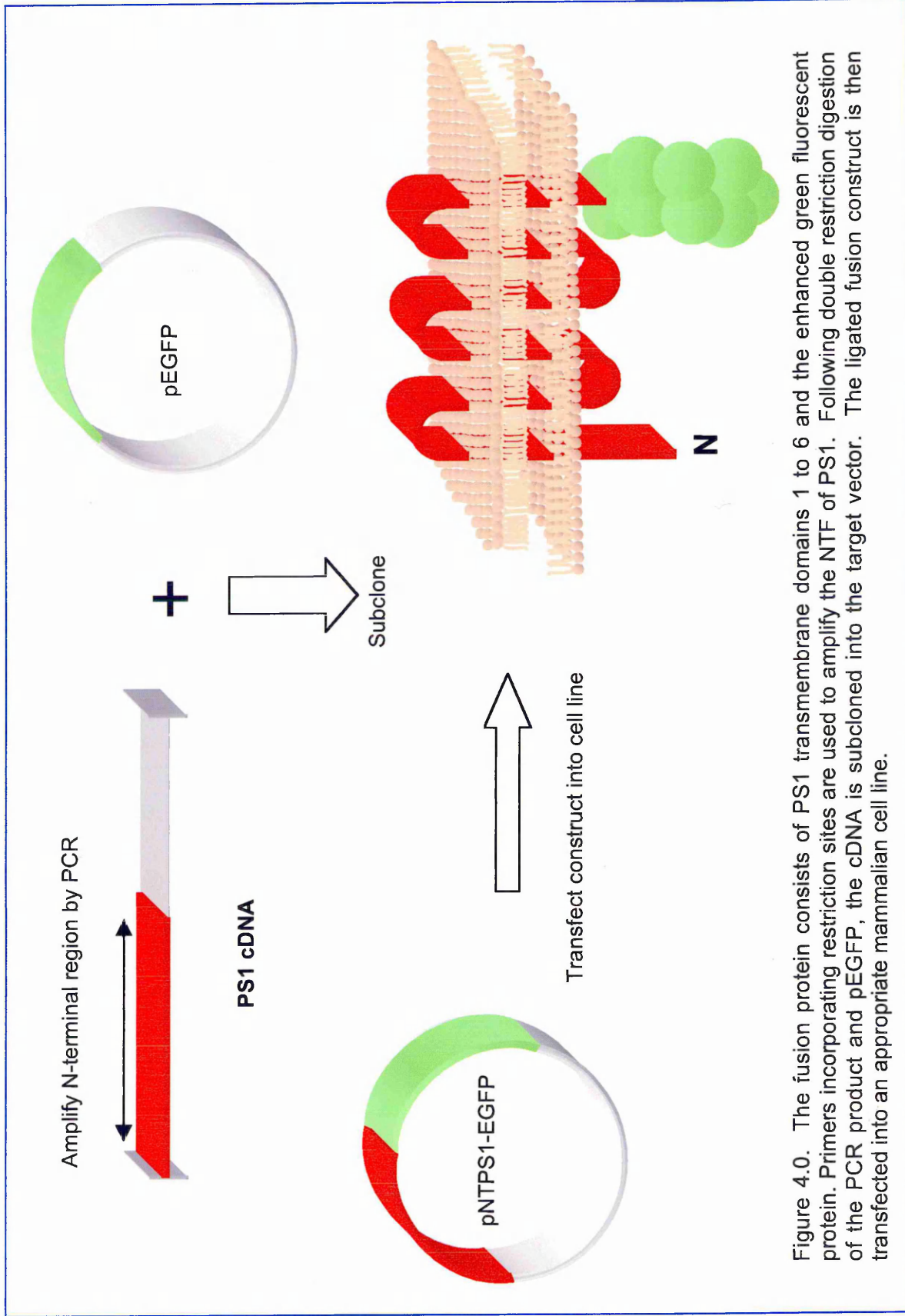
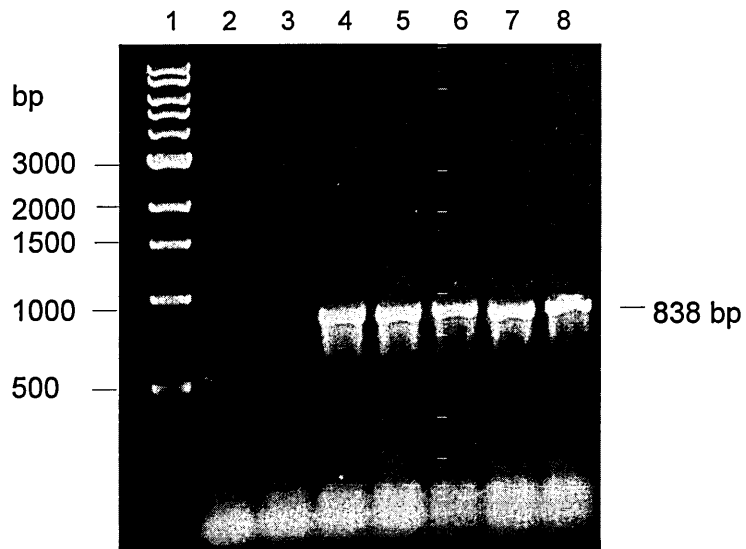


Figure 4.0. The fusion protein consists of PS1 transmembrane domains 1 to 6 and the enhanced green fluorescent protein. Primers incorporating restriction sites are used to amplify the NTF of PS1. Following double restriction digestion of the PCR product and pEGFP, the cDNA is subcloned into the target vector. The ligated fusion construct is then transfected into an appropriate mammalian cell line.

a.



Lanes	1	2	3	4	5	6	7	8
	1Kb	No DNA	No Mg	2.0 mM	2.5 mM	3.0 mM	3.5 mM	4.0 mM
	Ladder							

b.

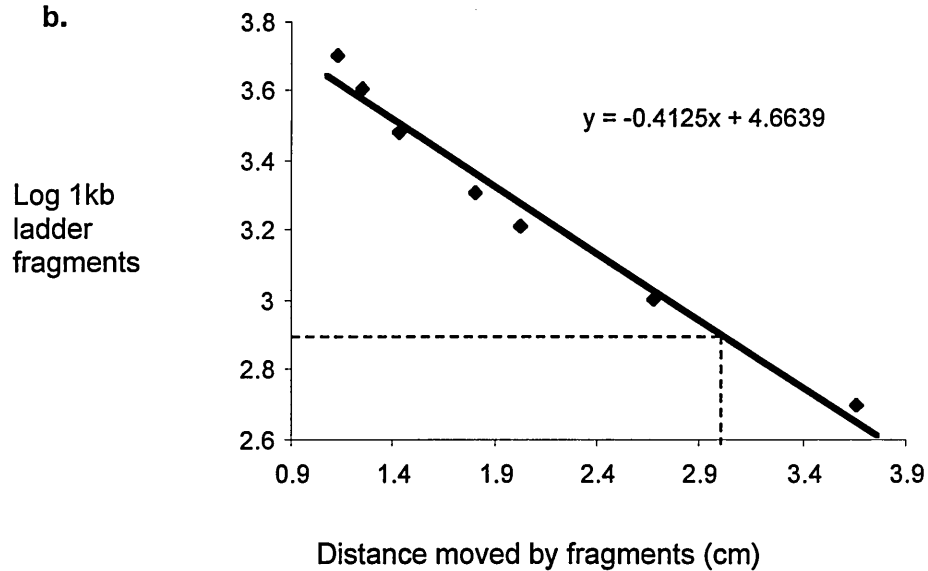


Figure 4.1. Amplification of N-terminal PS1 fragment by PCR. a. Incubation of 1 μ l pCIneoPS1 (1mg/ml) with Taq polymerase in the presence of varying MgCl₂ concentrations (mM) (annealing temperature 55°C). 1.5% TAE agarose gel stained with ethidium bromide. b. Log plot of 1kb ladder fragments. Estimate of PCR product size (bp) using linear regression analysis.

expected, the absence of pCIneoPS1 (lane 2) and Mg (lane 3) within the reaction mixture did not generate any PCR product.

Table 4.0. Primer sequences used to amplify by PCR truncated (NTPS1) and full length (FLPS1) PS1 mutant and wild-type cDNAs from pCLneoPS1

NTPS1 conserved construct Forward. Code: 0-05 Reverse. Code: 0-06	5'- GAATTTTGGGAATCCTCCTTTGAGCTTCCGGGT-3' 5'-GAGCGAAAAAAATTCAAGCGTTTCATTTCT-3
FLPS1 conserved construct Forward 712-748. Code: 0-10 Reverse 1404-1427. Code: 0-12	5'TTAGTGCCCTCATGGCCCTGGTGTGTTTATCAAGTACCT 3' 5'GAGCGAATTCGA ATAAAATTGATGGAATGCTAA 3'
NTPS1/FLPS1 FAD (L235P) Forward 712-748. Code: 0-11 Reverse 712-748. Code: 0-09	<div style="text-align: center;">L→P</div> 5' TT AGT GCC CTC ATG GCC <u>CCG</u> GTG TTT ATC AAG TAC CT 3' <div style="text-align: center;">L→P</div> 5'AG GTA CTT GAT AAA CAC <u>CGG</u> GGC CAT GAG GGC ACT AA 3'

Varying the magnesium concentration had no obvious effect on the amount of PCR product generated even under reaction conditions using annealing temperatures of 45°C, 50°C (data not shown) and 55°C. In view of these results, future PCR experiments were carried out in the presence of 2.0 mM Mg and an annealing temperature of 55°C. The lower bands shown in figure 4.1 represent unused excess primer.

By plotting the Log of the 1kb ladder fragments against the distance traveled by the marker DNA allows the size of the PCR product to be estimated. Using the equation for the line of best fit an observed value of 838 bp is obtained, close to the predicted size of the PCR product of 846 bp (Figure 4.1).

4.4 Subcloning of N-terminal PS1 cDNA into N2-pEGFP

The amplified PCR fragments were excised from the agarose gel and recovered using a Qiagen gel extraction kit. Following EcoR1/Xho1 restriction enzyme, double digestion of the NTFPS1 PCR product and the pEGFP vector, several attempts were made at ligating the insert into the target vector, however none of

these attempts was successful. It was therefore decided to adopt an alternate strategy using a TA cloning kit (Promega) whereby the insert was first sub-cloned into the pGEM-T vector. The Taq polymerase (Biolines) used for the PCR generates single 3'-5' adenine overhangs in the PCR product. The linearised pGEM-T vector incorporates single 3'-5' thymidine overhangs designed to complement that of the PCR product and so facilitate the ligation of PCR products into pGEM-T vector. Following ligation of the insert into the vector, DH5 α *E.coli* was transformed and plated-out on LB agar containing IPTG and X-Gal. The following day putative recombinant white colonies were picked and grown overnight in LB broth containing ampicillin. DNA samples were prepared from the overnight cultures and double digested to screen for the insert. Lanes 5 and 12 (figure 4.2 a) show inserts of the expected size (~800 bp) and linearised plasmid at ~3000 bp. A scaled-up double digestion was then carried out to provide sufficient DNA for subcloning into the EGFP vector. Double digested EGFP and the insert were ligated together and the resulting mixture used to transform DH5 α *E.coli*. Selected colonies were incubated in LB overnight and minipreped the following day. Double digestion of the putative pNTPS1-EGFP samples generated insert close to the expected size (figure 4.2 b, lane 7).

4.5 Restriction digestion analysis of putative N-terminal PS1 cDNA

To confirm that the identity of the insert was that of NTFPS1, a series of diagnostic restriction enzyme assays were carried out with the restriction enzymes BspH 1, Sty 1 and Xho 1. Digestion of the construct with these enzymes revealed a unique banding pattern distinct from pEGFP digestion alone (figure 4.3). Linear regression analysis was used to compare the actual band sizes obtained experimentally with those predicted from a restriction map of the plasmid containing the insert (table 4.1).

Finally, sequence confirmation of the pNTPS1-EGFP cDNA was carried out by Lark Technologies. The sequence obtained matched that of the wild type N-terminus fragment, however an error appears to have been introduced at position 49, N-terminus from the start methionine of the wild type PS1 cDNA. Because of

Colony screening for pNTPS1

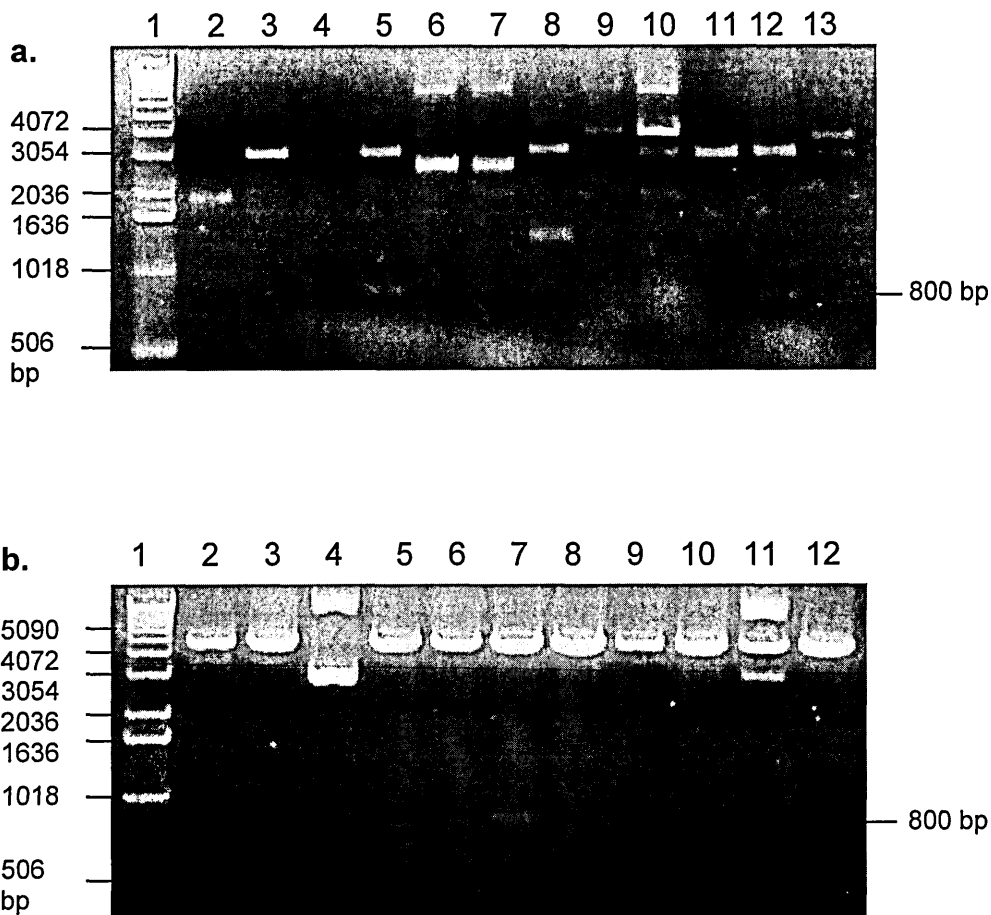


Figure 4.2. Restriction digest of cDNA recovered from transformed DH5 α *E.coli*. Individual clones were double digested with EcoR1/Xho1 (0.1 units/ μ g DNA). a. pGEM-T restriction digestion shows putative inserts of the correct size (~800 bp) in lanes 5 and 12. b. Following double digestion of the NTPS1-GEM-T plasmid, the recovered insert was ligated into double digested pEGFP. DH5 α *E.coli* was transformed, cultured overnight and plasmid DNA prepared for restriction digestion. Restriction digestion of the putative NTPS1-EGFP in lane 7 yields an insert of the expected size. Lane 1 shows a 1 kb ladder. Samples were analysed on a 1% TAE agarose gel stained with ethidium bromide. Insert sizes estimated using linear regression analysis.

the copying error at this position translation of the open reading frame would generate an arginine residue instead of the amino acid glycine. However, according to the Presenilin Mutation Directory at www.alzforum.org there is no known FAD PS1 mutation located at this position, nevertheless, this does not rule out the possibility of a pathogenic effect associated with this mutation. Though not ideal, it was decided as a matter of economy and convenience to continue with the next stage of the project, that of transfecting the construct into Cos-7 cells.

4.6 Cos-7 cells transfected with pNTPS1-EGFP display several phenotypes

Cos-7 cells grown to varying densities on glass coverslips were transfected with differing cDNA concentrations to Lipofectamine ratios to achieve the best transfection rate. Cells were transfected with either the fusion construct or pEGFP alone as a control. Cells were left for 24 hours post transfection before being prepared for fluorescent microscopy. The number of transfectants was assessed by counting the total number of cells viewed under the microscope using the x 400-objective and comparing them with those expressing the fusion protein. This procedure was repeated three times per slide. The x and y stage adjusters on the microscope were moved blindly to obtain a random sample for counting. Given that the EGFP fluorescence faded rapidly following exposure to the light source no transfected cell could be mistakenly counted a second time. In general transfection rates ranged from 5% to 10%, depending on the cell type and the construct being transfected (see later).

Four distribution phenotypes were consistently observed following transfection of the N-terminal fusion construct into Cos-7 cells: reticular, perinuclear, vesicular and circumnuclear 'blob-like' aggregates (figure 4.4). These phenotypes contrast sharply with those observed in Cos-7 cells expressing EGFP, which displays a diffuse, cytoplasmic distribution (figure 4.4 b). Taken as an average of several transfection experiments, the proportion of cells displaying a particular phenotype remained roughly constant: 28% of transfected Cos-7 cells displayed an reticular-like phenotype, 13% displayed a peri-nuclear like phenotype, 27% displayed a vesicular phenotype and 30% displayed blob-like aggregates. On the whole, cells expressing the fusion protein displayed a mixture of phenotypes

within the same cell, e.g. an ER-like reticular distribution of the fusion protein typically might have vesicles and blobs dispersed throughout the cell (figure 4.5). Expression levels of the fusion protein varied significantly between low levels that could be discerned under the microscope but were too weak to be recorded by the CCD camera, to runaway levels of expression that appear as a single fluorescent mass that obscured any obvious phenotype.

4.7 Western blot analysis of NTPS1-EGFP fusion protein locates to the cell membrane

The presenilins are multipass membrane proteins with several transmembrane domains (Thinakaran et al, 1996; Tomita et al, 1997). The N-terminal region, the loop domain between TM 6 and 7 and the C-terminus region are all orientated towards the cell cytoplasm (Li and Greenwald, 1996; Doan et al, 1996; De Strooper et al, 1997). It would be expected that a crude preparation of Cos-7 cells expressing the fusion protein would, when divided into soluble and insoluble fractions, immunoblot for the membrane fraction only. However, the observation that some transfected cells display an aggregate-like phenotype, possibly as an artefact of overexpression of the fusion protein, suggests a soluble cytoplasmic component. To address this question soluble and membrane fractions taken from control, non-transfected cells, pEGFP transfected cells, and cells transfected with the NTPS1-EGFP construct, were immunoblotted with the anti-EGFP antibody (figure 4.6).

As expected immunoreactive bands were absent from non-transfected Cos-7 control samples (lanes 1 and 2). Cells transfected with pEGFP show an immunoreactive band at ~29 kD within the cell soluble fraction corresponding to the EGFP protein (lane 3). Western analysis of transfected Cos-7 cells expressing the fusion protein show immunoblotting of the membrane fraction at ~61 kD and ~120 kD. Whilst the smaller band was expected corresponding to the sum of the individual sizes of both the EGFP moiety and the N-terminus of PS1, the band at ~120 kD was not expected and may therefore represent dimerisation or aggregation of the fusion protein (lane 6). In an attempt to resolve the larger protein species into one band, the experiment was repeated a second time with the

Restriction digest of pNTPS1-EGFP

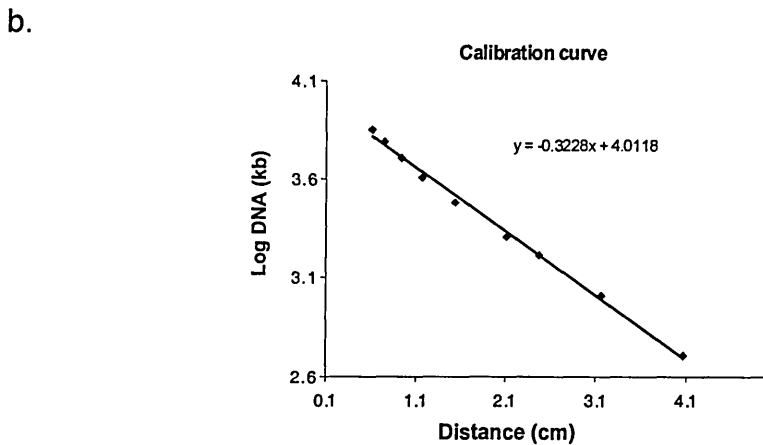
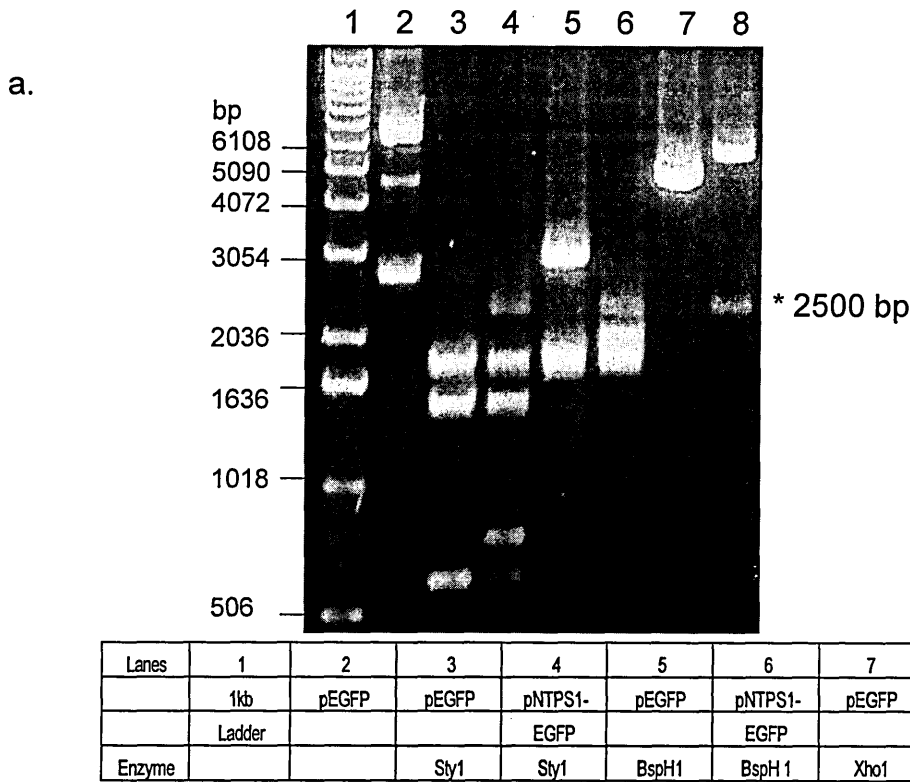


Figure 4.3. a. Restriction digest of pNTPS1-EGFP recovered from transformed DH5 α *E.coli*. 1% TAE agarose gel stained with ethidium bromide. NB the bands at ~2500 bp (-) represents incomplete digestion of the plasmid. b. Log plot of 1kb ladder fragments. PCR product size (bp) was estimated by linear regression. Plasmid samples digested with BspH 1, Sty 1 and Xho1 (0.1 units/ μ g DNA).

Table 4.1 Predicted versus observed fragment sizes generated following restriction enzyme digestion of plasmid DNA.

Fragment sizes (bp) obtained following BspH1, Xho1 and Sty I restriction digest of pNTPS1-EGFP											
pEGFP				pNTPS1-EGFP				pEGFP		pNTPS1-EGFP	
BspH1		Sty 1		BspH1		Sty I		Xho1		Xho1	
Predicted	Observed	Predicted	Observed	Predicted	Observed	Predicted	Observed	Predicted	Observed	Predicted	Observed
2966	3000	1809	1832	1941	2110	1809	1832	4737	4886	5610	5586
1776	1887	1499	1499	1839	1887	1499	1499				
		610	592	1776		610	620				

addition of urea to the gel; however, the result was identical to that shown in figure 4.6. That the addition of urea made no difference to the band at 120 kD may be more indicative of insoluble fusion protein aggregates rather than dimerisation of the protein. The Coomassie stain in figure 4.6 b shows approximately equal loading of protein samples into each of the gel lanes.

Since the phenotypes exhibited by transfected cells are distinct from that of EGFP, and that no immunoreactive bands corresponding to EGFP alone was found within the soluble fraction of cells, it can be concluded that the EGFP moiety is not cleaved from the C-terminus of PS1NTF and that the fusion protein resides within the membranous compartment of the cell. Similarly, the anti-EGFP antibody co-localises with the fusion protein for all phenotypes displayed by transfected Cos-7 cells (figure 4.7).

4.8 The NTPS1 fusion protein localises to the ER and Golgi compartments

To investigate the identity of the membranous compartment in which the fusion protein resided, several antibodies specific to cell marker proteins were used for immunolocalisation experiments. The NTPS1 fusion protein localises to varying degrees with markers for the ER (Colligin and PDI), the medial Golgi (Mannosidase II), the trans Golgi (GalNac) and the Trans Golgi Network (Golgin 245) (figure 4.8 & 4.9). Colligin, a 47 kDa stress protein that resides within the ER is thought to participate in intracellular processing, folding, assembly and secretion of procollagens (Nagata & Yamada, 1986). Similarly, PDI is thought to interact with nascent proteins during their folding and assembly within the ER as part of the ER quality control mechanism (Bottomly et al, 2001). Colligin and PDI display a reticular distribution in both transfected and non-transfected cells and show partial overlap with the fusion protein. However, where the fusion protein displays a perinuclear and vesicular distribution there is no localisation with these ER markers (figure 4.8, merged panel). Unexpectedly, PDI staining is increased in some cells expressing high levels of the fusion protein compared to neighbouring non-transfected cells (Figure 4.8, bottom row).

Antibody staining by markers to the Golgi apparatus is distinctly peri-nuclear in both transfected and non-transfected cells. Mannosidase II and Golgin 245

Distribution of N-terminal PS1 fusion protein in transfected Cos-7 cells shows four distinct phenotypes

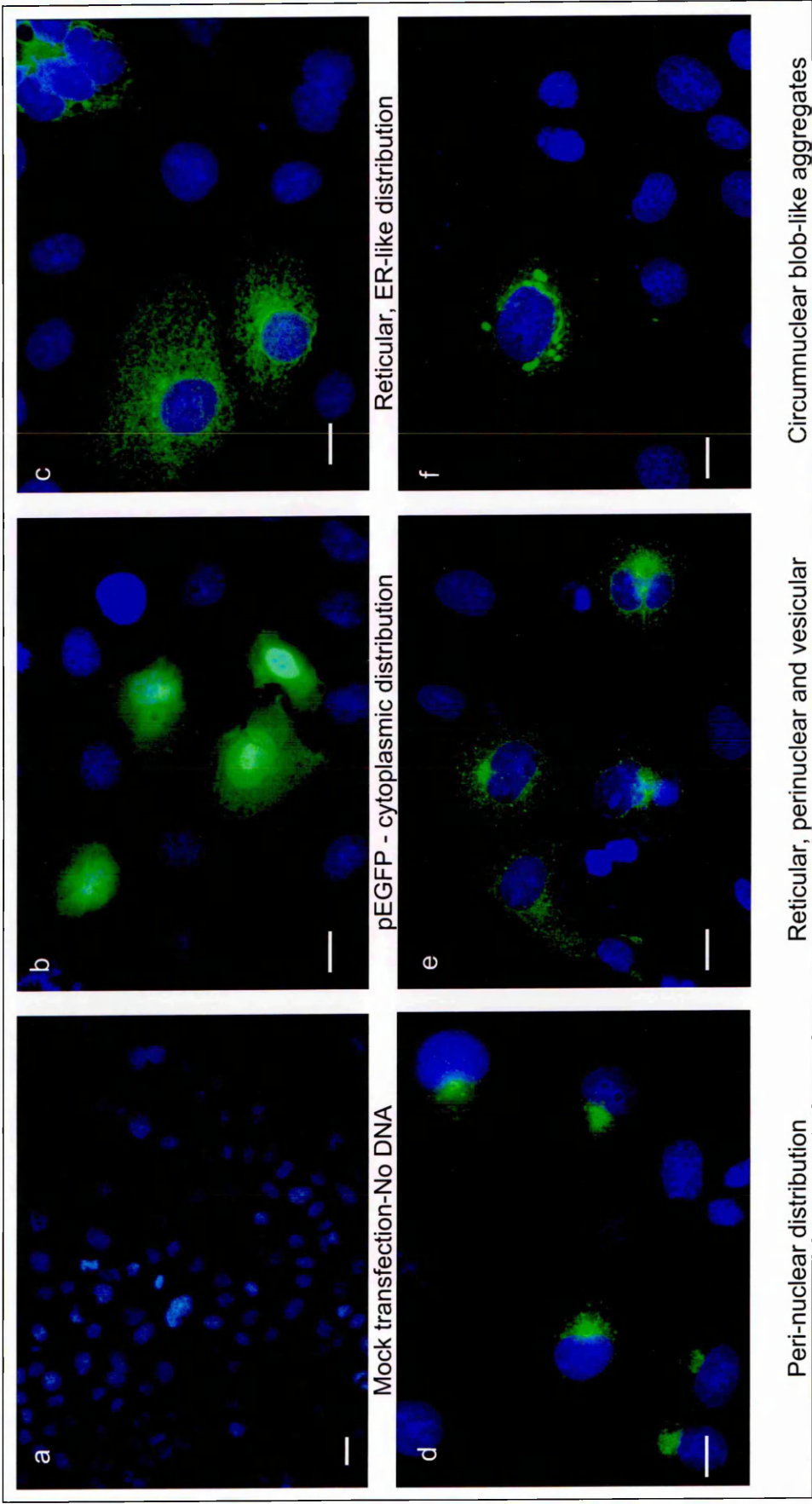


Figure 4.4. Transfection of Cos-7 cells with the N-terminal PS1 fusion construct generates four distinct phenotypes i.e reticular (c), perinuclear (d), vesicular (e) and circum-nuclear blob-like aggregates (f). Mock transfection (a) does not generate fluorescence. Transfection with EGFP (b) resulted in diffuse cytoplasmic phenotype distinct from that of the fusion protein. DAPI stain in blue. Bars, 15 μ m.

Cos-7 cells expressing the fusion protein display a range of phenotypes

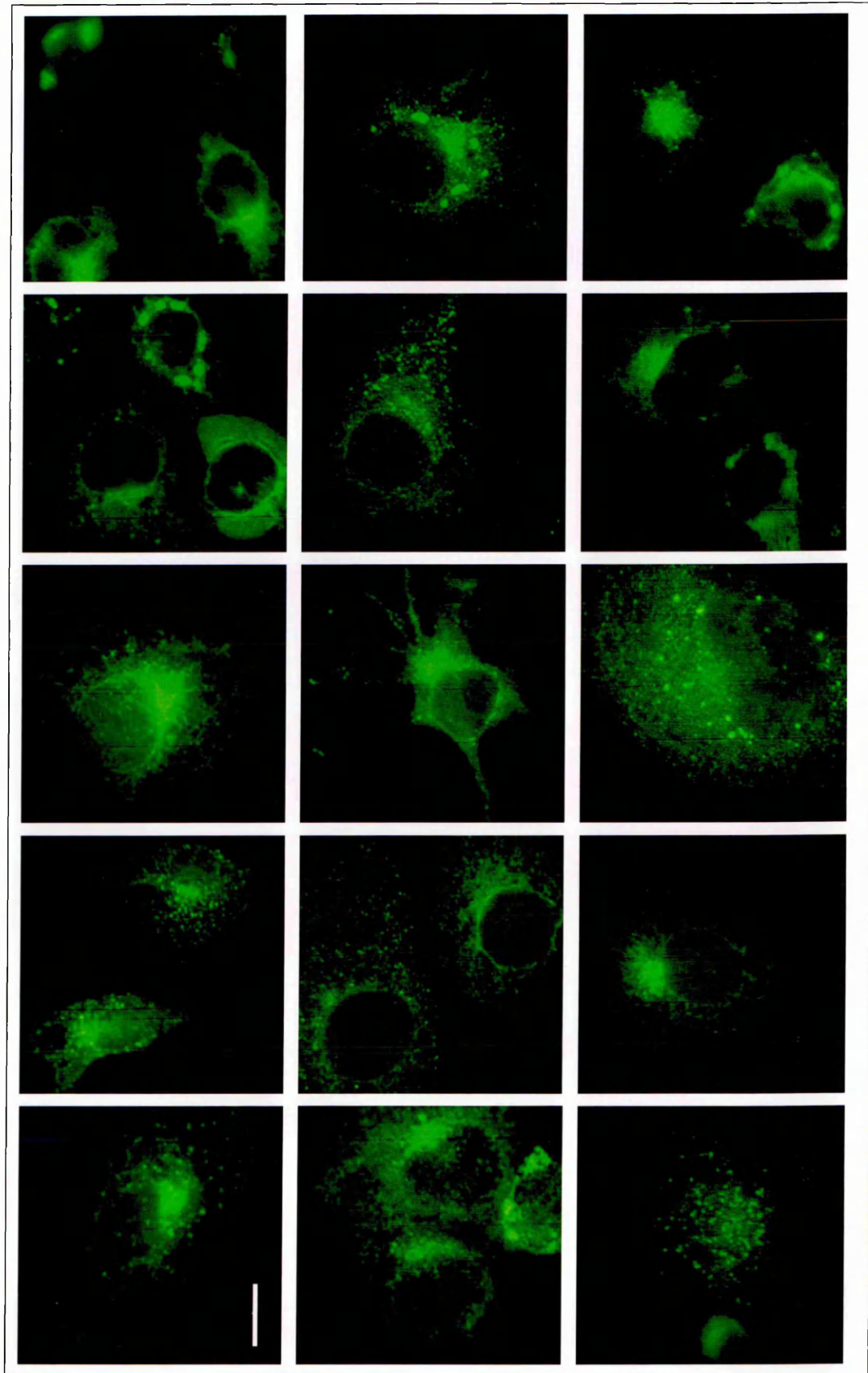
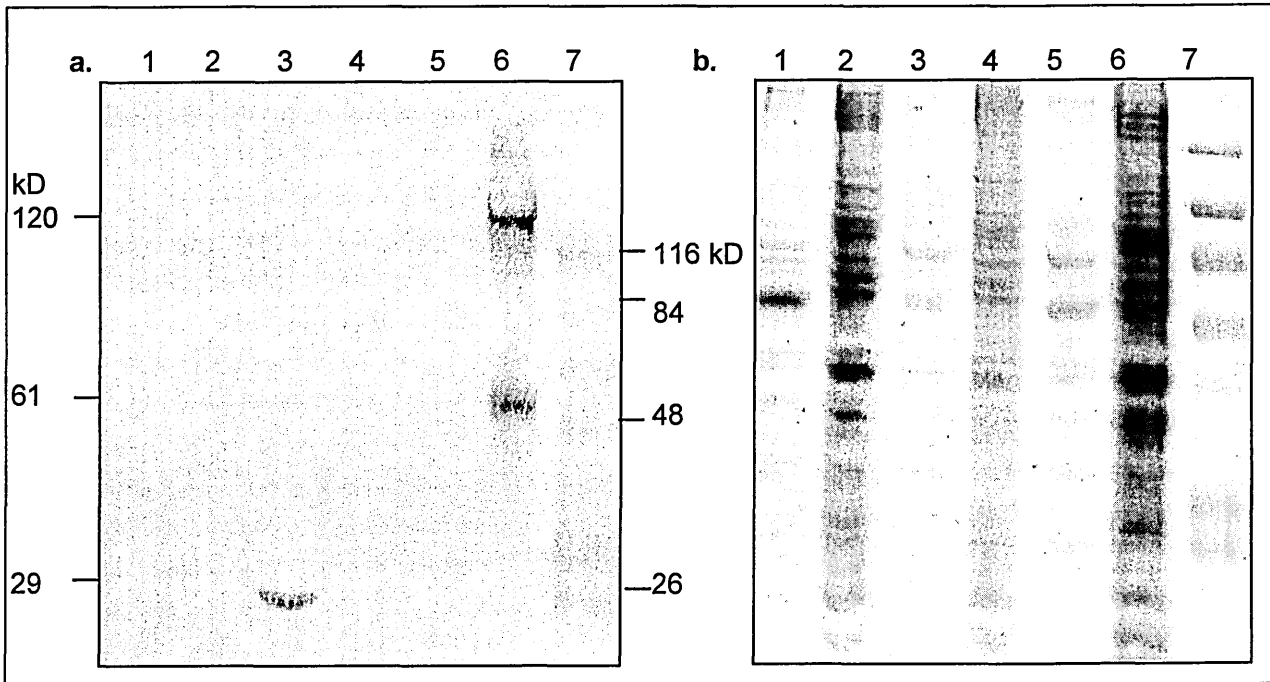


Figure 4.5. Phenotypes expressed by Cos-7 cells transfected with the fusion construct. Typically, transfection resulted in a reticular, vesicular and blob-like aggregate phenotype, all within the same cell. Nuclei omitted for clarity. Bar, 20 μm .

Cos-7 cells expressing the fusion protein show immunoreactivity within the membrane fraction only



Lanes:

1. Control non transfected - soluble fraction
2. Control non transfected membrane fraction
3. pEGFP transfection - soluble fraction
4. pEGFP transfection - membrane fraction
5. pNTPS1-EGFP transfection - soluble fraction
6. pNTPS1-EGFP transfection - membrane fraction
7. 7 Blue marker

Predicted molecular weights

N-terminal PS1fragment	35 kD
EGFP	27 kD
NTPS1-EGFP	62 kD

Figure 4.6. Western analysis of Cos-7 cells expressing the fusion protein. a. Cell soluble and membrane bound fractions prepared from control and transfected Cos-7 cells (pEGFP or pNTPS1-EGFP) stained with the anti-EGFP antibody. Using linear regression analysis EGFP alone resolves as a band at ~29 kD (lane 4). Two bands represent the membrane-bound fusion protein in lane 7 at 61 kD and 120 kD. The higher molecular weight species may represent dimerisation of the fusion protein. Samples analysed by 10% SDS Urea PAGE. b. Corresponding comassie stain shows approximately equal sample loading per lane.

antibody staining show significant overlap with the perinuclear phenotype of the fusion protein. Whereas the majority of untransfected cells stained for GalNac display a Golgi stack phenotype, staining in transfected cells is both reduced and in patches, scattered throughout the cell showing only partial overlap with the fusion protein (middle row figure 4.9). Interestingly, neither the vesicular phenotype nor the blob-like phenotype co-localise with the above cell compartment markers, possibly indicating that these two structures have similar origins.

4.9 The NTPS1 fusion protein does not co-localise with 923 staining and returns to the ER following BFA treatment in Cos-7 cells

Confident that the NTPS1-EGFP fusion protein had been successfully generated, the earlier experiment in which 923 antibody staining of endogenous PS1 was shown to be predominantly vesicular following BFA treatment (figure 3.3), was repeated, this time with Cos-7 cells expressing the fusion protein. From the top row in figure 4.10, the fusion protein shows a reticular and aggregated blob phenotype, whereas 923 antibody staining displays an Ergic/Golgi-like phenotype. Close examination reveals very little overlap between the fusion protein and the 923 antibody. Following BFA treatment, cells expressing the fusion protein were stained with antibodies to Colligin (figure 4.10, bottom row) and Ergic53 (figure 4.11). In the case of Colligin staining there was little change in the phenotype before and after BFA treatment (figure 4.11, bottom row). Similarly, following BFA treatment, the fusion protein locates to the ER, whilst Ergic53 staining remains largely vesicular (figure 4.11, bottom row).

Although raised against the N-terminus of PS1 (amino acids 10-24), staining with the 923 antibody of transfected cells failed to show co-localisation with the fusion protein. Similarly, when the BFA experiment was repeated and the cells were stained with the 923 antibody, there was very little co-localisation between it and the fusion protein (figure 4.10, upper panels). Additionally, PS1 transgene expression has been reported to displace endogenous PS1 expression. In the case of 923 staining, this appears to be unaffected by expression of the fusion protein, raising doubts as to the ability of the 923 antibody to recognise PS1. As expected the 1039 antibody does not co-localise with N-terminal fusion protein nor

does the latter displace endogenous C-terminal PS1 staining, which is similar in both transfected and non-transfected neighbouring cells, suggesting that full-length exogenous PS1 but not exogenous N-terminal fusion protein alone, is required to displace endogenous levels of the holoprotein (figure 4.12).

4.10 Chapter summary

In summary, the distinctive phenotypes displayed by the fusion protein within the cell compartment of transfected Cos-7 cells and its immunoreactivity within the membrane-only fraction, would indicate correct folding of the NTPS1 fusion protein and its maturation from the ER/IC to the Golgi, consistent with previously published reports (Yu et al, 1998; Capell et al, 1998). The distribution of the fusion protein within the cell compartment shows some overlap with markers to the ER and Golgi. In the case of PDI staining, this is increased in some cells expressing relatively high amounts of the fusion protein compared to non-transfected cells. Conversely, GalNac staining is reduced in some cells expressing the fusion protein. The absence of co-localisation of the fusion protein with the putative PS1NTF 923 antibody, and the discrepancy between their phenotypes following BFA treatment, indicates that the 923 antibody does not recognise either transgene NTPS1-EGFP nor endogenous PS1.

The anti EGFP antibody co-localises with NTPS1 fusion protein

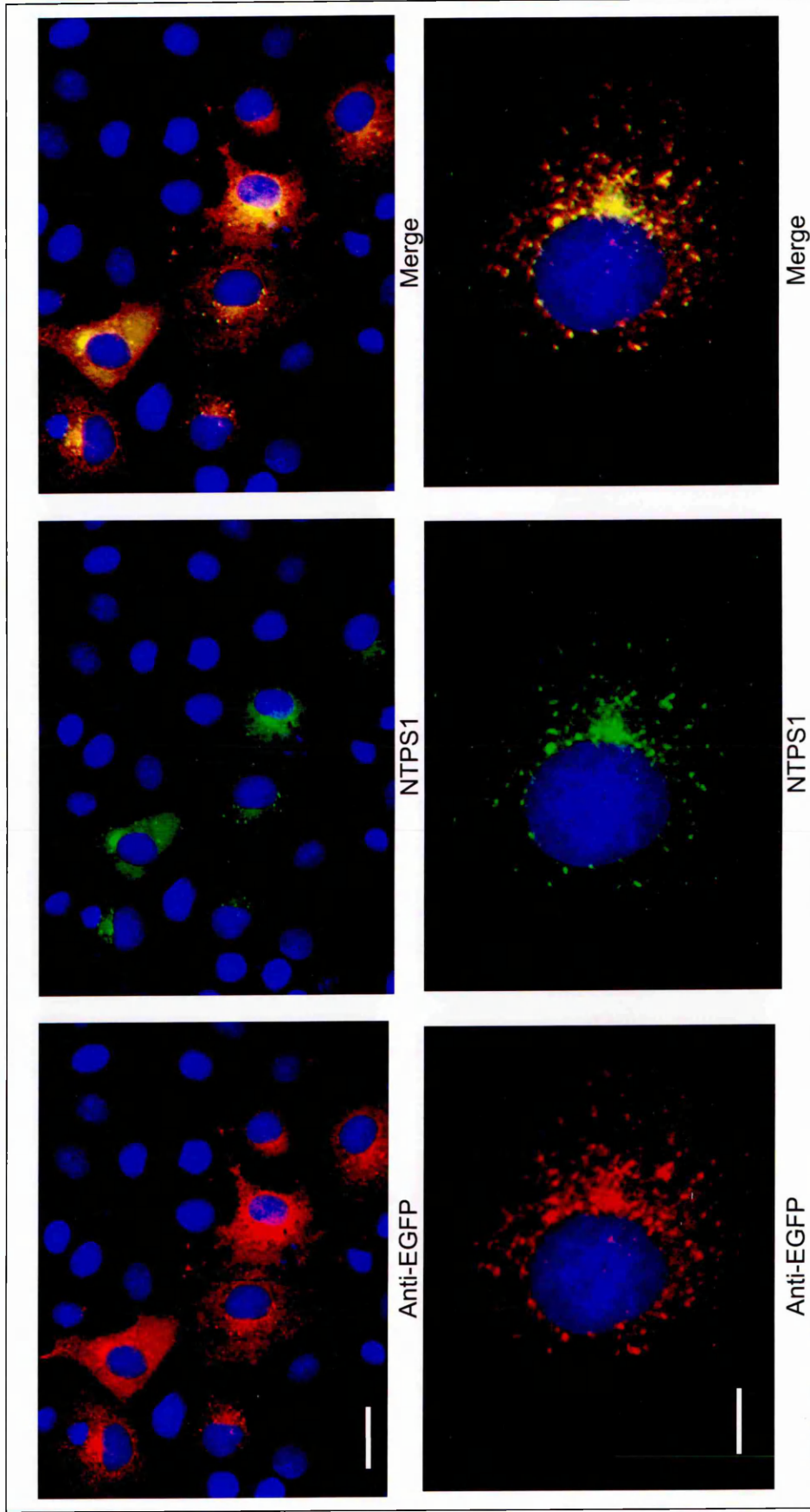


Figure 4.7. Anti-EGFP antibody staining of Cos-7 cells expressing the NTPS1 fusion protein. The high degree of overlap between the fusion protein and the anti-EGFP antibody suggest cleavage of the EGFP moiety does not occur. DAPI stain in blue. Bars, 20 μm .

The NTPS1 fusion protein shows partial co-localisation with the ER markers Colliglin and PDI

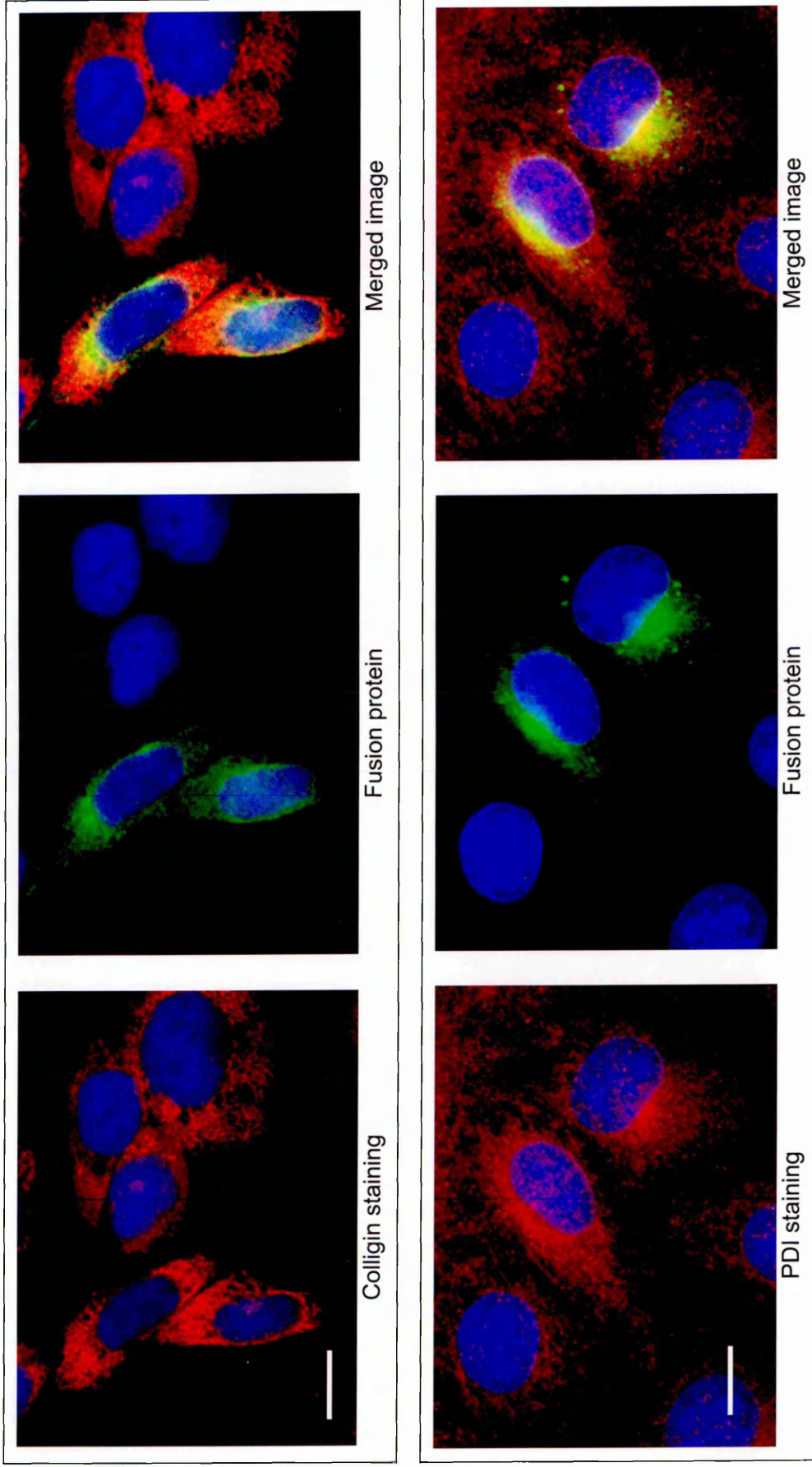


Figure 4.8. ER antibody staining of Cos-7 cells expressing the NTPS1 fusion protein. Top row: Colliglin staining (red) shows a reticular distribution. Bottom row: PDI staining (red) shows partial overlap with the reticular fusion protein phenotype but does not localise with perinuclear or vesicular phenotype. PDI and colliglin staining is marginally brighter in transfected cells compared to neighbouring cells. DAPI stain in blue. Bars, 20µm.

The NTPS1 fusion protein partially overlaps with markers to the Golgi apparatus

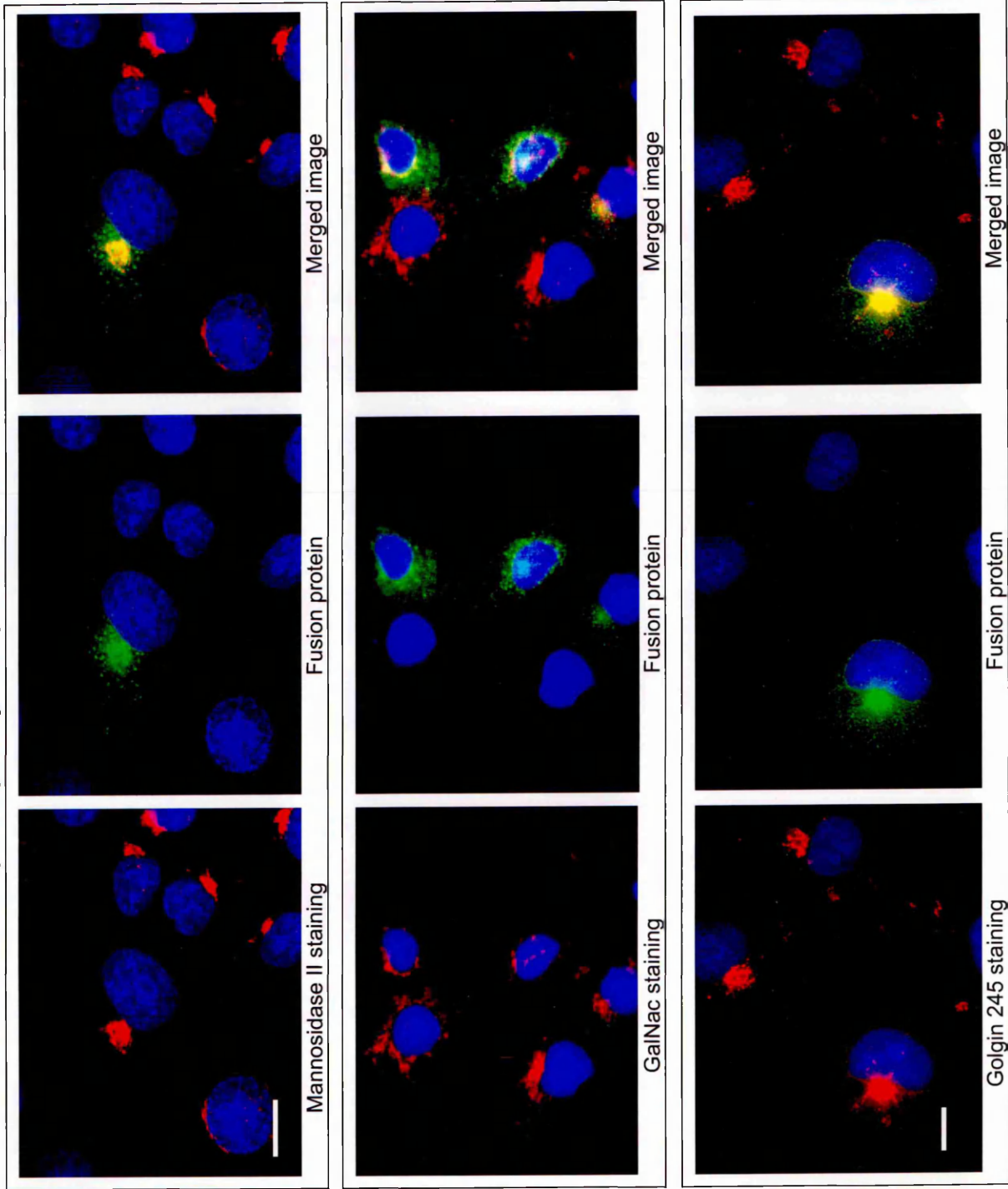
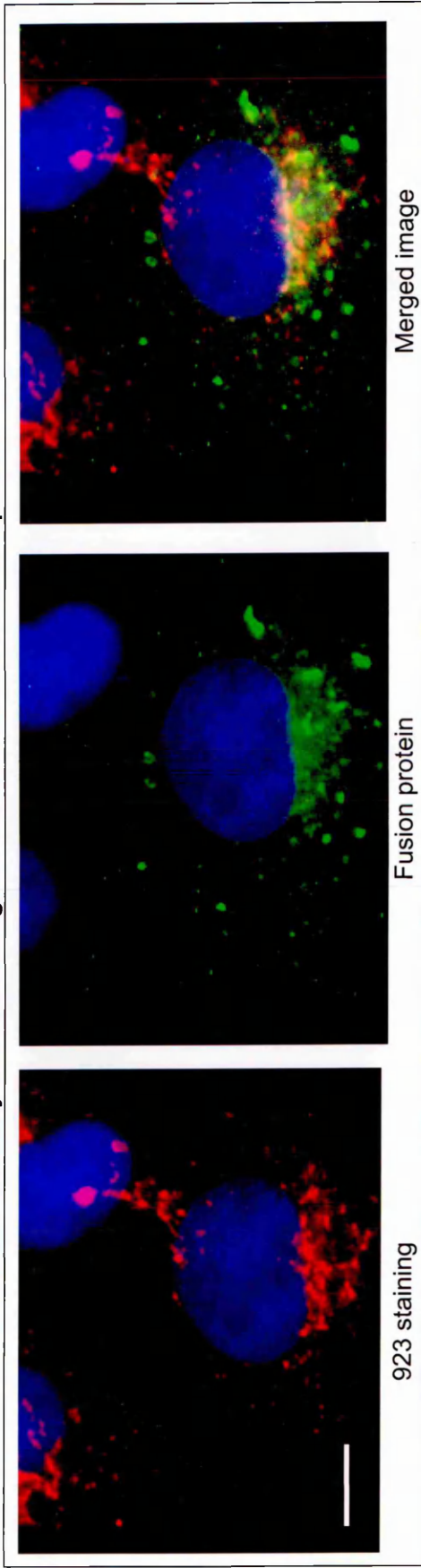


Figure 4.9. The fusion protein overlaps to varying degrees with markers to the Golgi. Top row: Mannosidase II staining of the medial Golgi (red); middle row GalNac staining of trans Golgi (red); bottom row Golgin 245 staining of the TGN (red). Note: GalNac staining is reduced compared to neighbouring, non-transfected cells (see also figure 6.1). DAPI stain in blue. Bars, 20 μ m.

The 923 antibody does not recognise the N-terminal PS1 fusion protein



The NTPS1 fusion protein localises to the ER following BFA treatment of transfected Cos-7 cells

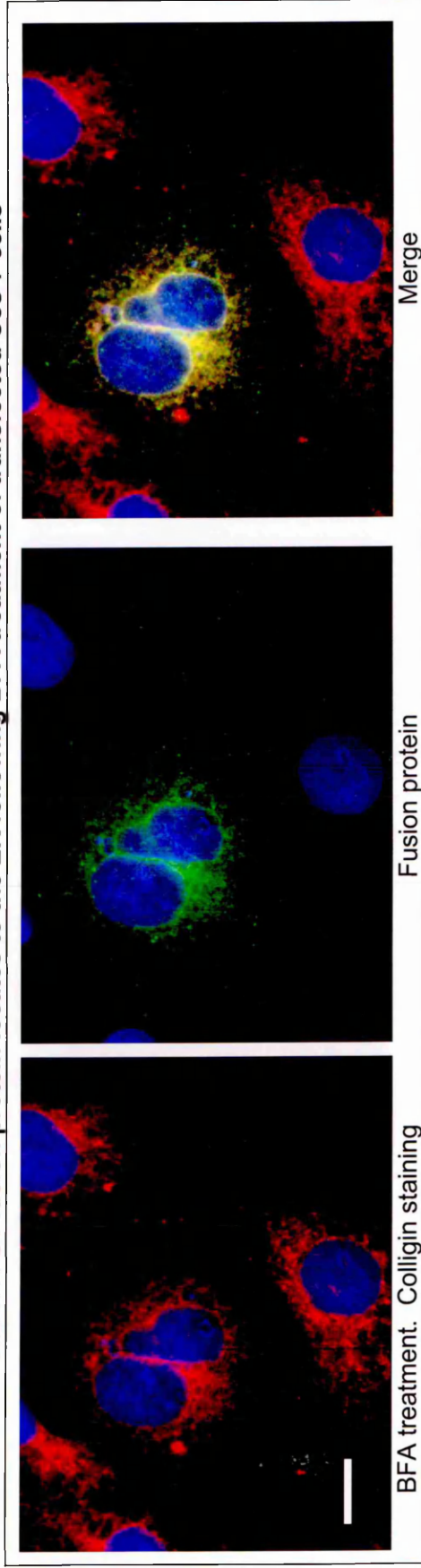


Figure 4.10. 923 antibody staining and BFA treatment of transfected Cos-7 cells. Top row: The putative PS1 antibody 923 does not co-localise with the fusion protein in Cos7 cells. Bottom row: BFA treatment of Cos7 cells expressing the fusion protein. Following BFA treatment the fusion protein maintains a reticular distribution that localises closely with the ER marker Colliglin (compare with 923 staining of BFA treated cells shown in figure 3.3). DAPI stain in blue. Bars, (top row) 10 μ m, (bottom row) 20 μ m.

The NTPS1 fusion protein does not localise with ERGIC53 staining following BFA treatment of transfected Cos-7 cells

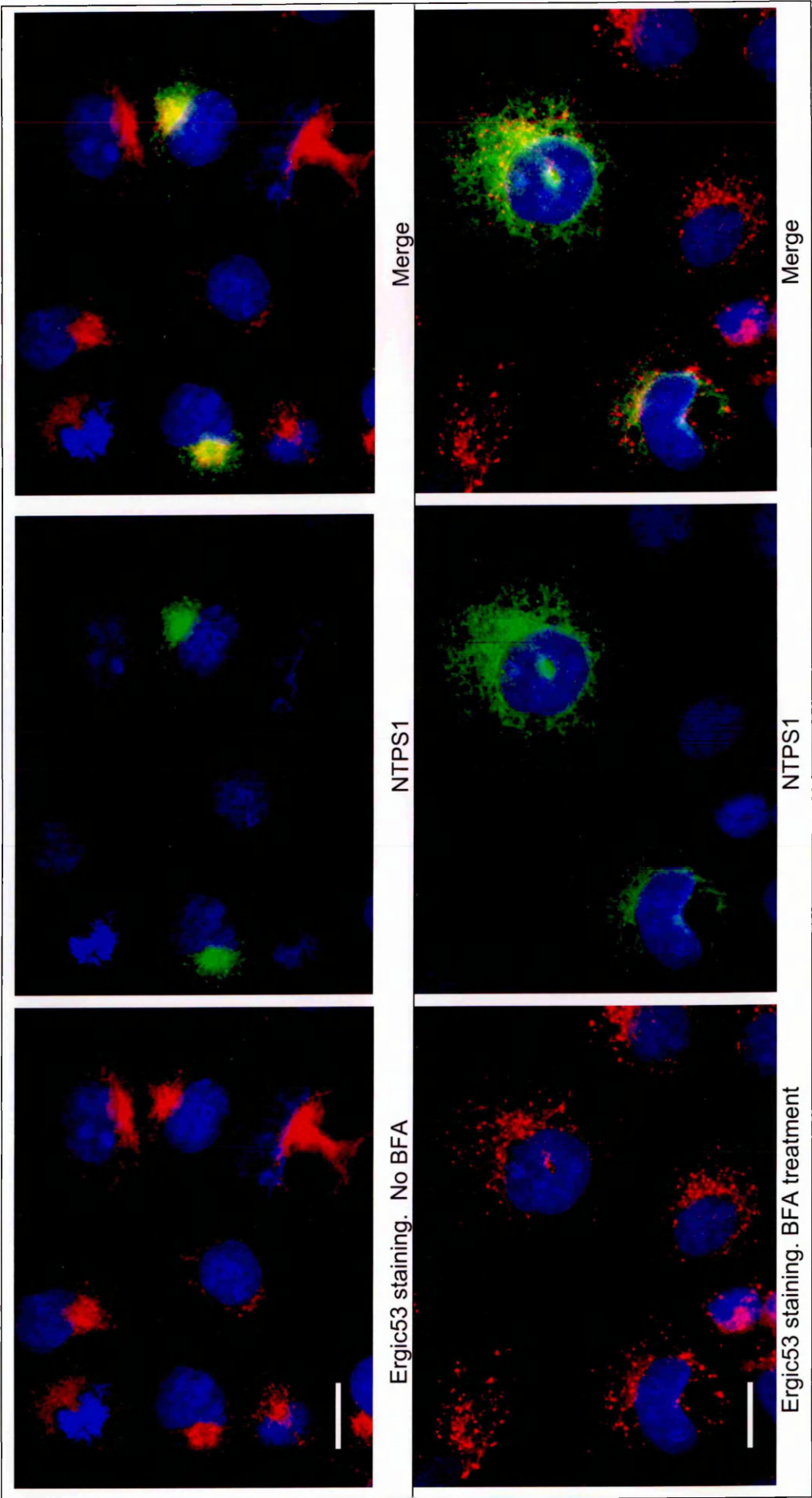


Figure 4.11. Ergic53 antibody staining of BFA-treated Cos-7 cells expressing the NTPS1 fusion protein. Upper panels: The fusion protein and Ergic53 staining display a predominantly perinuclear phenotype. Lower panel: Following BFA-treatment the fusion protein localises to the ER, whilst ERGIC53 staining is distinctly vesicular. DAPI stain in blue. Bars, 20 μ m.

The 1039 antibody neither co-localises with the PS1 N-terminal fusion protein nor displaces endogenous PS1

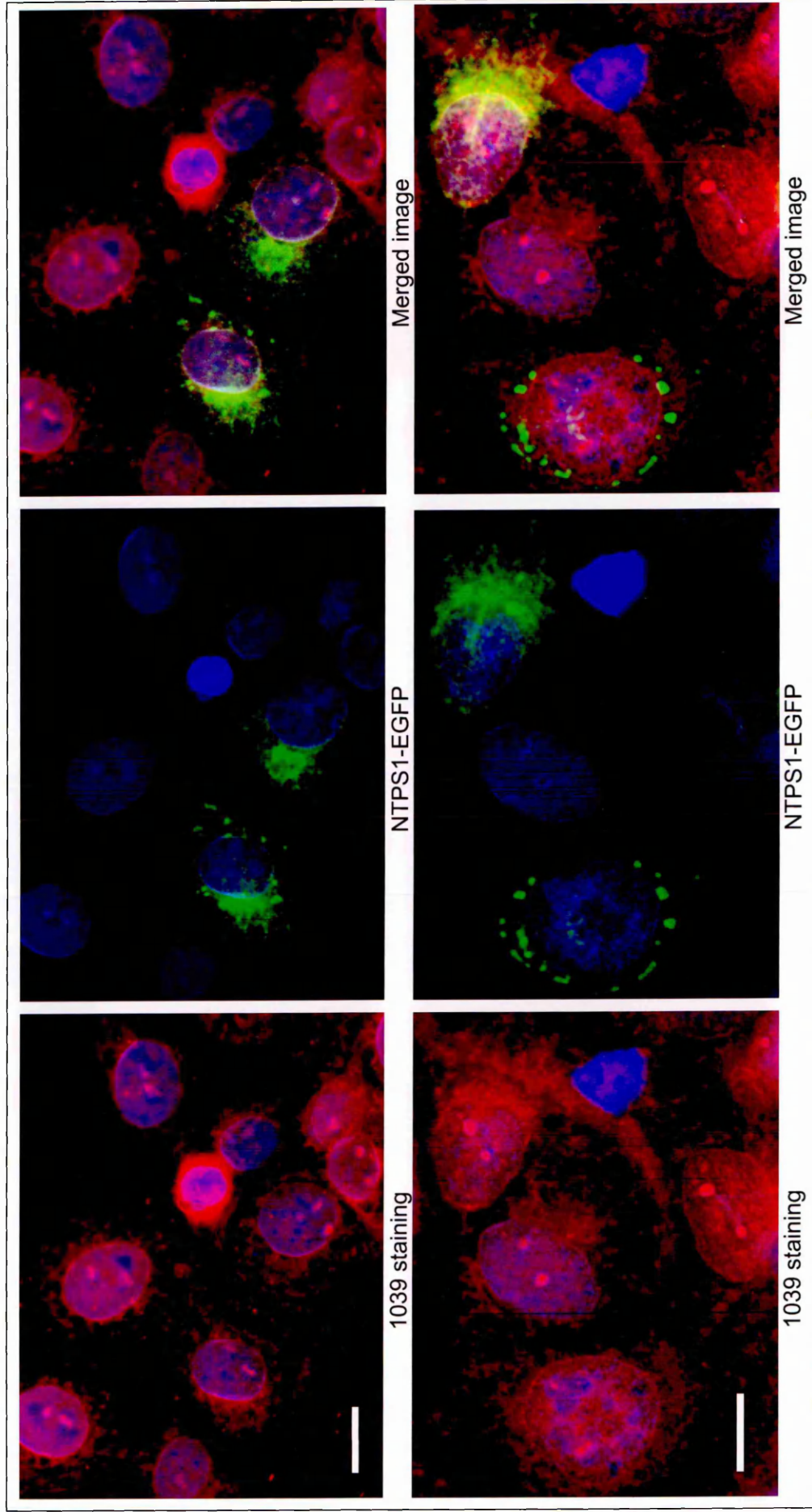


Figure 4.12. 1039 antibody staining of Cos-7 cells expressing the NTPS1 fusion protein. The 1039 anti-PS1CTF antibody displays a reticular phenotype as does a proportion of the fusion protein, however this staining is coincident since the 1039 antibody does not stain for the other fusion protein phenotypes. Note that the fusion protein does not displace endogenous PS1 staining. DAPI stain in blue. Bars, 20 μ m.

5.1 Introduction

The observation that the 923 antibody did not recognise the fusion protein as expressed in transfected Cos-7 cells raised doubts as to whether or not this was in fact an anti-PS1 antibody. The simplest conclusion to be drawn at this stage was that the 923 antibody recognised some other protein other than PS1. Consequently any further investigation with the 923 antibody in the characterisation of the fusion protein was abandoned. Instead it was decided to examine more closely the phenotypes displayed by the fusion protein and any biological effect they might have within the cell. To address the issue as to whether the phenotypes observed for the fusion protein were specific to this NTPS1 construct, a full-length wild type fusion protein (FLCPS1) was constructed and compared in Cos-7 cells with the phenotypes exhibited by the presence of the NTPS1 fusion protein. Additionally, full-length (FLMPS1) and an N-terminal PS1 (NTMPS1) fusion constructs harbouring a known FAD mutation were generated for the purpose of investigating what effect, if any, these mutations have on the trafficking of the fusion protein within the cell and any associated effects these mutation might have on the cleavage of APP.

5.2 The phenotypes exhibited by the fusion protein are not an artefact of the cell fixation process

Methanol fixation of cells in preparation for microscopic examination was chosen because of the lower toxicity associated with its handling and its ease of use. However, issues arose as to whether the phenotypes observed were in fact artefacts generated as a consequence of the fixation process. To address this concern, Cos-7 cells expressing the fusion protein were treated with an alternate fixative, paraformaldehyde. Transfected Cos-7 cells expressing the fusion protein were fixed separately in methanol or paraformaldehyde and examined for differences in the phenotypic distribution of the fusion protein. Figure 5.0 shows that there are no marked differences between the two fixation methods since each treatment results in the same ER/Golgi, vesicular/blob phenotypes. Similarly, live

cells affixed to coverslips were imaged. In this instance a diffuse-ER and blob phenotype could be discerned within the same cell not dissimilar to that observed in fixed cells (data not shown), though it could be argued that the removal of the cells from a constant CO₂/temperature environment to the microscope, regardless of how rapid the transfer was, may have contributed to the phenotypes observed. Had the phenotypes been an artefact of the fixation procedure, it is reasonable to expect that all transfected cells would similarly be affected and therefore exhibit the same phenotypes, as opposed to the actual ones observed. Since the phenotypes are independent of the fixation method, methanol was used throughout the remainder of the project given its ease of use and reduced toxicity compared to paraformaldehyde.

5.3 The phenotypes displayed by the fusion protein are found within other cell types

As a corollary to the above experiment, the construct was transfected into several additional mammalian cells with a view to establishing whether the fusion protein phenotypes were unique to Cos-7 cells. The fusion construct was therefore transfected into HEK 293, CHO, HeLa, NRK and mouse PS1^{-/-} knockout cells. The images shown in figure 5.1 shows no difference between the phenotypes displayed by Human HeLa/HEK 293 cells and rodent NRK cells and those displayed by monkey Cos-7 cells (figure 5.1). To rule out the possibility that the observed phenotypes were not the result of the transgene protein interacting with endogenous PS1, mouse PS1^{-/-} cells were transfected with the fusion construct. As with the other transfected mammalian cells there was no difference in the phenotypes expressed by this cell line (figure 5.1, bottom panel). To ascertain whether the EGFP moiety and the fusion protein remained intact when expressed by other cells, the cells were stained with the anti-EGFP antibody (HEK 293 cells, middle panel). No diffuse staining, indicative of soluble, cleaved EGFP was observed, instead both the ER and blob phenotypes co-localised strongly with the antibody.

Since there are no discernable differences in the phenotypes displayed by Cos-7 cells and those displayed by other transfected mammalian cell types, including

The N-terminal PS1 fusion protein displays the same phenotype regardless of the fixation method

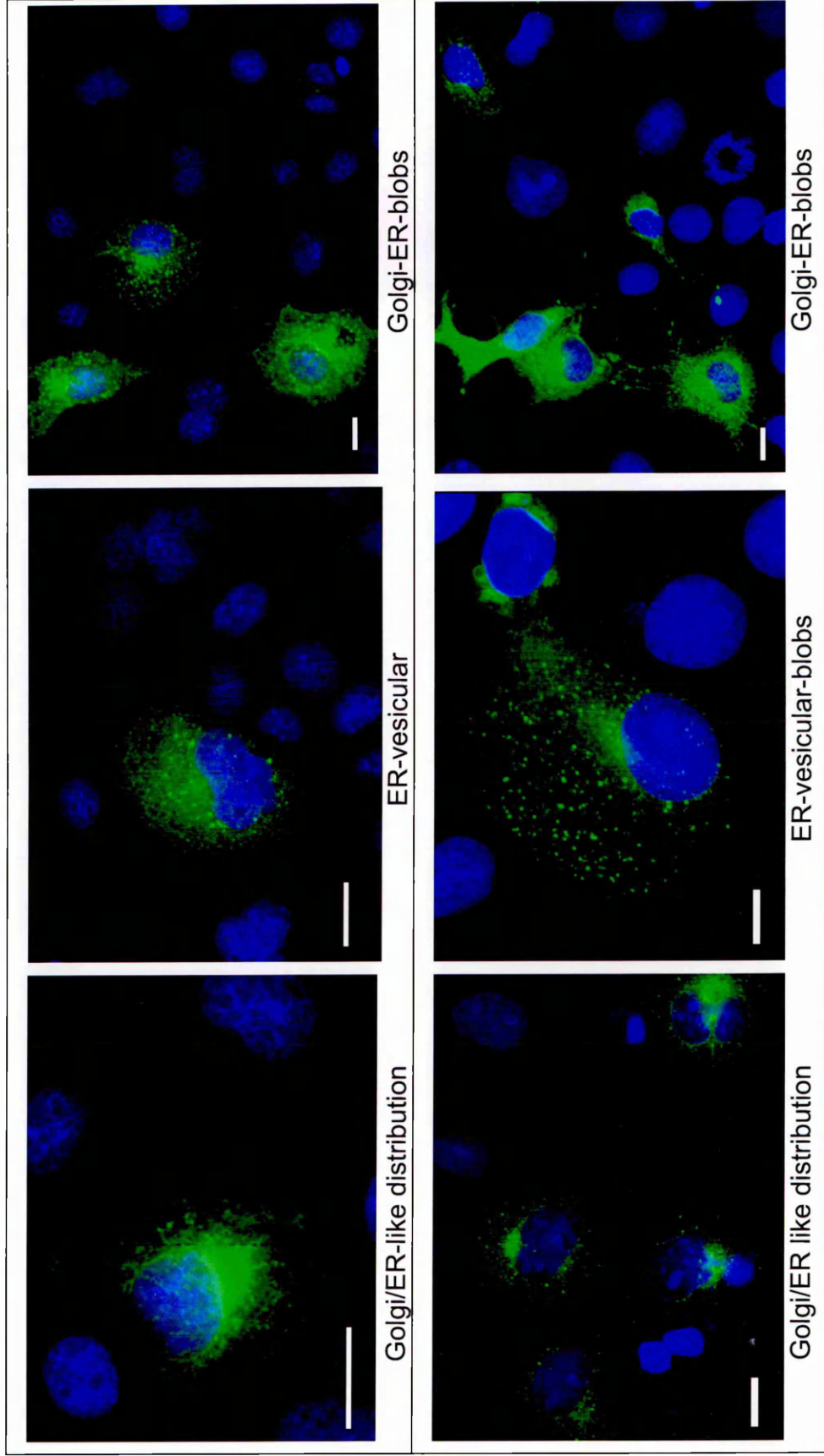


Figure 5.0. Cell fixation method. Transfected Cos-7 cells expressing the fusion protein were fixed in formaldehyde (upper row) or methanol (lower row). No appreciable difference in phenotypes is observed between the two fixation methods. DAPI stain in blue. Bars, 20 μm .

The fusion protein phenotypes displayed by various mammalian cells are identical

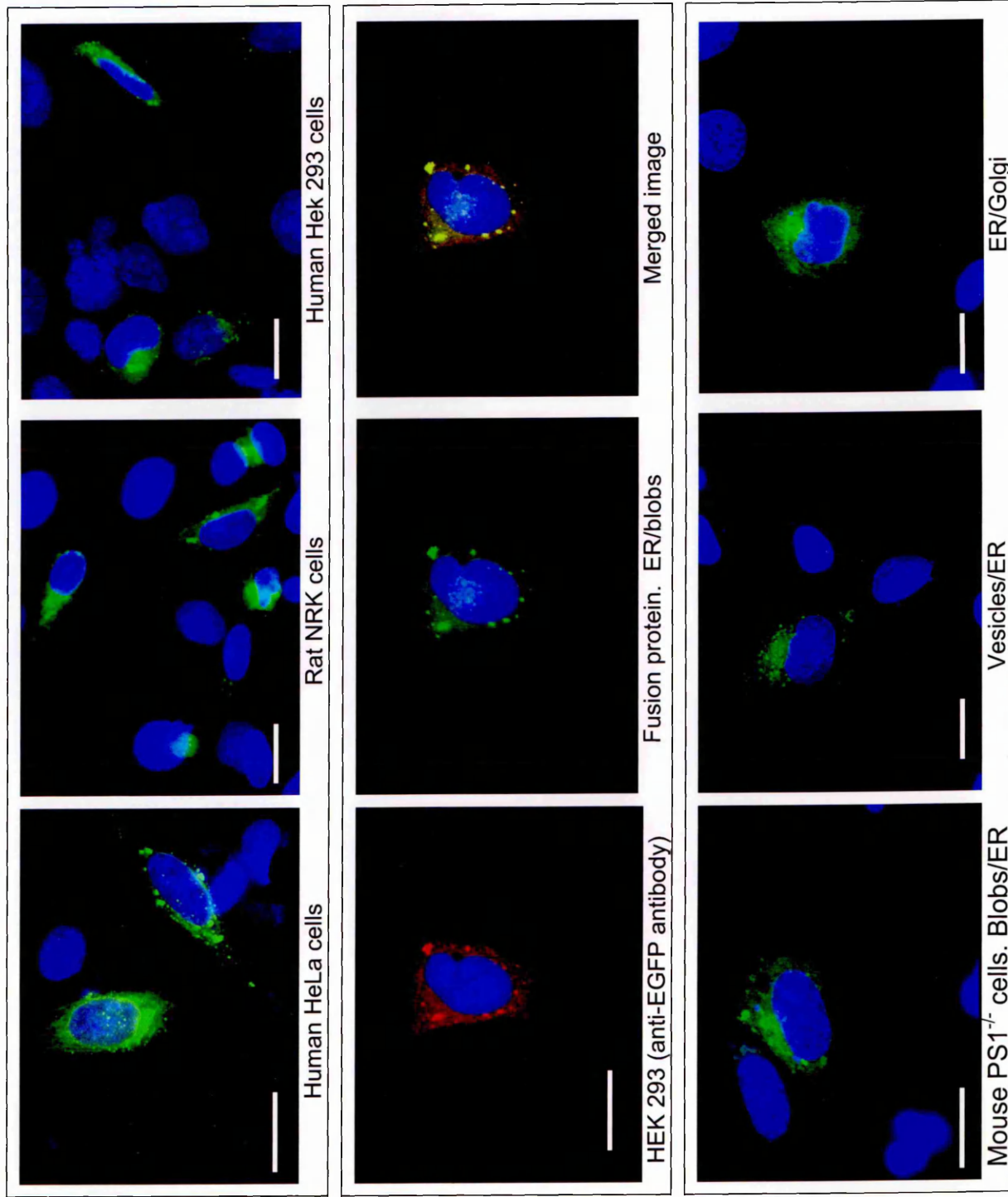


Figure 5.1. Transfection of different cell types with pNTPS1-EGFP. Top row: HeLa, NRK and HEK 293 cells display the same phenotypes. Middle row: The anti-EGFP antibody co-localises with the fusion protein expressed by HEK 293 cells. The degree of overlap in the yellow merged image is more intense for the blobs. Bottom row: Transfection of PS1^{-/-} mouse cells resulted in the same phenotypes as those seen in Cos-7 and other cells, i.e. ER and Golgi-like, vesicular and blob-like aggregates. DAPI stain in blue. Bars 20 μ m.

PS1 knockout cells, it is reasonable to assume that the above results reflect a general cellular response to the presence of the fusion protein.

5.4 Construction of wild type and FAD mutant PS1 plasmids

In all reported cases of FAD there is an increase in the production of the amyloidogenic $A\beta_{42}$ species by proteolytic processing of APP (Scheuner et al, 1996). To examine what affect FAD mutations had on the generation of $A\beta$ a course of action was taken to generate both wild type and mutant full-length PS1 fusion proteins and a mutant N-terminal PS1 protein. Additionally, the introduction of a FAD mutation into the construct will be of use for examining the passage of the fusion protein through the cell compartment.

(i) Alteration of PS1 cDNA base sequences by site directed mutagenesis

A novel approach used to alter the amino acid sequence of a protein involves the use of site directed mutagenesis (SDM). Here, selected bases within a DNA molecule can be altered and the effects on protein function studied (Deng, 1992). At the molecular level mutations may be in the form of insertion, point or deletion mutations. In site-directed mutagenesis mutations are directed specifically to a target region of a protein. This achieved by introducing a mutation inot a cloned segment of DNA corresponding to this region.

A general feature of SDM is that the oligonucleotide encoding the desired mutation is annealed to one strand of the DNA of interest and serves as a primer for initiation of DNA synthesis. This way the mutagenic oligonucleotide is incorporated into the newly synthesized strand. Mutagenic oligonucleotides incorporate at least one base change but can be designed to generate multiple substitutions, insertions or deletions. The synthetic oligonucleotide is complementary to the target template except for a region of mismatch near the center. This mismatched region contains the desired mutation. Following hybridization, the oligonucleotide is extended with DNA polymerase to create a double-stranded structure. The nick is then sealed with DNA ligase and the duplex structure is transformed into a suitable host cell.

If no selection method is employed, the theoretical yield of mutants using this procedure is 50% (due to the semi-conservative mode of DNA replication). In practice, however, the mutant yield in the absence of selection may be much lower, often only a few percent or less. This is assumed to be due to such factors as incomplete in vitro polymerization, primer displacement by the DNA polymerase used in the fill-in reaction and in vivo host-directed mismatch repair mechanisms that favour repair of the unmethylated newly synthesized DNA strand. Off the shelf kits like the 'GeneEditor in vitro Site-Directed Mutagenesis System' uses antibiotic resistance to select only for plasmid derived from the mutant strand, resulting in a greatly increased frequency of mutations. According to the manufacturer's claims, 80-90% recovery is possible.

(ii) Site directed mutagenesis by PCR

Originally the PS1 FAD mutation was to be introduced using a site directed mutagenesis kit, however, given the success of the previous PCR it was decided to explore the possibility that the desired mutation could be introduced into PS1 using mutant primers in a PCR involving two stages. The first stage used two mutant primer pairs to generate the complete, but fragmented product in two separate PCR reactions. The second stage exploited the complementary overlap region of the fragmented products in a third PCR reaction. In this reaction polymerase effectively fills-in the gaps using flanking (conserved) primers to generate the complete molecule incorporating the FAD mutation (figure 5.2). In terms of economy, it was estimated that this two-stage method of introducing a mutation is both quicker, involving fewer steps and less expensive when compared to the SDM kit method.

A general rule when attempting PCR is to limit the size of the read performed by the polymerase since the longer the DNA sequence to be copied the greater the likelihood that an error will be introduced. Bearing this in mind the simplest approach to introducing a mutation into the transgene was to design mutant primers that only generate a portion of the target cDNA during the PCR (table 4.0). For reasons of practicality the L235P mutation (AD onset 32 years) located within TM5 of PS1 (Campion et al, 1997) was chosen since PCR of the

PS1 cDNA would generate PCR products of approximately 700 bp, half the size of the full-length molecule. Figure 5.3 shows the amino acid sequence of PS1 and the location of the L235P FAD mutation within TM 5 of the molecule. By selectively amplifying the cDNA in two stages, the reaction products can then be incubated together in a final PCR to generate PS1 containing the FAD mutation.

To generate the full length PS1 mutant for example, required two separate PCR reactions, the first with the primer pair 0-05/0-09, and the second reaction with the primer pair 0-11/0-12 (table 4.0). In stage 2 the resultant PCR products were separated on an agarose gel, excised and purified. Equal molar quantities of the two PCR products were incubated together along with dNTPs/Mg, Taq polymerase and the necessary flanking primers in a third PCR reaction (figure 5.2).

(iii) Optimisation of PCR conditions

The PCR conditions were optimised as before to give the best product yield with the least non-specific binding (NSB) component (figure 5.4), however after several attempts it became clear that the NSB could be reduced, but not entirely eliminated altogether. The results from this PCR show bright bands of the expected size of approximately 700 bp and 150 bp. The assumption was made that these were the required PS1 cDNAs and were therefore excised from the gel and purified for the second PCR (figure 5.5 a).

To generate the full-length mutant PS1 molecule, the PCR products from lanes 5 and 6 (figure 5.4) were mixed in equal molar amounts. Similarly, to generate the mutant NTMPS1 molecule the products from lanes 5 and 7 were incubated together. Further optimisation of the reaction conditions yielded both NTMPS1 and FLMPS1 products of the correct size (figure 5.5 b, lanes 2 to 5, and lanes 6 to 9, respectively). From figure 5.5 it is clear that the reactions did not precede to completeness and that the yield of NTMPS1 DNA was greater than that for FLMPS1. However, the results were encouraging enough that the experiment was scaled-up and the resultant products were separated on an agarose gel, excised and purified for restriction enzyme analysis.

Site directed mutagenesis of PS1 cDNA by two step PCR using primers incorporating FAD mutation L235P

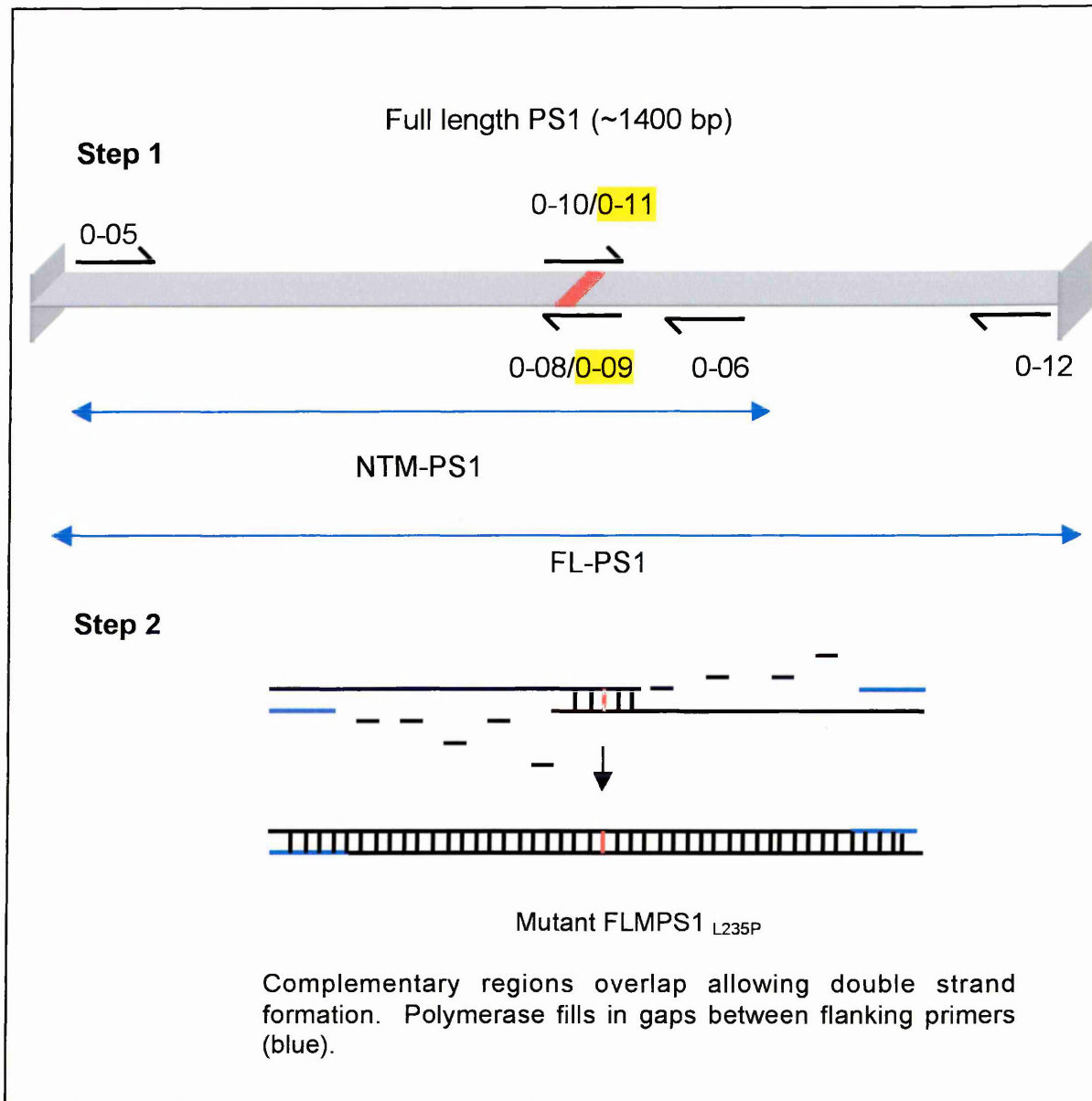


Figure 5.2. Schematic representation of the PCR used to generate PS1 cDNAs. Step 1: To generate the full-length PS1 mutant molecule required two PCR reactions, the first with the primer pair 0-05/0-09, and the second reaction with the primer pair 0-11/0-12. Step2: The resultant reaction products are then mixed together to generate the full-length construct in a third PCR using the flanking primers 0-05 and 0-12. The advantage to this scheme is that the two intermediate PCR products overlap at complementary sequences to form a double stranded region with flanking single stranded arms, which the polymerase fills-in during the final PCR. The red bar represents the site at which the mutated primers (highlighted) introduce the FAD L235P mutant.

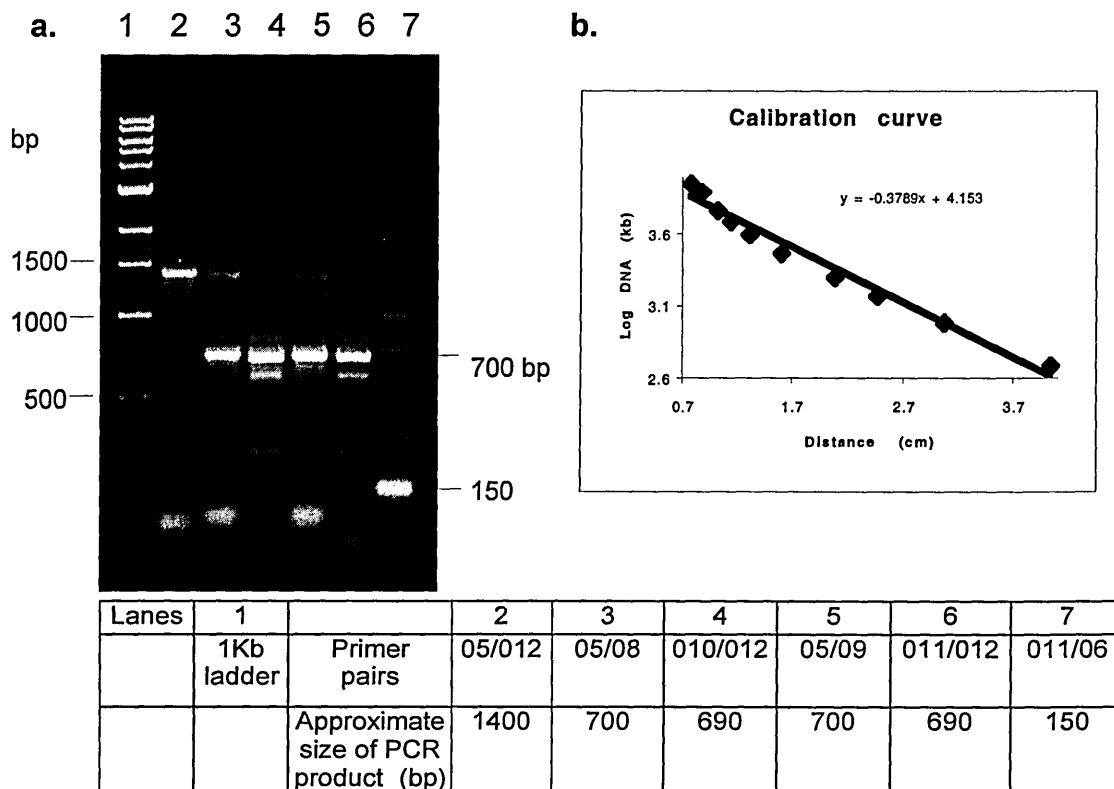


Figure 5.4 Amplification by PCR of pCLneoPS1. **a.** Mutated and conserved primers (table 4.0) were used to generate truncated PS1cDNAs by PCR. 1.5% TAE agarose gel stained with ethidium bromide. **b.** Log plot of 1kb ladder fragments. Estimate of PCR product size (bp) using linear regression analysis.

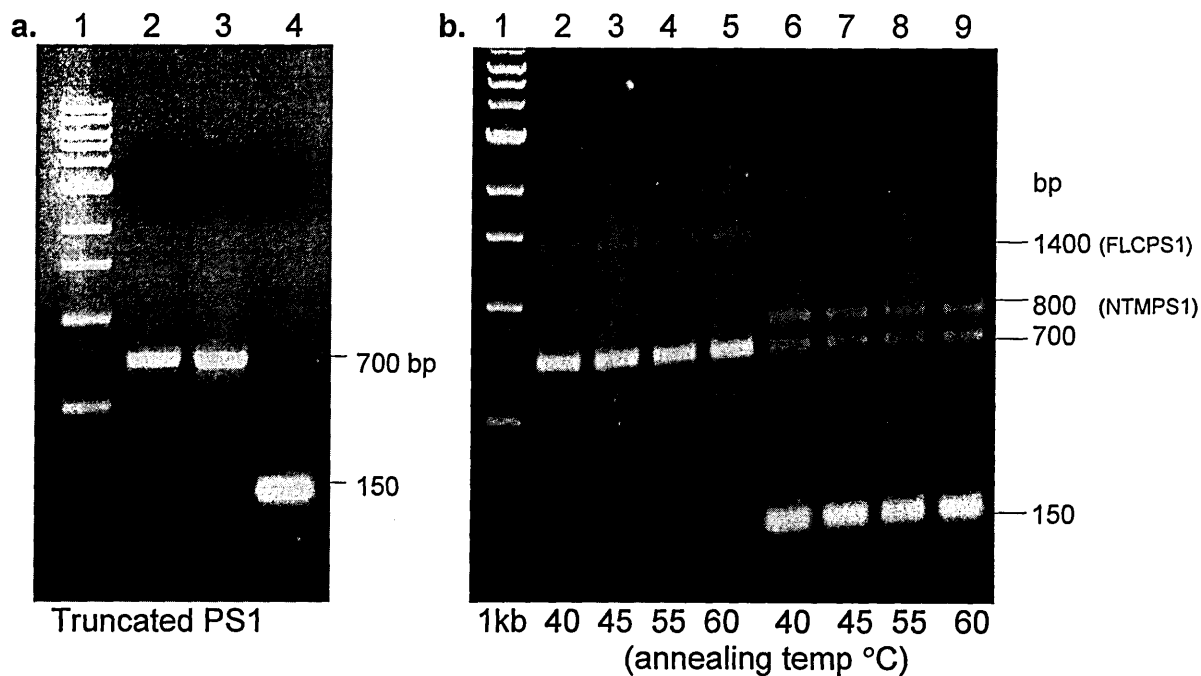


Figure 5.5. Analysis of PCR product. **(a)** The PCR products shown in figure 5.4 were excised and recovered (lanes 2 to 4) to eliminate the NSB component. **(b)** The increased PCR cycle time from 2 min to 10 mins generated FLMPS1 (lanes 2 to 5) and NTMPS1 DNAs (lanes 6 to 9) approximating in size to those for FLMPS1 (1447 bp) and NTMPS1 (856 bp). Different annealing temperatures did not improve the yield of the PS1 cDNAs. Each lane shows 1 μ l of product taken from a total reaction volume of 25 μ l. Samples analysed on a 1.5% TAE agarose gel stained with ethidium bromide.

(iv) Restriction analysis of PCR products

To confirm that the identity of NTMPS1 and FLMPS1 a series of diagnostic restriction digestion assays were performed (Figure 5.6). The fragments generated by restriction digestion are close in size to the values calculated from a restriction map of PS1 (table 5.0). The mutant PS1 cDNAs were subcloned, firstly into the pGEM-T vector as before then secondly into the pEGFP vector. Once subcloning of the cDNAs was completed the putative FLM/NTMPS1-EGFP vectors were analysed by a second series of restriction digestion reactions (Figure 5.7). The resultant fragments were close in size with the predicted values calculated from a restriction map of pEGFP (table 5.1). Finally, the DNA sequences of the new constructs were confirmed for that of the wild type and mutant full-length PS1 and N-terminal PS1 molecules (Lark Technologies).

5.5 Expression of NTMPS1-EGFP by Cos-7 cells

Transfection of the NTMPS1 construct into Cos-7 and HEK 293 resulted in phenotypes identical to those displayed by the NTPS1 fusion protein i.e. ER, Golgi-like, vesicular and blob-like aggregates. Transfection rates for both truncated constructs were comparable as was the percentage of cells displaying the various phenotypes. This is most readily seen by comparing figures 4.5 with those images in figure 5.8 showing anti-EGFP staining of the NTMPS1 fusion protein (top row). Similarly, Colligin and Golgin antibody staining localises with the NTMPS1 fusion protein reticular and perinuclear phenotypes (data not shown).

The earlier attempt at characterising the NTF with the 923 antibody failed to show co-localisation with the fusion protein. The availability of a second putative anti-N-terminal PS1 rabbit polyclonal antibody (NT7) produced by this laboratory, which both Western blots and recognises PS1 in fixed cells, was used to stain for both endogenous PS1 and exogenous NTMPS1. NT7 staining of endogenous PS1 displays an ER-reticular and Golgi-like perinuclear pattern consistent with the reported distribution of PS1. Challenge with the peptide immunogen used in the production of NT7 in a competition assay significantly reduces staining to a diffused speckled pattern (figure 5.8, bottom row). Unlike the putative anti N-

terminus PS1 antibody 923, NT7 readily stains both NTPS1 fusion proteins showing a high degree of co-localisation (figure 5.8, middle row).

5.6 Expression of Full length PS1-EGFP and Full length mutant PS1-EGFP by Cos-7 cells

Interestingly, there were significant differences in the transfection rates between full-length PS1 and the truncated PS1 constructs. Cells expressing the full-length fusion proteins consistently display transfection rates <1%, compared to the 5-10% transfection rate found for both N-terminal PS1 plasmids. In addition, the overall fluorescence of the full-length fusion protein was much fainter compared to the truncated proteins. Although visible under the microscope, cells expressing the full-length fusion proteins were barely detectable by the CCD camera. To capture these images by camera required a maximum gain typically +18 and a shutter setting >40 frames. This compares starkly with the NTPS1-EGFP images, which typically required a gain of +0 and a shutter <10 frames. This presented difficulties when capturing 'clean' images due to the high noise to signal ratio, however this was minimised by utilising the 'dust and scratch' facility found in Adobe Photoshop without significantly altering the information content of the image. Where visible, phenotypes displayed by the full-length fusion proteins were chiefly reticular and blob-like/vesicular (figure 5.9), yet no clear perinuclear distribution was observed. The absence to date of a Golgi-like phenotype for the full-length fusion proteins may be of significance for the distribution of the CTF, however caution is required in ruling out a perinuclear phenotype given the consistently low transfection rates associated with these constructs.

5.7 Endoproteolysis of the full-length fusion protein generates separate pools of NTF and CTF in a proportion of cells expressing the transgene

To characterise the location of the full-length fusion protein within the cellular compartment, cells were stained with the anti-NTFPS1 antibody NT7 and the anti-CTFPS1 antibody 1039 and imaged for fluorescence. Unlike the NTPS1 fusion protein, which does not stain for the anti-PS1 C-terminal antibody 1039 (figure

4.12), full length PS1, as expected, co-localises with the 1039 antibody i.e. the PS1 C-terminus fused to the EGFP moiety shows co-localisation with 1039 staining (figure 5.10). Of more immediate interest is the staining pattern observed for the NT7 antibody in transfected cells expressing the full-length fusion proteins, since it appears that there are two separate CTF and NTF pools; one for the NTF as detected with the NT7 antibody, and one pool for the CTF-EGFP protein, indicating that the full-length transgene product undergoes endoproteolysis to generate both fragments. In figure 5.11 (upper row) NT7 stains the blob-like aggregates (as does 1039), however, in a proportion of cells exhibiting this phenotype, NT7 staining is distinct from the green fluorescence generated by the C-terminus EGFP moiety, of which the latter shows a predominantly reticular pattern of distribution (figure 5.11, lower row).

Close examination of the middle panel of the bottom row shows that the lower of the two transfected cells is weakly fluorescent. In comparison NT7 staining shown in the adjacent panel is considerably stronger, indicating possible differences in the lifespan between NTF and CTF-EGFP molecules. Similarly, the earlier 923 antibody staining showed a distinct phenotype from that of the PS1CTF 1039 antibody, however, in this instance the NT7 phenotype is clearly blob-like and not perinuclear, unlike the 923 phenotype.

5.8 BFA treatment of Cos-7 cells expressing the full-length fusion protein

Previously it was shown that following BFA treatment of transfected cells, the NTPS1 fusion protein returned to the ER as opposed to the ERGIC-like compartment seen for BFA treated cells stained with the 923 antibody (figures 3.4). In light of the above finding that the full-length protein forms two separate pools in some cells expressing the protein, it was necessary to investigate whether this held true following BFA treatment i.e. do the PS1 fragments derived from the full-length fusion protein return to different cellular compartments in the presence of BFA? To answer this question, cells were treated with BFA as indicated previously (figure 5.9 row d). No vesicular/ERGIC-like staining was observed; rather the fusion protein remained distinctly ER-like, as per the earlier experiment when cells expressing the NTPS1 fusion protein were treated with BFA (see figure 4.10). This

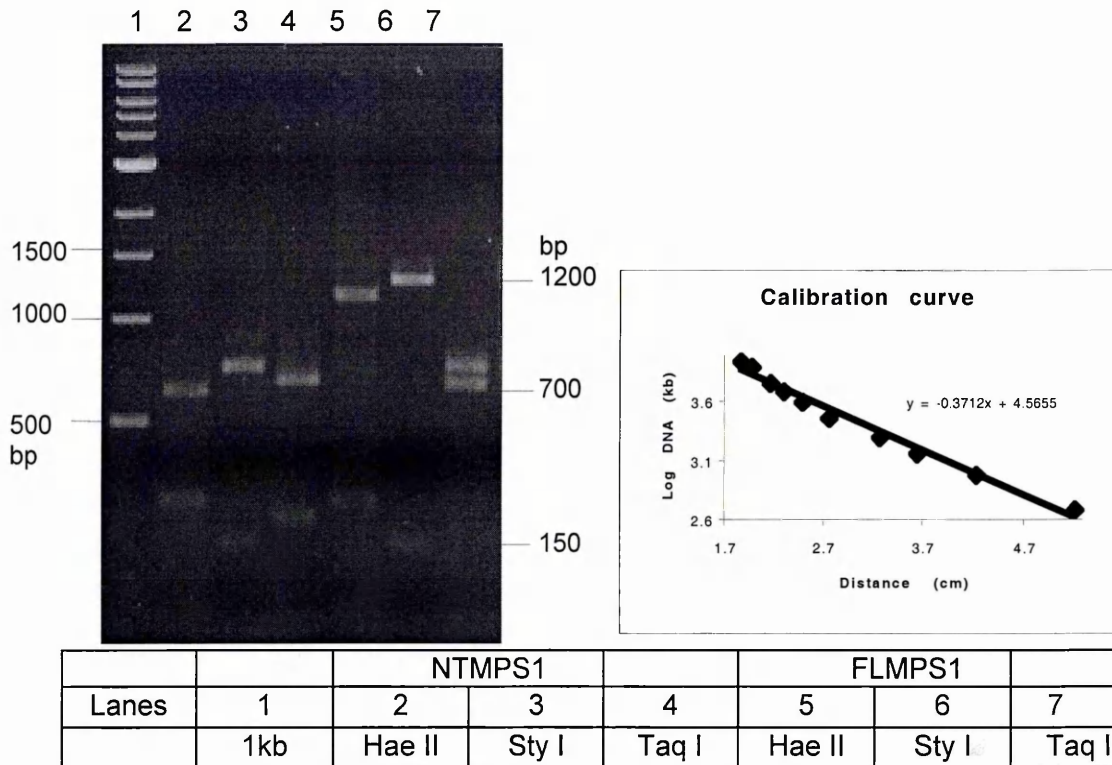
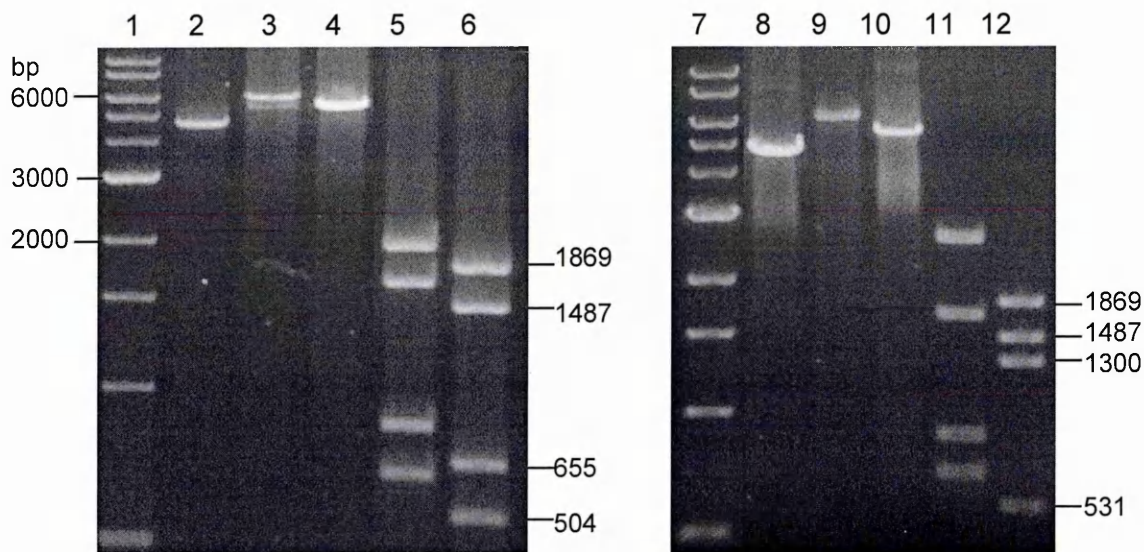


Figure 5.6. Restriction digestion of putative FLMPS1 and NTMPS1 cDNAs. To confirm that the identity of NTMPS1 and FLMPS1 a series of diagnostic restriction digestion assays were performed. The fragments generated by restriction digestion are close in size to the values calculated from a restriction map of PS1 (table 5.0 below). Recovered samples digested with Hae II, Sty I and Taq I (0.1 units/ μ g DNA). 1.5% TAE agarose gel stained with ethidium bromide. The size of the cDNAs were estimated by linear regression analysis.

Table 5.0. Fragment sizes of PCR products following single site restriction digest (bp)

Restriction site	Full length PS1/ Full length mutated PS1		N-terminal PS1	
	Predicted	Observed	Predicted	Observed
Hae II	258, 1153	225, 1235	258, 598	217, 539
Sty I	155, 1256	164, 1440	155, 701	161, 835
Taq I	683, 728	597, 708	173, 683	196, 607



Lanes	1	2/8	3/9	4/10	5	6	7	11	12
	1 kb Ladder	pEGFP	pEGFP-FLMPS1	pEGFP-NTMPS1	pEGFP-NTMPS1	pEGFP-NTMPS1	1 kb Ladder	pEGFP-FLMPS1	pEGFP-FLMPS1
Restriction enzyme		Xho I	Xho I	Xho I	Hae II	Sty I		Hae II	Sty I

Figure 5.7 Single restriction digest of pEGFP, and putative pEGFP-containing FLMPS1 and NTMPS1 plasmids. Plasmids digested with Hae II, Sty I and Xho I (0.1 unit/0.1 mg/ml) for 1 hour at 37°C. Samples analysed on a 1.5% TAE agarose gel stained with ethidium bromide.

Table 5.1 Comparison of fragment sizes (bp) generated by Hae II, Sty I and Xho I single restriction digestion of putative pEGFP-NTMPS1 and pEGFP-FLMPS1. Calculated values obtained from a restriction map of pEGFP.

pEGFP-NTMPS1				pEGFP-FLMPS1			
Hae II		Sty 1		Hae II		Sty 1	
Calculated	Observed	Calculated	Observed	Calculated	Observed	Calculated	Observed
2014	2138	1809	1869	2423	2475	1809	1907
1675	1724	1499	1487	1675	1771	1499	1527
896	820	770	655	896	861	1334	1300
728	686	610	504	728	663	610	531
Fragment sizes (bp) following Xho I restriction digest							
pEGFP		pEGFP-NTMPS1		pEGFP-FLMPS1			
Calculated	Observed	Calculated	Observed	Calculated	Observed		
4737	4895	5610	5576	6200	6267		

The NTMPS1 fusion protein phenotypes are identical to those of NTPS1

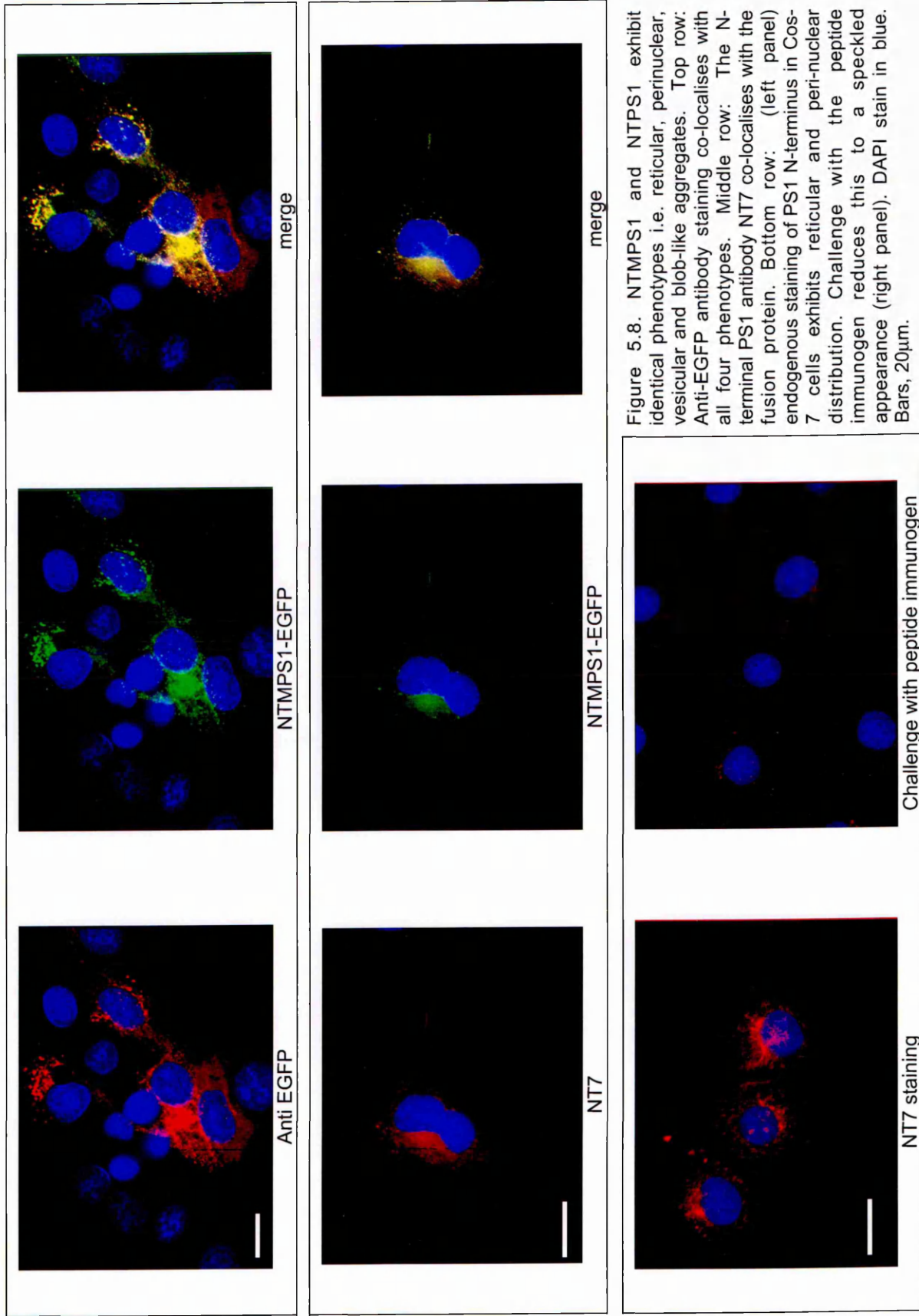


Figure 5.8. NTMPS1 and NTPS1 exhibit identical phenotypes i.e. reticular, perinuclear, vesicular and blob-like aggregates. Top row: Anti-EGFP antibody staining co-localises with all four phenotypes. Middle row: The N-terminal PS1 antibody NT7 co-localises with the fusion protein. Bottom row: (left panel) endogenous staining of PS1 N-terminus in Cos-7 cells exhibits reticular and peri-nuclear distribution. Challenge with the peptide immunogen reduces this to a speckled appearance (right panel). DAPI stain in blue. Bars, 20µm.

result shows that transfected cells expressing the fusion protein do not display differences in N- or C-terminal PS1 distribution following BFA treatment. Taken together these data suggest that the two separate PS1 pools form following cleavage of the full-length molecule within the ER, and that these pools have different turnover rates.

5.9 Western analysis of Cos-7 cells expressing FLPS1-EGFP, FLMP51-EGFP and NTMP51-EGFP fusion proteins

Cos-7 cells were transfected with pEGFP and the full-length and N-terminus PS1 constructs. Twenty-four hours post transfection cells were separated into soluble and membrane fractions and analysed by SDS PAGE. From figure 5.12, non-transfected control cell fractions did not stain with the anti-EGFP antibody (lanes 2 and 3), nor the membrane fraction prepared from cells transfected with pEGFP (lane 5). Anti-EGFP antibody staining of the soluble fraction (lane 4) resolves a single immunoreactive band of approximately 26 kDa, close to that predicted for EGFP (27 kDa). The absence from lanes 6-11 of a single band corresponding to EGFP would indicate that the EGFP moiety remains attached to the fusion constructs and does not undergo cleavage. As with the earlier Western blot for NTPS1-EGFP (figure 4.6), immunoreactive bands are absent from soluble fractions prepared from cells expressing the three new fusion proteins. In lane 11 the NTMP51-EGFP membrane fraction shows several bands, two of which approximate to 57 kDa and 127 kDa, very close in size to those bands seen for the NTPS1 fusion protein (figure 4.6) which correspond to the sum of the individual sizes of both the EGFP moiety and the N-terminus of PS1 (62 kDa). As before, the band at ~127 kD may represent aggregation of the fusion protein (figure 5.12, lane 11).

The blotting profiles obtained for both full-length fusion proteins are identical. Immunoreactive bands corresponding to the sum of the individual sizes of both the EGFP moiety (27 kDa) and full-length PS1 (55 kDa) resolve at approximately 83 kDa, very close to the predicted size of the full-length PS1 fusion protein (lanes 7 and 9). The strongly staining nature of these bands suggests that the fusion holoprotein is the predominant species. From figure 5.11 the C-terminus

PS1-EGFP moiety remains distinct from NT7 antibody staining in a proportion of cells expressing the full-length fusion constructs. Close examination of figure 5.12, lanes 7 and 9 at ~47 kDa reveal faint bands approximate in size to those expected if the full-length fusion proteins undergo endoproteolysis to yield C-terminus PS1-EGFP. Smaller bands for all three constructs at ~30 kDa or less may represent proteolytic fragments generated as the result of physiological specific cleavage events e.g. caspase activity, or could be artefacts produced due to the manner in which the tissue was prepared (Dewji et al, 1997).

As with the N-terminal fusion proteins, the full-length proteins show additional higher molecular weight bands, in this case at approximately 132 and 155 kDa, again possibly representing aggregation of the fusion proteins. Whereas consistently low transfection rates were observed for the full-length constructs, membrane fractions blot with a comparable intensity to that of NTMPS1 (compare lanes 7 & 9 with lane 11) adding weight to the notion that the holoprotein or CTF has a more rapid turnover.

5.10 Chapter summary

In summary, PCR was used to construct mutant PS1 cDNA by a two-stage process. The phenotypes displayed by the fusion proteins in a variety of cells are identical as is their immunoblotting profiles when comparing like with like, and the various phenotypes displayed are not a product of the fixation process. In all four constructs EGFP immunoreactivity occurs within the membrane-only fraction indicating correct folding of the fusion proteins consistent with their maturation from the ER to the Golgi, though the presence of the full-length fusion protein within the Golgi compartment is yet to be established. One of the stated intentions within this chapter was to assess what effect the L235P FAD mutation would have on the trafficking of the fusion proteins. The introduction of the mutation within the fusion protein and its expression by several mammalian cell lines appears to have no effect on its distribution as evidenced by the identical phenotypes for all four constructs, ie FLPS1-EGFP vs FLMPS1-EGFP, and NTPS1-EGFP vs NTMPS1-EGFP. Additionally, the difference in C- and N-terminal PS1 fragment distribution indicates that the full-length molecules undergo endoproteolysis, and that CTF-

EGFP turnover exceeds that of the NTF, which appears to aggregate more readily as seen for NTPS1-EGFP and NTPS1 derived from the full-length fusion proteins. The fluorophore intensity and transfection rate of NTPS1-EGFP exceeds that observed for the full-length molecules suggesting a greater stability for this fragment.

Full-length PS1-EGFP displays reticular, vesicular and blob-like aggregate phenotypes

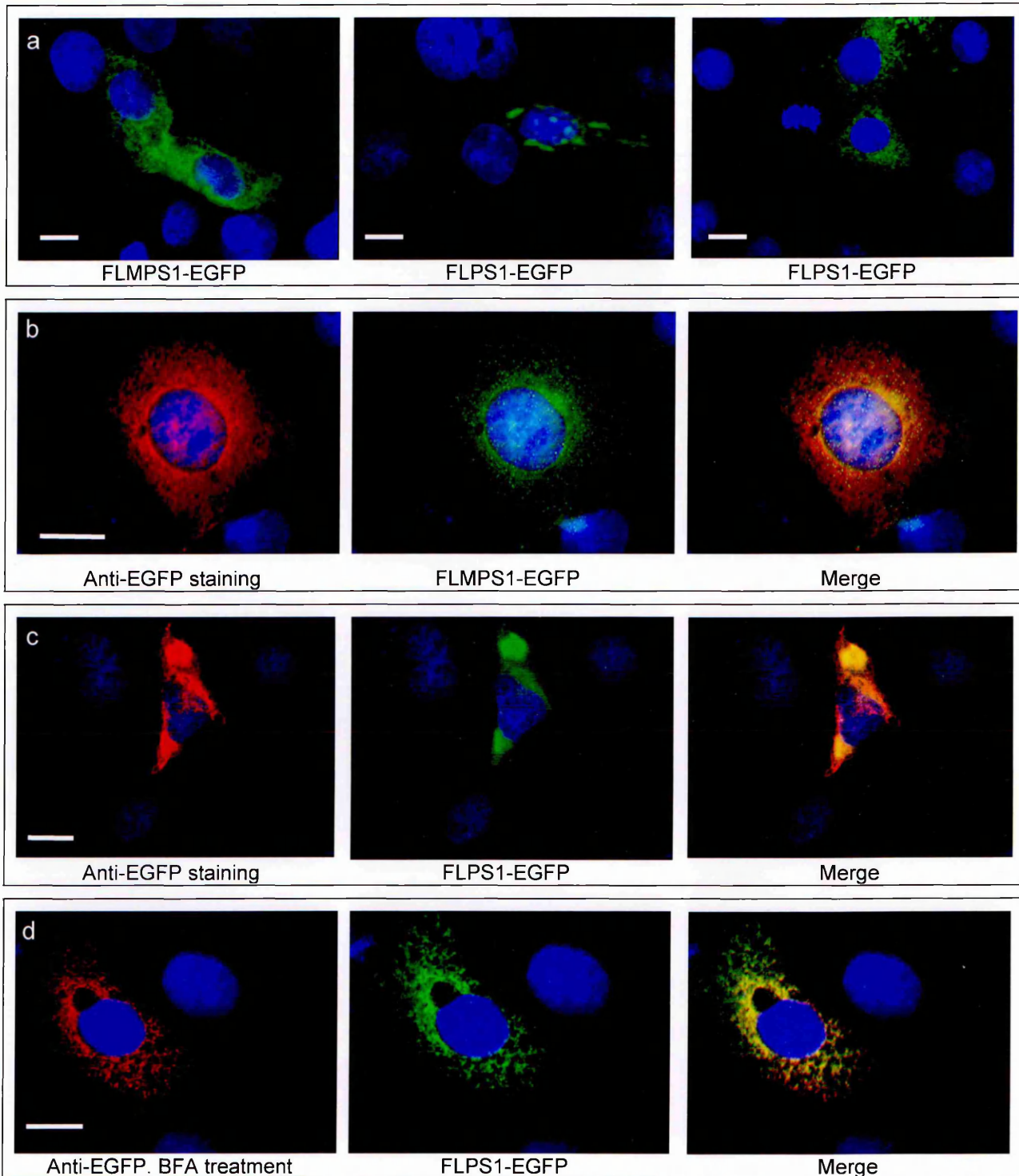


Figure 5.9. Phenotypes displayed by full-length proteins. (a) Cos-7 cells expressing the FLPS1 or FLMPS1 fusion proteins show no difference in distribution when compared with each other or with NTPS1, with the exception of the peri-nuclear phenotype, which to date, has not been observed for the full-length molecules. (b) and (c) The anti-EGFP antibody stains all phenotypes exhibited by the fusion proteins. The distinct staining pattern displayed by the anti-EGFP antibody indicates that the EGFP moiety is not cleaved from the fusion protein. (d) BFA treatment of transfected cells results in a reticular distribution of the fusion as with the NTPS1 molecules (compare with figures 3.4 & 4.10). DAPI stain in blue. Bars, 20 μm.

1039 staining co-localises with the full-length PS1 fusion proteins

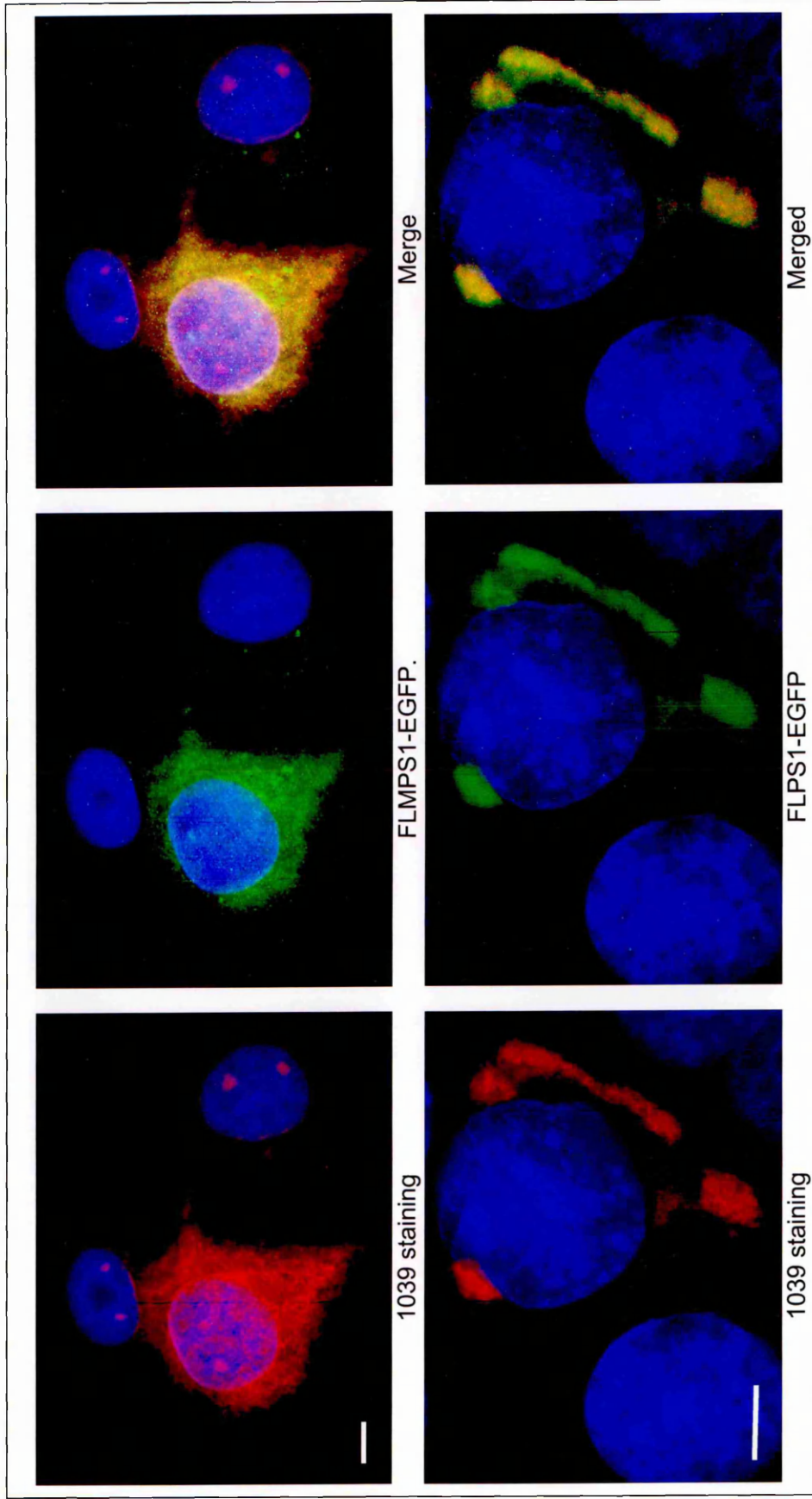


Figure 5.10. Transfection of Cos-7 cells with the full-length fusion constructs. Top row: 1039 staining co-localises with the FLMPS1 fusion protein. Although visible through the microscope, staining of endogenous PS1 in neighbouring non-transfected cells could not be captured in the same frame as the 1039 antibody staining due to differences in fluorescent intensity. Bottom row: 1039 staining co-localises with the blob-like aggregate phenotype displayed by FLPS1-EGFP. DAPI stain in blue. Bars, 10 μ m.

NT7 staining of the blob-like aggregate phenotype is distinct from that of the C-terminus PS1-EGFP moiety

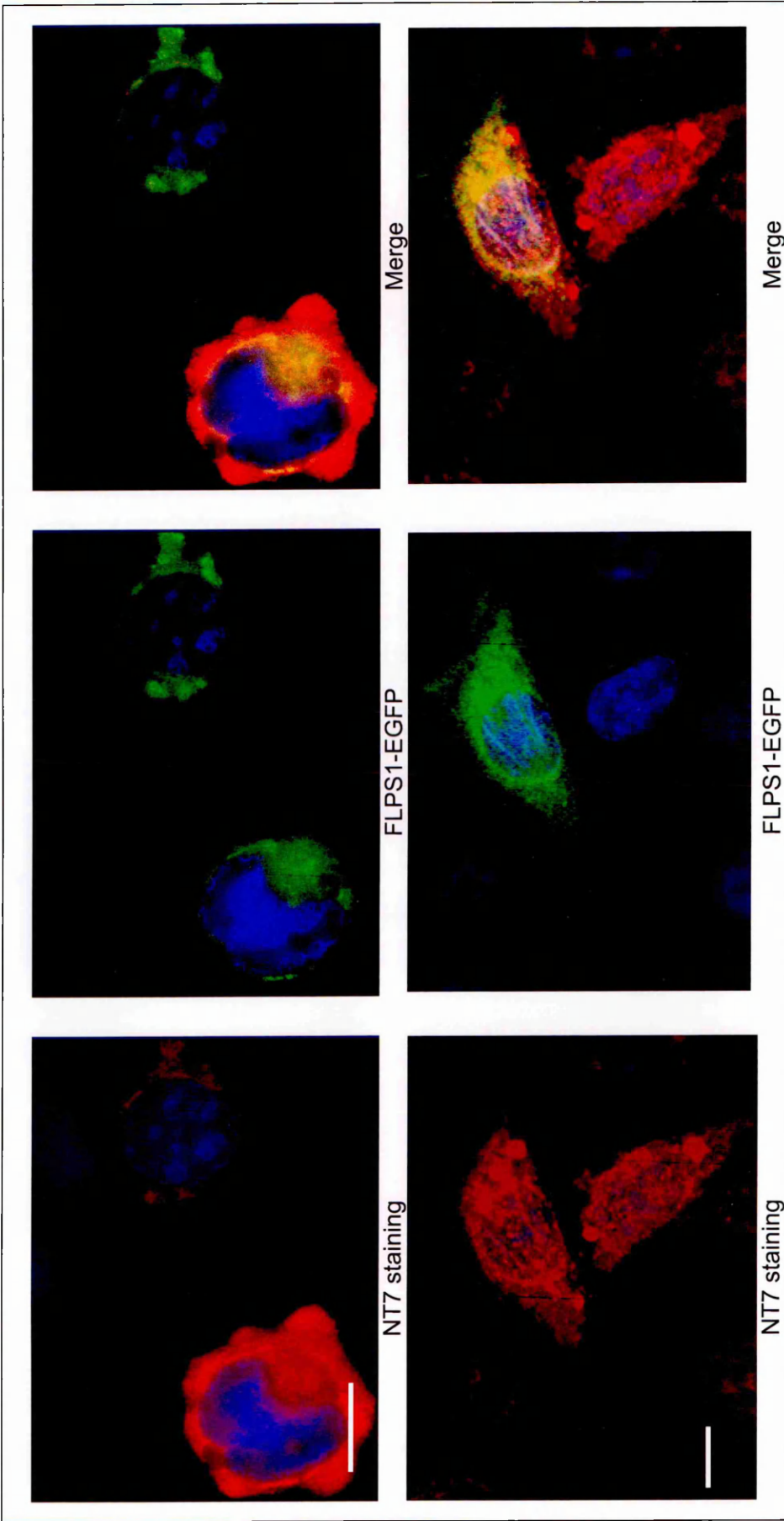
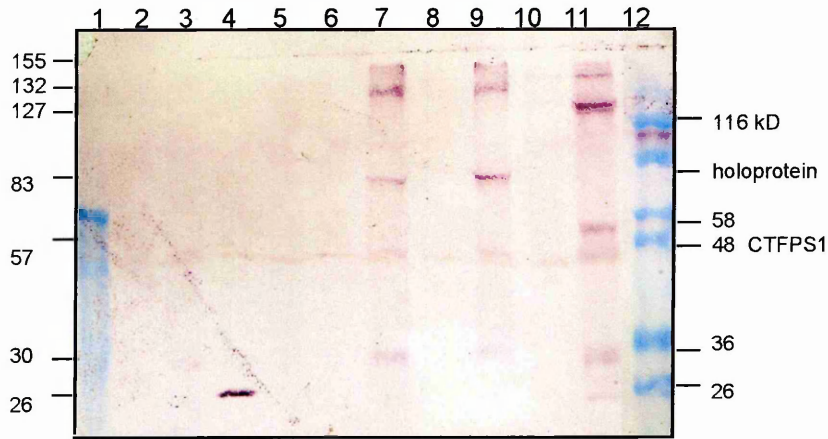


Figure 5.11. Transfection of Cos-7 cells with the full-length fusion constructs. Top row: NT7 staining shows partial overlap with the full-length fusion protein. Bottom row: NT7 antibody staining is reticular in adjacent non-transfected cells. Close examination of the merged image reveal NT7 staining of blobs remains distinct from the fusion protein. DAPI stain in blue. Bar 20 μ m.

Western analysis of NTMPS1, FLPS1, and FLMPS1 fusion proteins



LANES:

1. 1 blue
2. Control soluble fraction
3. Control membrane fraction
4. EGFP soluble
5. EGFP membrane
6. FLPS1-EGFP soluble
7. FLPS1-EGFP membrane
8. FLMPS1-EGFP soluble
9. FLMPS1-EGFP membrane
10. NTMPS1-EGFP soluble
11. NTMPS1-EGFP membrane
12. 7 blue

Predicted mol wt for fusion proteins (approx):

EGFP	27 kDa
C-terminal PS1-EGFP	47 kDa
FLPS1-EGFP	82 kDa
NTPS1-EGFP	62 kDa

Figure 5.12 Cos-7 transfected with pEGFP and PS1-EGFP fusion constructs were separated into soluble and membrane fractions. Samples analysed by 10% SDS/urea PAGE gel stained with anti-EGFP antibody.

6.0 Introduction

Having successfully generated the additional constructs the biological properties and functional relevance of the fusion proteins was investigated. Cells expressing the fusion protein were stained with antibodies to the cell compartment, anti- β -catenin and anti-APP. Additionally, functional aspects of the fusion protein were considered, in particular, their ability to cleave APP. Thus to measure $A\beta$ generation in stable APP₇₇₀-CHO cells transfected with the fusion protein, a bicine SDS PAGE gel was prepared since this can discriminate between the $A\beta_{40}$ and $A\beta_{42}$ peptides.

6.1 Reduction in antibody staining of the ER resident proteins Colligin (Hsp47) and PDI

To investigate the identity of the compartment in which the fusion protein resided, several antibodies specific to cell marker proteins were used in immunolocalisation experiments. All three fusion proteins exhibited localisation to varying degrees with the ER markers Colligin and PDI (data not shown). Only the NTMPS1-EGFP fusion protein localised with the anti-Golgi antibodies Mannosidase II, GalNac and Golgin 245. The lack of a perinuclear phenotype in cells expressing the full-length proteins cannot be ruled-out since the transfection rate for these constructs was significantly less when compared to NTMPS1-EGFP.

Unexpectedly, in a proportion of cells expressing both full-length and truncated fusion proteins and in particular cells exhibiting the blob-like aggregates, markers for both the ER and Golgi compartments were either significantly reduced and/or dispersed to such a degree as to suggest that these compartments have fragmented. Colligin and PDI antibody staining was reduced in cells over-expressing both full length and truncated fusion proteins (figure 6.0). Antibody staining was either considerably weaker in transfected cells compared to neighbouring, non-transfected cells or else antibody staining exhibited a vesicular distribution pattern. Colligin staining was most affected compared to the loss in PDI staining, though both show vesicle-like structures

scattered throughout the cytoplasm, possibly indicating fragmentation of the ER (rows a-c).

6.2 Reduction in antibody staining of Golgi-associated proteins Mannosidase II and GalNac.

As with the ER markers, there were visible differences in antibody staining of the medial Golgi protein Mannosidase II, and the trans Golgi protein GalNac in Cos-7 cells expressing both full-length and truncated PS1 fusion proteins (figure 6.1). Both antibodies show reduced staining compared to neighbouring cells which typically display a peri-nuclear phenotype. Mannosidase II staining is barely detectable in cells exhibiting the blob-like phenotype or those cells where the fusion protein has occupied the majority of the cell cytoplasm. GalNac staining appears to localise with the juxta-nuclear blob-like aggregate. The fragmented appearance of the GalNac antibody staining contrasts to the classic, stack morphology displayed by non-transfected neighbouring cells. Additionally, some cells expressing moderate levels of the fusion protein also showed a reduction in GalNac staining compared to neighbouring non-transfected cells (see figure 4.9, middle row).

The alterations in the structure of the ER and Golgi compartments indicate that moderate to high levels of the fusion protein may disturb intracellular trafficking or exhibit toxicity in some cells.

6.3 β -Catenin does not associate with NTMPS1-EGFP in Cos-7 and HEK293 cells

PS1 has been detected as a high molecular weight complex in vivo (Seegar et al, 1997; Capell et al, 1998), associated with several co-factors such as Nicastrin, APH, PEN2 and β -catenin. The latter has been implicated in cell-cell interaction and signalling in the Wnt pathway. PS1 interaction with β -catenin regulates levels of the protein by its association with GSK-3 β that targets β -catenin for proteosomal destruction via its phosphorylation motif. PS1 FAD mutations alter the trafficking of β -catenin arising from a dominant 'gain of aberrant function'. Lithium induced Wnt activation in FAD human fibroblasts

decreases the nuclear trafficking of β -catenin compared to wild type fibroblasts (Nishimura et al, 1999a).

To investigate what effect the fusion protein had on β -catenin levels and whether both proteins formed a complex within the cell, Cos-7 and HEK293 cells expressing the truncated fusion proteins were stained with an anti- β -catenin antibody and imaged by fluorescent microscopy (figure 6.2). β -catenin antibody staining is present at the cell membrane/cell-cell contacts and within the cytoplasmic of HEK293 and Cos-7 cells. Additionally, β -catenin staining is just discernable in the nuclei of both cell types regardless of whether the fusion protein is being expressed, and that this expression does not appear to influence the level of antibody staining. As shown in figure 6.2, β -catenin does not localise with the NTMPS1-EGFP fusion protein, nor does it seem that the fusion protein alters this phenotype compared to untransfected/low level expressers in adjacent cells. In this experiment there is no evidence that mutant NTMPS1-EGFP affects β -catenin trafficking. The lack of NTF- β -catenin interaction is consistent with previous studies showing that the CTFPS1 or full-length PS1 but not NTF, contain the β -catenin binding domain (Murayama et al, 1998; Yu et al, 1998; Kang et al, 1999; Singh et al, 2001).

6.4 The fusion protein shows limited localisation with the anti-APP antibodies 874, 993 and DE2

One of the major pathological hallmarks of Alzheimer's disease is the deposition of APP-derived β -amyloid within the senile plaque of AD brains. APP proteolysis is dependent on α -, β - and PS1 associated γ -secretase activity to generate several proteolytic fragments. Three main APP species have been recognised: a 751 and a 770 amino acid protein commonly found in both neurons and non-neuronal cells, and a 695 amino acid protein found exclusively in neurons. Data from studies examining the proteolysis of APP reveal the presence of different peptide fragments at various points along the secretory pathway, i.e. ER, ERGIC, Golgi compartments, lysosomes/endosomes and the plasma membrane (many authors). However, a discrepancy exists between the ER location of the secretases responsible for the cleavage of APP, and the site of $A\beta$ generation. PS1, for instance, is localised to the ER/Golgi yet generation

Colligin and PDI antibody staining is reduced in some cells over expressing the fusion proteins

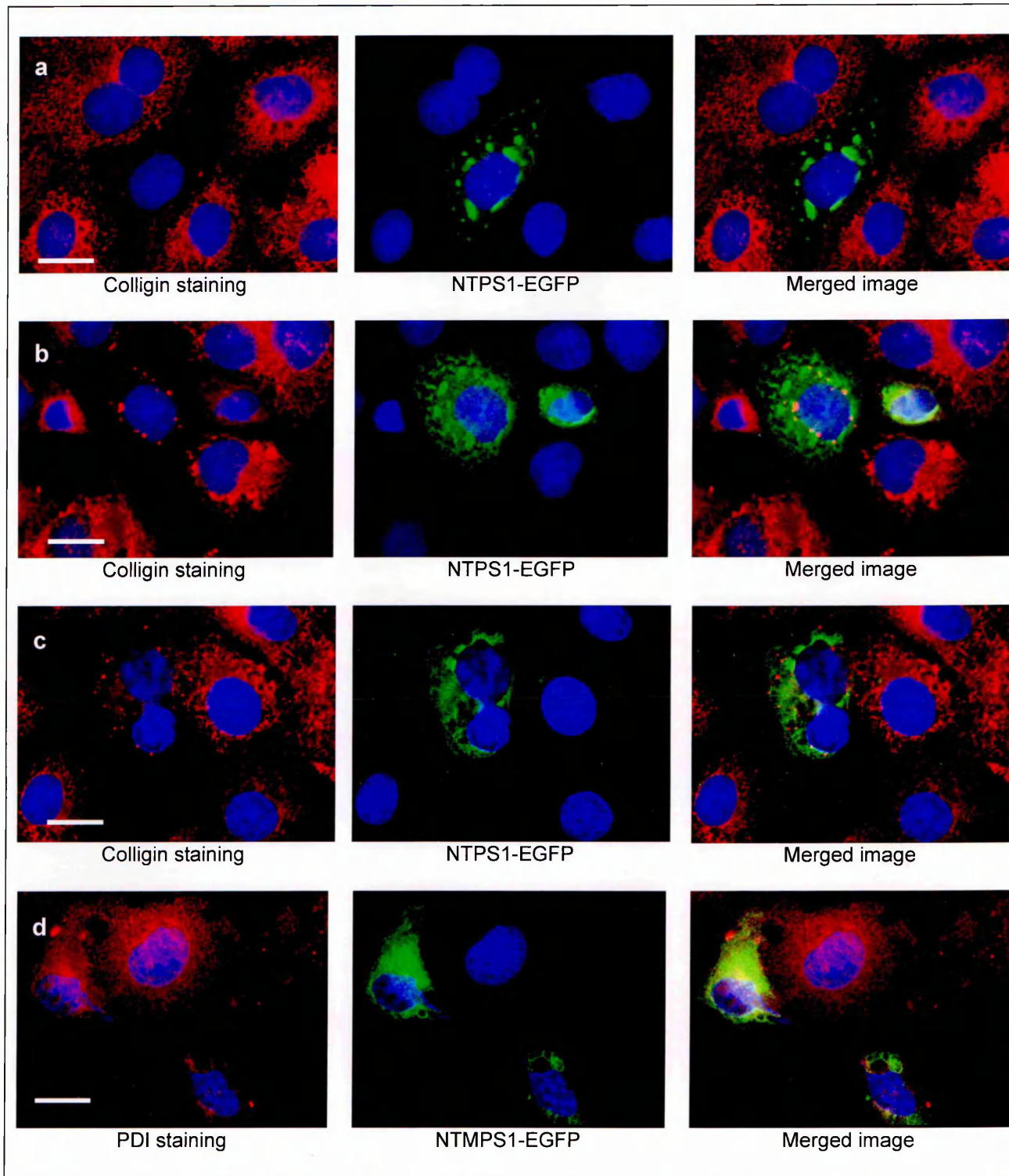


Figure 6.0. Altered ER antibody staining. A proportion of Cos-7 cells over-expressing both full length and truncated fusion proteins show reduced Colligin (rows a-c) and PDI antibody staining (rows d-f). Antibody staining was either considerably weaker in transfected cells compared to neighbouring non-transfected cells or else the antibody staining was fragmented. DAPI stain in blue. Bars 20 μ m.

Golgi antibody staining is reduced in some cells over-expressing the fusion protein

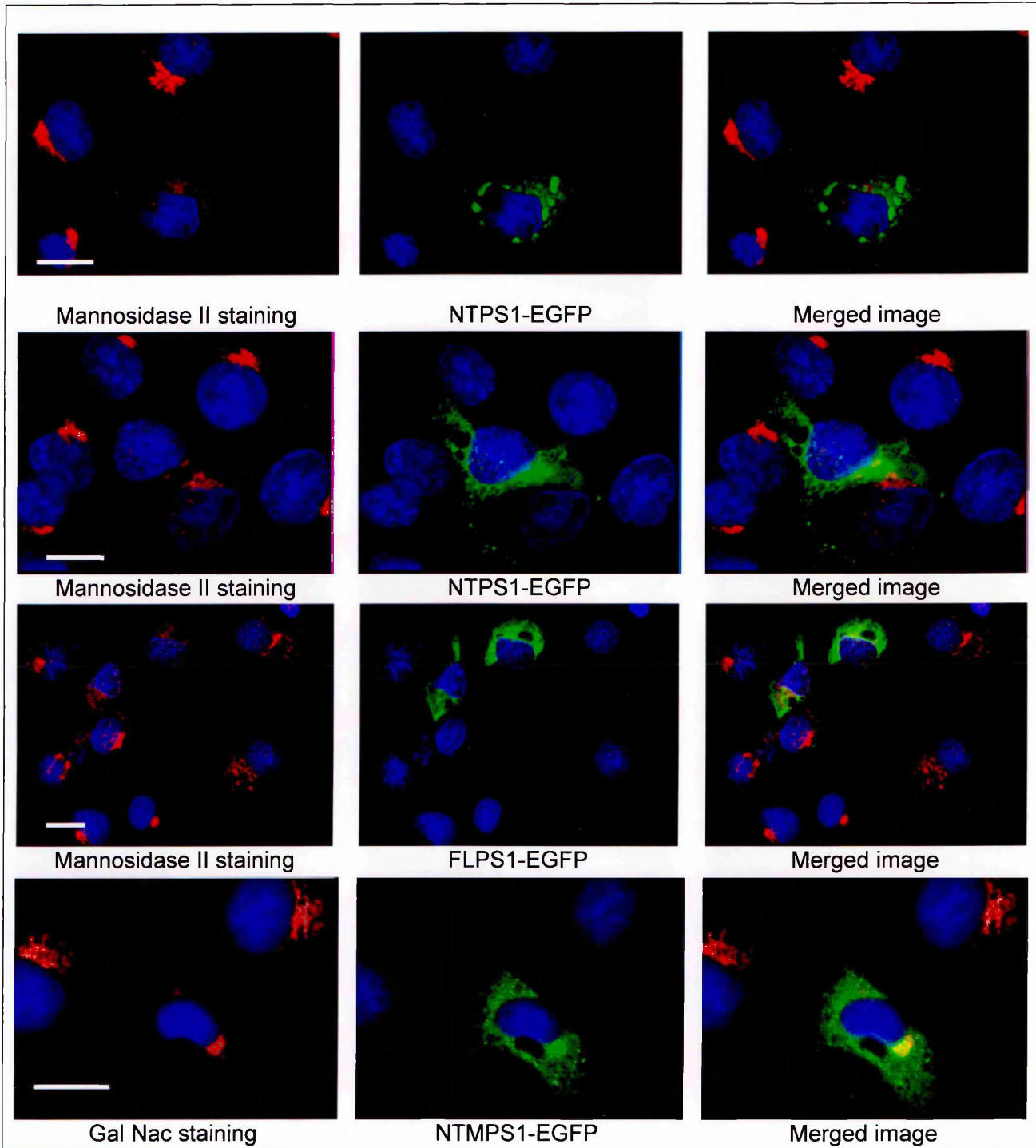


Figure 6.1. Altered Golgi antibody staining. A proportion of Cos-7 cells over-expressing both full length and truncated fusion proteins show reduced Mannosidase II and Gal Nac antibody staining. Antibody staining was reduced in transfected cells compared to neighbouring, non-transfected cells. GalNac staining is fragmented compared to neighbouring cells, which typically show ribbon/stack morphology. DAPI stain in blue. Bars 20 μ m.

β -Catenin does not localise with the NTMPS1-EGFP fusion protein

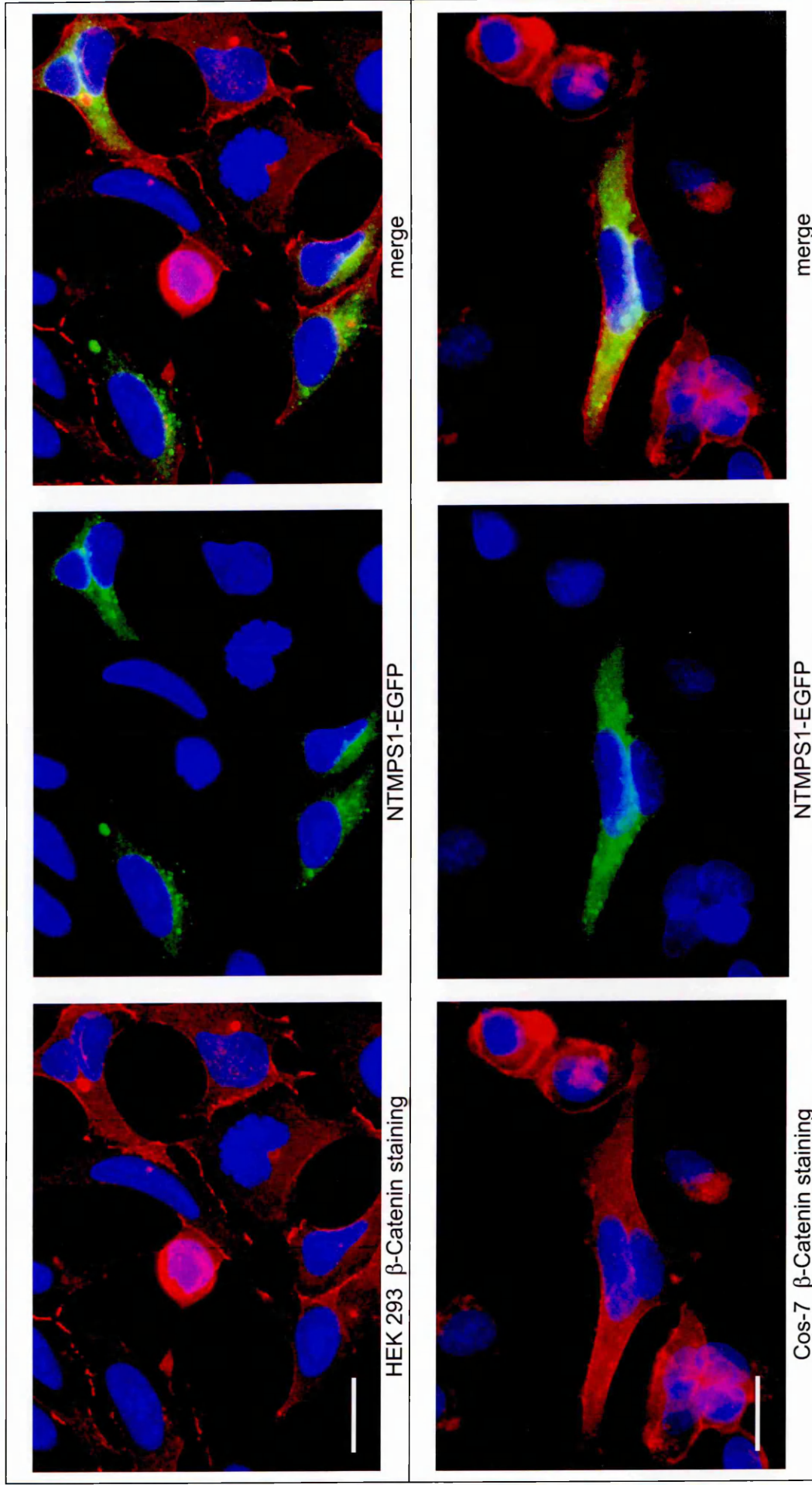


Figure 6.2. β -Catenin antibody staining of HEK293 (top row) and Cos-7 cells (bottom row) expressing NTMPS1-EGFP. β -Catenin is confined to the cytoplasm and cell-cell contacts and does not associate with the fusion protein. DAPI stain in blue. Bars, 20 μ m.

of the toxic A β ₄₂ peptide occurs within the ER/ERGIC, whilst the production of the A β ₄₀ is thought to occur more distally within the secretory pathway (Selkoe, 1999).

To investigate whether the fusion protein localises with APP within the cell compartment, transfected Cos-7 cells were stained with three polyclonal anti-APP antibodies referred to as 993, 874 and DE2. The 993 antibody recognises the 770 and 751 isomers of APP containing the KPI domain. Staining with the 993 antibody, which has been described previously, requires reduction and alkylation (Campbell et al, 1999). Staining with 993 reveals an unusual network of fibrils, which do not localise with any of the phenotypes displayed by the fusion protein (figure 6.3). The top row shows that the blob-like aggregates are intimately associated with the nucleus. This circumnuclear phenotype appears to disrupt the 993 pattern of staining in the immediate vicinity of the nucleus (figure 6.3, all rows).

The 874 antibody recognises the C99 stub derived from the action of β -secretase on APP. 874 staining of Cos-7 cells display a reticular, peri-nuclear and vesicular phenotype. Staining of cells expressing the fusion protein appears to partially overlap with the peri-nuclear phenotype, but not with the numerous vesicles scattered about the cell (figure 6.4). However, closer examination of the peri-nuclear phenotype exhibited by the fusion protein suggests that localisation with the 874 antibody is coincident since this phenotype appears to be composed of much larger vesicles compared to those stained by the 874 antibody, which are considerably smaller in diameter (figure 6.5, top row). This is seen more clearly by the vesicular phenotype, which does not localise with the 874 antibody (figure 6.4, middle row). The blob-like phenotype similarly does not localise with the 874 antibody and effectively excludes staining in the region occupied by the fusion protein (left panel, bottom row).

The DE2 antibody only recognises the 'free-end' C-terminus epitope of the β -secretase generated C99 stub and the α -secretase generated stub, thus uncleaved full-length APP is not recognised by the DE2 antibody. DE2 staining displays a largely reticular/ punctate and peri-nuclear phenotype (figure 6.5). Close inspection of the latter phenotype of neighbouring non-transfected cells reveals a cluster of vesicles reminiscent of the ERGIC. In cells expressing the fusion protein DE2 staining partially overlaps with the peri-nuclear and blob-like

aggregate phenotype but not the reticular or vesicular phenotype (figure 6.5). As with the 874 antibody, DE2 staining of the peri-nuclear located fusion protein may be coincident. Similarly, staining of the blob-like aggregate may also be coincident since the antibody staining is arranged as small vesicles, whereas the fusion protein appears opaque (figure 6.5, bottom row).

6.5 Detection and separation of synthetic $A\beta_{40}$ and $A\beta_{42}$ by bicine SDS PAGE

The aim of this next study was to investigate what affect wild type and mutant fusion proteins had on the generation of $A\beta_{40}$ and $A\beta_{42}$ peptides in a stable CHO-APP₇₇₀ expressing cell line transfected with the pNTMPS1-EGFP and pFL/FLMPS1-EGFP cDNAs. To date, attempts by other researchers at resolving $A\beta_{40}$ and $A\beta_{42}$ by conventional reverse-phase liquid chromatography, capillary zone electrophoresis, acid-urea-PAGE or SDS PAGE has not been successful. Previously, separation has proven difficult because of solubility problems and interaction of $A\beta$ with the separation matrix. To measure the metabolic fate of APP₇₇₀ a bicine SDS PAGE gel employed because of its ability to discriminate between the different $A\beta$ peptide species (Wiltfang et al, 1997).

To detect $A\beta$ production synthetic $A\beta_{40}$ and $A\beta_{42}$ was first used as a control to gauge the effectiveness of this gel system in discriminating between the two peptides. Various nanogram quantities of $A\beta_{40}$ and $A\beta_{42}$ were loaded onto the gel and immunoblotted using a polyclonal antibody AB10, that recognises both APP and $A\beta$. In the first experiment 10 ng and 50 ng of synthetic $A\beta_{42}$ were separated on gel and analysed by AB10 (figure 6.6, a). Immunoreactivity was greatest with an antibody dilution of 1:3 (50 ng $A\beta_{42}$), and least reactive at 1:30 dilution (50 ng). 10 ng of the peptide did generate any immunoreactivity.

Next, using the 1:3 antibody dilution, 1ng to 50 ng $A\beta_{40}$ was analysed by immunoblotting (figure 6.6, b). AB10 immunoreactivity detected $A\beta_{40}$ in the 10-50 ng range (lanes 4-6). $A\beta_{42}$ (lane 7) migrates at just over 4 kD, above $A\beta_{40}$, demonstrating size separation of the two peptides. To establish the limit of detection and test whether this system could resolve a mixture of the two peptides, varying peptide amounts were loaded and immunoblotted using a range of antibody dilutions (figure 6.6 c). AB10 was able to detect 5 ng of the peptide mixture at 1:50, and 25 ng at 1:400. 50 ng of the peptide mixture showed immunoreactivity with AB10 at 1:800. For comparison purposes, 50 ng

of peptide mixture was detected using ECL. AB10 antibody immunoreactivity was seen in the 1:200 -1:3200 dilution range for 50 ng A β ₄₀ and A β ₄₂ (fig. 6.6 d).

6.6 Immunoprecipitation of APP₇₇₀ from conditioned and complete media

To effectively measure the generation of A β peptides in cell cultures expressing the fusion protein requires immunoprecipitation of the conditioned media into which the A β ₄₀ and A β ₄₂ peptides are secreted. From the previous immunoblotting experiments it was established that the best antibody dilution/peptide quantity that gave a consistently clear signal was 1:100/50ng. Stable CHO-APP₇₇₀ expressing cell lines were transfected with the pNTMPS1-EGFP and pFL/FLMPS1-EGFP cDNAs. Transfection of CHO-APP₇₇₀ cells was confirmed by fluorescent microscopy. Condition media was removed following a 24 hour incubation period. As a control to test recovery, 50 ng of each peptide were added to a known volume of complete media. Immunoprecipitation of the samples was performed using the AB10 antibody at a 1:100 dilution (figure 6.7 a). APP immunoreactivity was detected at ~113 kD in complete media (lanes 2-4) and in conditioned media from transfected cells (lanes 6-8). A β immunoreactivity was detected in lane 5 (control), whereas recovered or secreted A β ₄₀/A β ₄₂ peptides were not detected in any of the control lanes or transfected samples. That the synthetic A β peptides were not recovered from complete media suggests that the AB10 antibody, whilst recognising the peptide by immunoblotting, cannot immunoprecipitate either A β ₄₀ or A β ₄₂ from solution.

The above result might be due to insufficient AB10 antibody at the immunoprecipitation stage. However, repeat experiments this time with higher concentrations of AB10 yielded the same result (data not shown). Given that the antibody recognises the same epitope in both APP and A β , the relative abundance of both the peptides within the culture medium might lead to competition for the AB10 binding site. Thus, excessive amounts of APP compared to A β might effectively out-compete A β antibody binding thereby explaining the APP immunoreactivity only.

To test this hypothesis, a second antibody that recognises APP but not A β , DP23/2, was used to twice-immunoprecipitate complete media containing

993 antibody staining does not localise with the fusion protein

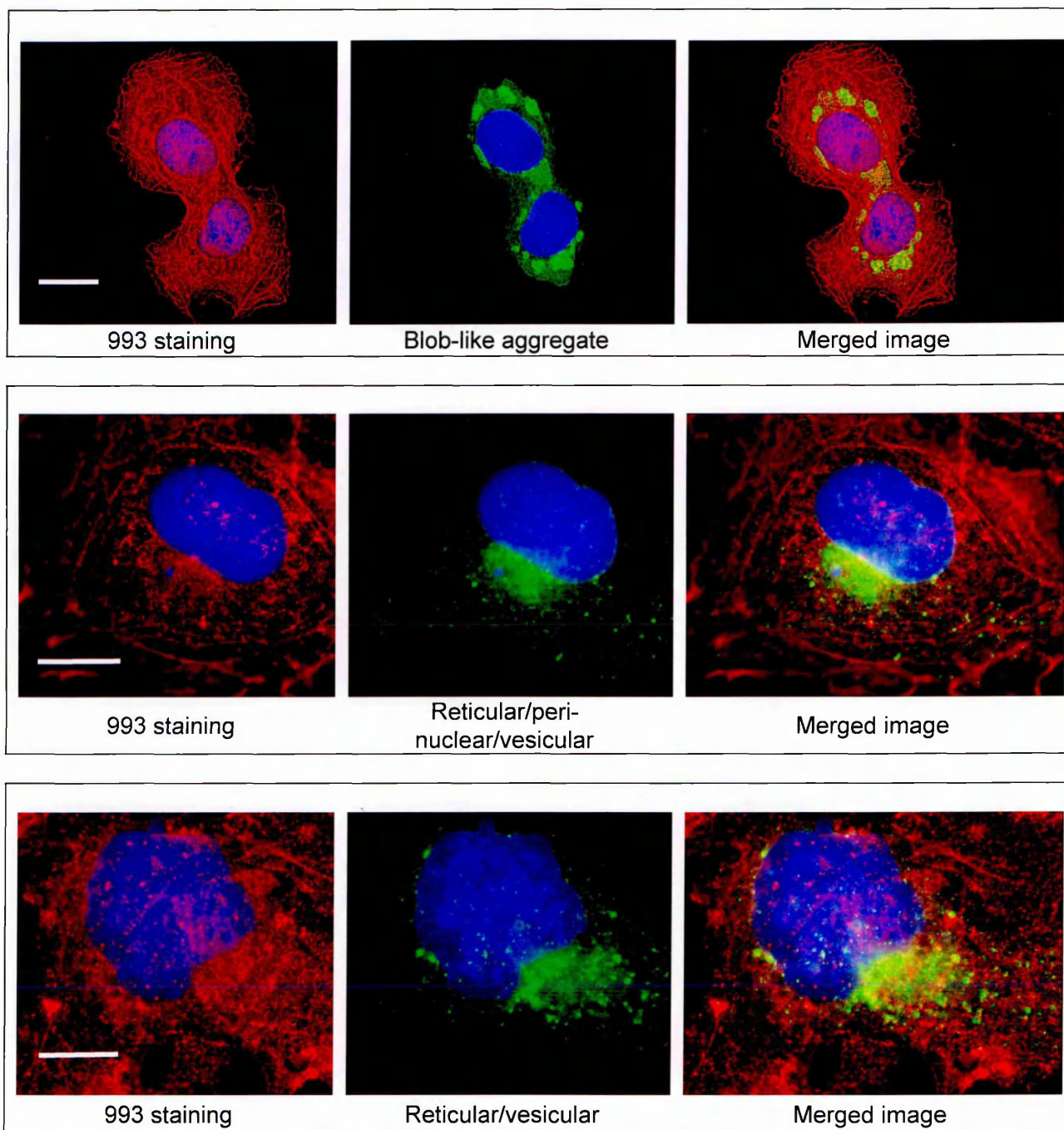


Figure 6.3. APP 993-antibody staining. Cos-7 cells transfected with pNTPS1-EGFP stained with reduced and alkylated α APP 993 antibody. 993 recognises the 770 and 751 KPI containing isomers of APP. The fusion protein displays a reticular, peri-nuclear and vesicular phenotype that does not localise with the 993 antibody. The 993 antibody displays a fibril pattern of staining. Notice the overall lack of vesicular 993 staining and disruption around the immediate vicinity of the nucleus. DAPI stain in blue. Bars, top and middle rows 20 μ m, bottom row 10 μ m.

874 antibody staining partially overlaps with the fusion protein

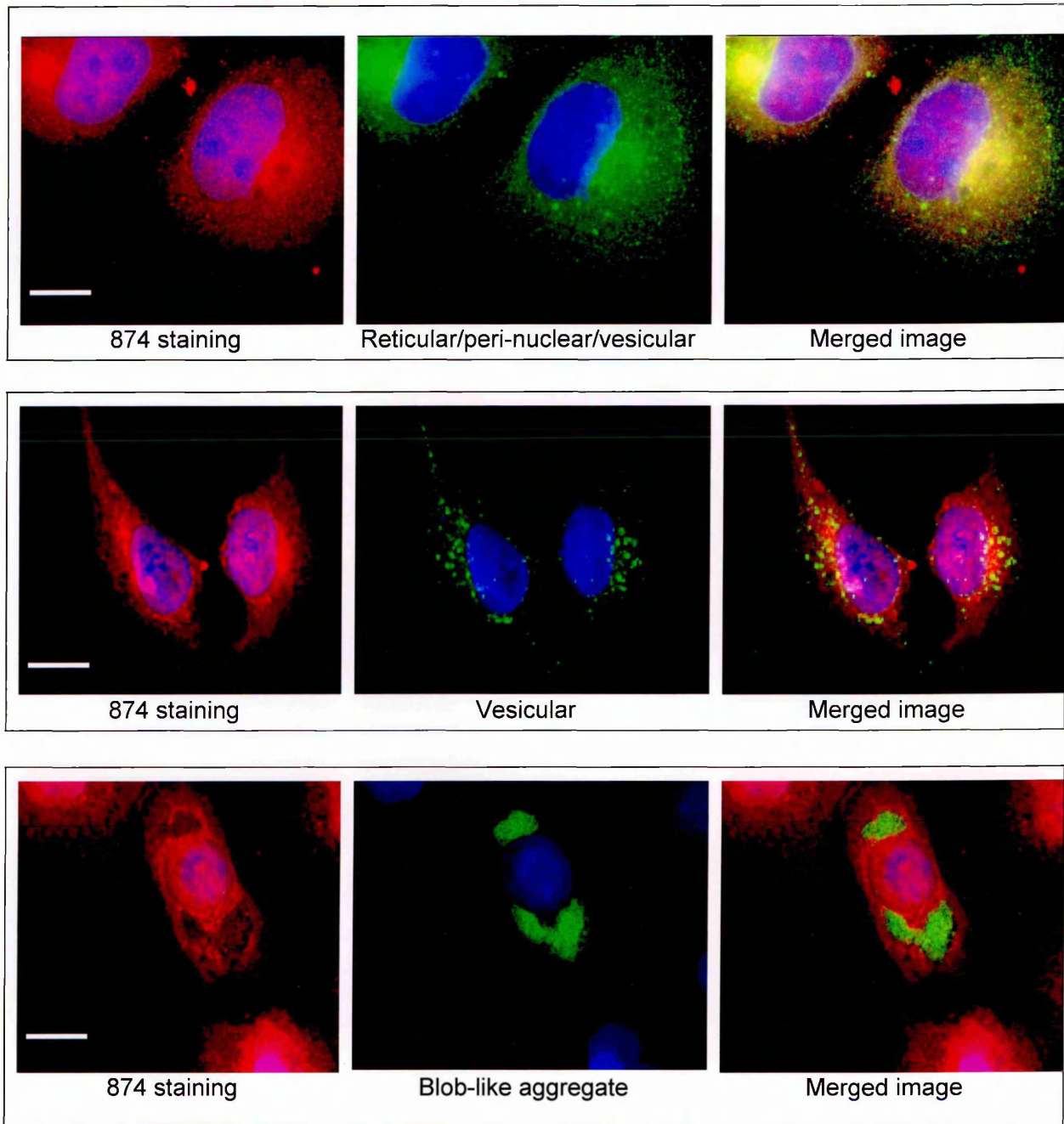


Figure 6.4. APP 874-antibody staining of Cos-7 cells expressing NTMPS1-EGFP. 874 staining display a reticular, peri-nuclear and vesicular phenotype. In transfected cells 874 staining partially overlaps with the peri-nuclear phenotype displayed by the fusion protein (top row) but not with the vesicular phenotype (middle row). The blob-like phenotype likewise does not localise with 874 antibody staining and effectively excludes 874 from the region occupied by the blob (lower row). DAPI stain in blue. Bars, 20 μm .

DE2 antibody staining partially overlaps with the fusion protein

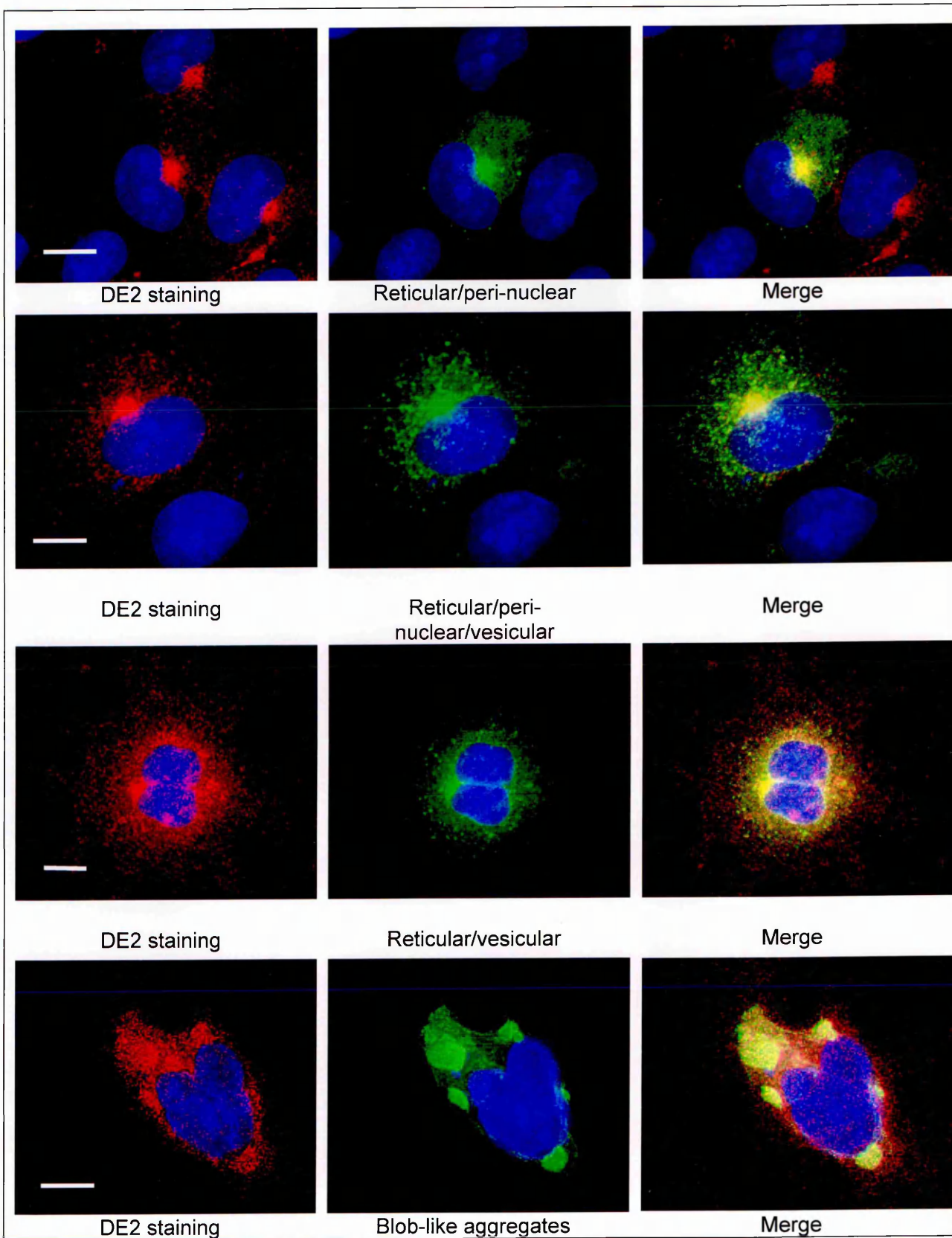


Figure 6.5. DE2 staining of Cos-7 cells expressing the NTMPS1 fusion protein. DE2 partially overlaps with the peri-nuclear and blob-like aggregate phenotype but not the reticular or vesicular phenotype. DAPI stain blue. Bars, 20 μ m.

50 ng each of the A β peptides. To ensure sufficient recovery of APP, three different volumes of DP23/2 were used. The resulting supernatant was then immunoprecipitated for a third time with the AB10 antibody in order to recover the A β peptides (figure 6.8 b).

Samples were immunoblotted with DP23/2 (lanes 2-5) and AB10 (lanes 7-9). Strong immunoreactivity was seen in lanes 2-4, but whether this smear represents APP is unclear. Presumably AB10 and DP23/2 APP staining intensities should be approximately equal. APP staining in lanes 7-9 representing the third immunoprecipitation is less intense compared to figure 6.7a, indicating that some APP had been removed by serial immunoprecipitation. As expected DP23/2 does not stain A β_{40} /A β_{42} (lane 5), unlike the AB10 antibody (lane 10). No synthetic A β_{40} /A β_{42} was detected by AB10 in those samples thrice immunoprecipitated even though APP immunoreactivity had decreased.

In the current investigation Tris buffer and anti-mouse beads had been used to immunoprecipitate APP, whereas RIPA buffer and protein-A beads had been specified in the protocol developed by Wiltfang et al, who previously described immunoprecipitation of APP derived A β (Klafki et al, 1996; Wiltfang et al, 1997). The current protocol was therefore modified to take account of the original conditions in which A β was immunoprecipitated. In addition to the above protocol modifications, the complete media containing A β peptides was reduced and alkylated since the DP23/2 antibody displays greater immunoreactivity for reduced/alkylated APP.

Following modifications to the immunoprecipitation protocol, complete media containing 50 ng A β peptides was immunoprecipitated with protein-A/DP23/2 or IgG beads/AB10 in RIPA or Tris buffer following reduction/alkylation. Samples were immunoblotted with the AB10 antibody. Overall, the modified protocol had little effect on the amount of APP immunoprecipitated. Similarly, under the changed conditions A β immunoreactivity was not detected (figure 6.8).

The earlier encounter with the 923 antibody whilst useful for immunofluorescence imaging defied attempts at Western blotting and immunoprecipitation. Similarly the AB10 antibody whilst able to detect both APP and the A β peptides would not immunoprecipitate A β . In conclusion, the

Detection of synthetic A β peptides by bicine SDS/PAGE

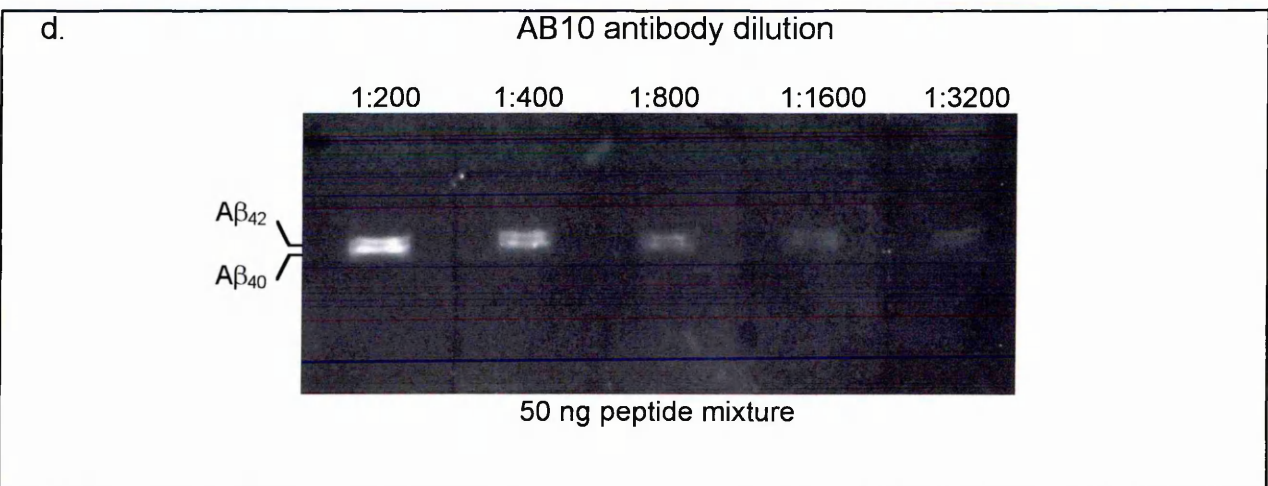
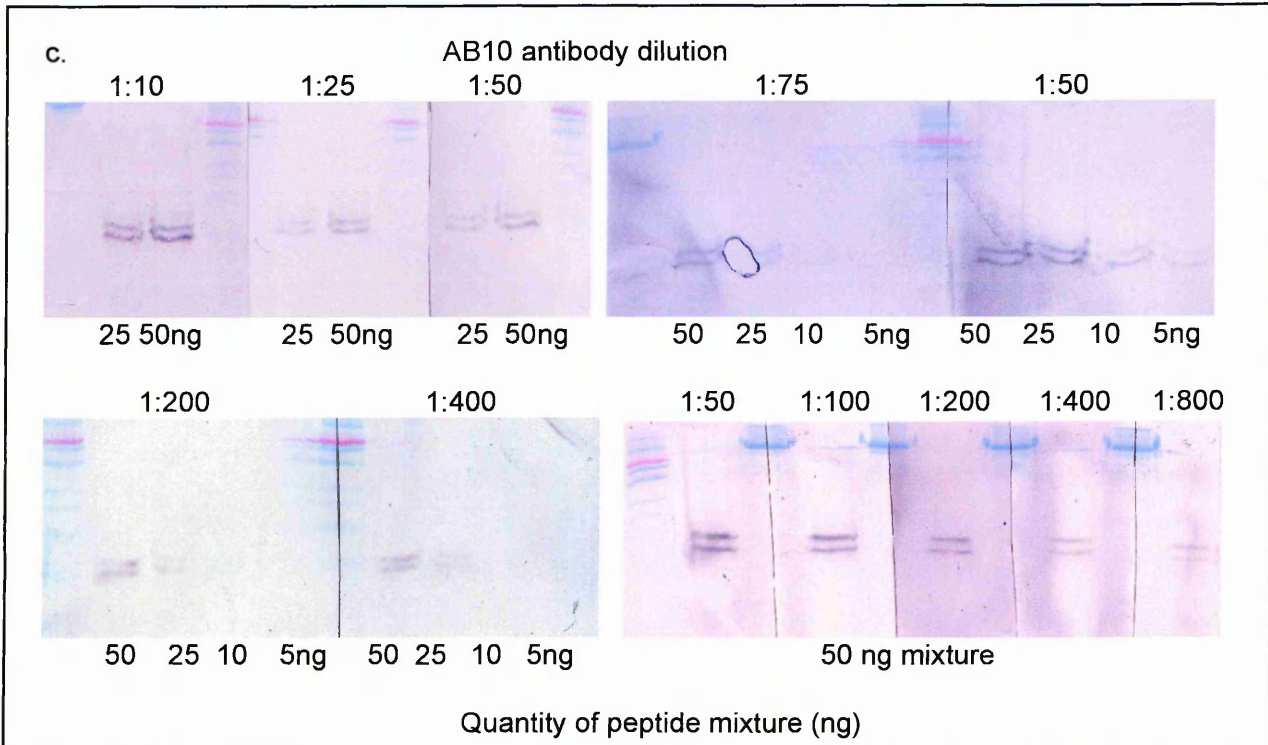
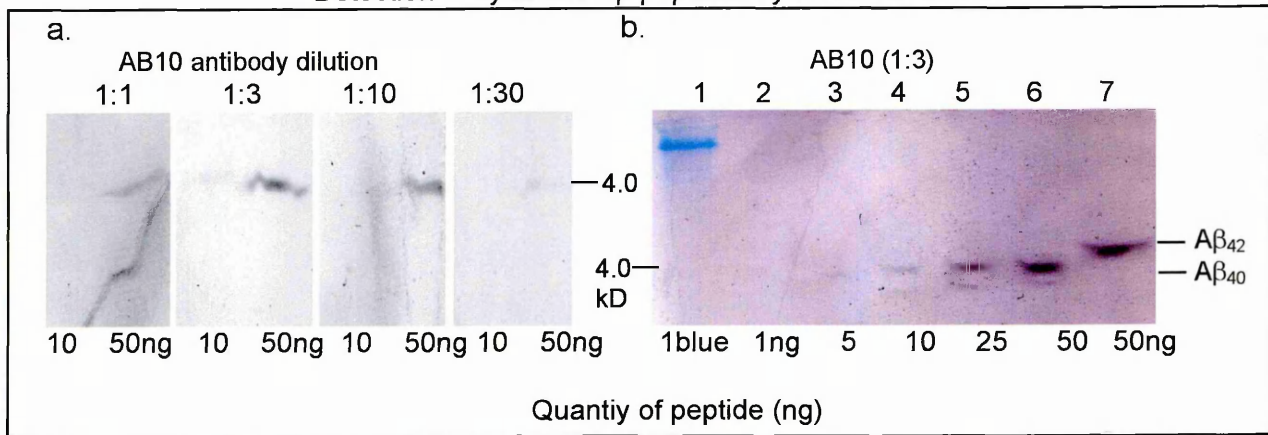


Figure 6.6. Detection and separation of synthetic A β_{40} and A β_{42} peptides by bicine SDS/PAGE. **a.** Detection of A β_{40} (10 and 50ng) by immunoblotting with AB10 (1:30). **b.** Detection of A β peptide (1-50 ng) by immunoblotting with AB10 (1:3). **c.** Resolution of varying amounts of peptide mixture immunoblotted with AB10 (1:10 -1:800). **d.** Detection of 50 ng peptide mixture by ECL. Peptides resolved by SDS 10% Urea Bicine gel. Samples immunoblotted with primary antibody AB10 and detected by alkaline phosphatase (a-c) or HRP (ECL) secondary antibody (d).

Immunoblotting of conditioned media detects secreted APP₇₇₀ but not synthetic or secreted A β peptides

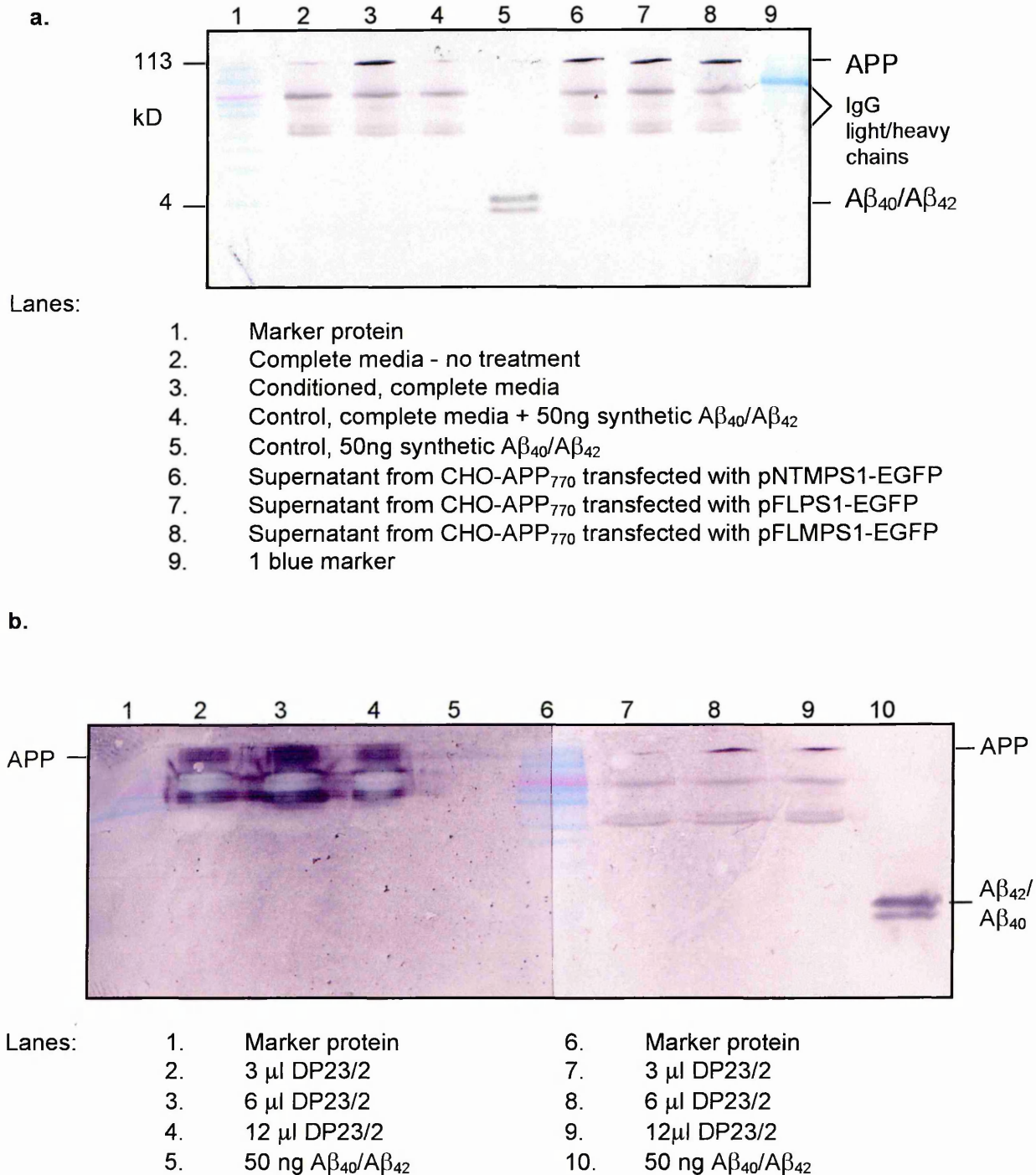


Figure 6.7. a. Immunoprecipitation of A β_{40} /A β_{42} from stable CHO/APP cell supernatant using anti-APP antibody AB10. Samples immunoblotted with AB10 (1:100). Transfection of CHO-APP₇₇₀ cells was confirmed by fluorescent microscopy. b. Immunoblotting of complete media containing 50 ng A β peptides. Samples twice immunoprecipitated with DP23/2, followed by a third immunoprecipitation with AB10. Three different DP23/2 volumes were used for the first two immunoprecipitations. Samples immunoblotted with DP23/2 (1:1000) lanes 2-5 or AB10 (1:100) lanes 7-10. Note, as expected both DP23/2 and AB10 stain APP₇₇₀, whereas DP23/2 does not recognise A β_{40} /A β_{42} . Samples resolved by SDS 10% Urea Bicine gel.

A β immunoreactivity absent following modifications to immunoprecipitation protocol

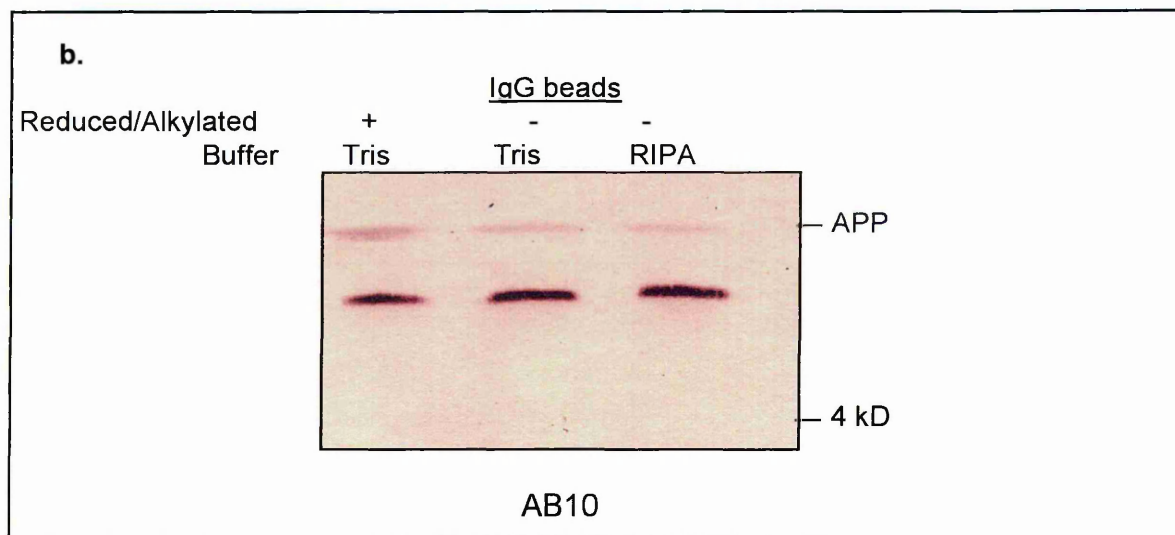
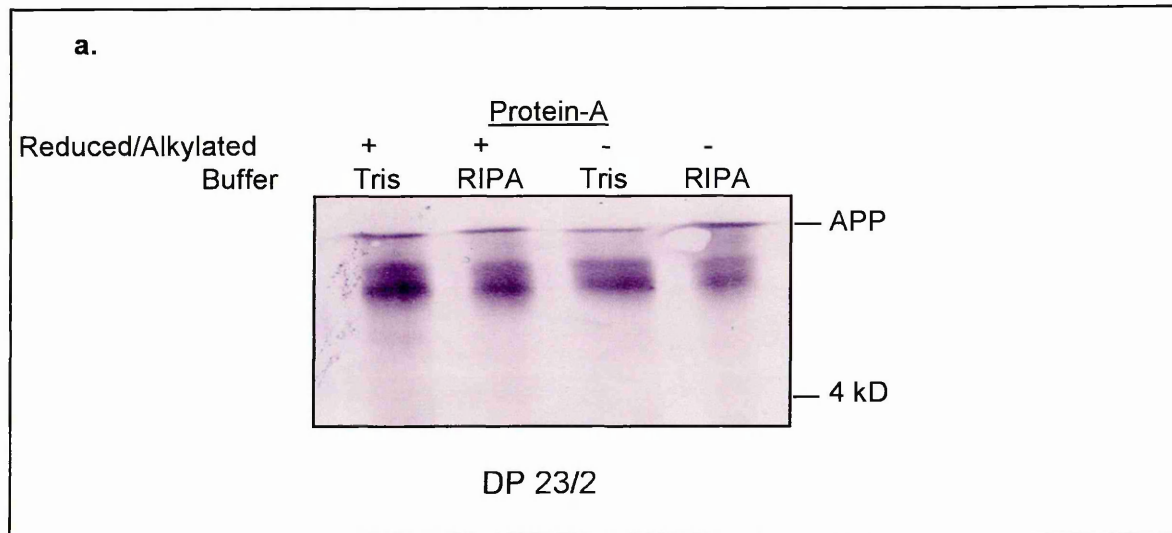


Figure 6.8. Complete media containing 50 ng A β 40/A β 42 was immunoprecipitated under varying conditions. Samples immunoprecipitated by DP23/2 (a) and AB10 (b). Samples resolved by SDS 10% Urea Bicine gel and immunoblotted with AB10.

bicine SDS PAGE gel system is able to resolve an admixture of A β ₄₀ and A β ₄₂ peptides detectable in nanogram quantities by the anti-APP/A β antibody AB10 using AP or HRP secondary antibodies. The inability of the AB10 to immunoprecipitate A β from solution or conditioned media would suggest that this antibody is epitope conformation specific.

6.7 Selection of HEK293 cells stably expressing full length and truncated PS1-EGFP

Several attempts at cloning a stable Cos-7 cell line expressing the truncated fusion protein failed. This lack of success was considered to be due technical difficulties, however in light of the earlier observation that ER and Golgi markers are severely reduced in transfected Cos-7 cells, it is feasible that cells may be unduly stressed by the presence of the fusion protein. As a consequence, over-expression of the fusion protein may be associated with toxic events that trigger a variety of cellular responses, such as apoptosis, thereby reducing the chances of selection. The extent to which a cell is affected by stress varies depending on the cell type and the cellular response elicited by the stressor. For instance, HEK293 and Neuro2a cells have been characterised as 'robust' and less susceptible to ER stress compared to other cell types such as Cos-7 cells (Imaizumi et al, 2001). The selection procedure was therefore repeated with the more robust HEK 293 cell line on account of their availability and their ease of transfection as evidenced by earlier transfection experiments.

HEK293 cells were transfected with FLPS1-EGFP and NTMPS1-EGFP cDNAs as described previously. Transfectants were treated with G418 and resistant colonies were trypsinised and diluted into a 96 well plate to yield individual clones. Confluent wells were split onto coverslips and analysed by fluorescent microscopy. Several stable cell lines expressing varying levels of the fusion proteins were obtained. The phenotypes displayed by the full length and truncated fusion proteins were typically reticular-like with dispersed circumnuclear, blob-like aggregates and vesicles (figure 6.9). Noticable was the absence of a phenotype typical of the Golgi apparatus in any of the cells imaged. Whilst the absence of a Golgi phenotype had been previously observed in cells transiently expressing the full-length proteins, the absence of this phenotype in NTMPS1-EGFP clones was unexpected. However, unlike

Cos-7 cells, which have a flattened, fried-egg-like appearance and are therefore ideally suited for microscopy, HEK293 cells due to their rounded-up morphology are more difficult to image, therefore the presence of a Golgi phenotype cannot be entirely ruled out.

The overall fluorophore intensity of all the stable expressers was considerably weaker compared to transiently transfected Cos-7 or HEK293 cells. On average a gain of +12/+18 was required to capture a given field of cells by the CCD camera. The fusion proteins in the NTMPS1-EGFP cells shown in figure 6.9 (top panel) have uniform fluorophore intensity, unlike some clones, which varied considerably such that neighbouring cells appear not to express the fusion protein (see figure 6.9, middle and lower panels). A simple explanation for the heterogeneity in protein levels is that these cells are in fact not clones, more than likely due to technical limitations. Less likely, levels of the fusion protein may vary significantly depending on the degree of cell-cycle synchronization amongst the cell population.

HEK293 cells stably expressing the fusion protein display the same phenotypes as encountered previously in transiently transfected cells, however the overall fluorophore intensity of these proteins was considerably less compared to the transients suggesting that too high a level of the proteins may be toxic even to HEK293 cells.

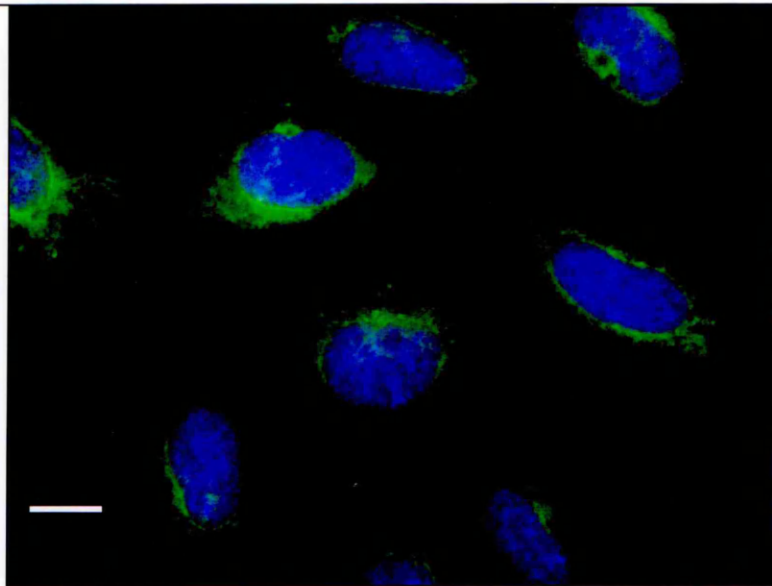
6.8 Western analysis of stable HEK293 cells expressing the fusion proteins

Western analysis of the clonal cell lines expressing the fusion protein varied in their immunoreactivity. Immunoblotting with the anti-EGFP antibody of the NTMPS1-EGFP expressing cell lines (figure 6.10) shows immunoreactive bands at ~57 kD and ~122 kD close in size with those already seen in Cos-7 cells transfected with the truncated PS1 construct (figure 4.6). The clones 1/27 and 2/23 that produce the blob-like phenotype also show immunoreactive bands at ~150 kD (figure 6.10, lanes 11 and 13). These data suggests that HEK293 cells can tolerate the presence of the blob phenotype since clearly these cells are able to divide. However, that these cells cannot be captured by the low gain-settings used to capture transiently transfected Cos-7 cells, would indicate that there is a limit to the amount of fusion protein that can be tolerated by stable HEK293 cells.

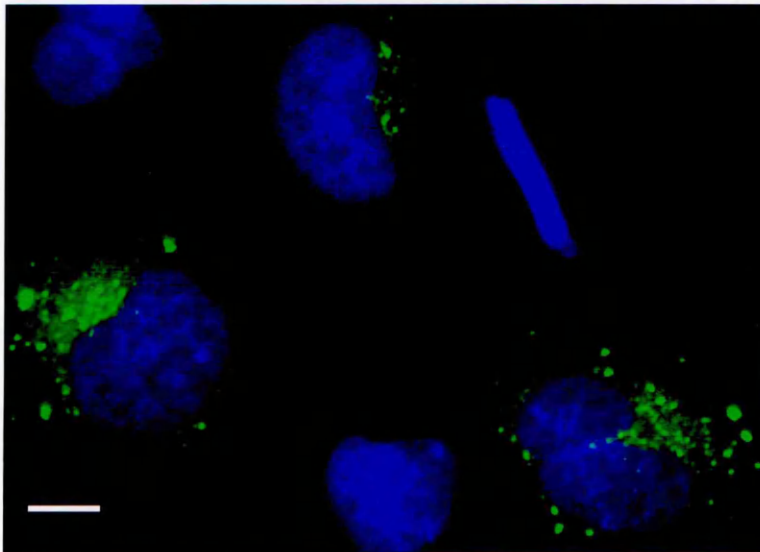
Immunoblotting of the FLPS1-EGFP expressing cell lines with the anti-EGFP antibody is considerably weaker in intensity compared to the HEK293 NTPS1-EGFP cell lines (figure 6.11, panel a, compare lane 2 with lanes 3-7). Anti-EGFP immunoreactive bands were present at ~88, 55, 48, 32, and 28 kD. Bands were close in size with those already seen in Cos-7 cells transiently transfected with the full-length PS1 construct (figure 5.12) however, the immunoreactive band of ~130 kD analysed from transients is absent indicating that over expression of the full length fusion protein may not be tolerated by the cell. The immunoreactive bands at ~88 kD is close to the calculated size predicted for the holoprotein plus EGFP (~82 kD), and indicates that a fraction of the fusion protein does not undergo proteolysis. The fraction that does undergo proteolysis is represented by the immunoreactive band at ~48 kD corresponding to CTFPS1-EGFP. The remaining bands at ~28 and ~32 kD may represent caspase cleavage of the full-length fusion protein known to occur under conditions of apoptosis.

Immunoblotting with the anti-CTPS1 antibody 1039 showed multiple immunoreactive bands in the size range ~10-150 kD (figure 6.11, panel b). The doublet at ~20 kD is typical of the 1039 antibody and corresponds to endogenous CTF. The addition of the EGFP moiety to the CTF increases the band size to ~45 kD, close in size to the calculated value of 47 kD for CTFPS1-EGFP. No immunoreactive bands of this size are present in control cells and NTMPS1-EGFP HEK293 cells (lanes 1 and 2 respectively). Present in all samples is an immunoreactive band at ~55 kD possibly corresponding to the holoprotein. This is unusual since levels of the holoprotein (uncleaved FLPS1) are normally very low or undetectable. Similarly, uncleaved FLPS1-EGFP is present at ~90 kD close in size to the calculated value of 82 kD. As with CTFPS1-EGFP, the full-length fusion protein is absent from lanes 1 and 2. The immunoreactive bands shown in lane 2 were similar in intensity to the bands from the control in lane 1, suggesting that NTMPS1-EGFP does not displace endogenous CTF. The higher immunoreactive bands at ~150 kD may represent the blob-like aggregates. The doublet bands at ~12 kD may represent proteolytic fragments generated as the result of physiological specific cleavage events e.g. caspase activity (Kim et al, 1997; Kovacs et al, 1999; Van de Craen et al, 1999), since the lower of these bands are more reactive when compared to the control lane. Alternatively, Dewji, et al (1997) has reported that such

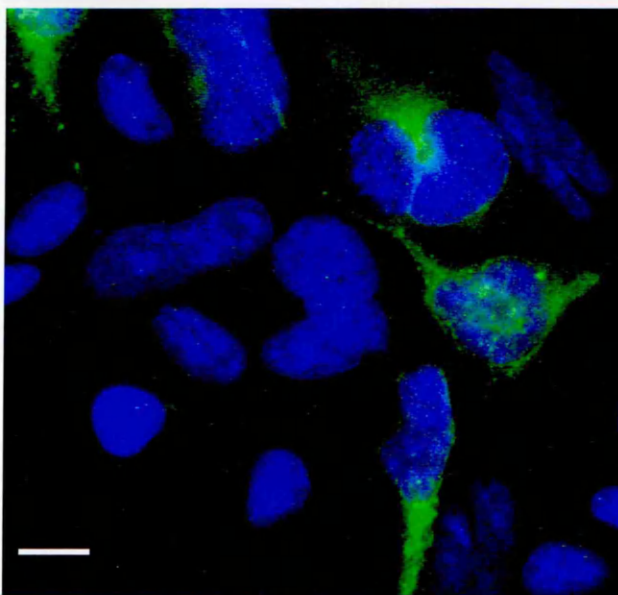
HEK293 cells stably expressing the PS1 fusion proteins



NTMPS1-EGFP
(clone 2/23)
expression is largely
uniform in intensity
between cells. Cells
display a mixture of
phenotypes. Bar
10 μ m.

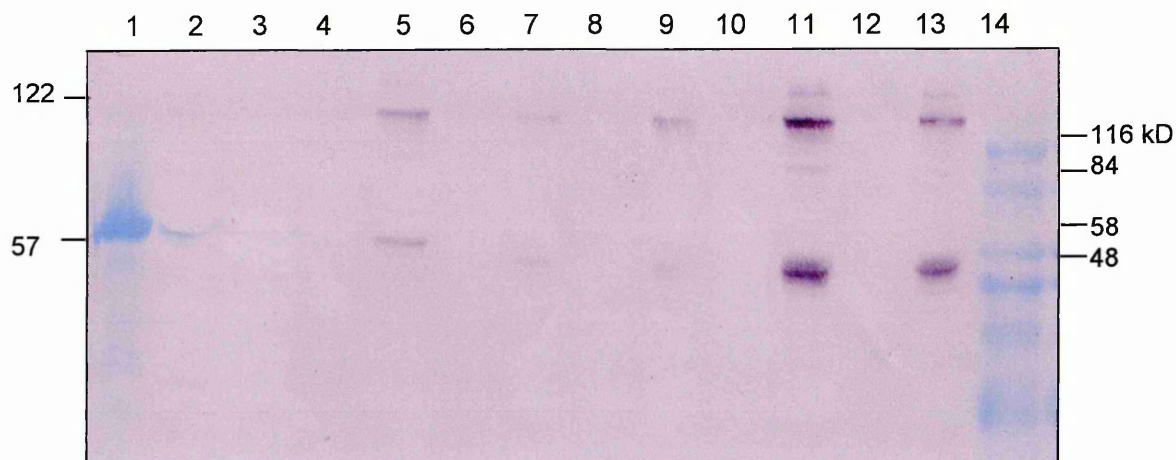


NTMPS1-EGFP
(clone 1/27). In
this clonal cell
line the fusion
protein is
reticular but the
vesicular/ blob-
like phenotype
predominates.
Bar 5 μ m.



Full-length PS1-EGFP
(clone 1/10). Fluorophore
intensity differed between
cells such that although
visible through the
microscope, cells
expressing low levels of
the fusion protein could
not be captured by the
CCD camera. A
maximum Gain of +18
was required to capture
this image. Bar 10 μ m.

Figure 6.9. HEK293 cells stably expressing FLPS1-EGFP or NTMPS1-EGFP fusion proteins. DAPI stain in blue.



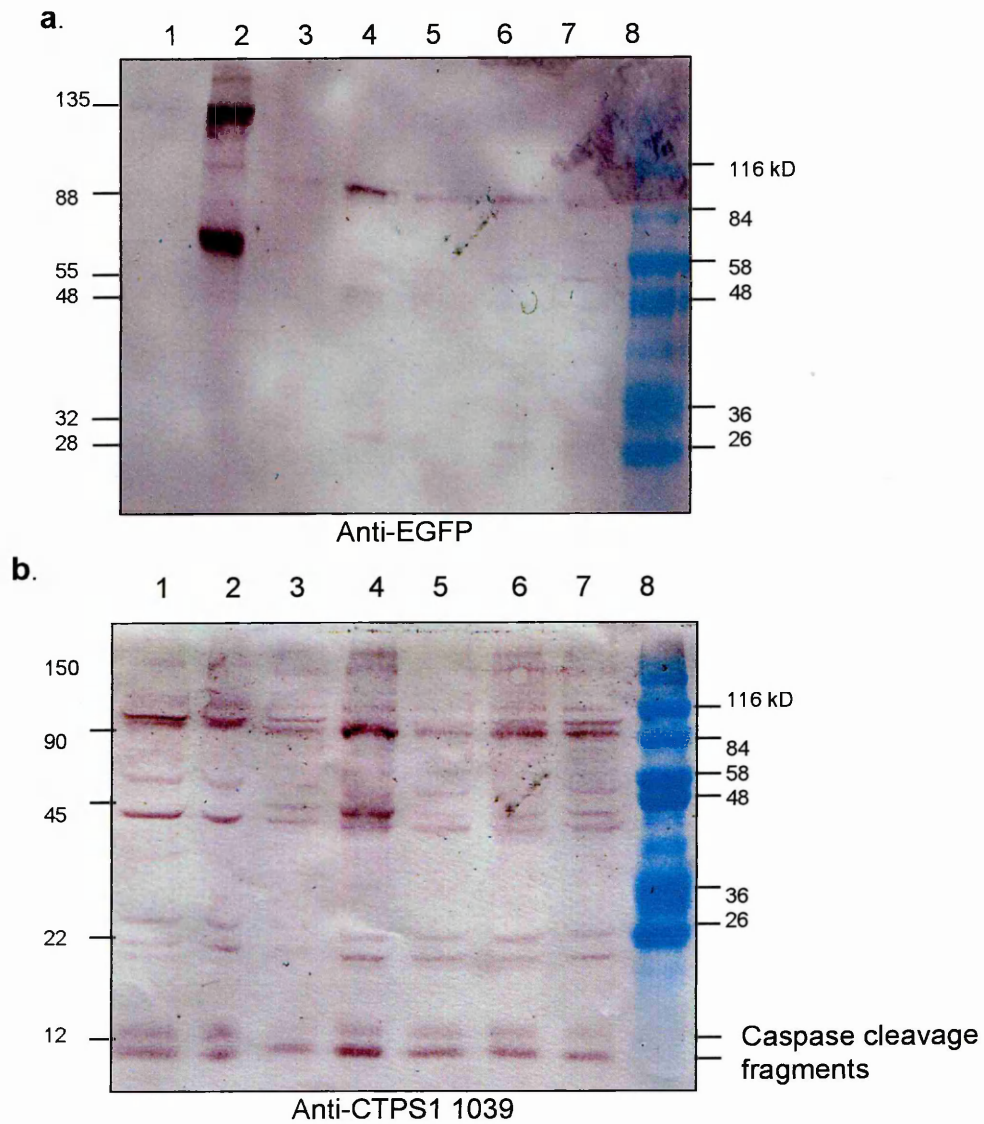
Key to lanes:

1. 1 blue
2. Control soluble fraction
3. Control membrane fraction
4. Clone 1/10 NTPS1-EGFP soluble
5. Clone 1/10 NTPS1-EGFP membrane
6. Clone 2/47NTPS1-EGFP soluble
7. Clone 2/47NTPS1-EGFP membrane
8. Clone 1/14NTMPS1-EGFP soluble
9. Clone 1/14NTMPS1-EGFP membrane
10. Clone 1/27NTMPS1-EGFP soluble
11. Clone 1/27NTMPS1-EGFP membrane
12. Clone 2/23NTMPS1-EGFP soluble
13. Clone 2/23NTMPS1-EGFP membrane
14. 7 blue

Predicted mol wt for fusion constructs:

EGFP	27 kDa
Holoprotein	55 kDa
C-terminal PS1	20 kDa
N-terminal PS1	35 kDa
FLPS1-EGFP	82 kDa
NTPS1-EGFP	62 kDa

Figure 6.10. Western analysis of HEK 293 cells stably expressing N-terminal PS1-EGFP fusion proteins. Membranes immunoblotted with the anti-EGFP antibody. Soluble and membrane fractions analysed by 10% SDS tricene/urea gel. Actual values obtained by linear regression analysis. Discrepancies between actual values and calculated values differ due to the error associated with a line of best fit.



Key to lanes:

1. Control membrane fraction
2. Clone 1/27NTMPS1-EGFP membrane
3. Clone FAC FLC-EGFP membrane
4. Clone I/10 FLC-EGFP membrane
5. Clone J/11 FLC-EGFP membrane
6. Clone K/9 FLC-EGFP membrane
7. Clone T/11 FLC-EGFP membrane
8. 7 blue marker

Predicted mol wt for fusion constructs (approx):

EGFP	27 kDa
Holoprotein	55 kDa
C-terminal PS1	20 kDa
N-terminal PS1	35 kDa
FLPS1-EGFP	82 kDa
CTPS1-EGFP	47 kDa
NTPS1-EGFP	62 kDa

Figure 6.11 Western analyses of HEK 293 cells stably expressing full length PS1-EGFP fusion protein. Samples immunoblotted with (a) anti-EGFP antibody and (b) anti-CTPS1 antibody 1039. Bands corresponding to caspase fragments may indicate apoptotic activity. Membrane fractions analysed by 10% SDS tricine/urea gel.

banding patterns are a common artifact due to the manner in which the cells are prepared for PS1 immunoanalysis, however, extensive laddering was not observed for samples blotted with the anti-EGFP antibody. Both the anti-EGFP and the anti-CTF PS1 1039 antibodies show membrane-only immunoreactive bands approximate in size with the calculated values of the NTF- and CTF-fusion proteins.

6.9 Mannosidase staining in control cells

The previous data from transfected Cos-7 cells and stable HEK293 cells expressing the fusion protein suggest that high levels of the fusion proteins may be toxic/have a pro-apoptotic effect. The latter is suggested by the caspase cleavage shown in figure 6.11, b. Previous research has implicated PS associated apoptosis in AD and suggests that the proteolytic fragments may have differential actions being pro or anti-apoptotic (Vito et al, 1996; Roperch et al, 1998; Wolozin et al, 1998; Alves da Costa et al, 2002). To investigate what effect if any, the truncated fusion protein had on apoptosis, Cos-7 cell morphology was assessed following STS treatment of transfected and non-transfected cells. STS is a wide spectrum kinase inhibitor that induces apoptosis by mediating a sustained increase in intracellular calcium ion concentration associated with mitochondrial disturbance and later to caspase activation (Kruman & Mattson, 1999).

The general features of apoptosis are characterised by changes to the cell morphology including nuclear fragmentation, chromatin condensation, cell body shrinkage, and membrane blebbing (Kerr et al, 1972). By assessing cell morphology and nuclear fragmentation as an end point of apoptosis, transfected and non-transfected Cos-7 cells were exposed to varying concentrations of STS over time. A series of control experiments were carried out to first gauge the effect STS would have on Cos-7 cells (figure 6.12). Golgi morphology was assessed as an indicator of cell structural integrity by examining mannosidase II staining. Mannosidase staining in control cells was classically peri-nuclear and tubular in appearance, whereas staining in STS treated cells is condensed and indistinct (indicated by arrows, lower panels). At higher STS concentrations cell body and nuclear shrinkage is widespread indicating that all cells have entered apoptosis.

6.10 The NTMPS1-EGFP sensitizes Cos-7 cells to STS-induced apoptosis

Using the above criteria for assessing apoptosis the previous experiment was repeated this time with Cos-7 cells transfected with the NTMPS1-EGFP construct. The number of transfected cells showing apoptosis was expressed as a percentage of the total number of cells exposed to STS (figure 6.12 and table 6.0). Staurosporine-induced apoptosis was appreciably greater in transfected cells expressing NTMPS1-EGFP compared to control (no treatment) and non-transfected STS-treated cells for all concentrations, with the maximum effect seen after 280 min (figure 6.13, 2 μ M STS). The number of apoptotic cells increased in a time dependent manner for both cell populations in response to treatment with 2 μ M STS, though the increase in transfected cells was greater at all time points compared to the non-transfected, STS-treated cells.

Table 6.0. Data for staurosporine treatment of NTMPS1-EGFP transfected Cos-7 cells. The number of transfected cells showing apoptosis was expressed as a percentage of the total number of cells exposed to STS. See text for criteria used to assess apoptosis in STS-treated cells.

		Control non STS-treated, non-transfected Cos-7 cells				
		No. of cells	No. apoptotic	% apoptotic		
		347	29	8		
0.5 μ M STS						
Exposure to STS (min)	Total no. of cells	No. apoptotic cells	% apoptotic	No. of transfectants	No. apoptotic	% apoptotic
70 min	233	35	15	47	28	60
140 min	248	37	15	46	29	63
280 min	241	42	17	74	48	65
1.0 μ M STS						
	Total no. of cells	No. apoptotic cells	% apoptotic	No. of transfectants	No. apoptotic	% apoptotic
70 min	629	77	12	61	36	59
140 min	681	75	11	71	41	58
280 min	402	58	14	75	48	64
2.0 μ M STS						
	Total no. of cells	No. apoptotic cells	% apoptotic	No. of transfectants	No. apoptotic	% apoptotic
70 min	302	73	24	70	35	50
140 min	389	117	30	65	40	61
280 min	172	73	42	44	33	75

6.11 Staurosporine induced apoptosis in NTMPS1-EGFP expressing NRK cells show increased Grasp65 cleavage compared to untransfected cells

Although the above experiment represented an $n=1$, the results suggest that the PS1 fusion protein sensitizes the cells to STS-induced apoptosis above that observed for STS-treated, non-transfected cells. One criticism, however, concerning the design of this experiment is that changes in cell morphology were measured as an end point of apoptosis. A more definitive experiment would be one in which the early events of apoptosis could be measured in cells transfected with the fusion protein. One such early event in the execution stage of apoptosis is the caspase-3 mediated cleavage of the cis-Golgi stacking protein GRASP65 (Golgi reassembly and stacking protein of 65 kD). During mitosis and apoptosis GRASP65 cleavage results in the Golgi ribbon fragmenting into tubulo-vesicular membranes (Barr et al, 1997; Lane et al, 2002).

To investigate what affect the fusion protein had on the early events of apoptosis in transfected cells was measured using a monoclonal anti-GRASP65 antibody (gifted by M. Lowe). The GRASP65 antibody was used to assess GRASP65 staining in transfected and untransfected NRK cells following STS treatment. Cells affixed to coverslips were treated over 4 hours with 1 μ M STS at 37°C, and prepared for immunofluorescent microscopy. Figure 6.14 shows GRASP65 staining as a peri-nuclear ribbon in transfected and untransfected cells. Two transfected cells show a reduction in GRASP65 staining similar to the decrease seen for the other compartment markers. The bar chart in figure 6.15 show the number of STS-treated transfected GRASP65-negative cells expressed as a percentage of the total number of non-transfected STS-treated cells. Figure 6.15 shows a dose-dependent relationship between staurosporine exposure and Grasp65 staining in both transfected and untransfected NRK cells. This loss in staining is more statistically significant in cells expressing the fusion protein compared to control cells treated with or without staurosporine (figure 6.15 and table 6.1). Though not statistically significant, apoptosis was nonetheless greater in control-transfected cells compared to non-transfected control cells indicating that the fusion protein may have a small pro-apoptotic effect.

For Western analysis, STS treated NRK whole cell lysate was immunoblotted with a GRASP65 polyclonal antibody (figure 6.16). Whilst Grasp65 cleavage is clearly evident in STS treated NRK cells processed for immunofluorescent microscopy (figure 6.14), GRASP65 cleavage was not detected by immunoblotting in STS-treated NRK cells. Instead an immunoreactive band was identified at ~66 kD corresponding to uncleaved full-length GRASP65. Lane et al, (2002) have previously shown that the anti-Grasp65 antibody stains immunoreactive bands at approximately 50, 45 and 40 kD corresponding to caspase-3 cleavage fragments. Although GRASP65 cleavage was not detected, the overall immunoreactivity was nevertheless weaker in control (no STS) transfected and STS-treated-transfected cells (figure 6.16, lanes 5-8), compared to STS-treated non-transfected cells (lanes 2-4), consistent with the previous observation that the fusion protein reduces antibody staining to some cell compartment markers, in this case, cis-Golgi GRASP65 staining is affected.

The failure to demonstrate GRASP65 cleavage by immunoblotting may, in part, be due to different experimental techniques. In this experiment crude cell lysate was prepared from NRK cells exposed to 1 μ M STS for 4 hours. The concentration of STS and the length of exposure were determined by the immunofluorescence microscopy data, which showed reduced GRASP65 staining after 4 hours in the presence of 1 μ M STS. GRASP65 cleavage has previously been demonstrated in a cell-free system where apoptotic Hela cell lysate was prepared by treatment with cytochrome c, a potent apoptotic inducer (Lane et al, 2002). Here, apoptotic cytosol was incubated with purified rat liver Golgi membranes for various times at 37°C. Immunoblotting of these samples showed major proteolytic fragments one hour after incubation. In the current experimental set-up, GRASP65 would have been cleaved following STS treatment, however, the caspase-generated fragments would have been exposed to the action of several additional cellular proteases during apoptosis, hence full length membrane-bound GRASP65 was detected by immunoblotting, but not its proteolytic fragments.

6.12 Chapter summary

In summary, co-localisation experiments with antibodies to APP and β -catenin show little or no co-localisation with the NTF fusion protein consistent with the notion that the full-length molecule, as an entity is necessary to bind with β -catenin and APP. In a sub set of cells expressing the fusion protein there was an appreciable reduction or absence of antibody staining directed at some markers for the ER and Golgi indicating fragmentation of these compartments. Furthermore, Western analysis of PS HEK293 clone cell lines indicates the presence PS caspase cleavage fragments suggesting toxicity or an apoptotic event associated with the fusion protein. Moreover, the truncated fusion protein significantly sensitises Cos-7 and NRK cells to apoptotic stimuli, in this case following STS treatment.

Cell shrinkage and altered Golgi morphology occurs following staurosporine treatment of Cos-7 cells

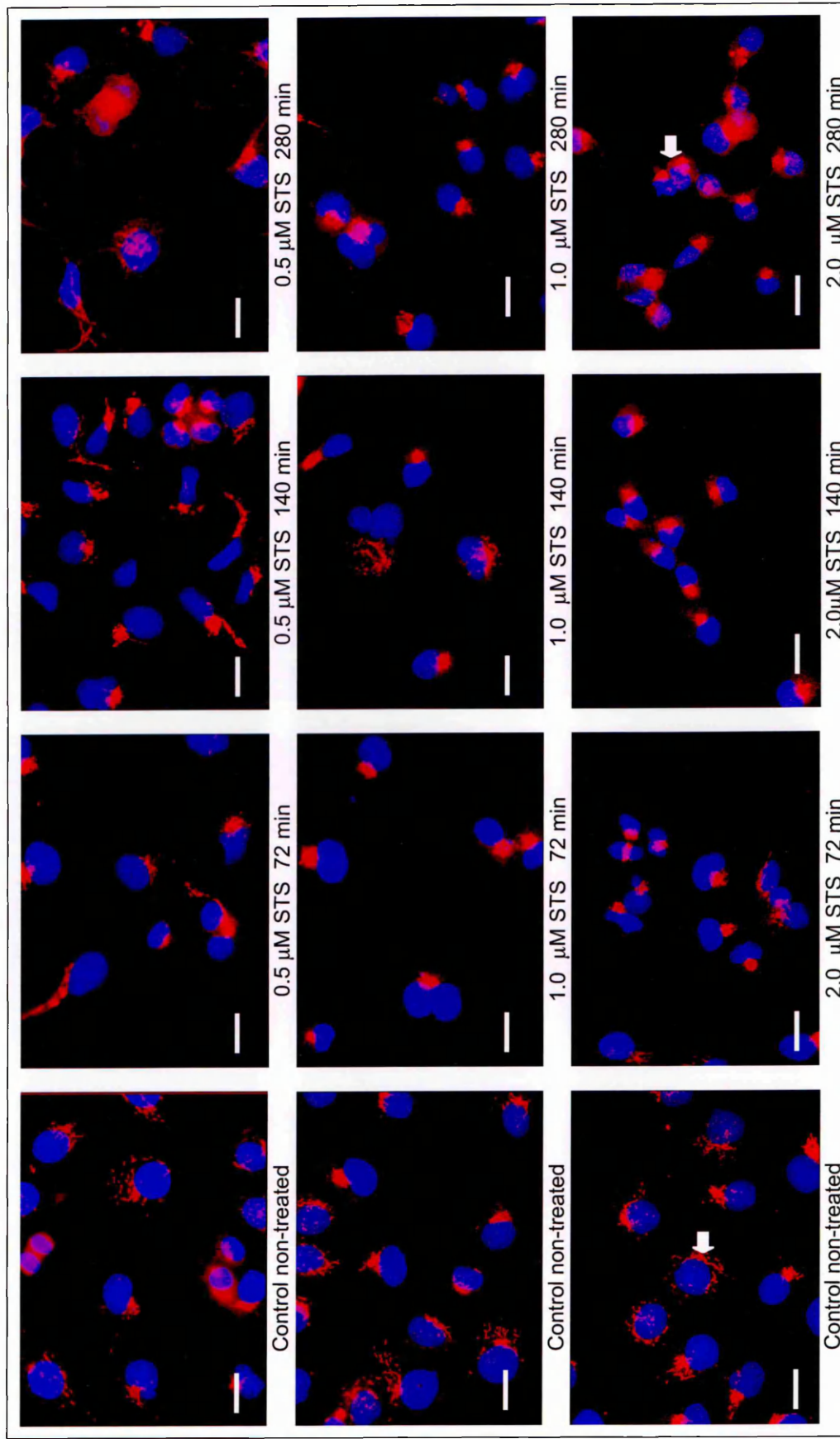


Figure 6.12. Effect of varying staurosporine concentrations on Cos-7 morphology over time. Golgi morphology was assessed as an indicator of cell structural integrity by examining Mannosidase II staining (red). Mannosidase staining in control cells is distinctly perinuclear and tubular in appearance, whereas staining in STS treated cells is dense and indistinct (arrows). At higher STS concentrations cell body and nuclear shrinkage is widespread. DAPI stain in blue. Bars, 20 μm .

Cell shrinkage and altered Golgi morphology occurs following staurosporine treatment of Cos-7 cells

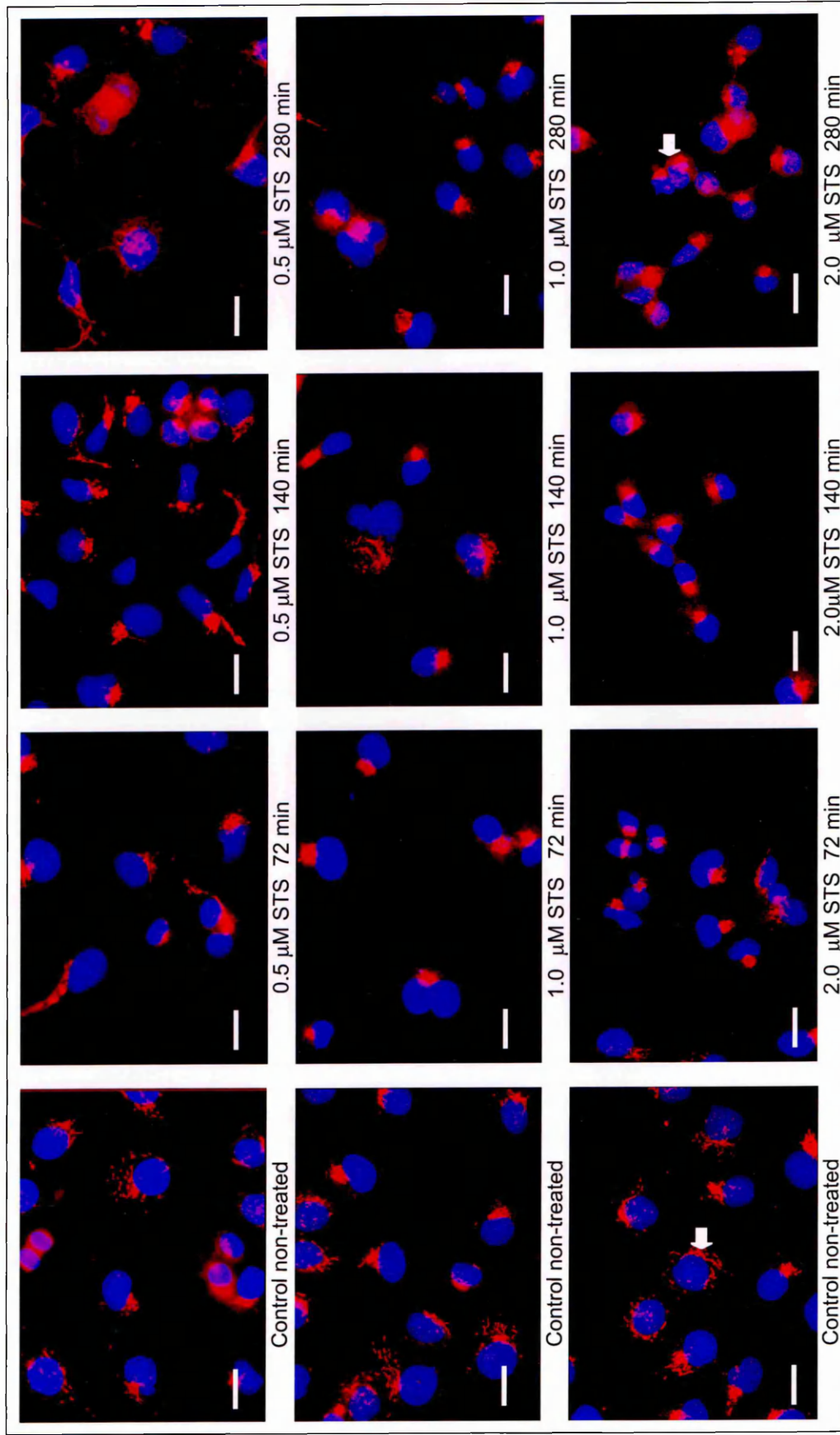


Figure 6.12. Effect of varying staurosporine concentrations on Cos-7 morphology over time. Golgi morphology was assessed as an indicator of cell structural integrity by examining Mannosidase II staining (red). Mannosidase staining in control cells is distinctly perinuclear and tubular in appearance, whereas staining in STS treated cells is dense and indistinct (arrows). At higher STS concentrations cell body and nuclear shrinkage is widespread. DAPI stain in blue. Bars, 20 μ m.

The NTMPS1-EGFP fusion protein sensitizes Cos-7 cells to staurosporine-induced apoptosis

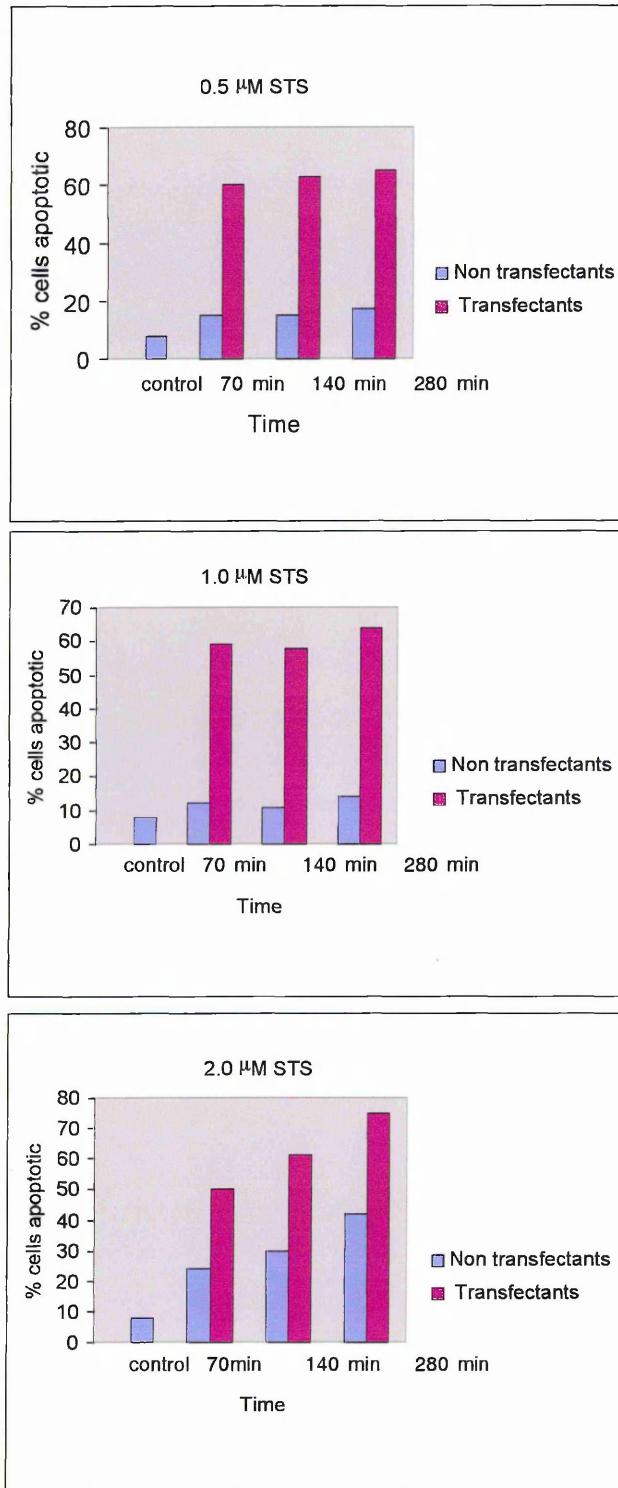


Figure 6.13. Staurosporine (STS) treatment (0.5 μM, 1.0 μM, 2.0 μM) of Cos-7 cells expressing the truncated fusion protein over time. The number of dysmorphic cells showing cell body shrinkage and nuclear fragmentation as an end point of apoptosis was greater in transfected cells compared to control non-transfected cells. See text for criteria used to assess apoptosis.

STS treatment reduces GRASP65 staining in transfected and non-transfected NRK cells

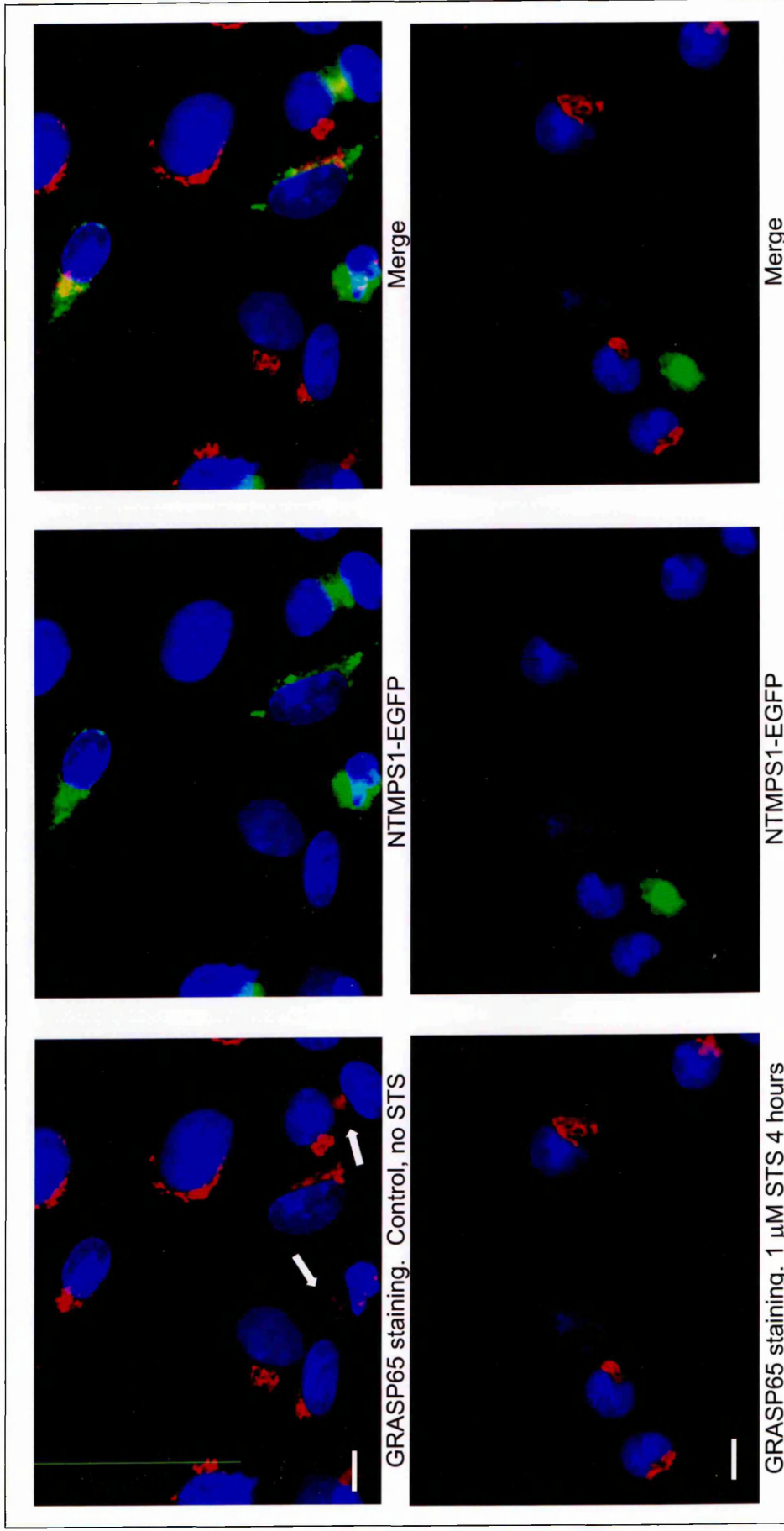


Figure 6.14. GRASP65 staining of pNTMPS1-EGFP transfected NRK cells treated for 4 hours with 1 μ M staurosporine. GRASP65 staining does not localise with the fusion protein. Notice that in two cells expressing the fusion protein GRASP65 staining is reduced (arrows) or fragmented in control cells. DAPI stain in blue. Bar, 10 μ M.

The fusion protein sensitises NRK cells to STS induced apoptosis

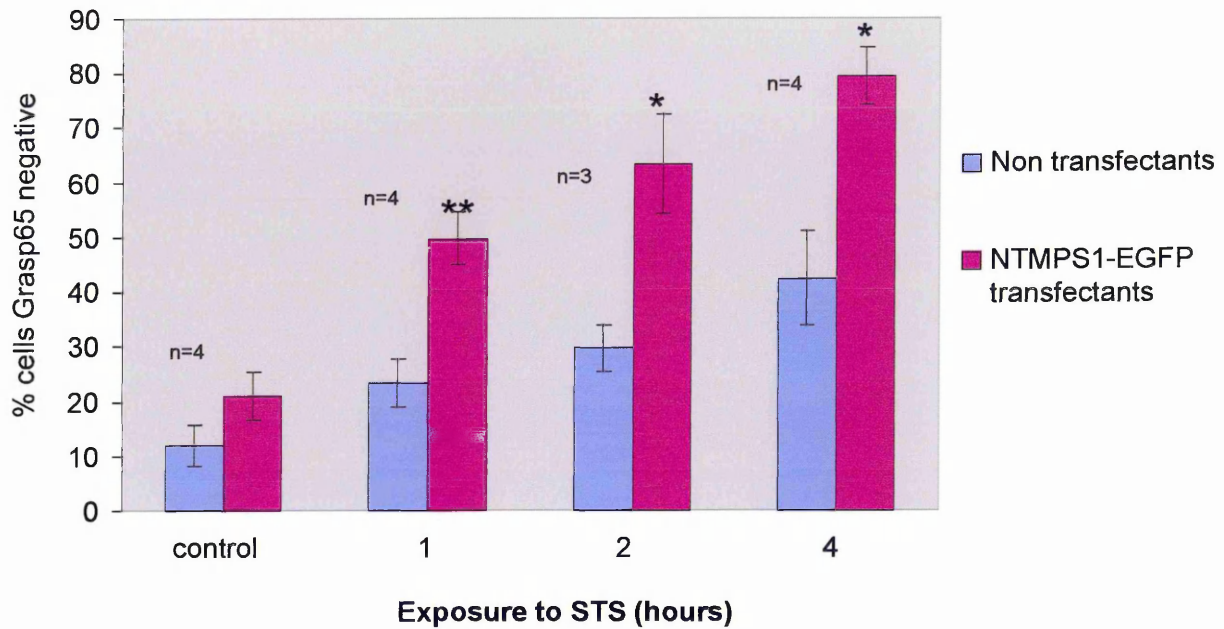
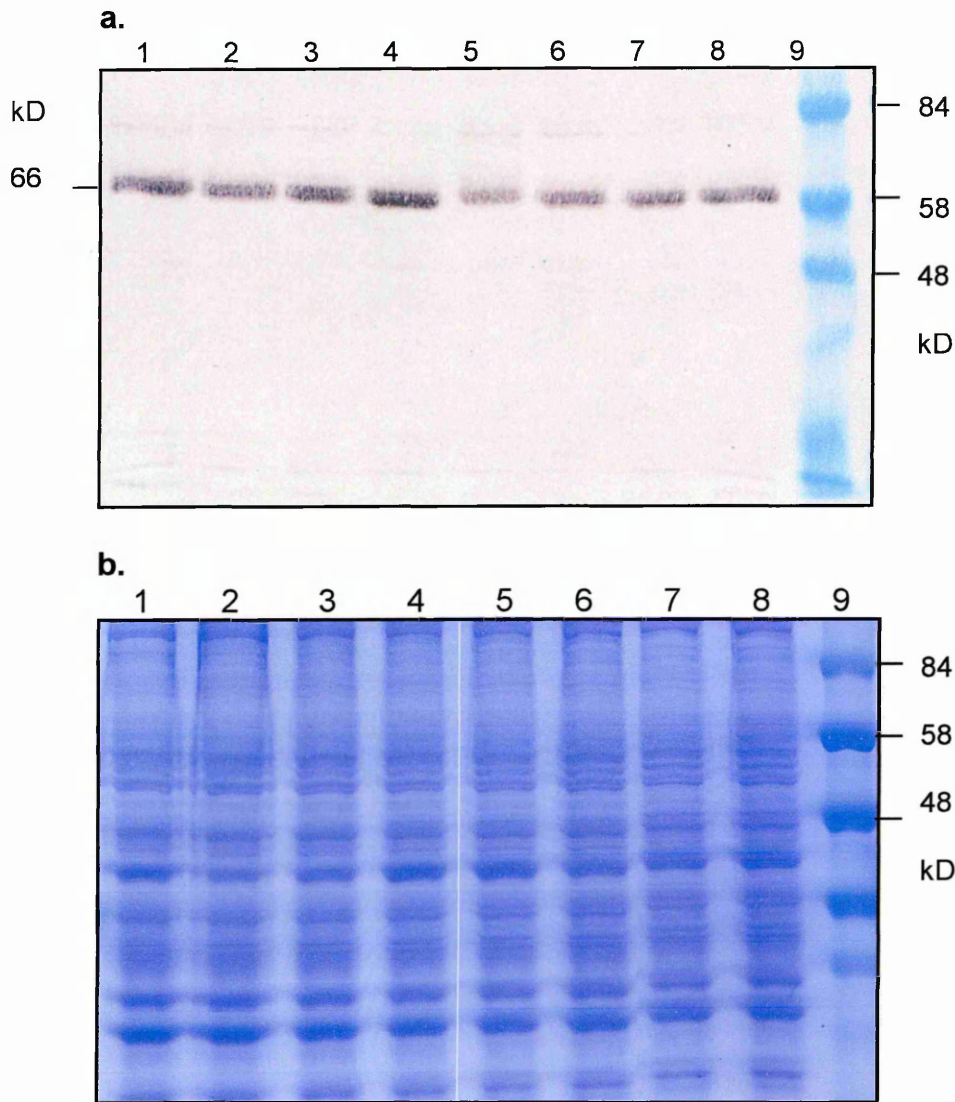


Figure 6.15. Quantitation of Grasp65 staining of pNTMPS1-EGFP transfected and untransfected NRK cells treated with 1µM staurosporine over 4 hours. Bars represent the mean \pm SEM ($n = 3-4$ for each time point). Using the students t-test there was a significant difference in the number of apoptotic STS-treated, transfected cells compared to STS-treated, non-transfected cells. * $P < 0.05$ and ** $P < 0.0065$ vs. non-transfected, GRASP65 negative cells within the same time point.

Table 6.1. Summary of data for Grasp65 staining of pNTMPS1-EGFP transfected (tfx) NRK cells treated with 1µM staurosporine. Data represents Grasp65 negative cells (%).

Expt No.	Control		1 Hour		2 Hours		4 Hours	
	Non Tfx	Tfx	Non Tfx	Tfx	Non Tfx	Tfx	Non Tfx	Tfx
1	10	13	22	51	26	51	36	78
2	23	27	35	43	25	58	21	67
3	8	30	14	63	-	-	57	92
4	7	14	22	42	38	81	56	81
Mean	12.0	21.0	23.3	49.8	29.7	63.3	42.5	79.5
STDEV	7.44	8.76	8.69	9.71	7.23	15.70	17.29	10.28

Grasp65 cleavage is not detected in staurosporine treated NRK cells expressing the NTMPS1-EGFP fusion protein



- Lanes: 1. Control non transfected, no STS
 2. 1 μ M STS for 1hour
 3. 1 μ M STS for 2hour
 4. 1 μ M STS for 4hour
 5. Control transfected no STS
 6. Transfected 1 μ M STS for 1hour
 7. Transfected 1 μ M STS for 2hour
 8. Transfected 1 μ M STS for 4hour
 9. 7 blue marker

Figure 6.16. a. Polyclonal Grasp65 immunoblotting of whole cell lysate taken from NRK cells expressing the NTMPS1-EGFP fusion protein following treatment with 1 μ M staurosporine (STS) over 4 hours. Unusually, transfected cells (lanes 5-9) show less GRASP65 immunoreactivity compared to control, non-transfected cells (lanes 1-4). This is in keeping with the earlier observation that overexpression of the fusion protein reduces some ER and Golgi markers. 8% SDS PAGE gel. b. Corresponding coomassie gel showing approximate equal sample loading per lane.

Chapter 7 Functional and morphological characteristics of the blob phenotype

7.0 Introduction

In the previous chapter it was demonstrated that transfected cells show altered antibody staining within the ER and Golgi compartments and increased susceptibility to apoptosis. In this section, concerns that the phenotypes exhibited by the fusion proteins were in fact a direct result of the EGFP moiety were addressed. Lastly, because of their unusual morphology the nature of the blob-like aggregates was further investigated by immunofluorescent microscopy, immunoblotting, and electron microscopy.

7.1 Introduction of an in-frame STOP codon between PS1 and EGFP cDNA

Before investigating further the properties of the fusion proteins, the role of the EGFP moiety in generating the fusion protein phenotypes was first investigated. Although there is little evidence to suggest that the EGFP tag affected the distribution of the fusion protein, it was necessary to consider whether or not the phenotypes were an artefact induced by the EGFP moiety. Because of the similarity of the phenotypes generated by all four constructs, mutant and non-mutant NTPS1 and CTPS1 proteins minus the EGFP moiety were constructed. To achieve this, an oligo-linker sequence containing a STOP codon (TGA) was ligated into the open reading frame between position 1427 for full-length PS1 and position 827 of NTPS1, and the start of the EGFP cDNA sequence (figure 7.0). Transcription of these constructs should therefore terminate after the STOP codon thus generating full-length and truncated proteins devoid of the EGFP moiety. To aid in the selection of putative clones, a Pst1 restriction site not found within the existing constructs was introduced into the oligo-linker sequence. PS1 cDNAs from putative clones transformed by the PS1-STOP constructs were screened by restriction digestion analysis (data not shown). The purified plasmids were then used for the transfection of Cos-7 cells. To analyse PS1 expression in Cos-7 cells, the NTF antibody NT7 and the CTF antibody 1039 were used for immunofluorescence and immunoblotting.

Oligo Linker sequence for insertion into Full-length PS1-EGFP (red)

Last codon of full-length PS1 (1427) stop Pst 1 First codon of EGFP
 ORF ↓ ↓ ↓
 (forward) 5' CAA TTT TAT ATC GAA TTG TGA CGA AAA CTG CAG TTC GAT CGA TCC ATC GCC3'
 (reverse) 3' GTT AAA ATA TAG CTT AAC ACT GCT TTT GAC GTC AAG CTA GCT AGG TAG CCG5'

Oligo Linker sequence for insertion into N-terminal PS1-EGFP (red)

Last codon of N-terminal PS1 (872) stop Pst1 First codon of EGFP
 ↓ ↓ ↓
 (forward) 5' AAT GAA ACG CTT GAA TTG TGA CGA AAA CTG CAG TTC GAT CGA TCC ATC GCC3'
 (reverse) 3' TTA CTT TGC GAA CTT AAC ACT GCT TTT GAC GTC AAG CTA GCT AGG TAG CCG5'

Figure 7.0. Oligo linker sequence. To investigate whether the blob phenotype displayed by cells expressing the fusion protein was an artefact generated by the presence of the EGFP moiety, an oligo-linker sequence incorporating a STOP codon (TGA) was introduced between the PS1 and EGFP DNA sequences (red type).

Primers incorporating an in-frame stop codon between the end of the PS1 and the start of the EGFP cDNA were designed for all four plasmids (Invitrogen). To aid in the screening of putative PS1-STOP-EGFP clones, the Bam H1/Eco R1 restriction site was abolished and a Pst 1 restriction site was re-introduced (underlined). Annealing reactions were carried out according to the manufacturers instructions. Briefly, 19.2 nmoles primer Pstp01 (47.5 μl) and 25.4 nmoles primer Pstp02 (47.5 μl) were incubated together with 10 μl 10X annealing buffer (0.5 M Tris Hcl (pH 7.5), 2.0 M NaCl, 0.25 M EDTA) at 65°C for 10 minutes, then for a further 2 hours at room temperature. The annealed double stranded linkers were ligated into the double digested fusion constructs using T4 ligase. Confirmation of the linker insertion was established following restriction enzyme analysis of the constructs.

7.2 Removal of the EFGP moiety does not alter the phenotypes displayed by cells expressing truncated or full-length PS1

Cos-7 cells transfected with the pNTPS1-STOP, pNTMPS1-STOP, pFLPS1-STOP or pFLMPS1-STOP constructs displayed identical phenotypes to those exhibited by the fusion protein i.e. reticular, peri-nuclear, vesicular and blob-like aggregates (figure 7.1). Similarly, the transfection rates for the new constructs were approximately the same as those observed for the fusion proteins. The overall fluorescent intensity of the full-length constructs was less compared to those cells expressing the NT-STOP constructs. As was the case for the full-length PS1-EGFP fusion proteins, it was necessary to maximise the camera gain in order to capture images of the cells expressing full length-STOP-PS1. Moreover, staining of the full-length-STOP proteins with the anti-PS1 antibodies did not reveal an obvious peri-nuclear phenotype, consistent with that already observed in cells expressing the full-length fusion proteins. Endogenous staining with NT7, however, reveals a punctate and a peri-nuclear phenotype (figure 7.1, first panel).

As expected, cells expressing the PS1-STOP proteins did not exhibit EGFP fluorescence or stain with the anti-EGFP antibody (data not shown). Also, the anti-CTF antibody 1039 similarly failed to stain the NTFPS1-STOP fusion proteins (data not shown). Noticeably, cells expressing the full-length PS1 STOP constructs, whether stained with the NT7 or 1039 antibodies, all show similar phenotypes (figure 7.1). Whether this indicates that the two fragments form blobs separately or represent full-length (uncleaved) PS1 is unclear. Ideally, this issue could be resolved by double immunolabelling using an anti-mouse PS1CTF monoclonal antibody and the NT7 rabbit polyclonal antibody.

7.3 Western analysis of soluble and membrane fractions prepared from cells expressing full-length and truncated PS1-STOP proteins

Membrane and soluble fractions prepared from cells transfected with the four PS1-STOP constructs were immunoblotted with the NT7 and 1039 antibodies (figure 7.2). As expected, the soluble cell fraction did not show any immunoreactivity to the NT7 antibody. Membrane fractions taken from cells

transfected with the four PS1-STOP constructs show similar immunoreactivity profiles following NT7 staining (figure 7.2, a). Bands common to all four samples are shown at approximately 31, 33, 57, 73 and 83 kDa. The latter two bands may represent dimerised or aggregated protein. The bands at ~57 kDa are close in size to the holoprotein, whilst all samples show a doublet at ~32 kDa, close in size to the NTF fragment. Significantly, the bands at ~28 and 66 kDa are absent from the FL-STOP samples. The higher weight bands suggest that the NTFs are more susceptible to aggregation compared to the full-length-derived NTF, possibly indicating that a disturbance in the 1:1 (CTF:NTF) stoichiometry results in aggregation of the NTF fragment. The smaller bands at ~28 kDa could be the result of caspase cleavage of the NTF or due to the manner in which the cells were prepared for immunoanalysis (lanes 6 and 8). Overall, the immunoreactivity of the full-length samples in lanes 2 and 4 were generally weaker compared with the NT-STOP samples.

Membrane fractions taken from cells transfected with the four PS1-STOP constructs also show similar immunoreactivity profiles following 1039 staining (figure 7.2, b). Bands common to all four samples plus the control membrane fraction range in size from approximately 11 to 134 kDa. The bands at ~20/22 kDa and ~52 kDa are close in size to the CTF and holoprotein, respectively. Overall, immunoreactivity in cells expressing the transgene is higher when compared to endogenous levels of the protein (lane 1). This observation is in keeping with previous studies that show that over expression of transgene PS1 results in a modest increase in steady state levels of PS1 (Thinakaran et al, 1996). As before, bands corresponding in size to the caspase fragments appear at approximately 11 and 13 kD in control as well as transfected cells, however, the immunoreactivity is significantly greater in fractions taken from transfected cells. This data is consistent with the CTF undergoing alternative cleavage by caspase-3 (Kim et al, 1997; Podlisny et al, 1997; Kovacs et al, 1999).

7.4 Analysis of the cell compartment in which the fusion protein resides

Transfection of the fusion protein constructs both full-length and truncated consistently display the same overall phenotype in several different cell lines. In particular, the blob-like aggregate phenotype appears to dominate, forming numerous pleomorphic bodies varying in both size and number. Western

The fusion protein phenotypes are not an artefact due to the presence of the EGFP moiety

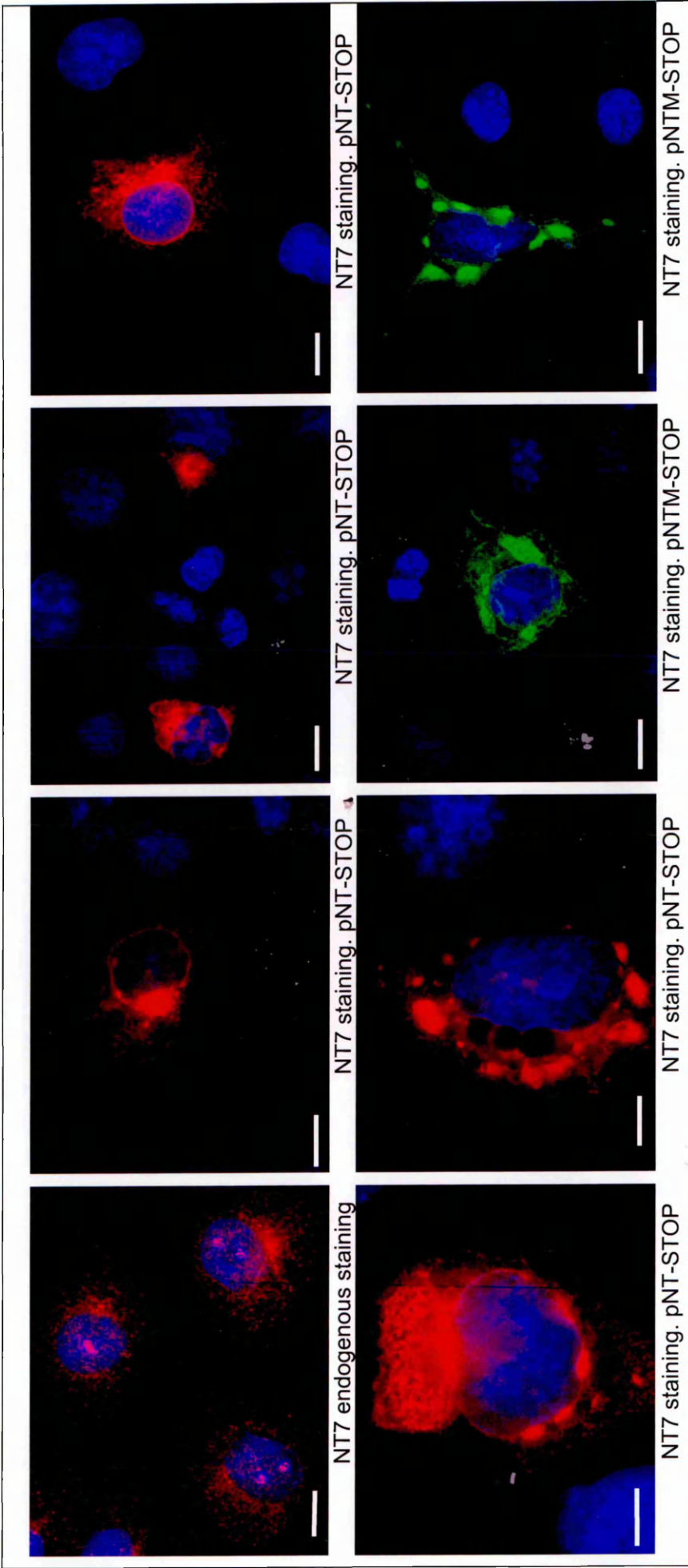


Figure 7.1. NT7 and 1039 staining of Cos-7 cells transfected with PS1-STOP-EGFP constructs. The range of phenotypes displayed by the PS1-STOP proteins was identical to those exhibited by the fusion proteins. Endogenous staining with NT7 reveals a punctate and a peri-nuclear phenotype. The overall intensity of the full-length constructs was less compared to those cells expressing the NT-constructs. As was the case for the full-length PS1-EGFP fusion proteins, it was necessary to maximise the camera gain in order to capture the full length-STOP images. Cells stained with Alexa 594 (red) or Alexa 495 (green) secondary antibodies. DAPI stain in blue. Bars, 20 μ m.

(continued overleaf)

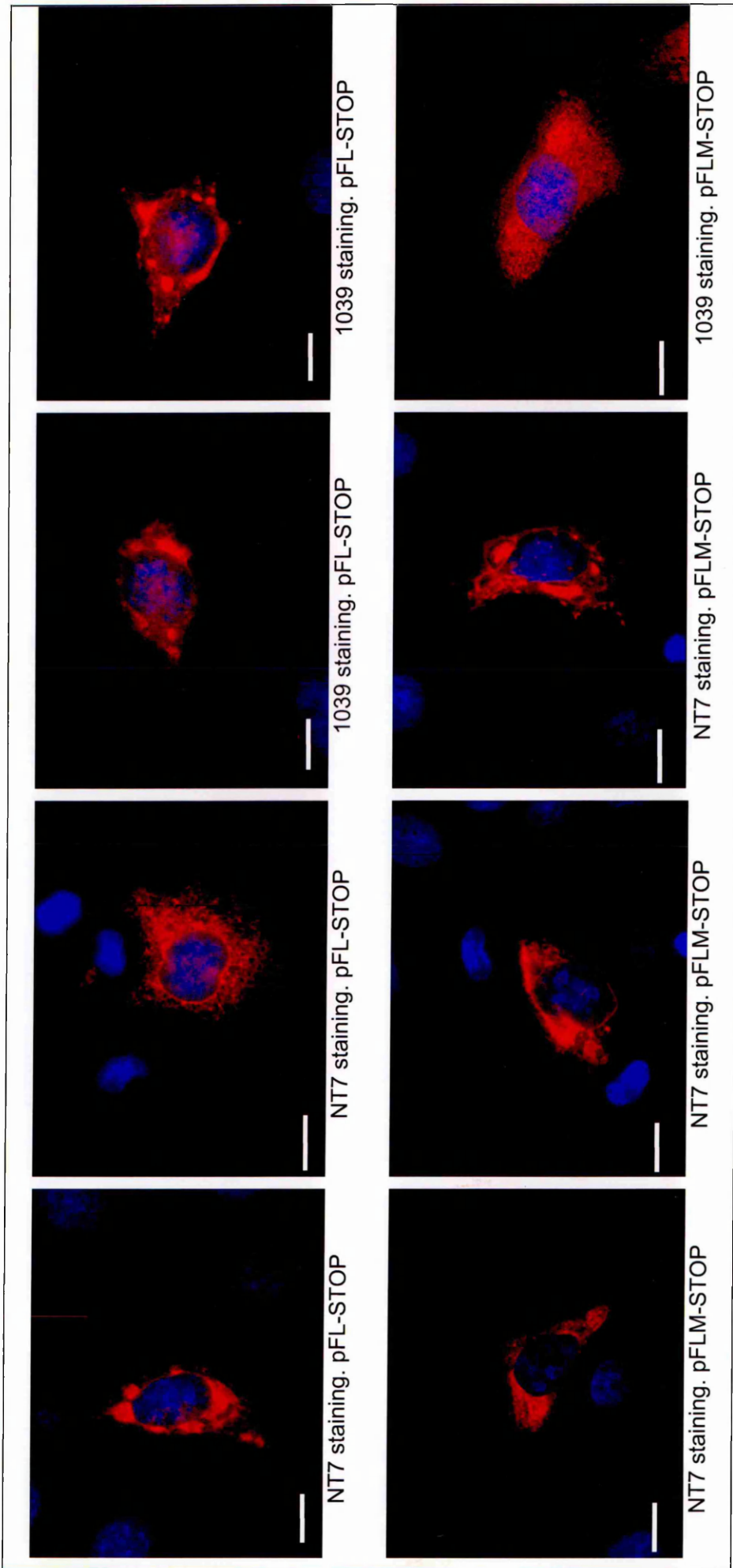
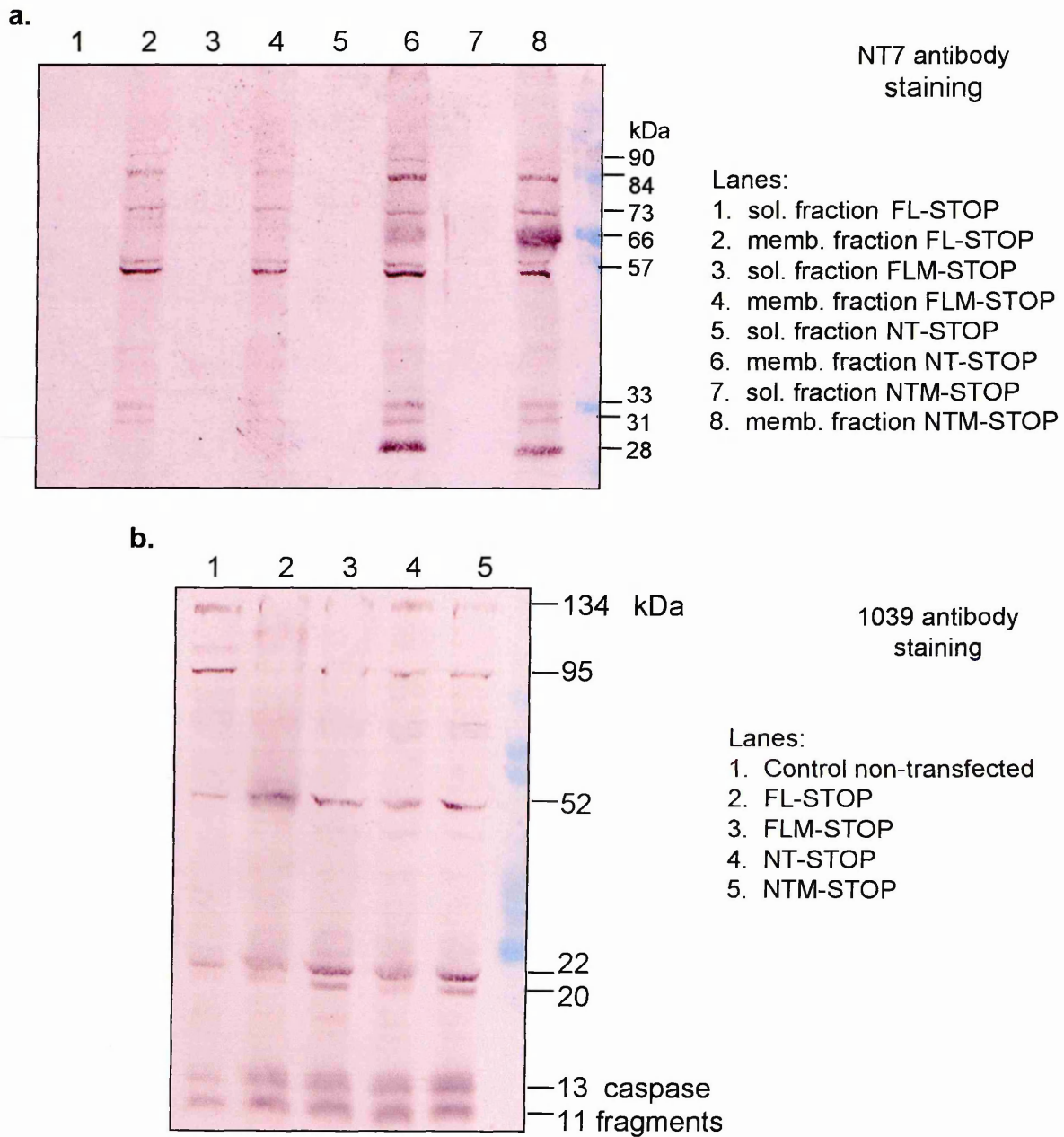


Figure 7.1 (continued)

Western analysis of PS1-STOP proteins



Predicted mol wt for fusion proteins (approx):

PS1 holoprotein	55 kDa
N-terminal PS1 fragment	35 kDa
C-terminal PS1 fragment	20 kDa

Figure 7.2. Western analysis of full-length and truncated PS1-STOP proteins. a. NT7 immunostaining of soluble and membrane cell fractions. b. 1039 immunostaining of cell membrane fractions. Samples analysed by 10% SDS/urea PAGE gel. Band sizes estimated by linear regression.

analysis of transfected cells demonstrates that these blobs are associated with the insoluble/membrane fraction. Given their general morphology, the blobs are either insoluble aggregates or membrane-sheathed structures derived from the cell compartment. An intuitive guess regarding their genesis might consider the fusion protein accumulating over time eventually resulting in 'swellings' of the ER or Golgi, or some other membrane derived organelle. Alternatively, the blobs may be the result of vesicles undergoing successive fusion events with one another, assuming membrane kinetics allow for such a process. A parsimonious explanation is that the blobs are cytoplasmic aggregates.

In order to justify the next investigation and address the origins of the fusion protein blobs, it is helpful to first consider the fate of proteins trafficking through the cell. The dogma surrounding the passage of membrane proteins (in this instance PS1) through the cell compartment can be stated thus: (1) the protein is first co-translationally inserted within the ER membrane. (2) Correct folding is followed by selected packaging of PS1 into COP II coated transport vesicles at ER transitional elements (TE- ER exit sites) either central or peripheral. (3) Vesicles containing the cargo protein bud off from the TE. (4) Transport vesicles lose their COPII coats and vesicles fuse together to form vesicular tubular clusters (VTCs/ERGIC compartment) at the cis-Golgi interface. At peripheral TE, vesicles form smaller VTCs that constitute transport complexes (TC) of tubulovesicles that are transported to the cis-Golgi via microtubules. (5) Finally, especially at VTCs but also from the distal TGN, COPI-coated vesicles are formed. COPI vesicles return proteins by retrograde transport thereby concentrating proteins in the VTCs (Klumperman, 2000; Gorelick and Shugrue, 2001). Ultimately, functional PS1 is then trafficked to its final destination, be it the synapse/plasma membrane, endosome, etc.

If the blobs arise from fragmented ER or the Golgi apparatus or are in fact the result of fused vesicles, it is reasonable to assume that resident proteins from these compartments may still be present. To test this hypothesis and therefore better understand the identity of the blob-like aggregates, cells expressing the fusion protein were stained with a variety of antibodies to the ER, ERGIC and Golgi compartments.

7.5 The blob phenotype does not co-localise with antibodies to the ER, Golgi or the ERGIC compartment.

Cos-7 and HEK293 cells expressing the NTMPS1-EGFP fusion protein were stained with Colligin, Mannosidase II (figure 7.3) and ERGIC53 (figure 7.4, top and middle rows) antibodies. No co-localisation with the blob phenotype was observed. From earlier experiments it was demonstrated that BFA treatment of cells expressing moderate levels of the fusion protein co-localise with the ER marker Colligin but not with the ERGIC53 marker. Assuming that the blobs were derivatives of the cis or trans Golgi complex, BFA treatment should result in either an ERGIC or ER phenotype for the fusion protein. To investigate this possibility HEK293 cells displaying the blob phenotype were treated with BFA and stained with the ERGIC53 antibody as demonstrated previously (figure 7.4, lower row). Treatment with BFA does not disperse the blob-like aggregates nor affect their size, morphology or cellular distribution. Following BFA treatment, moderate levels of the fusion protein redistribute to the ER, whereas ERGIC53 staining is distinctly vesicular.

An additional test as to whether the blobs originated from VTCs following the fusion of transport vesicles was investigated by staining with the anti-membrin antibody. Membrin is a 27 kDa integral membrane protein that serves as a t-SNARE in ER-to-Golgi transport. T-SNAREs facilitate the fusion of ER derived membrane vesicles with their cognate v-SNARE partner (Lowe et al, 1997). Again, no co-localisation of the membrin antibody with the blob phenotype was observed (figure 7.5) indicating that the blob phenotype is not a post-ER/pre-Golgi derived structure.

7.6 Altered COP II antibody staining in Cos-7 cells exhibiting the blob phenotype

To examine whether the blobs associated with vesicles derived from the TE or distal Golgi compartment, cells were stained with antibodies markers for COP-II and COP-I coat proteins. β -Cop is the major component of the COP-I complex, which is critical for vesicular traffic between the ER and Golgi and useful as a marker for the VTCs found at the cis face of the Golgi stack, as well as the cis Golgi itself (Oprins et al, 1993). β -COP antibody-staining exhibits a

reticular/vesicular phenotype in both cell lines (figure 7.6). The difference in size between the β -COP vesicles and the fusion protein and the absence of any co-localisation shows that the blob phenotype neither associates with nor affects COP-I trafficking.

COP II staining of HEK293 cells exhibits a punctate and peri-nuclear phenotype. The COP II antibody overlaps with the peri-nuclear phenotype displayed by the fusion protein (figure 7.7, top row), but not with the blob phenotype (middle and bottom row). The presence of the fusion protein appears not to affect COP II staining in HEK293 cells, however the blob phenotype either reduces or alters COP II staining from a peri-nuclear ribbon, to a fragmented or diffuse/cytoplasmic phenotype in Cos-7 cells (figure 7.8). Because of the rounded-up appearance of HEK293 cells making visual analysis difficult, altered COP II antibody staining cannot be ruled-out entirely.

7.7 The blob-like aggregates do not associate with the Lysosomal compartment.

Within the cell, the lysosomal and proteasomal systems are the two major intracellular pathways responsible for the degradation of damaged or unwanted proteins. Lysosomes are membrane-bound, acid hydrolase-containing vesicles derived from the TGN/endosome that deal primarily with extracellular proteins, such as plasma proteins that are endocytosed by the cell, or cell-surface membrane proteins used in receptor-mediated endocytosis. In trying to identify whether the blob-like aggregates were membrane-bound structures associated with the lysosome, Cos-7 cells expressing the NTMPS1-EGFP fusion protein were stained with the anti-lysosomal antibody LAMP-1 (lysosomal associated membrane protein), which stains a 10.5 kDa membrane protein in a characteristic ring pattern (Chen et al, 1985). LAMP-1 displays a discrete vesicular phenotype that does not co-localise with any of the phenotypes displayed by the fusion protein. Similarly, the blob phenotype remains distinct from LAMP-1 antibody staining (figure 7.9), which exhibits a distinctive ring-like vesicular phenotype (figure 7.9, insert).

The blob-like aggregates do not co-localise with markers to the ER or Golgi compartments

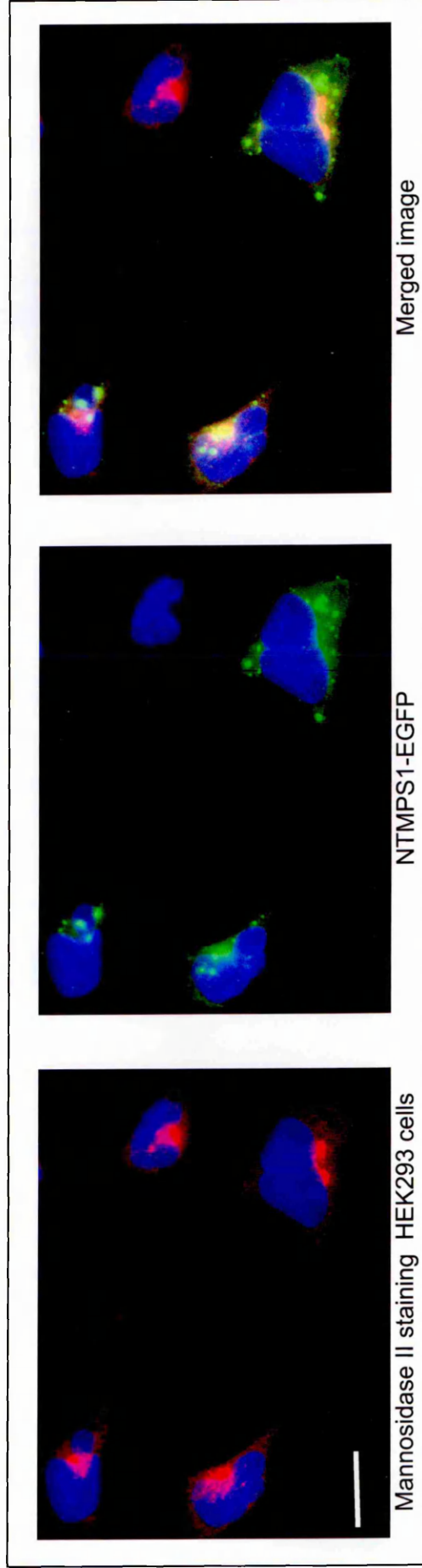
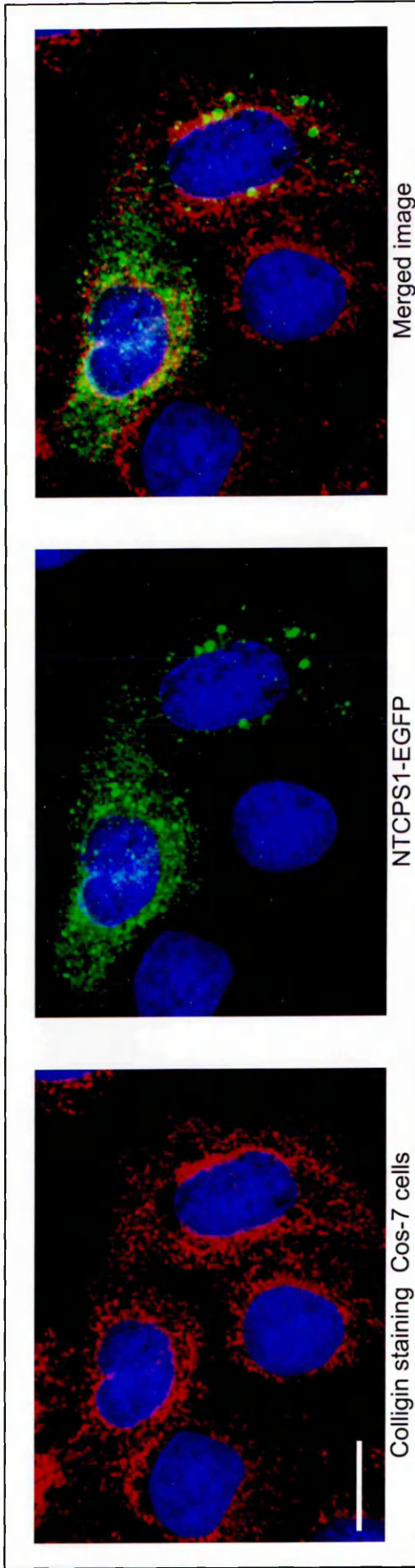


Figure 7.3. Colligin and Mannosidase II antibody staining of Cos-7 and HEK293 cells. Antibodies to the ER (top row) and Golgi (bottom row) do not stain the blob-like aggregate phenotype in either cell line, indicating that the blobs do not contain these marker proteins and by extension are not ER or Golgi fragments. DAPI stain in blue. Bars, 20 μm .

ERGIC53 does not localise with the blob-like aggregates

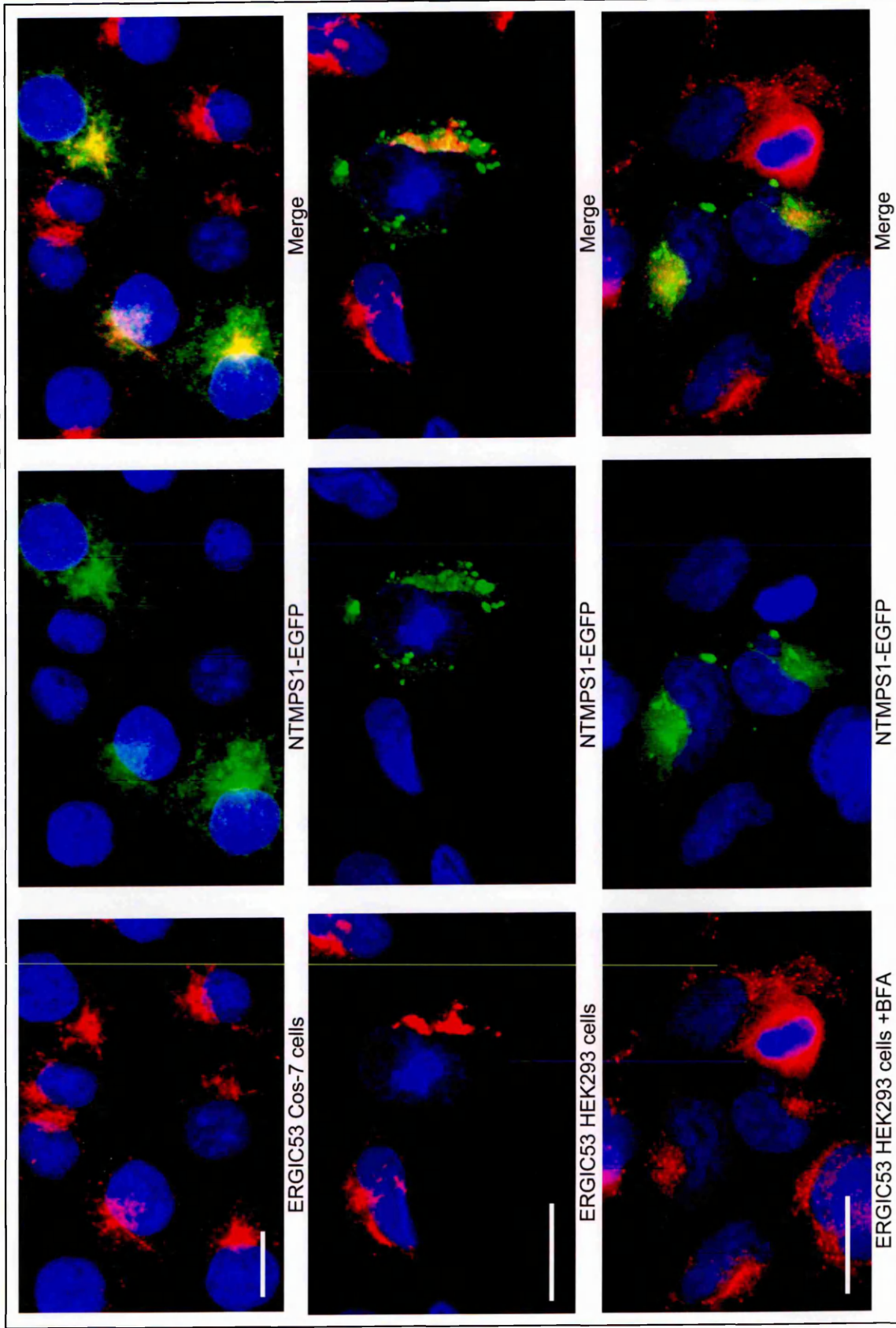


Figure 7.4. ERGIC53 antibody staining of Cos-7 and HEK293 cells expressing the NTMPS1-EGFP fusion protein. The blob-like aggregates do not stain for ERGIC53 (top and middle rows), indicating that this phenotype does not arise from the ERGIC/ vesicular tubular clusters. BFA treatment does not disperse the blob phenotype into the ER (bottom row). DAPI stain in blue. Bars, 20 μ m.

Membrin antibody-staining does not localise with the blob phenotype

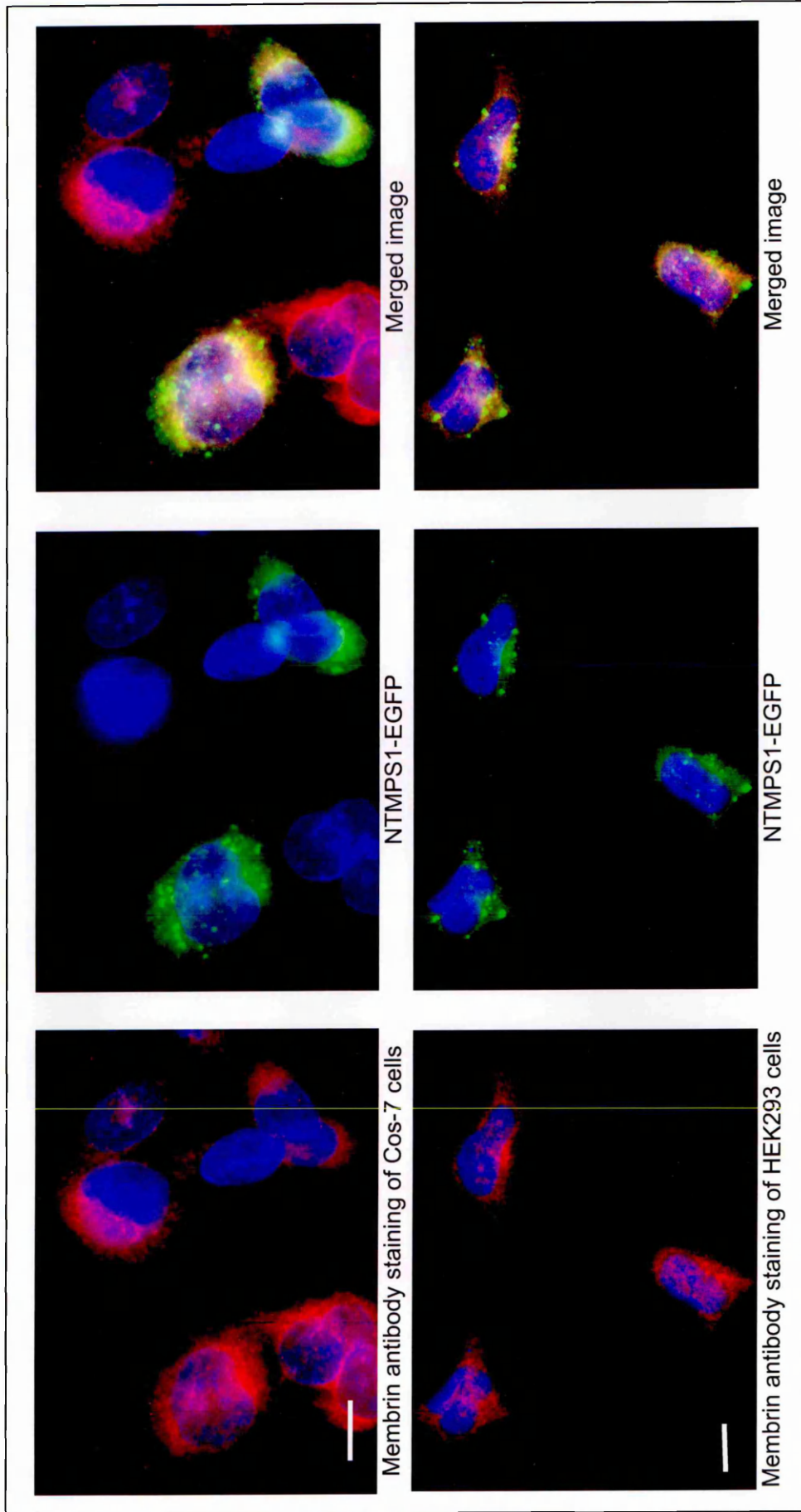
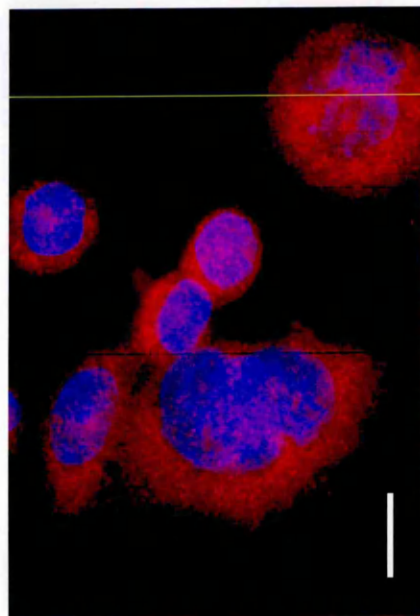
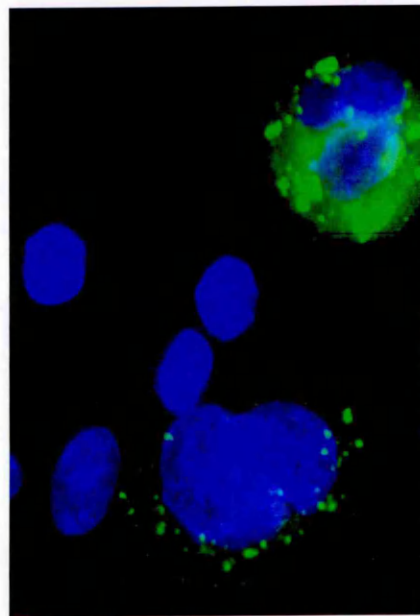


Figure 7.5. Membrin antibody staining of Cos-7 and HEK293 cells displaying the blob phenotype. Membrin is a 27 kDa integral membrane protein that serves as a t-SNARE in ER-to-Golgi transport. No co-localisation is seen between the membrin antibody and the fusion protein blobs. DAPI staining in blue. Bars, 20 μm .

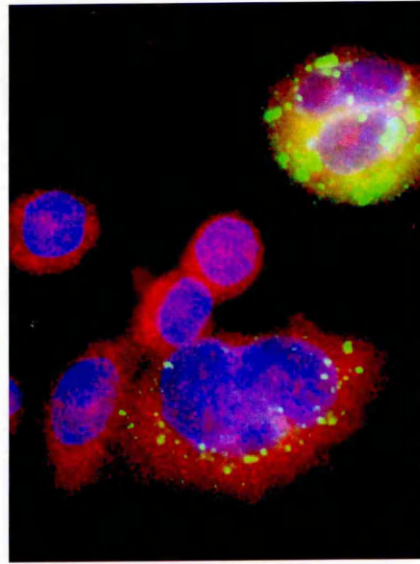
Blob-like aggregates do not co-localise with β -COP antibody staining



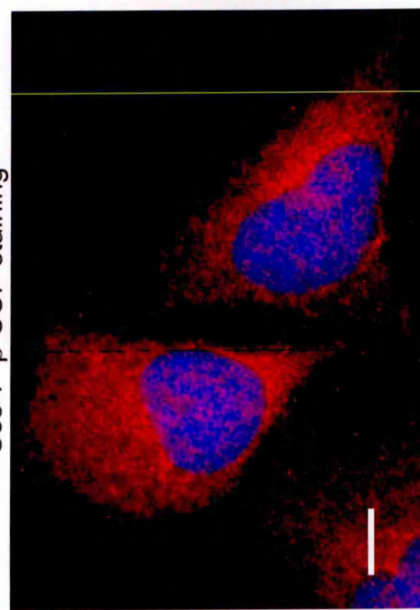
Cos-7 β -COP staining



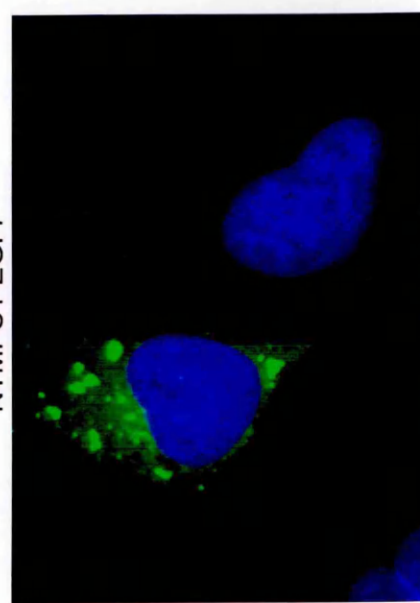
NTMPS1-EGFP



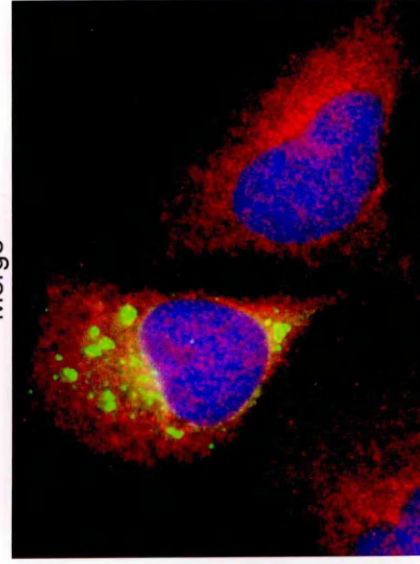
Merge



HEK 293 β -COP staining



NTMPS1-EGFP



Merge

Figure 7.6. β -COP staining of Cos-7 and HeK293 cells expressing NTMPS1-EGFP. β -COP antibody-staining exhibits a reticular/vesicular phenotype in both cell lines. The difference in size between the β -COP vesicles and the fusion protein and the absence of any co-localisation shows that the blob phenotype is not associated with COP-I trafficking. DAPI stain in blue. Bars, 10 μ m.

COP II does not co-localise with the blob phenotype in HEK293 cells

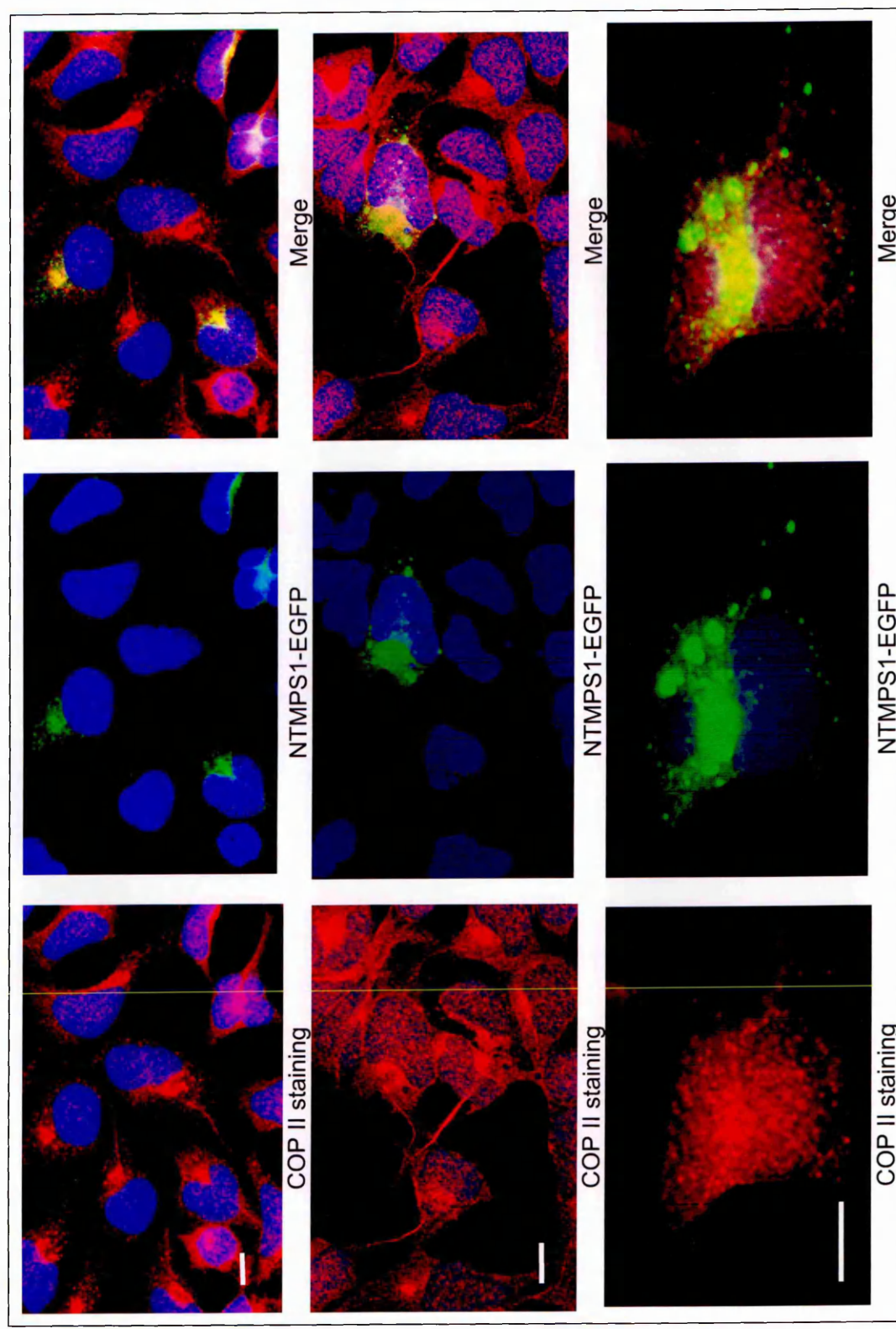


Figure 7.7. COP II staining in HEK 293 cells displays a peri-nuclear and punctate phenotype. The COP II antibody shows partial overlaps with the peri-nuclear phenotype but not the blob phenotype. DAPI stain in blue. Bars, 10µm.



Cos-7 cells over-expressing NTM PS1 fusion protein show altered Anti-COP II antibody staining

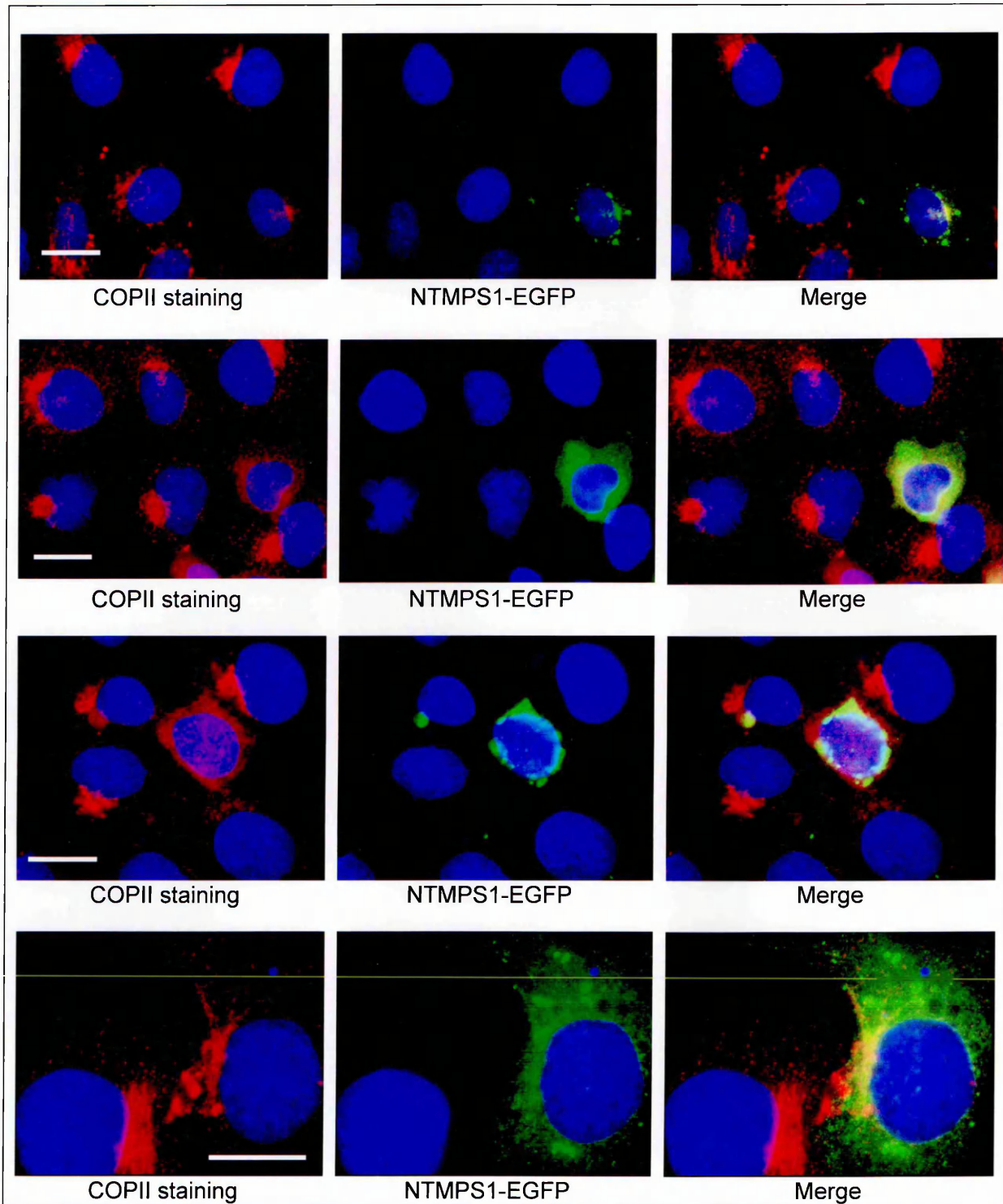


Figure 7.8. COP II staining of Cos-7 cells expressing moderate levels of the fusion protein exhibits a peri-nuclear phenotype. COP II staining does not localise with the blob-like aggregates. In cells expressing high levels of the fusion protein the Golgi ribbon-like staining pattern is absent or in a state of fragmentation. DAPI stain in blue. Bars, 20 μ m.

The blob phenotype does not associate with the lysosome marker LAMP-1

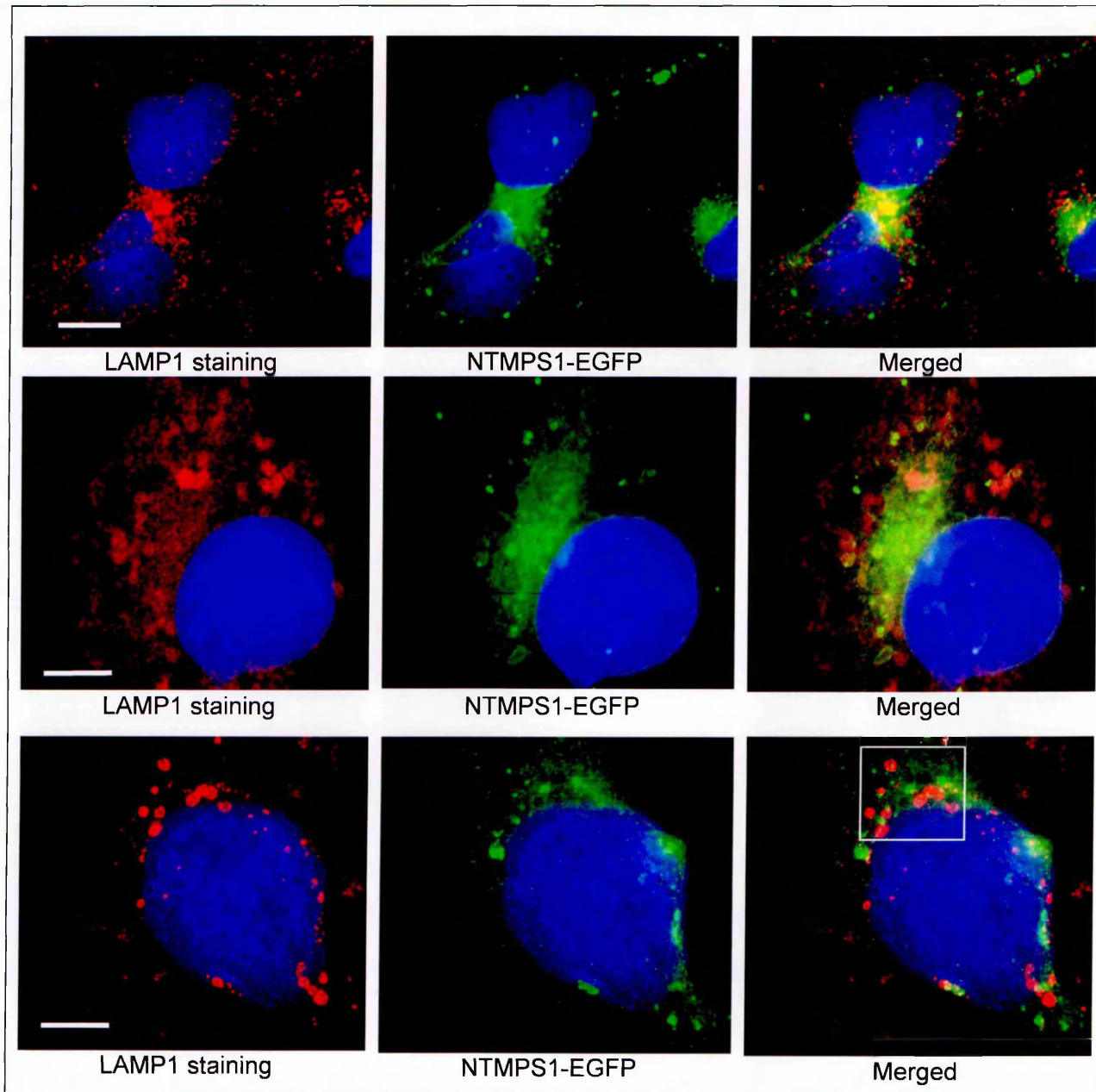
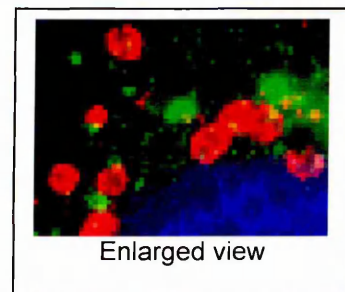


Figure 7.9. LAMP-1 staining of Cos-7 expressing the NTPS1-EGFP fusion protein. LAMP-1 displays a discrete vesicular phenotype (red) that does not co-localise with any of the phenotypes displayed by the fusion protein (green). The LAMP-1 antibody recognises a lysosomal membrane protein that produces a distinctive ring pattern quite separate from the blob phenotype (insert right). DAPI stain in blue. Bars, 20 μ m.



7.8 Proteasome 20S antibody staining of the fusion protein

The second intracellular proteolytic pathway involves the proteasome, a 26S (200 kD) complex, which in mammalian cells contains a 20S (673 kD) multi domain catalytic protein responsible for the degradation of a wide variety of polyubiquitinated proteins, including PS (Kim et al, 1997; Steiner et al, 1998). Excess holoprotein and non-incorporated fragments are degraded by the 26S proteasome. Using an interaction trap/two-hybrid assay and by immunoprecipitation, a direct physical interaction between PS1 and the 20S catalytic core of the 26S proteasome has been established (Van Gassen et al, 1999). To investigate whether the fusion protein similarly interacts with the proteasome, Cos-7 cells and PS1^{-/-} (mouse) cells exhibiting the blob phenotype were stained with a monoclonal anti-20S antibody. The results however were ambiguous since the 20S antibody showed poor staining in both cell lines. The fluorescence intensity of the 20S antibody in these cells was equivalent to primary-only antibody incubation in the absence of the alexxa 594 secondary. In the case that the fixation method affected antibody binding, the experiment was repeated with cells fixed in paraformaldehyde, however only non-specific binding was observed (data not shown).

7.9 The blob-like aggregates show ubiquitination

Whilst the interaction of the fusion protein with the proteasome could not be demonstrated definitively, involvement with the ubiquitin-proteasome system (UPS) can be inferred by examining the ubiquitin status of the fusion protein. Cells were stained with the anti-ubiquitin antibody and prepared for immunofluorescent microscopy. The anti-ubiquitin antibody co-localises with the blob-like aggregate phenotype, but not the reticular phenotype in HEK293 and Cos-7 cells expressing the fusion protein (figure 7.10, rows a and b). As a control, the extent of bleed-through by the fusion protein into the red channel was assessed. Bleed-through from the green channel was not detected in cells stained with the secondary antibody only, indicating that the fusion protein is intact ubiquitinated (figure 7.10, panel d). Additionally, HEK 293 cells were analysed by immunoblotting using the anti-EGFP and anti-Ubiquitin antibodies. Only those higher weight bands from the membrane fraction show weak

immunoreactivity to the anti-ubiquitin antibody (figure 7.10, panel d). These data show that only the blob-like aggregates are ubiquitinated and provide evidence that the higher weight immunoreactive bands seen in previous immunoblots may correspond to the blob-like phenotype.

The usage of the term 'blob-like aggregate' within the context of this thesis was meant purely as a general description for this phenotype. However, recent work by Johnston et al (1998) have characterised the existence of a single, stable, juxtannuclear aggregate referred to as an aggresome. Aggresomes are a general response by the cell to protein over-expression and can be generated artificially by inhibiting the proteasome. Once the degradative capacity of the proteasome is exceeded, polyubiquitinated protein aggregate at the microtubule organising centre (MTOC), and is accompanied by the rearrangement of the intermediate filament protein (IF) vimentin, which forms a containment cage around the aggregated protein core (Johnston et al, 1998). Previous reports show that PS2 is targeted for degradation by the proteasome (Kim et al, 1997) and that PS1 readily form aggresomes following proteasome inhibition (Johnston et al, 1998). To evaluate whether the NTMPS1-EGFP fusion protein similarly forms aggresomes, cells expressing the fusion protein were treated with the proteasome inhibitors lactacystin and MG132. Cells were then stained with several antibodies diagnostic for the presence of aggresomes.

7.10 The NTMPS-EGFP fusion protein accumulates as a distinct perinuclear structure following inhibition of the proteasome

To evaluate the effects of proteasome inhibition on Cos-7 cells, cells were treated for 12 hours with 25 μ M MG132 or 10 μ M lactacystin and stained with the anti-IF vimentin antibody (figure 7.11). Staining of untreated cells with the anti-vimentin antibody produces a fine thread-like pattern that ramifies throughout the cell (figure 7.11, panel a). This contrasts sharply with vimentin staining in cells treated with lactacystin and MG132. Here, cells display a characteristic collapsed halo phenotype that impinges on the nuclear membrane causing a significant deformation of the nucleus (figure 7.11, panels b and c). Next, cells expressing the fusion protein were stained for vimentin following proteasome inhibition and prepared for fluorescent microscopy (figures 7.12 and 7.13). Three general observations were made, namely: (1) Vimentin forms

a cage around the fusion protein in lactacystin and MG132-treated cells (figures 7.12, rows c, d, and figure 7.13, rows b, c, d). (2) Vimentin antibody staining in the absence of proteasome inhibition does not form a cage around the fusion protein blobs in Cos-7 or HEK293 cells (figures 7.12, rows a, b, and 7.13, row a). (3) The blob phenotype persists in cells treated with the proteasome inhibitors and forms a distinctive ring of blobs around the aggresome. This latter observation was more readily observable in HEK293 cells (figure 7.13, rows b, c, d).

7.11 Higher weight fusion protein aggregates show increased ubiquitin immunoreactivity in cells treated with proteasome inhibitors

Overall EGFP fluorescence was greater in cells treated with the proteasome inhibitors when compared to control cells. Similarly, western analysis of cells with the anti-EGFP and anti-ubiquitin antibodies show greater immunoreactivity in drug treated cells compared to control cells expressing the fusion protein (figure 7.14, panel a and b). As expected, EGFP immunoreactivity was absent from the cell soluble fraction in all the samples analysed (panel b, lanes 2-4). In the membrane fractions prepared from drug treated cells, EGFP immunoreactivity is greater in lactacystin treated cells when compared to MG132 treated cells, which in turn shows greater immunoreactivity compared to untreated control cell samples (panel b, lanes 6-8). Soluble fractions immunoblotted with the anti-ubiquitin antibody like wise show greater immunoreactivity following proteasome inhibition compared to control cells expressing the fusion protein (panel a, lanes 2-4).

Interestingly, the membrane derived cell fraction show a decrease in ubiquitin immunoreactivity for the 56 kD species following drug treatment. Conversely, the higher weight bands at approximately 120 kD show increased immunoreactivity following lactacystin treatment, compared to immunoreactivity in MG132 treated cells, which in turn is greater than the band intensity seen in control cells (panel a, lanes 6-8). This higher ubiquitin-staining band demonstrates that only a fraction of the fusion protein corresponding to the aggregated protein at 120 kD is targeted for proteasome degradation. Similarly, immunofluorescent microscopic examination of cells expressing the fusion protein shows co-localisation with the anti-ubiquitin antibody following lactacystin or MG132 treatment in some but not all cells (figure 7.14, panel c).

7.12 MG132 concentrations in the nanomolar range are sufficient to cause the collapse of vimentin around the aggresome

Whilst the above data demonstrate a clear physiological response by the cell to the presence of the proteasome inhibitors, a chief concern was the concentration of lactacystin and MG132 needed to obtain these results. For instance, MG132 is a potent, reversible proteasome inhibitor that has a K_i of 4 nM (Calbiochem data sheet), yet under the current experimental conditions cells were treated with 25 μ M MG132, presumably well in excess of that needed to inhibit the proteasome. Although such high concentrations of proteasomal inhibitors have been used by other laboratories investigating aggresome formation (Johnston et al, 1998; Garcia-Mata et al, 1999), the possibility exists that any observations made may be the result of other, unrelated systems being affected by too high a drug dose. To address this issue, cells were treated with a series of MG132 concentrations in the nanomolar range. To assess the degree of aggresome formation cells were stained for vimentin (figure 7.15). The number of cells displaying a peri-nuclear vimentin phenotype were then counted and expressed as a percentage of the total number of cells showing antibody staining (figure 7.16, a). Although the concentration series used here are not typical of a pharmacological range of concentrations, there is nonetheless a clear dose response affect (figure 7.16, b). Sub maximal concentrations of MG132 (5 nM to 50 nM) were sufficient to collapse the vimentin cage around the aggresome. Subsequent experiments using MG132 were therefore carried out with 50 nM to lessen any possible artefacts induced by too high a concentration.

7.13 MTOC staining is altered in Cos-7 cells expressing high levels of the fusion protein

Previous work has shown that the aggresome localises to the MTOC region of the cell in the immediate vicinity of the Golgi (Johnston et al, 1998) and is able to recruit mitochondria from the cell periphery to the region immediately surrounding the aggresome. To verify the presence of the aggresome in the present study, cells expressing the fusion protein were treated with 50 nM MG

132 for 12 hours and stained with antibodies for the MTOC or mitochondria. Staining in untreated cells reveals co-localisation of the fusion protein with the MTOC antibody, but only in those cells expressing high levels of the fusion protein (7.17, row a). Furthermore, MTOC staining appears to be altered in these cells. MTOC staining in untransfected neighbouring cells is widespread and ramifies throughout the entire cell. In transfected cells MTOC staining is limited to a much smaller region of cell radiating out from the edge of the nuclear region. Following proteasome inhibition, MTOC antibody staining and the fusion protein form as a perinuclear body that displays partial co-localisation (figure 7.17, row b).

Cells stained with the mitochondria antibody show an even distribution throughout Cos-7 and HEK293 cells in untreated, transfected and untransfected cells (Figure 7.17 rows c and d), though in Cos-7 cells exhibiting the blob phenotype, the mitochondria are effectively excluded from the immediate region of the cell occupied by the blobs (row c). Similarly, row c also shows the exclusion of mitochondria from a perinuclear site in an untransfected cell that exhibits a deformed nucleus, typical of the aggresome. In this instance, aggresome formation is observed in the absence of proteasome inhibition. The addition of MG 132 however, causes a dramatic shift in the location of mitochondria from a scattered distribution throughout the cell, to a juxtannuclear position, where the fusion protein and the mitochondria partially overlap (figure 7.17, row d). Overall, the presence of the fusion protein had no effect on the number of mitochondria in transfected or untransfected cells.

7.14 Formation of the blob-like phenotype does not require intact microtubules

Previous studies have shown that aggresome formation at the MTOC requires an intact cytoskeleton (Johnston et al, 1998) and that disruption of the microtubule dynein/dynactin transport complex inhibits aggresome formation (Garcia-Mata et al, 1999). To test whether the aggresomes generated from the fusion protein require an intact microtubule system for their formation, cells expressing the fusion protein were treated with MG132 alone or in combination with the microtubule disrupting agent nocodazole and stained for the centrosome (MTOC) marker γ -tubulin or vimentin (figure 7.18). MG132 and

The blob-like aggregates are ubiquitinated

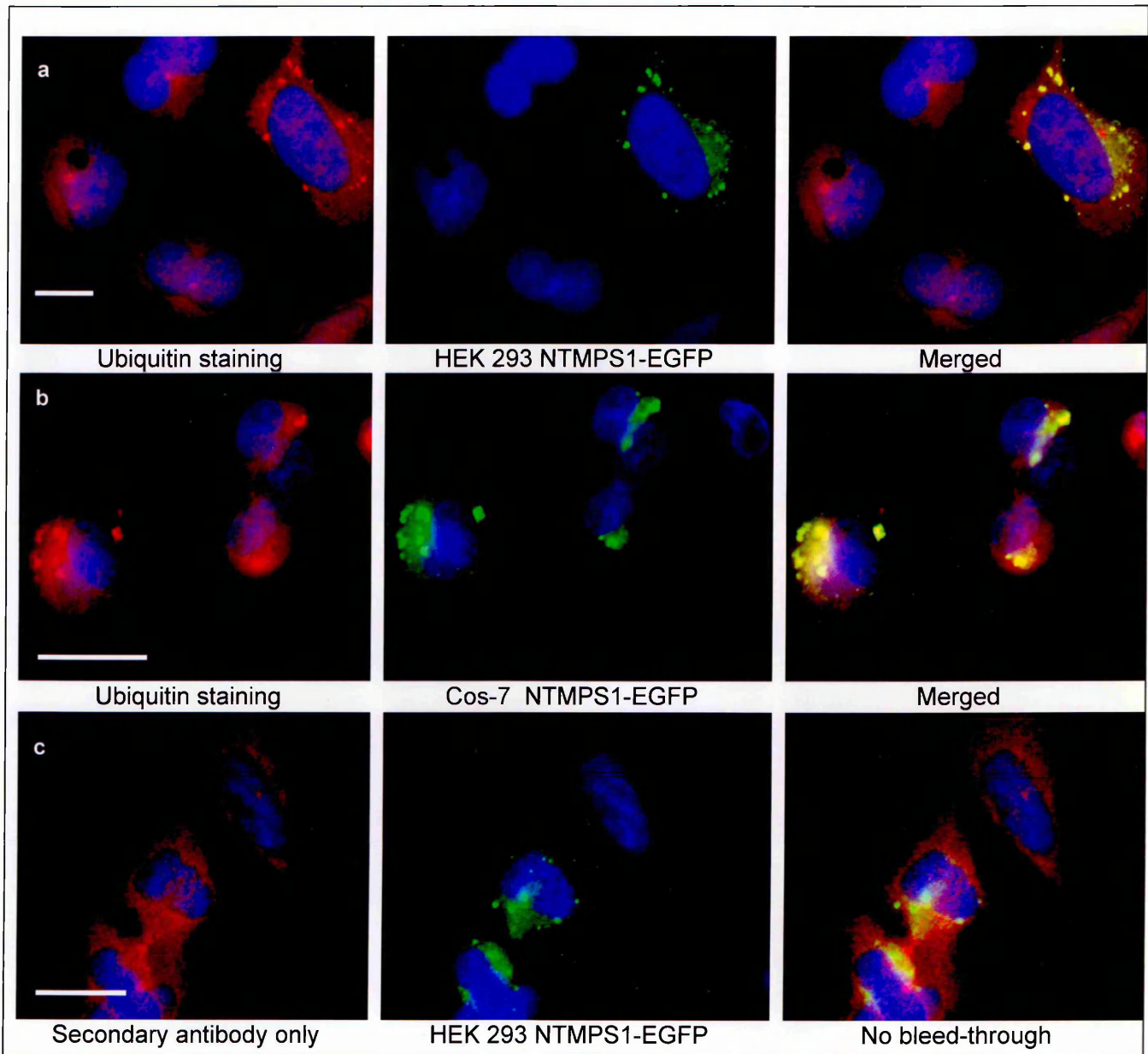
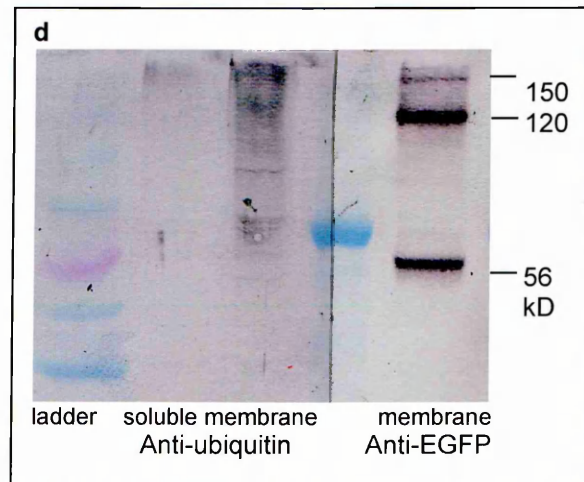


Figure 7.10. Ubiquitin antibody staining of cells expressing the NTMPS1-EGFP fusion protein. The blob phenotype stains for ubiquitin in (a) HEK293 and (b) Cos-7 cells. (c) Secondary antibody staining shows that the fusion protein does not bleed-through into the red channel (gain +9). DAPI stain in blue. Bars, 20 μ m. (d) Western analysis of HEK 293 cells stained with anti-EGFP and anti-Ubiquitin antibodies. The higher weight bands from the membrane fraction show weak immunoreactivity to the anti-ubiquitin antibody. Samples analysed by 7.5% SDS Urea PAGE.





The IF vimentin collapses at a perinuclear position in response to proteasome inhibition

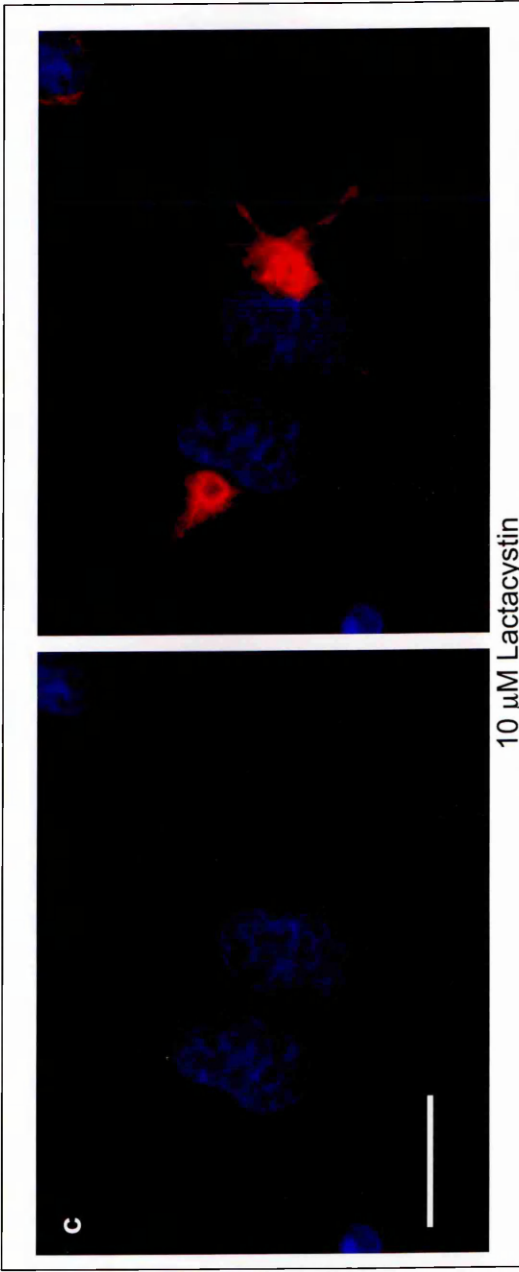
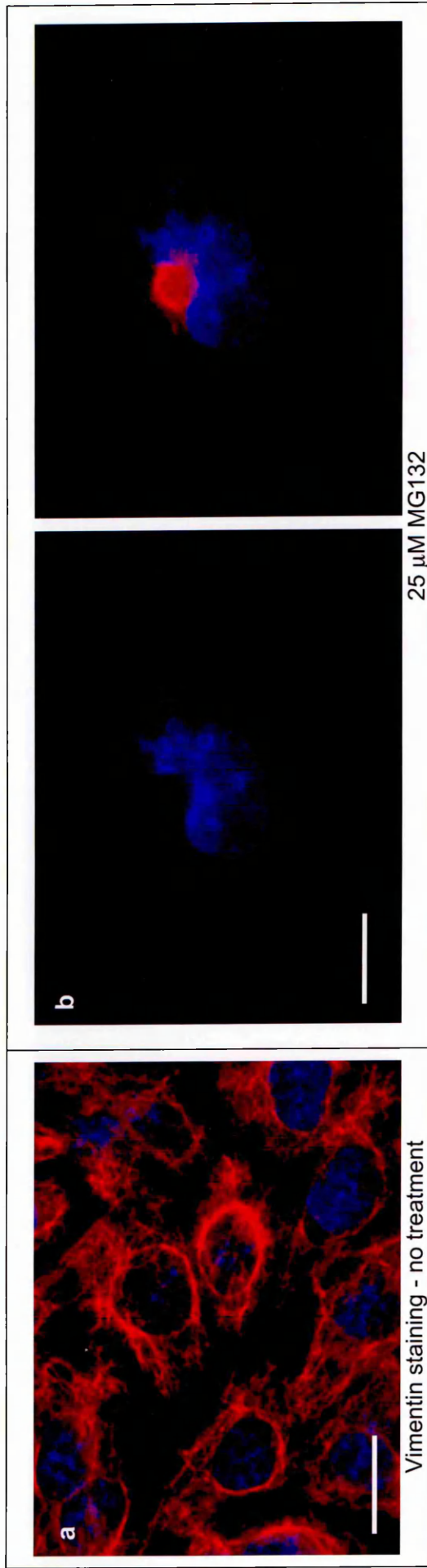


Figure 7.11. Aggresome formation causes a redistribution of the IF vimentin following proteasome inhibition. Cos-7 cells were treated for 12 hours with either 25 μM MG132 or 10 μM lactacystin. (a) Vimentin staining in untreated cells displays a fine thread-like pattern. Treatment with MG132 (b) or lactacystin (c) causes the collapse of vimentin into a halo and a significant deformation of the nuclear membrane. DAPI stain in blue. Bars, a 10 μm , b and c 20 μm .

The fusion protein forms aggresomes following proteasome inhibition in Cos-7 cells

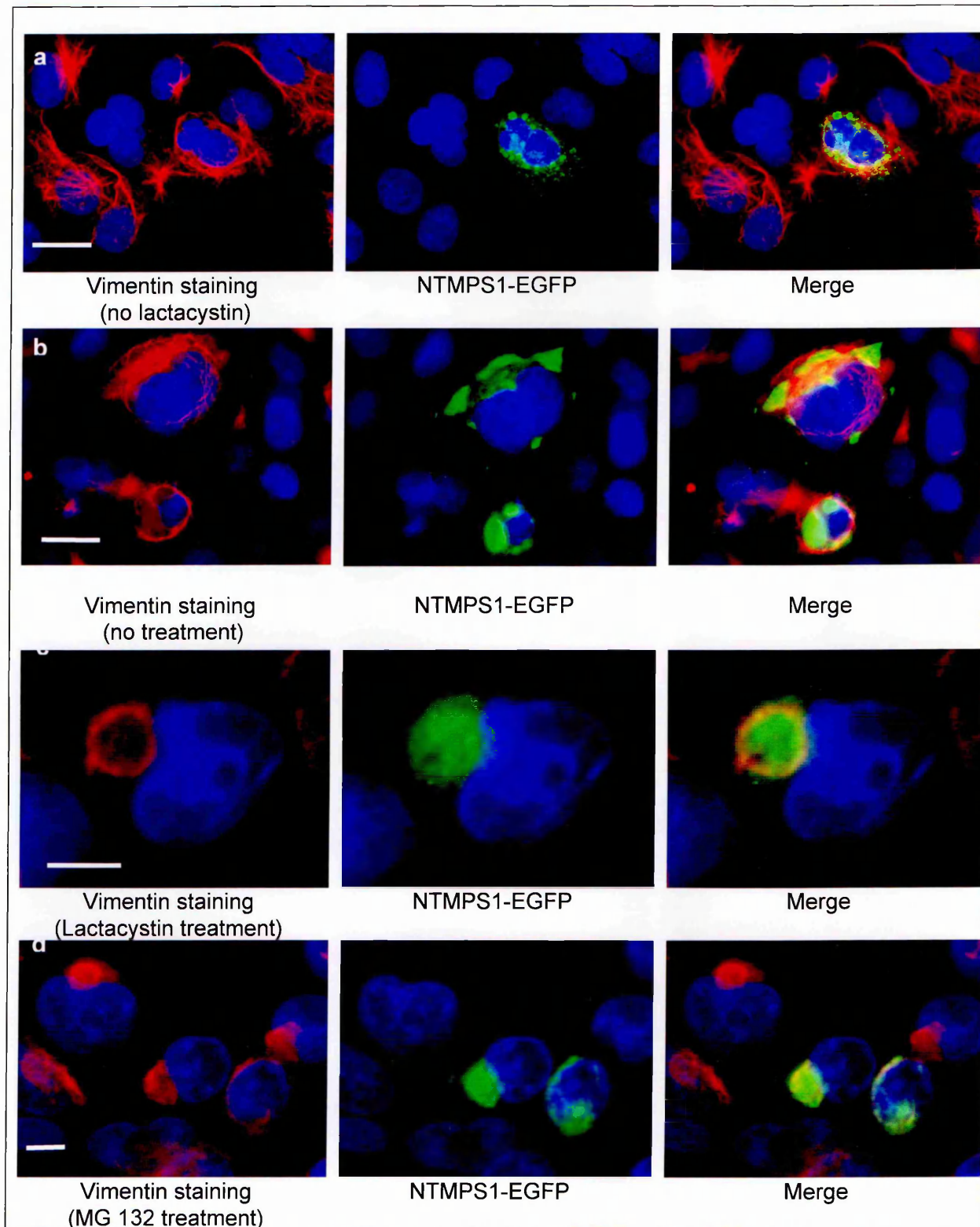


Figure 7.12. Vimentin staining of Cos-7 cells treated for 12 hours with the proteasomal inhibitors MG132 (25 μ M) and Lactacystin (10 μ M). Vimentin does not form a cage around the blobs in untreated cells (rows a and b). Following the inhibition of the proteasome, the fusion protein forms as a perinuclear aggresome surrounded by a vimentin cage (rows c and d). DAPI stain in blue. Bars, (a) and (b) 20 μ m, (c) 5 μ m, (d) 10 μ m.

The fusion protein forms aggregates following proteasome inhibition in HEK293 cells

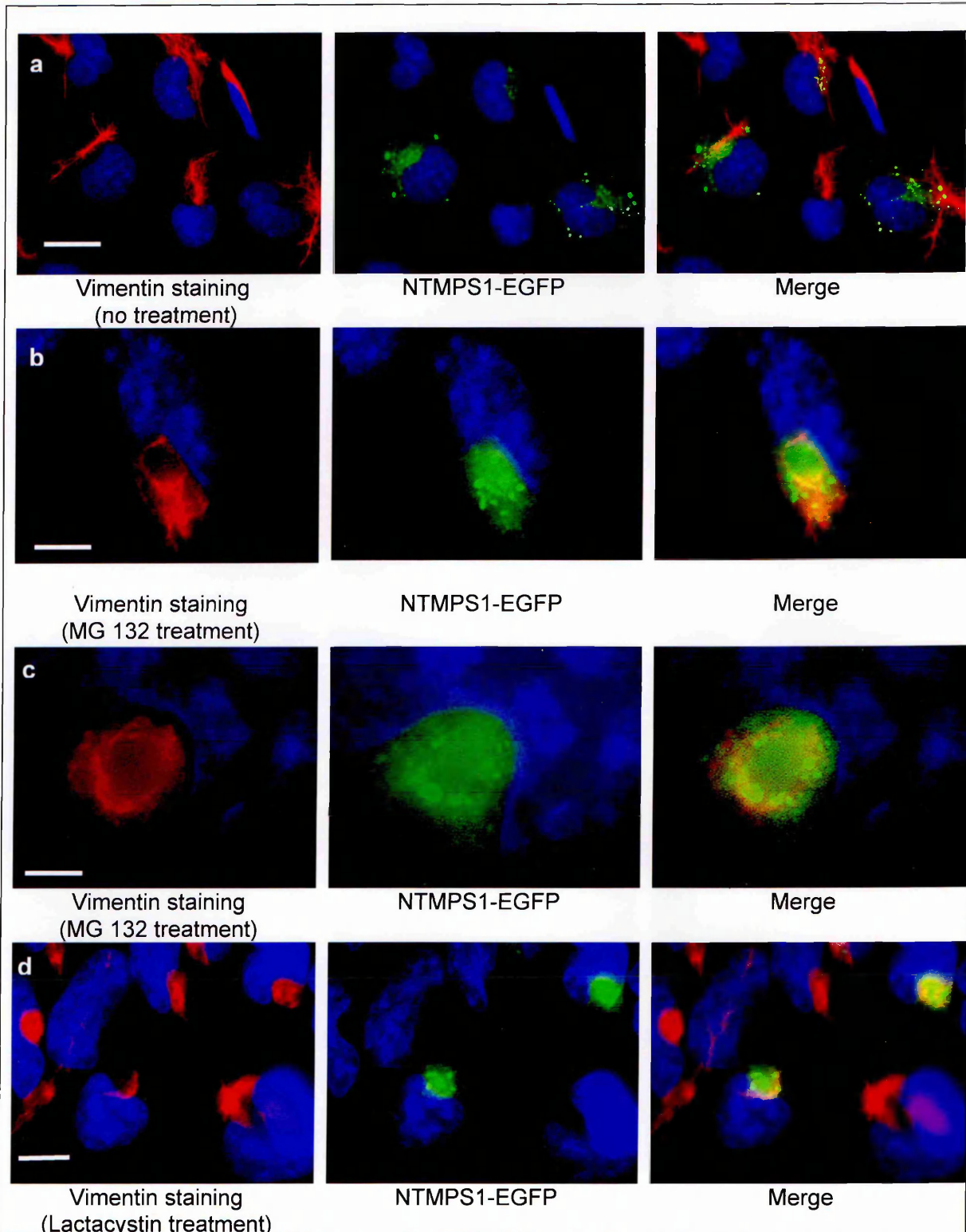


Figure 7.13. Vimentin staining of HEK293 cells treated for 12 hours with the proteasomal inhibitors MG132 (25 μ M) and Lactacystin (10 μ M). Vimentin does not form a cage around the blobs in untreated cells (row a). Following the inhibition of the proteasome, the fusion protein forms as a perinuclear aggregate (rows b-d), however, the vimentin cage appears to exclude the blobs, which are present as a ring surrounding the aggregate. DAPI stain in blue. Bars, (a) 20 μ m, (b) and (c) 2.5 μ m, (d) 10 μ m.

EGFP fluorescence increases following proteasome inhibition

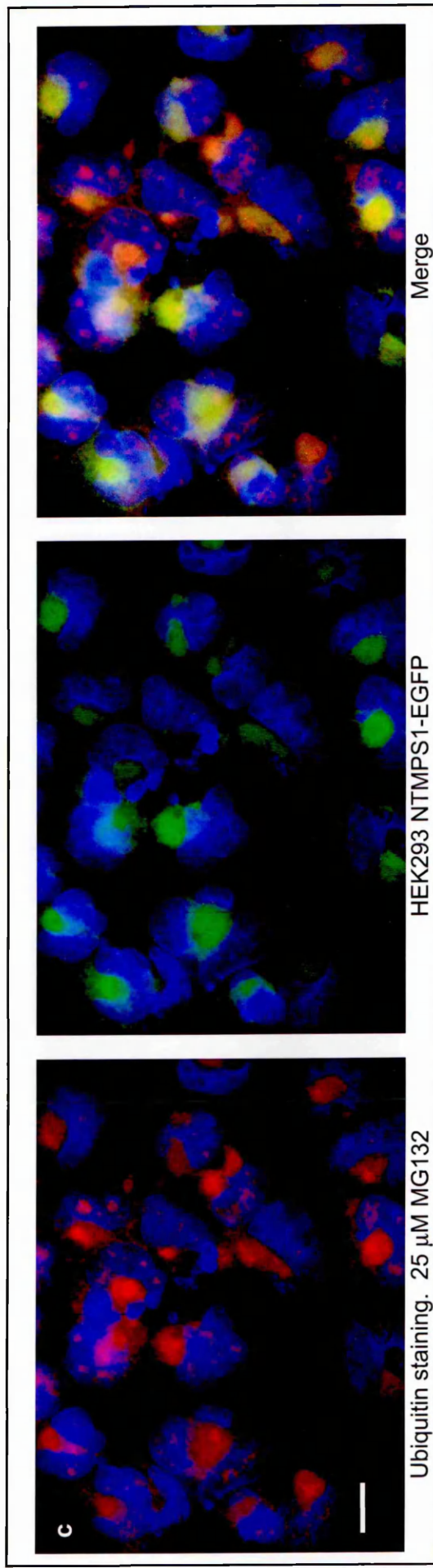
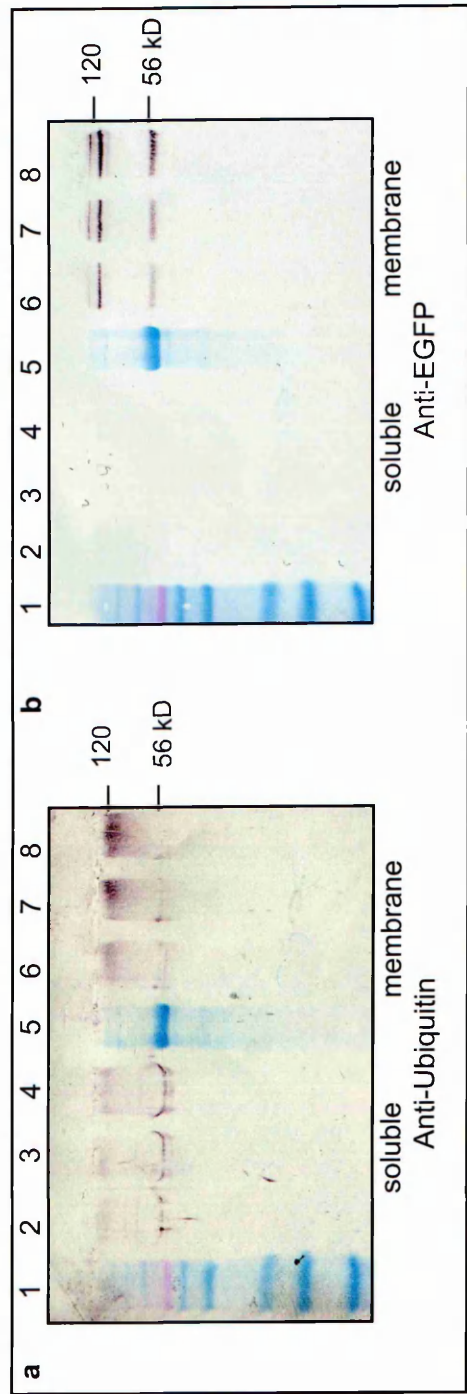


Figure 7.14. Proteasome inhibition of NTMPS1 HEK 293 cells. Cells were treated for 12 hours with 25 μ M MG132 or 10 μ M Lactacystin. Soluble and membrane fractions were immunoblotted with (a) anti-Ubiquitin (b) and anti-EGFP antibodies. Lactacystin treated cells show greater immunoreactivity when compared to MG132 treated cells, which in turn show greater immunoreactivity compared to the untreated control cell fraction. (c) Overall, EGFP fluorescence is greater in cells exposed to the proteasome inhibitors. Samples analysed by 10% Urea SDS PAGE. DAPI stain in blue. Bar, 20 μ m.

Proteasome inhibition of NTMPS1-EGFP HEK 293 cells with MG132 occurs in the nanomole range

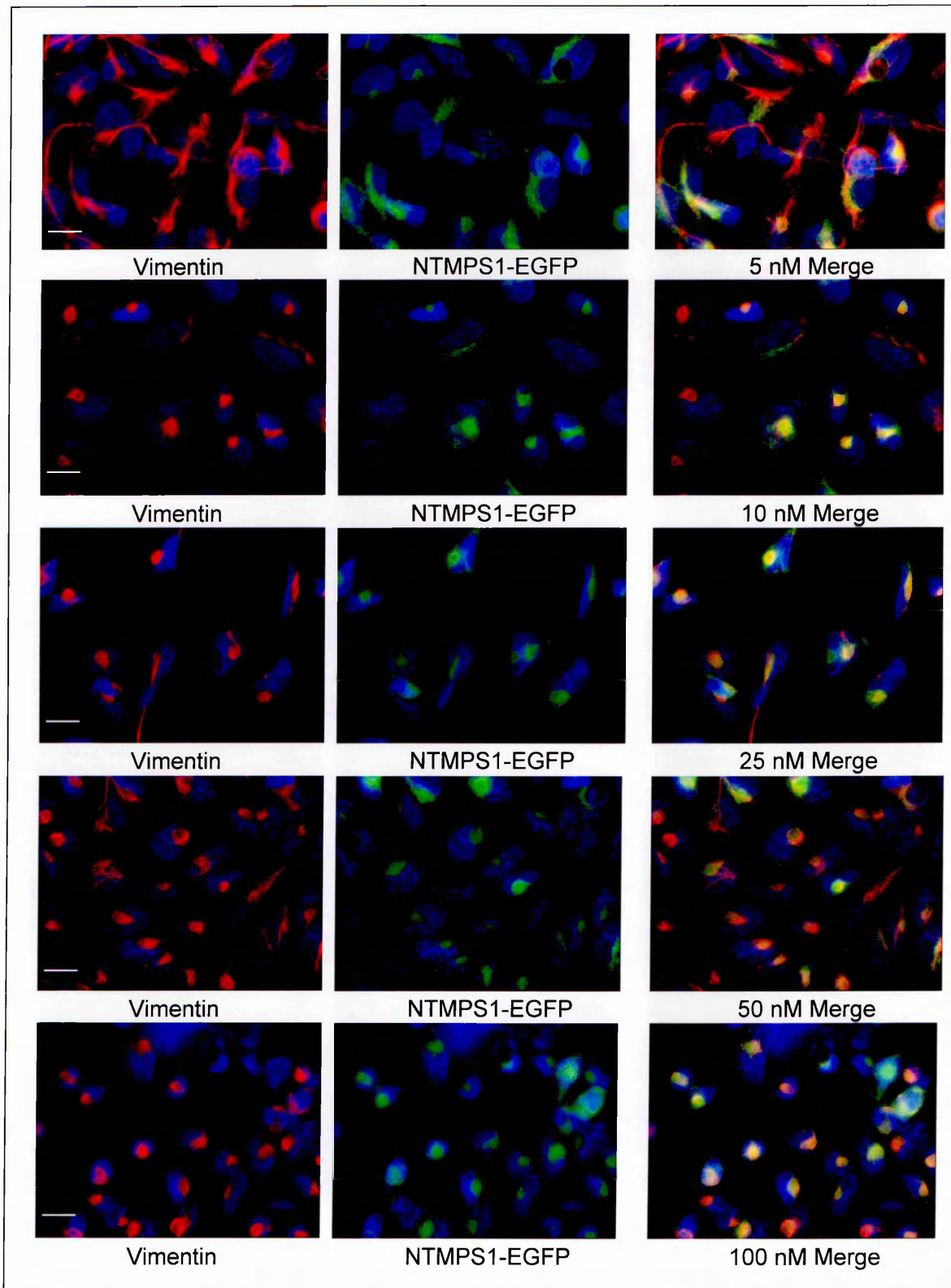


Figure 7.15. Overnight (12hr) treatment of NTMPS1 HEK 293 cells with 5 nM-250 nM MG132. Cells stained for Vimentin (red). DAPI stain in blue. Bars, 20 μ m.

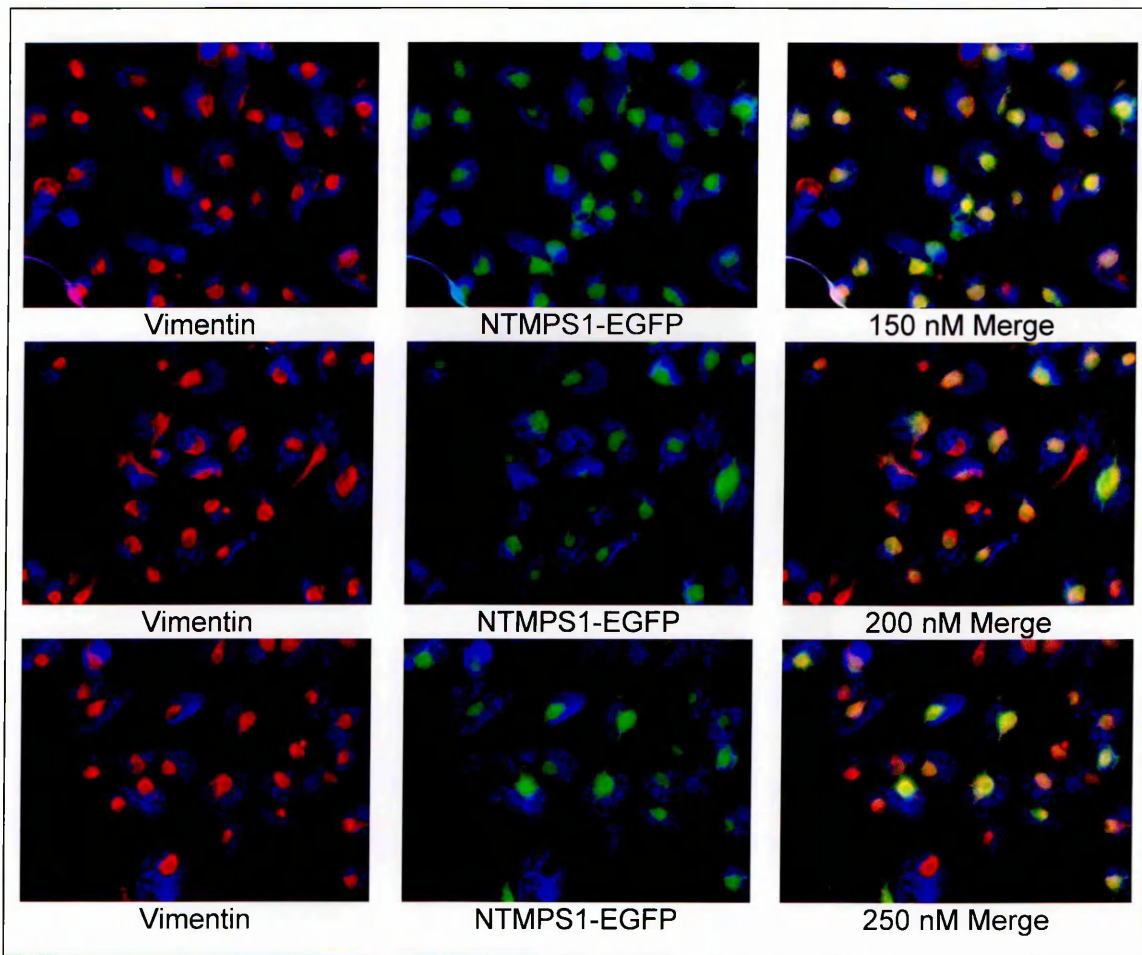


Figure 7.15 (continued)

a.

[MG132] nM	Number of cells displaying peri-nuclear Vimentin staining (%)
5	29
10	61
25	60
50	78
100	81
150	93
200	100
250	100

b.

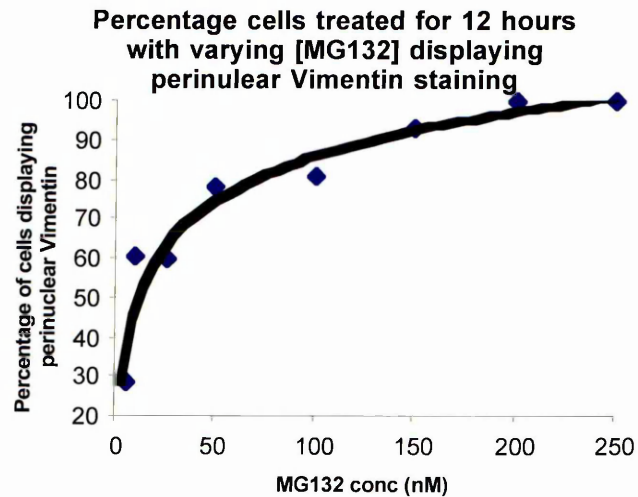


Figure 7.16. Effect of varying MG132 concentration on the distribution of vimentin in HEK 293 NTMPS1 cells. (a) The number of cells in figure 7.25 displaying a peri-nuclear vimentin phenotype were counted and expressed as a percentage of the total number of cells showing vimentin antibody staining. (b) Data from (a) generates a dose response curve following MG132 treatment of cells expressing the fusion protein.

MTOC staining is altered in cells over expressing the fusion protein

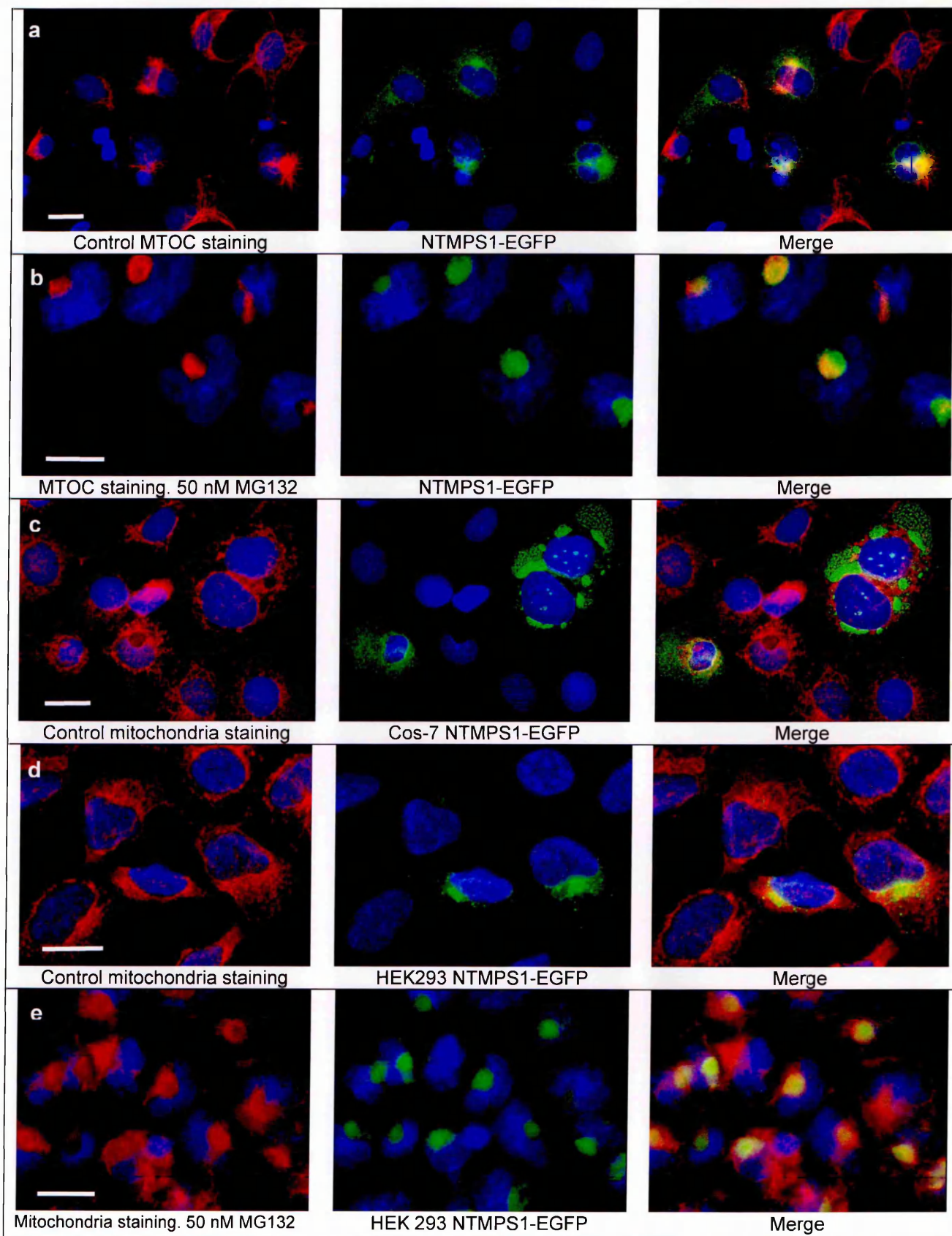


Figure 7.17. MTOC and Mitochondria antibody staining in HEK293 and Cos-7 cells. (a and b) MTOC staining is altered in cells over expressing the fusion protein. Following MG132 treatment, MTOC staining partially overlaps with the fusion protein at a juxtannuclear location. (c and d) Mitochondria staining in untreated Cos-7 and HEK 293 cells is distributed throughout the cell. (e) Treatment with MG132 results in a juxtannuclear phenotype containing mitochondria and the fusion protein. DAPI stain in blue. Bars, 20 μ m.

Aggresomes formed by over expression of the fusion protein or proteasome inhibition require an intact microtubule network

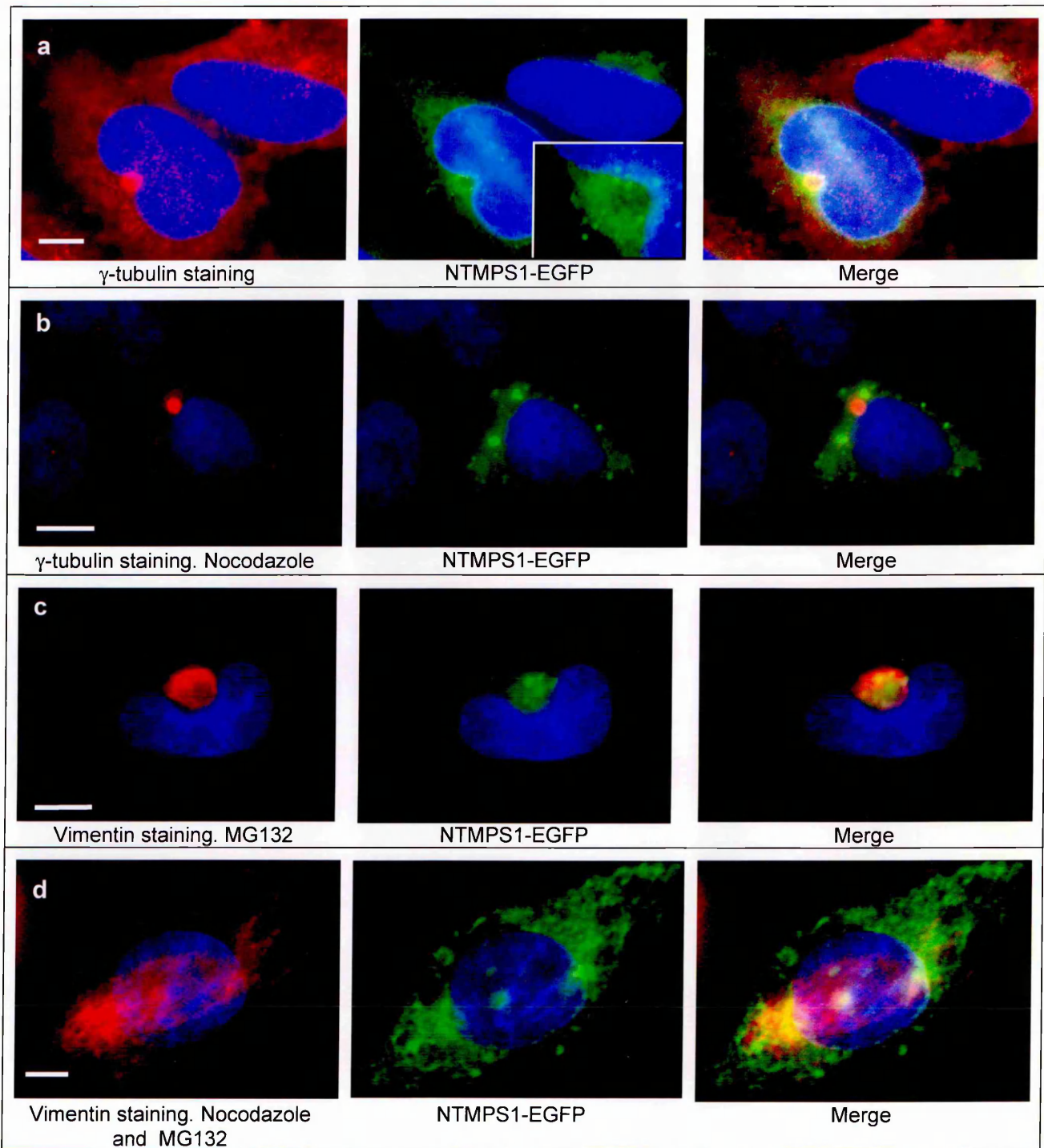


Figure 7.18. Cos-7 cells were treated for 12 hrs with 50 nM MG132 alone or in combination with the microtubule disrupting agent nocodazole (10 μ g/ml) and stained for the centrosome (MTOC) marker γ -tubulin, or the IF vimentin. (a) γ -tubulin staining co-localises with the fusion protein, which forms as a aggresome in the absence of proteasome inhibition. Small blobs are seen to gather around the aggresome (insert). (b) Nocodazole treatment does not affect γ -tubulin staining, or the formation of fusion protein blobs. (c) A vimentin cage forms around a perinuclear aggresome in cells treated with MG132. (d) Aggresome formation is prevented in cells treated with both nocodazole and MG132. Nocodazole treatment prevents both the collapse of vimentin into a cage surrounding the fusion protein and the characteristic distension of the nucleus. Notice that the fusion protein maintains a reticular and blob-like aggregate distribution throughout the cell, indicating that blobs do not require an intact microtubule system for their formation. DAPI stain in blue. Nocodazole and MG132 were added to lipofectamine-treated cells 5 hours post transfection prior to the appearance of the fusion protein. Bars, (a) and (b) 10 μ m, (c) and (d) 5 μ m.

The reticular phenotype appears prior to the blob phenotype

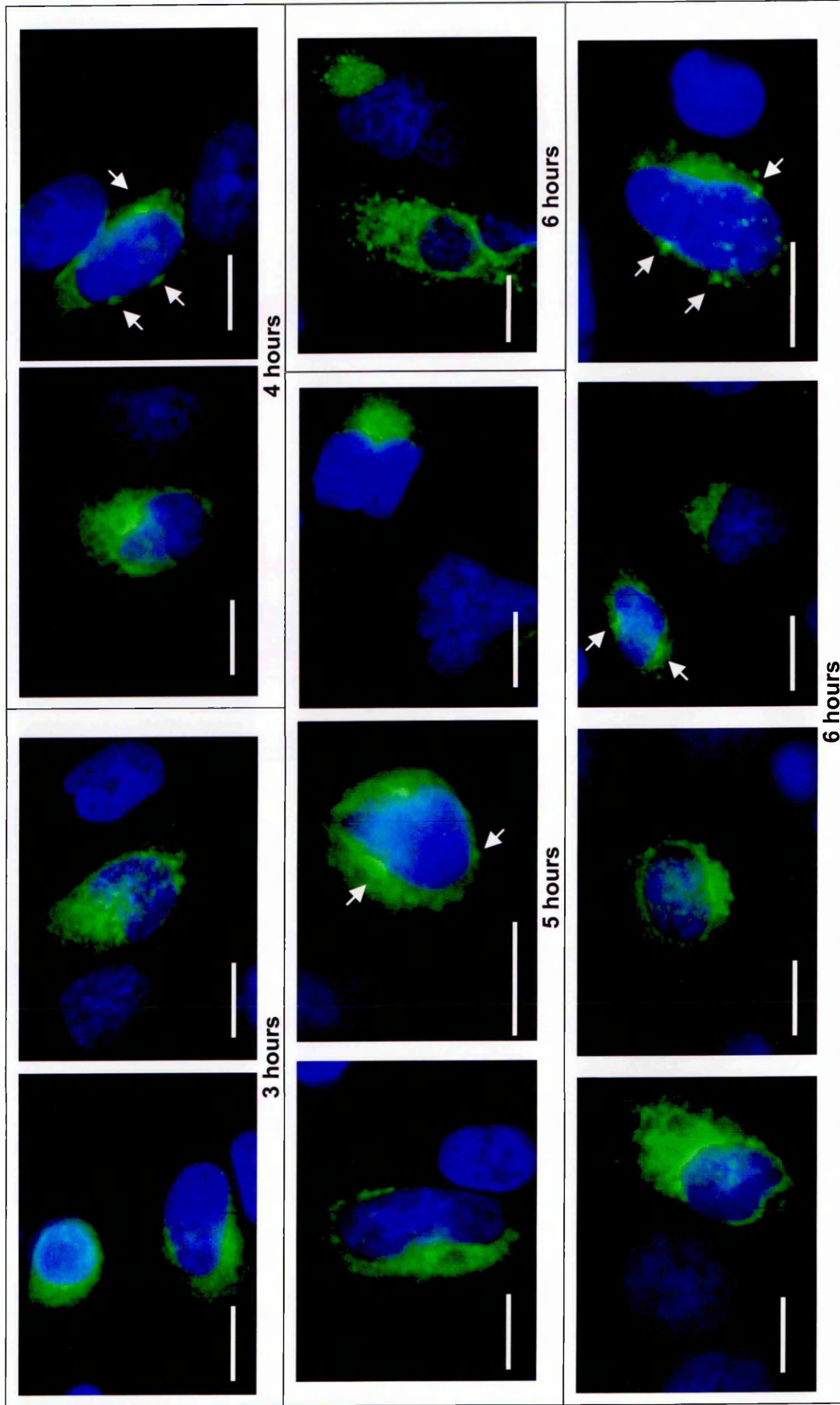


Figure 7.19. Analysis of transfected cells over time. The fusion protein appeared three hours after first transfection as a reticular phenotype. By four hours the first signs of the blob phenotype appear as 'swellings' intimately associate with the reticular-nuclear interface (arrows). The first signs of a peri-nuclear phenotype appear after 4 to 5 hours. By 6 hours cells exhibit the full range of phenotypes. Cells transfected using lipofectamine 2000. Cells fixed in methanol at times indicated. DAPI stain in blue. Bars, 10 μ m.

The blob phenotype arises as 'swellings' at the reticular-nuclear interface

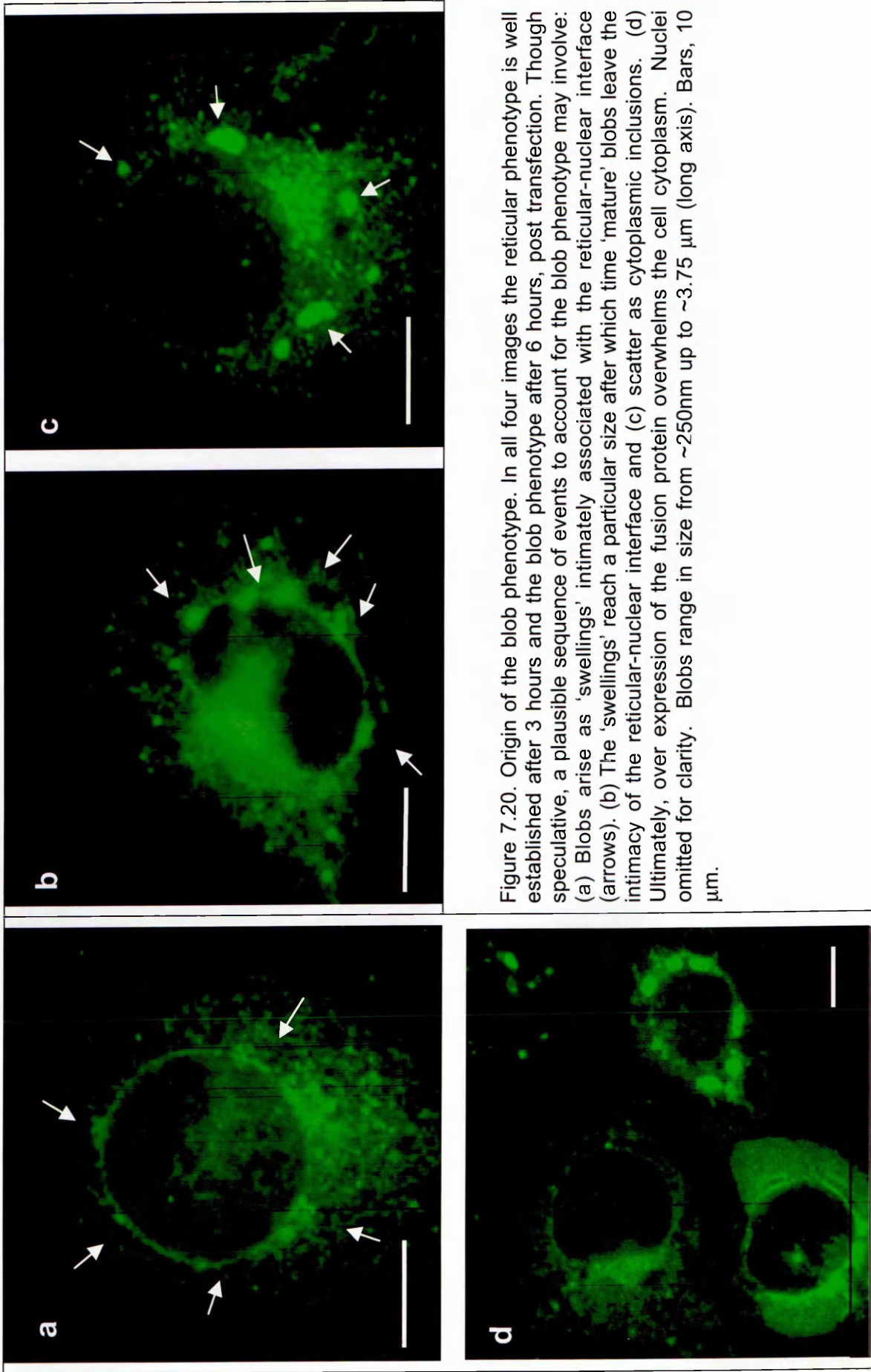


Figure 7.20. Origin of the blob phenotype. In all four images the reticular phenotype is well established after 3 hours and the blob phenotype after 6 hours, post transfection. Though speculative, a plausible sequence of events to account for the blob phenotype may involve: (a) Blobs arise as 'swellings' intimately associated with the reticular-nuclear interface (arrows). (b) The 'swellings' reach a particular size after which time 'mature' blobs leave the intimacy of the reticular-nuclear interface and (c) scatter as cytoplasmic inclusions. (d) Ultimately, over expression of the fusion protein overwhelms the cell cytoplasm. Nuclei omitted for clarity. Blobs range in size from ~250nm up to ~3.75 μm (long axis). Bars, 10 μm .

nocodazole were added 5 hours post transfection to Lipofectamine-treated cells prior to the appearance of the fusion protein. Staining of cells for γ -tubulin reveals a perinuclear phenotype that localises with fusion protein (row a), which appears as small blobs surrounding the aggresome (insert, row a). Moreover, high levels of the fusion protein results in the distension of nuclear envelope, indicating that fusion protein can spontaneously form aggresomes in the absence of proteasome inhibition (Johnston et al, 1998).

Importantly, unlike aggresomes, treatment of cells with nocodazole has no affect on the development of the blob-like aggregates, which maintain a scattered appearance throughout the cell indicating that intact microtubules are not required for their formation (row b). In cells treated with MG132, a vimentin cage forms around a perinuclear aggresome (row c). Conversely, aggresome formation is prevented in cells expressing the fusion protein following MG132 and nocodazole treatment, even after 12 hours incubation (figure 7.18, row d). In addition, vimentin staining exhibits a network of fibres, whereas the fusion protein maintains an ER and a blob-like aggregate distribution throughout the cell. Furthermore, distension of the nucleus, characteristic of the aggresome, is absent from drug treated cells.

7.15 The PS1 fusion protein phenotypes do not alter over time

Having established that the fusion protein forms aggresomes in response to its over expression and following proteasome inhibition, the identity of the blob phenotypes was further pursued. In particular, the cell compartment from which the blobs are derived and whether they are membrane-bounded structures or cytoplasmic aggregates remains unknown. The question arose as to whether the number of cells displaying the blob phenotype would increase over time. This would be a reasonable assumption to make if the phenotypes arose following maturation: ER/Golgi>Vesicles>Blobs.

To address this issue, the phenotypes of cells transfected with all four constructs were examined over a 6-hour period by fluorescent microscopy. Cells were transfected with lipofectamine and examined at 1-hour intervals over a 6-hour period. No EGFP fluorescence was detected over this time period. It was assumed that the absence of complete media was responsible for lack of expression of the fusion protein by the cells. This problem was overcome by

the use of lipofectamine 2000, a transfection agent which complexes with the cDNA even in the presence of complete media. As expected the number of cells expressing the fusion protein increased over time. The first signs of fluorescence appeared after 3 hours as a reticular phenotype (figure 7.19 & 7.20). By four hours post transfection, the first signs of the blob phenotype appear as circumnuclear 'swellings' intimately associate with the reticular-nuclear interface. Measurement of the blobs show that they range in size from ~250 nm up to ~3.75 μm (long axis). The first signs of a peri-nuclear phenotype appear after 4 to 5 hours. By 6 hours cells exhibited the full range of phenotypes (figure 7.20, a-d).

In a follow-up experiment the time intervals following transfection were extended. Cells expressing the fusion protein were examined after 10, 24, 36 and 58 hours. Overall there was no change in number of cells displaying the blob phenotype between each time point 10 hours after first transfection (data not shown).

7.16 TEM examination of the cells expressing the fusion protein reveals laminar structures and phagosomes

To examine the ultrastructure of the blobs, Cos-7 cells expressing the fusion protein were examined by transmission electron microscopy (TEM). Cells show a variety of structures such as mitochondria with visible cristae, lysosomes showing the tell-tale double unit membrane and phagosomes responsible for the degradation of certain cell components (Dunn, 1990), as well as the unexpected presence of unusual laminar bodies (figure 7.21). Structures resembling the blob phenotype in terms of their dimensions, distribution and numbers are seen in some, but not all cells. Approximately 1 in 3 cells display these structures, consistent with the transfection rate seen for control cells exhibiting fluorescence in samples fixed for conventional microscopy (data not shown).

Several regions throughout the cell show dark patches compared to the neighbouring regions, which on closer inspection are composed of compressed tubules (figure 7.21, A). Whole regions of the cytoplasm were occupied with multilaminar bodies, some of which consist of concentric, myelin-like whorls (figure 7.21, B & C). One of the multilaminar structures appears to be folding

back on itself possibly indicating how they form. A magnified view reveals that a unit membrane delimits part of this structure. Additionally, some regions of the cell containing the lamellar bodies appear to be loosely bounded by the ER. These bodies associate to varying degrees with the phagosomes, the contents of which vary in appearance (figure 7.21, D-G). Also, patches of the nuclear membrane in the region of the lamellar body are discontinuous or absent altogether (D-G).

Interestingly, associated with the lamellar bodies is the complete absence of any well-defined cytoplasmic structure (figure 7.21, H-K), suggesting that the contents have been engulfed by the phagosome and subsequently disposed off. The lamellar bodies appear to occupy one side of the vacuole, whilst the lumen contains various remnants suggesting that the specimens exhibit various stages of clearance. The presence of mitochondria showing intact cristae indicates that the lamellar bodies/vacuoles in these cells are not responsible for apoptosis, leastways; type 1 caspase-associated cell death (Clarke et al, 1990). Closer examination of the vacuoles reveals ragged margins in some places yet well-defined margins in others (figure 7.21, I-O). In these specimens the vacuole encloses the entirety of the lamellar bodies, which appear continuous with one another, however both structures remain separate when viewed at a higher magnification (figure 7.21, O). Interestingly, where the blob-like aggregates/multilamellar bodies predominate, the ER is barely present whilst there is little suggestion of the Golgi compartment.

7.17 Chapter summary

To summarise, the presence of the EGFP moiety is not a contributing factor in the phenotypes displayed by cells expressing the fusion protein. The blob phenotype does not appear to be ER or Golgi fragments since antibody staining with cell compartment markers such as Colligin, Ergic53, membrin, etc, do not show co-localisation. Furthermore, altered antibody staining for COPII and MTOC is seen in some cells expressing the fusion protein. Additionally, ubiquitin antibody staining is restricted to the blob phenotype. Proteosomal inhibition of cells expressing the fusion proteins generates juxtannuclear aggregates in a microtubule dependent manner, resulting in the collapse of vimentin around the fusion protein. The blob phenotype appears to originate

from the nuclear membrane/ER interface where formation is microtubule-independent. TEM reveals the presence of phagosomes and numerous, structured bodies that are composed of concentric myelin-like whorls associated with large vacuoles devoid of any kind of structure.

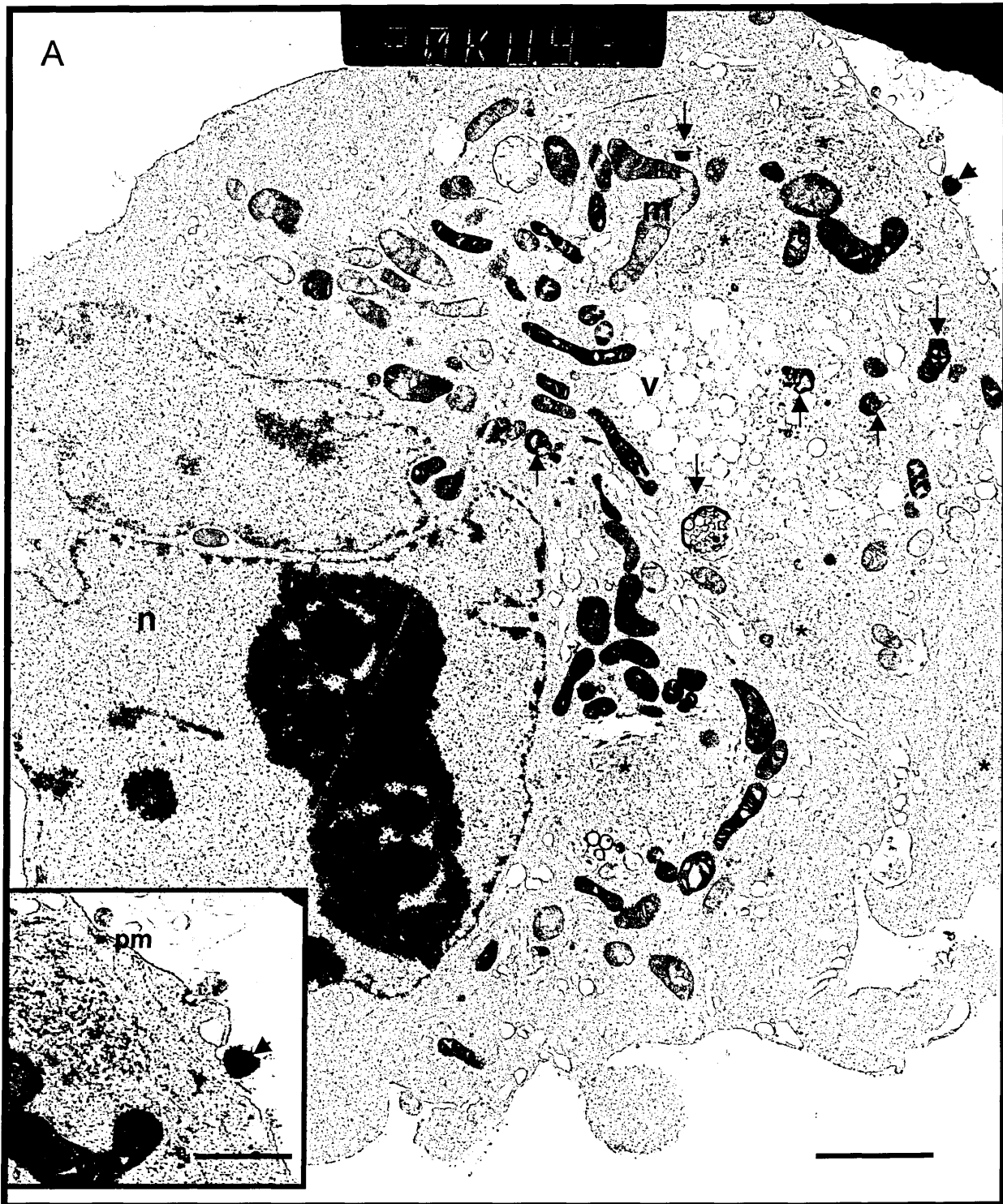


Figure 7.21. Transmission electron microscopy of Cos-7 cells expressing the fusion protein. A. Cos-7 cells affixed to coverslips were transfected with pNTMPS1-EGFP. Fixed Specimens were scraped off and prepared for EM as described under Methods and Materials. Cells show a nucleus (n) and numerous mitochondria (m) present throughout the cytoplasm. Close examination reveals the presence of cristae within the mitochondria. Numerous vacuoles are scattered throughout the cell (v). A few autophagosomal structures (arrows) were seen at various phases of maturation. The inset (left) from the top right of the picture shows the expulsion of an autophagosomal vacuole from the cell plasma membrane (pm). Noticeable was the presence of several darker regions (*), which on close examination are revealed to be composed of compressed tubules. Interestingly there is little sign of the ER or Golgi compartments. Bar, 2.5 μm , inset 1 μm .

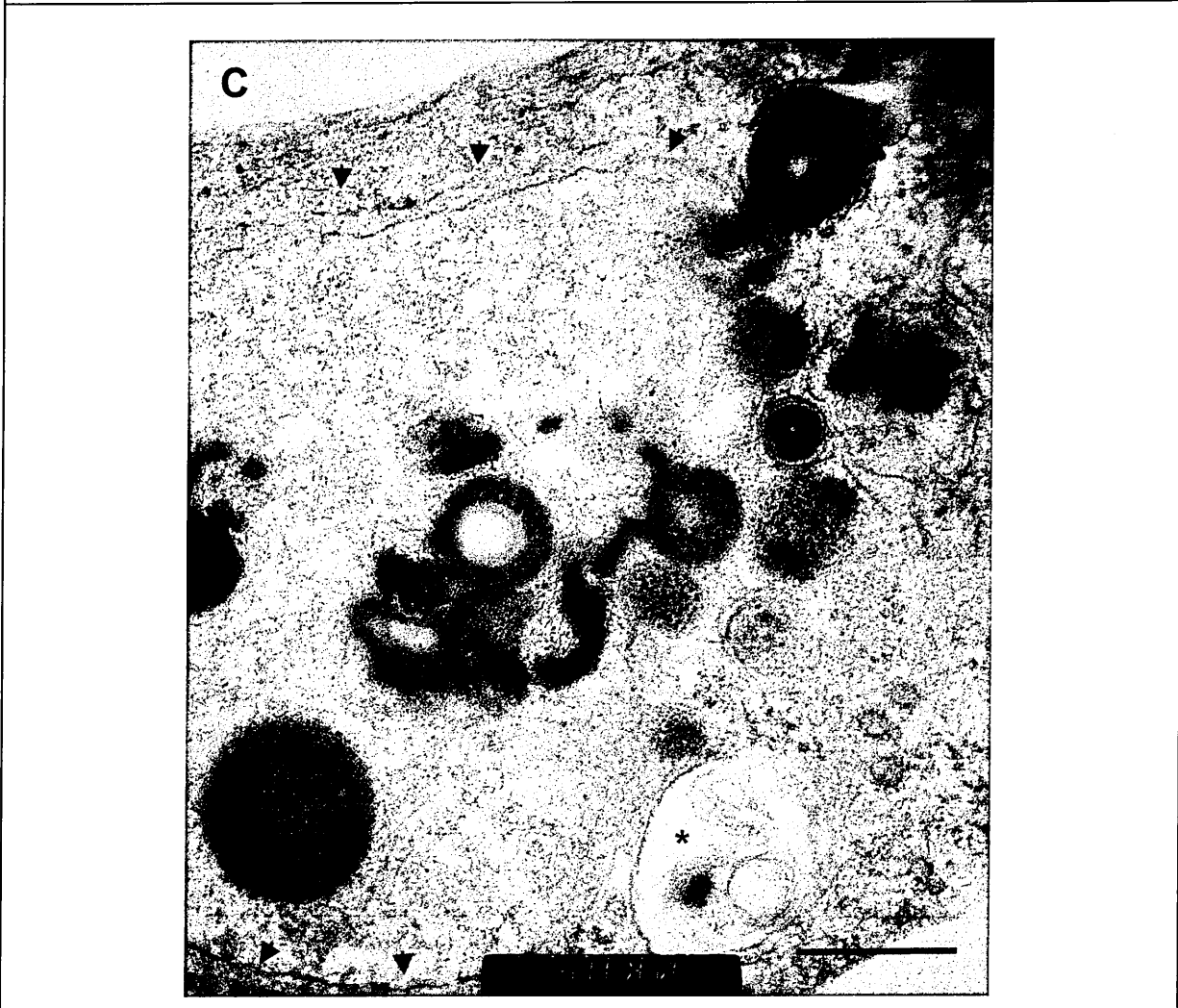
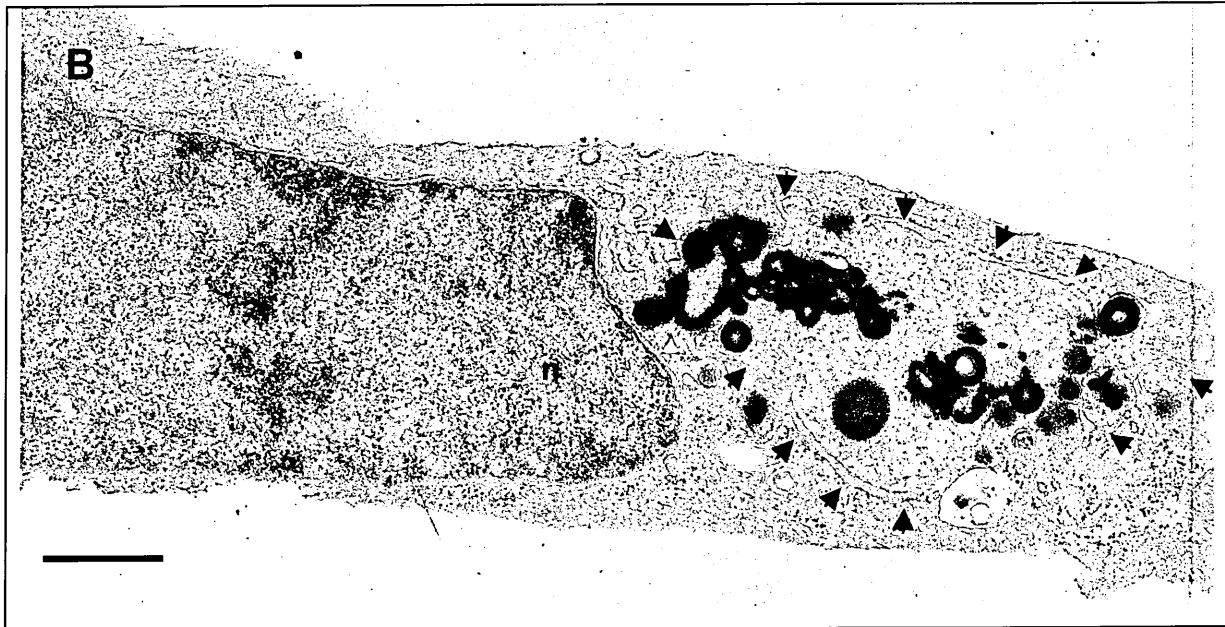


Figure 7.21. B. Electron dense inclusions exhibit a laminar structure that appears to be bounded by the ER (outlined by arrowheads in B). C. An enlarged view shows that the multilaminar structures are composed of concentric layers resembling myelin whorls. An autophagosome vacuole (*) has engulfed some of the cytoplasmic contents of the cell. The red arrowhead shows one of the multilaminar structures folding back on itself. Close inspection reveals that a unit membrane delimits part of this structure. Bars, (B) 1 μm , (C) 250 nm.

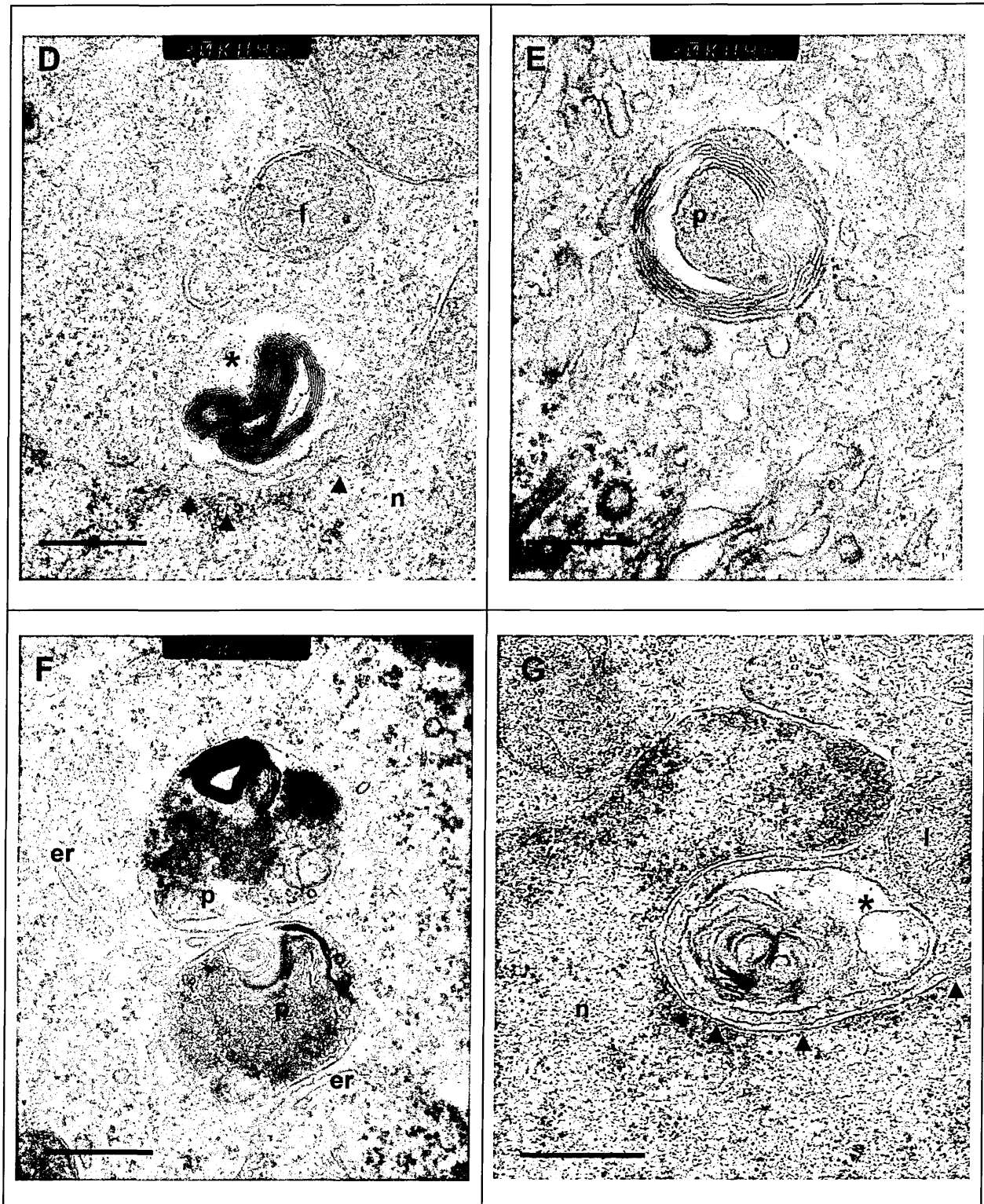


Figure 7.21. D-G. The phagosomes engulf the lamellar bodies along with other unidentified components of the cell. Abbreviations: (er) endoplasmic reticulum, (l) lysosome, (n) nucleus, (p) phagosome, (-) lamellar bodies associated with the nuclear membrane. In places, the nuclear membrane appears discontinuous (arrows). Bars, (D, E, F) 250 nm, (G) 500 nm.

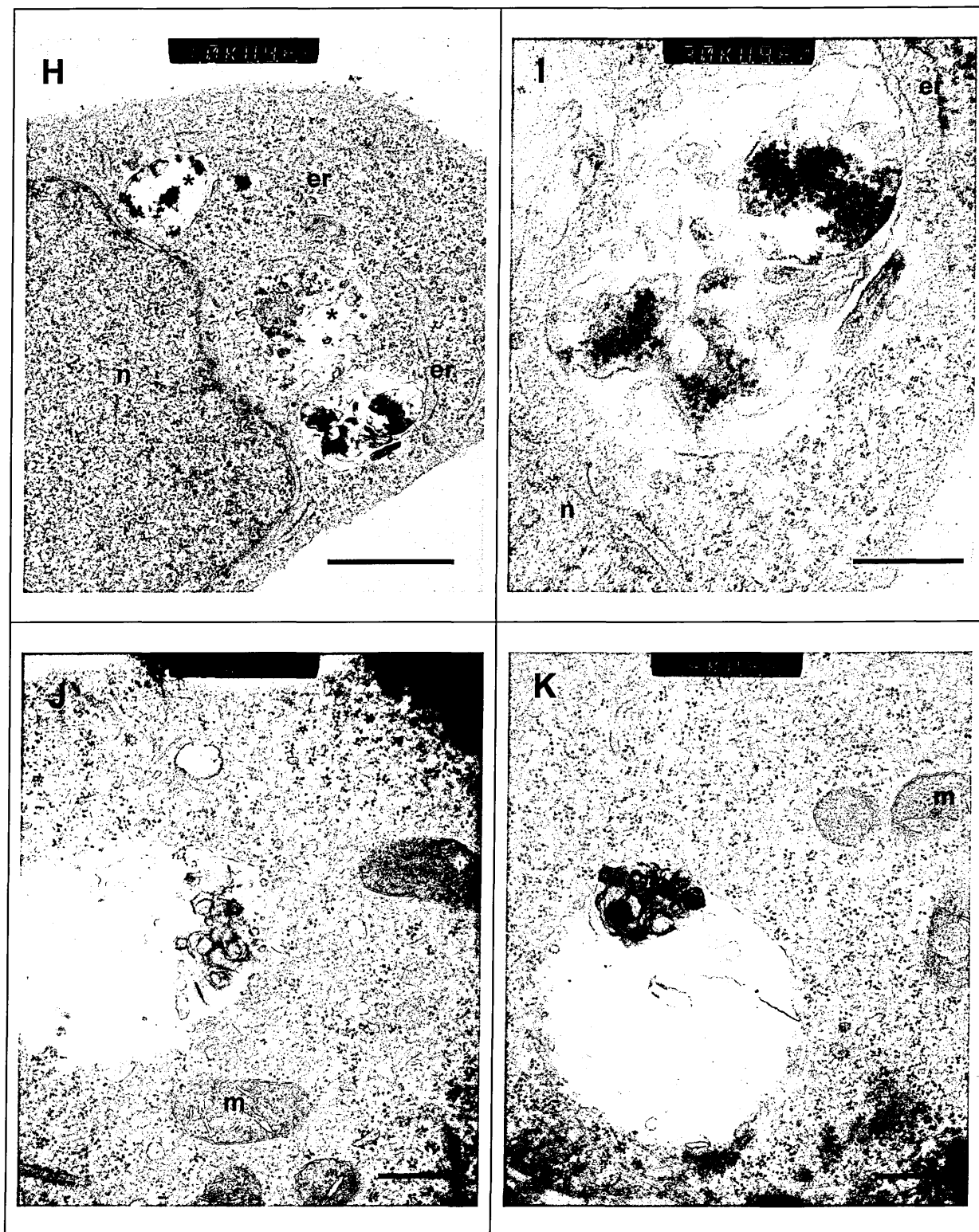


Figure 7.21, H-K. The cytoplasmic region adjacent to the lamellar bodies is devoid of any ordered structure suggesting that the phagosomes engulf the entire cytoplasmic contents (H) leaving behind a vacuole containing scattered fragments. (I) Enlarged view of (H) shows electron dense granular remnants surrounded by vacuole (v). (J, K) The presence of intact mitochondria (m) showing cristae indicate that caspase associated apoptosis (type 1 cell death) is not linked to the lamellar bodies/vacuoles. Bars, (H) 1 μ m, (I) 250 nm, (J, K) 500 nm.

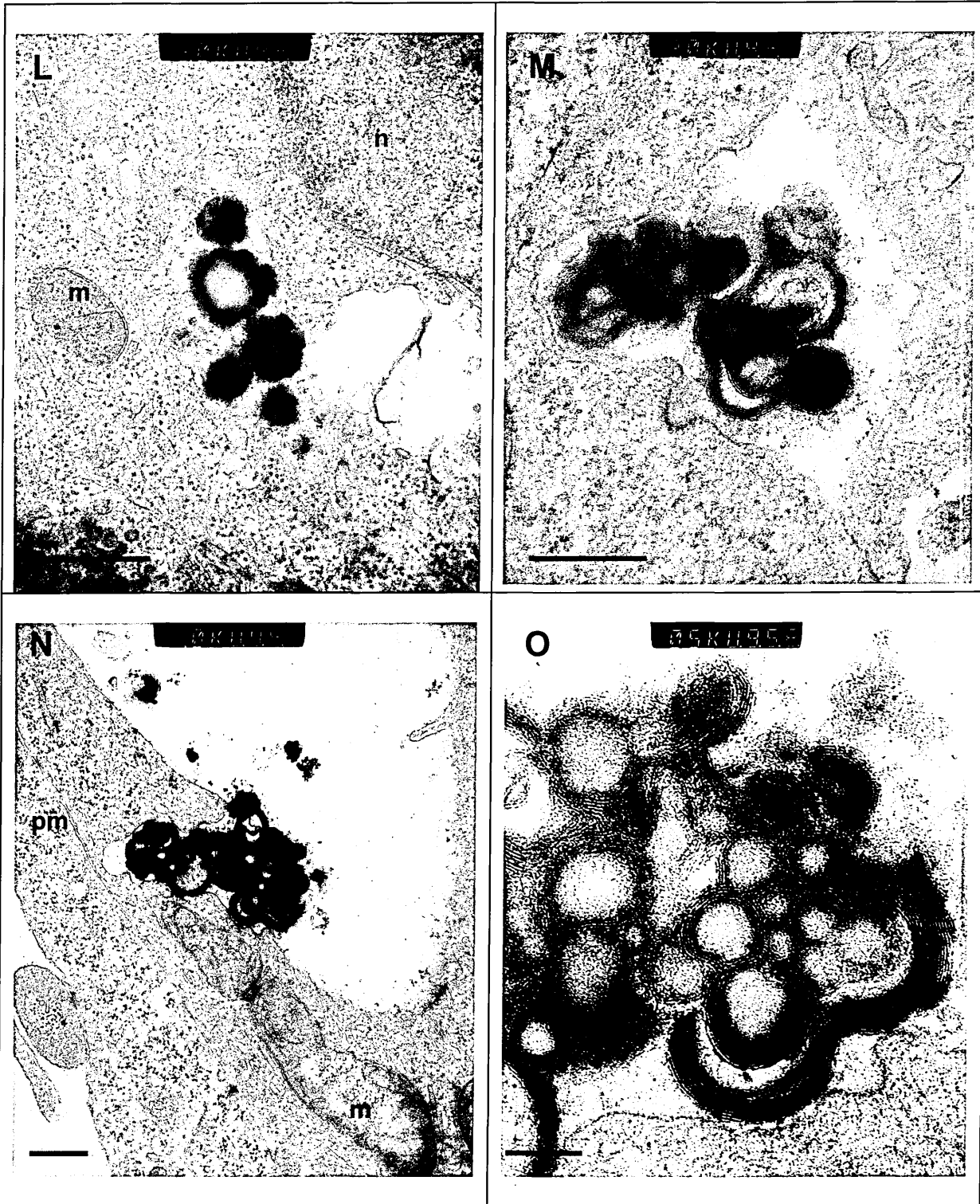


Figure 7.21, L-O. The margins of the vacuoles appear ragged in some places (L) but well defined in others (M). In the above cases, the vacuole encloses the lamellar bodies, which appear continuous, one with the other (N), though both structures remain separate as shown by the higher magnification view (O). Abbreviations: (pm) plasma membrane. Bars, (L, M, N) 500 nm, (O) 125 nm.

8.0 The putative PS1NTF 923 antibody staining is distinct from 1039 PS1CTF antibody staining

Initial investigations into the distribution of endogenous PS1 were carried out using the putative NTFPS1 antibody 923, and the CTFPS1 antibody 1039. The results shown in chapter 3 were consistent with the PS1 holoprotein undergoing proteolysis as part of the maturation process that gives rise to functional PS1. However, the novel observation that the two PS1 fragments appear to reside in separate compartments (figure 3.1) argued that the CTF and NTF may function separately to that of the mature PS1 complex and/or that the two fragments may be degraded by separate pathways. The current view holds that the PS1 holoprotein undergoes endoproteolysis within the ER to yield CTF and NTFs, which then re-associate within the Golgi compartment, along with additional factors to form the functional PS1 complex associated with γ -secretase activity (Kovacs, et al 1996). Moreover, the observation that the NTF displays a vesicular staining pattern following BFA treatment suggests that it may exit from the ER at a site different to that of the CTF.

Previous studies indicate that proteins exiting the ER pass via the ERGIC compartment en route to the Golgi or may pass directly to the Golgi within transport complexes originating from transitional ER sites (Scales et al, 1997). In this study 923 antibody staining co-localises very strongly with the Ergic53 antibody and that this co-localisation is not affected by BFA treatment indicating that the putative NTF originates from this compartment prior to its transport to the Golgi. A second compartment that also remains distinct from the ER following BFA treatment are structures referred to as 'Golgi remnants' that appear to house Golgi-matrix proteins (Nakamura et al, 1995; Seemann et al, 2000). However, it is unlikely that the PS1NTF are Golgi remnants given the intimacy of the Ergic53 and 923 antibody co-localisation.

One interpretation of the above data is that following endoproteolysis of PS1, the NTF and CTF traffic as two separate pools to the Golgi and that this separation may underlie different functions. Why this should be is unclear, although it has been speculated that PS1 may function in the transport of APP

in addition to its role as the putative γ -secretase (Kaether et al, 2002). However, other researchers have failed to demonstrate any interaction between PS1 and APP (Thinakaran et al, 1998). In this regard, a simple test would be to investigate whether the 923 antibody would co-immunoprecipitate PS1NTF along with APP and whether or not they co-localised within the same cellular compartment. It is worth noting that BFA-treatment of NTera 2 cells prevents A β secretion, in particular A β ₄₀ whereas BFA-treatment of cells has little effect on A β ₄₂ secretion suggesting that the toxic species is generated within the ERGIC compartment (Cook et al, 1997; Chen et al, 2000).

In light of the present data it is therefore possible that following endoproteolysis of the holoprotein, the PS1 fragments follow two separate routes from the ER before re-associating within the Golgi compartment and that within the ERGIC compartment the NTF associates with APP. However, given that the 1039 antibody does not stain for the ERGIC compartment (figures 3.1 and 3.2), it is difficult to envisage APP cleavage taking place in the absence of the CTF given the necessity for both fragments within the functional γ -secretase complex (Yu et al, 1998). Furthermore, the notion that PS1 undergoes endoproteolysis within the ER to generate NTF and CTF that then follow different routes to the Golgi, is in opposition to previous studies showing that PS1 fragments are maintained in a strict 1:1 stoichiometry and that the resultant heterodimer is not mixed but consists of a homogeneously derived pool (Kovacs, et al 1996; Podlisny et al, 1997; Yu et al, 1998; Tomita et al, 1999).

8.1 Construction and expression of N-terminal truncated PS1-EGFP

Unfortunately, to test whether the 923 antibody co-localises with APP or indeed immunoprecipitates APP along with PS1, could not be investigated, since the 923 antibody, unlike 1039, failed to Western blot (figure 3.5, lane 4). Furthermore, repeated attempts at immunoprecipitating PS1 have been unsuccessful raising concerns about the utility of the 923 antibody in fully characterizing the biology of PS1. In order to clarify this issue and effectively extend the previous observations, an NTFPS1-EGFP fusion protein was constructed with the aim of substituting for the 923 antibody in vitro. The use of

such a scheme scores over traditional antibody staining techniques in that fusion proteins have the advantage of not requiring fixation or permeabilisation steps thus making this reporter system suitable for kinetic studies concerned with protein localisation and trafficking within cells (Chalfie et al, 1994; Cubitt et al, 1995). Additionally, fusion proteins have been shown to maintain their fluorescence in living cells as well as retaining the normal biological function of the fusion partner. Such tagged proteins provide increased sensitivity and resolution when compared to antibody staining (Wang & Hazelrigg, 1994).

Expression of the PS1NTF fusion protein in Cos-7 cells generated four distinct phenotypes, two of which localised to varying degrees with antibodies to the ER and the Golgi compartments (figures 4.8 and 4.9). Unexpected was the presence of the blob-like aggregates and the much smaller vesicles within the cell, both of which do not co-localise with markers to the cell compartment, possibly indicating that these two structures have similar origins. Following Western blotting, a crude preparation of cells separated into soluble and membrane components should immunoblot for the membrane fraction only, given that PS are transmembrane proteins (Thinakaran et al, 1996; Tomita et al, 1997). Indeed, immunoreactivities for the membrane-only fraction were observed at ~61 kD corresponding to the sum of the individual sizes of both the EGFP moiety and the N-terminus of PS1 (figure 4.6, lane 6). As expected cells expressing EGFP showed immunoreactivity to the anti-EGFP antibody at ~29 kD within the soluble fraction only (lane 2). The absence of EGFP immunoreactivity within the soluble fraction prepared from transfected cells suggests no cleavage of the EGFP moiety from the PS1NTF (lane 5). This conclusion is further supported by the co-localisation of the anti-EGFP antibody with the fusion protein for all phenotypes (figure 4.7). Together these data indicate correct folding of the PS1NTF fusion protein and its maturation from the ER/IC to the Golgi, consistent with previously published reports (Yu et al, 1998; Capell et al, 1998).

Having successfully generated the PS1NTF-EGFP fusion protein, the earlier experiments investigating the novel distribution of the 923 antibody within the cell compartment was re-examined. Very little overlap between the fusion protein and the 923 antibody was observed (figure 4.10). Moreover, following BFA treatment the fusion protein displays a reticular phenotype distinct from

Ergic53 antibody staining, which is chiefly vesicular (figure 4.11). In conclusion these data and those from the previous experiments argue against 923 being a bonafide anti-PS1 antibody able to recognise either endogenous or exogenous PS1. Consequently, further characterisation of PS1 with the 923 antibody was abandoned. As to the identity of the 923 antibody, confocal microscopy reveals that 923 staining co-localises intimately with the Ergic53 antibody with the suggestion that, in terms of appearance, the one folds over the other (D. Parkinson).

8.2 Immunoanalysis of the NTF fusion protein

The initial aim of this study was to investigate the novel distribution of PS fragments within the cell compartment as revealed by specific PS antisera. Certain limitations in the properties of the 923 antibody were addressed by recourse to the construction of a PS1NTF-EGFP chimera. The results from this investigation demonstrated that the 923 antibody staining was not specific for PS1, consequently the present line of enquiry was concluded. However, in the course of this investigation fluorescent microscopy of transfected cells expressing the fusion protein revealed the unexpected presence of unusual intracellular bodies, the blob-like aggregates.

Also unexpected was the higher weight immunoreactive band at ~120 kD initially thought to represent dimerisation of the fusion protein since this is approximately twice the size of the lower immunoreactive band (figure 4.6 lane 6). Furthermore, attempts at resolving this species into one band using a denaturing SDS-urea gel were unsuccessful indicating a urea-insensitive, insoluble aggregate rather than dimerisation of the protein. Whilst the lower immunoreactive band of the expected size may represent correctly folded and membrane-located PS1 protein, drawing the same conclusion for the higher band may be premature. Conceivably, over expression of the fusion protein produces aggregates within the cytoplasm that show up in the membrane fraction, though how the hydrophobic transmembrane fusion protein could achieve this is not clear. One clue however is provided by the circumnuclear blob-like aggregates. These structures may in fact be represented by the higher band immunoreactivities seen in figure 4.6. Therefore the simplest

explanation to account for the existence of these aggregates is that they represent an artefact induced by the overexpression of the fusion protein. The difficulty with this interpretation is that all cells transiently expressing the fusion protein should contain aggregates since the same promoter drives expression of the transgene. Clearly they do not. Furthermore if the blobs were merely an amorphous mass of protein clumped together within the cytoplasm, then the difference in the size of the blobs should be reflected by a smear of protein following immunoblotting, rather than the single distinct band observed.

8.3 Expression of mutant full-length and truncated PS1 fusion proteins

Initial concerns about the fusion protein phenotypes arising as an artifact induced by the fixation method proved to be unfounded since all four phenotypes occur in cells fixed with either methanol or paraformaldehyde. Moreover, these same phenotypes are present in other mammalian cell types indicating a general cellular response to the presence of the fusion protein.

For the purpose of examining the effect selected FAD mutations have on the biochemistry of APP and the distribution of both full-length and truncated PS1-EGFP, cDNAs were successfully generated in a two-stage process using PCR. The transfection rate and the overall fluorophore intensity for the NTMPS1-EGFP fusion protein was identical to that seen for NTPS1-EGFP, whereas the converse was true for the full-length proteins, which consistently demonstrate low transfection rates and weak fluorescence. The availability of the N-terminal PS1 specific antibody NT7 unexpectedly revealed the presence of two separate CTF and NTF pools in some cells, indicating that the full-length fusion protein undergoes endoproteolysis consistent with previous reports (figure 5.11; Thinakaran et al, 1996). Additional evidence for the endoproteolysis of the full-length fusion protein is also provided by the Western immunoblot data (figure 5.12).

8.4 Endoproteolysis of the full-length PS1

Under normal physiological conditions PS1 is constitutively cleaved and quickly turned over ($T_{1/2} \sim 60$ min), in part to the two major fragments (Podlisny et al, 1997) that form a 1:1 heterodimer thought to be the biologically active form of PS1 (Thinakaran et al, 1996; Mercken et al, 1996; Podlisny et al, 1997; Ratovitski et al, 1997; Steiner et al, 1998). At first glance, staining with the NT7 antibody would support the earlier 923 antibody data showing two separate PS1 fragment pools. However, in this instance the NTF pool was distinctly Golgi-like (figure 3.1) whereas NT7 staining is typically blob-like in appearance. Moreover, BFA treatment of cells expressing the full-length fusion protein display the same reticular phenotype seen in earlier experiments examining the effects of BFA on the distribution of the NTPS1-EGFP protein (figure 5.9 d). These data therefore indicate a disturbance in the stoichiometry between the two endoproteolytically-derived fragments. As a consequence, C-terminal PS1-EGFP levels may be more tightly regulated over and above that of the NTF. Alternatively, both fragments may be equally susceptible to degradation but that the NTF may be more prone to aggregation and thereby thwarts attempts by the cell to regulate its numbers. Either way, this data indicate that both PS1 fragments are not regulated in the predicted 1:1 stoichiometry as previously reported (Thinakaran et al, 1996), leastways, under experimental conditions where Cos-7 cells express the full-length fusion protein. Previous reports indicate that steady state levels of the PS fragments are tightly regulated since transgene over expression does not increase the overall level of fragments within cells (Thinakaran et al, 1997).

The restricted incorporation of the PS1 fragments into a functional complex along with other cellular factors has been proposed as an explanation for their regulated accumulation (Yu et al, 1998), therefore excessive levels of the fusion protein both truncated and full-length, above that needed to complex with other unknown limiting factors may lead to the development of the blob-like phenotype. However, the tightly regulated accumulation of PS1 heterodimers as a means of regulating PS1 levels has been criticised as too simplistic. Additional influences appear to be at work in preventing aberrant accumulation of PS fragments and holoprotein such as proteasome, caspase, and leupeptin-sensitive cysteine proteinase activities. Inhibition of the proteasome, for

example, leads to the accumulation of NTF, CTF and polyubiquitinated holoprotein (Kim et al, 1997; Steiner et al, 1998; Honda et al, 1999; Marambaud et al, 1998). Other activities known to affect the fate of PS1 include GSK-3 β phosphorylation of C-terminal hydrophilic loop, which results in its degradation without affecting NTF levels (Kirschenbaum et al, 2001). Similarly, phosphorylation of the PS1 Ser³⁹⁷ residue is responsible for eliminating excess CTF prior to the appearance of a stable CTF in the long-lived heterodimer. Lithium chloride has been reported to have several biological effects including the specific inhibition of GSK-3 β in the millimolar range. Lithium treatment of HEK293 cells transfected with wild type PS1 results in a selective 3-fold increase in the CTF, whereas NTF levels remain unaffected (Kirschenbaum et al, 2001). Other reports demonstrate that the NTF residues 250-298 interact with GSK-3 β (Takashima et al, 1998; Khang et al, 1999) raising the possibility that in cells over expressing the full-length fusion protein, increased GSK-3 β activity is responsible for the low numbers of transfectants observed.

Previous studies show that over expression of PS1 results in modest increases in the steady state levels (Thinakaren et al, 1996; Kim, et al, 1999) and that the holoprotein (wild type as well as PS1_exon9) is rapidly degraded if not incorporated within the mature PS1 complex (Ratovitski et al, 1997; Steiner et al, 1998). The low levels of the full-length fusion proteins certainly fit in with these observations; however, levels of the truncated proteins are by comparison, consistently high. Earlier it was demonstrated that 1039 antibody staining does not co-localise with cells expressing the NTPS1 fusion proteins suggesting that exogenous NTF do not form a heterodimeric complex with endogenous CTF. Similarly, recombinant NTF₂₉₈ has been detected by short pulse labelling but not by steady state metabolic labelling (Citron et al, 1998), and that over expressed NTFs not incorporated into the complex are degraded by the proteosome (Steiner et al, 1998). The fluorescence and transfection rate of NTPS1-EGFP exceeds that observed for the full-length molecules suggesting a far greater stability. However, this observation conflicts with previous findings that demonstrate ectopically expressed NTFs from both PS1 and PS2 are not stabilised (Citron et al, 1998; Tomita et al, 1997; Steiner et al 1998), though whether this relates to stability within a complex or 'naked' NTF is unclear.

Given that the PS fragments are tightly regulated following endoproteolysis, and that holoprotein levels are consistently low, it can be concluded that the absence of the N- and CTF pair within a heterodimer upsets the stoichiometric regulation of PS leading to high levels of the truncated fusion protein.

A further explanation for the prevalence of NTFPS1-EGFP above that of CTFPS1-EGFP in transfected cells may well lie with the number of transmembrane domains. The former has 6 TM domains compared to the latter, which has 2 TM domains and is presumably less hydrophobic. In this scenario, over expression of the transgene leads to the accumulation of the hydrophobic NTF since limiting co-factors such as Aph-1 and Nicastrin needed for PS endoproteolysis, only associate with the holoprotein (Takasugi et al, 2003; La Voie et al, 2003). Stabilisation of the PS holoprotein is thought to occur through interaction with the Aph-1-Nicastrin complex to form a trimeric intermediate complex that then binds to Pen-2, allowing for PS endoproteolysis. Arguably excessive levels of 'naked' NTF are not recognised by these co-factors, leading the way clear for the hydrophobic truncated fusion protein to form stable, long lived aggregates.

8.5 Expression and sub cellular distribution of EGFP-tagged presenilin in this and previous studies

Studies in transfected cells as well as tissues show a wide distribution for PS depending on the cell type. At the sub cellular level, presenilins co-localise with markers for the ER and Golgi apparatus (Cook et al, 1996; Kovacs et al, 1996; Takashima et al, 1996; Zhang et al, 1998) and have been identified in a host of other cell compartments including the ERGIC compartment (Culvenor et al, 1997), at the plasma membrane (Takashima et al, 1996; Dewji and Singer, 1997; Kaether et al, 2002), in the nucleus and cytoplasm of the mouse embryo (Jeong et al, 2000), at interphase kinetochores and centrosomes (Li et al, 1997), within the inner membrane of rat mitochondria (Ankarcrona & Hultenby, 2002), and within growth cones of neurons (Singh et al, 2001).

In this study the PS fusion proteins have been identified within the ER and Golgi apparatus, though the full-length fusion is yet to be found in the latter compartment. Similarly antibody staining with 1039 and NT7 show endogenous

and exogenous PS within the ER and Golgi compartments. Additionally, mutant and non-mutant fusion proteins exhibit vesicular and blob-like aggregate phenotypes and that FAD mutations do not affect the intracellular distribution of the fusion proteins. This finding is in keeping with previous studies that similarly show that FAD mutations do not affect the trafficking of PS, although Kim et al, (2000) have found that four independent FAD-linked PS1 redistribute to the intermediate region of an Iodixanol gradient corresponding to the ER.

The use of GFP or EGFP as a tag to visualize PS within the cell is not unique to this study, since other researchers have previously reported the cloning of PS1 fusion proteins or their close homologues (Levitan & Greenwald, 1998; Singh et al, 2001; Kaether et al, 2002). In all these cases however, the position of the fluorescent tag within PS1 is not the same nor are the results. In one study the *C.elegans* PS holmologue SEL-12 was tagged after TM 6 within the large intracellular loop (Levitan & Greenwald, 1998). Assuming endoproteolysis of this fusion protein the GFP signal would be associated with the CTF of SEL-12. In functional studies this molecule was able to rescue a egg-laying defect of a *sel-12* reduction-of-function mutant. Additionally, this particular fusion protein locates to the ER/Golgi but not the plasma membrane consistent with a role for SEL-12 in the constitutive cleavage of Notch and the APP homologue LIN-12 (Levitan & Greenwald, 1998).

In another study investigating the role of PS in intercellular adhesion in human epithelial cells and mouse neurons, PS was tagged with GFP at the N-terminus region adjacent to TM1 using an ecdysone-inducible expression system (Singh et al, 2001). Localisation studies revealed the presence of this particular fusion protein within the cytoplasm and at cell-cell contacts of the plasma membrane where it complexes with β -catenin, but not within the ER or Golgi compartments. A truncated version of this molecule lacking the β -catenin binding region neither immunoprecipitates with β -catenin nor localises to the plasma membrane. Furthermore, L cells that do not form tight intercellular contacts, formed clusters of adhered cells after stable transfection with the full-length fusion construct (Singh et al, 2001). One obvious difficulty not addressed by the authors concerns the membrane localisation of their fusion protein. The accepted dogma for the insertion of a transmembrane protein asserts that the

N-terminus of the protein is first inserted within the lipid bilayer of the ER. How the N-terminal, soluble EGFP moiety is incorporated along with PS1 is a mystery. The cytoplasmic distribution of the fusion protein argues that the protein is not integrated within the membrane. Furthermore, in this study Western analysis was carried out using whole cell lysate but not the soluble or membrane fractions.

Lastly, a PS1 fusion protein has been used to examine the trafficking of nicastrin in transfected HEK293 cells, where a biologically active PS1-nicastrin complex is targeted to the cell surface (Kaether et al, 2002). In this study EGFP cDNA was inserted in-frame within the PS1 cytoplasmic loop, adjacent to TM6, downstream from the endoproteolytic cleavage site, thus generating an N-terminally located EGFP-CTF. In HEK 293 cells the fusion protein localised to the ER, vesicular structures, the nuclear envelope and to the cell-cell borders. Functionally, cells expressing the fusion protein generated A β at amounts comparable to those in cells expressing endogenous PS1. Additionally, this fusion protein promotes A β 40/42 ratio of ~9:1 in keeping with other reports (Selkoe, 1999). The majority of PS in this study localises to the ER, however a minority was detected at the plasma membrane. Kaether et al (2002) maintain that this latter finding contributes towards resolving the spatial paradox that exists between the site at which A β ₄₂ is generated and the ER/IC location of the β - and γ -secretases (De Strooper et al, 1997; Annaert et al, 1999).

Discrepancies in the distribution of the various PS fusion proteins more than likely reflect the position at which the tag is located, the cell type in which the fusion protein is expressed, and the overall level of expression. Moreover, the presence of the GFP tag itself may partially influence the distribution of PS1 in all the above studies making a direct comparison difficult. Interestingly none of these studies reported the appearance of blob aggregates, though Singh et al (2001) discarded PS1 over-expressing cell lines in favour of mild or moderate expression in response to work by Johnston and colleagues who showed that high levels of PS1 are associated with intracellular "aggresomes" (Johnston et al, 1998). Furthermore, Singh et al (2001) argue that the presence of their fusion protein at the plasma membrane is a reflection of the normal distribution of PS1 in polarized cells and neurons, and that an initial ER/Golgi localisation is

transient. Thus these authors conclude that the localisation of PS1 in early compartments in non-polarised cells such as HEK 293 or Cos-7 cells is due to the absence of late compartment trafficking signals.

8.6 Functional aspects of PS fusion proteins

In the preceding section the functional consequences of PS1-EGFP chimeras from previous studies were discussed. In the present study the functional relationship between the fusion protein and both APP and β -catenin was investigated by antibody staining. Furthermore, to investigate the biochemical properties of the fusion proteins, both mutant and non-mutant, in generating $A\beta$, a bicine gel capable of separating $A\beta_{40}$ and $A\beta_{42}$ was utilised.

Data from studies examining the proteolysis of APP reveal the presence of different peptide fragments at various points along the secretory pathway, i.e. ER, ERGIC, Golgi compartments, lysosomes/endosomes and the plasma membrane (many authors). However, a spatial paradox exists between the ER location of the secretases responsible for the cleavage of APP, and the site of $A\beta$ generation (De Strooper et al, 1997; Annaert et al, 1999). PS1, for instance, is localised to the ER/Golgi yet generation of the toxic $A\beta_{42}$ peptide occurs within the ER/ERGIC (Cook et al, 1997; Chen et al, 2000), whilst the production of the $A\beta_{40}$ is thought to occur more distally within the secretory pathway (Selkoe, 1999).

APP proteolysis is dependent on α -, β - and PS1 associated γ -secretase activity to generate several proteolytic fragments. To investigate the sub-cellular distribution of the APP and the NTPS1-EGFP fusion protein, cells were stained with APP antibodies specific to full length KPI-APP (993), the C99 fragment (874), and both the C99 and C83 stubs but not full-length, uncleaved APP (DE2). Staining with DE2 and 874 antibodies in transfected Cos-7 cells resulted in a reticular and peri-nuclear phenotype and showed only partial localisation with the fusion protein (figures 6.4 and 6.5). 993-antibody staining exhibited a distinctive microtubule-like staining pattern, which does not localise with any of the phenotypes exhibited by the fusion protein (figure 6.3). Recently APP was identified as a possible membrane receptor for the kinesin light chain,

a component of kinesin-1, a microtubule motor protein. Furthermore, a compartment has been identified containing kinesin-1 and APP, together with presenilin and β -secretase that are able to generate $A\beta$ (Kamal et al, 2001). 993 antibody staining may therefore provide additional evidence for the structural relationship between kinesin-1, APP and microtubules.

In light of recent data showing the necessity of full-length PS1 to associate with co-factors such as nicastrin, Aph-1 and PEN-2 prior to mature γ -secretase complex formation, it is not surprising that the truncated fusion protein did not localise with any of the APP antibodies. Previously, an APP binding domain has been mapped to the NTF of PS1, which interacts with the immature, N-glycosylated form of APP, consistent with the localisation of both immature APP and PS within the ER (Pradier et al, 1999). Full-length PS is therefore required to bind APP. For comparative purposes, the APP antibody experiment would be worth repeating in cells expressing both the mutated and non-mutated full-length fusion proteins.

Antibody staining of β -catenin in cells expressing the NTPS1 fusion proteins was restricted to the cytoplasm and the cell-cell contact (figure 6.2). No co-localisation of β -catenin with the truncated fusion proteins was observed, nor does it seem that the fusion protein alters this phenotype compared to untransfected/low level expression in adjacent cells. In addition, there is no evidence that mutant NTMPS1-EGFP affects β -catenin trafficking. However, lack of NTF- β -catenin interaction is consistent with previous studies showing that the CTFPS1 or full-length PS1 but not NTF, contain the β -catenin binding domain (Murayama et al, 1998; Yu et al, 1998; Kang et al, 1999; Singh et al, 2001). In this context it would be interesting to note what effect mutated and wild type full-length fusion proteins have on the β -catenin phenotype.

8.7 Detection of β -Amyloid

As a corollary to the section examining APP antibody staining, a bicine SDS PAGE gel capable of resolving $A\beta_{40}$ from $A\beta_{42}$ (Wiltfang et al, 1997) was prepared in anticipation that $A\beta$ levels would be assessed in transfected CHO cells stably expressing APP₇₇₀. However, although this gel system successfully

discriminated between synthetic A β peptides, and that AB10 immunoblotted both APP from conditioned media and synthetic A β , the peptide could not be immunoprecipitated from conditioned media or complete media to which synthetic A β had been added, though APP immunoprecipitated freely. Furthermore, serial immunoprecipitation and alterations to the protocol was unable to resolve matters. One of the pathological features of A β_{42} is its increased aggregation potential compared to A β_{40} . Under the present experimental conditions it is conceivable that A β_{42} may undergo a structural change (figure 1.3) therefore limiting the binding epitope and consequently AB10 immunoreactivity. However, if this were the case A β_{40} immunoreactivity should have been detectable since this peptide is not prone to aggregation. The experimental conditions used herein closely matched those of Wiltfang et al, who originally developed this gel system, except for the antibody used at the immunoprecipitation stage (Wiltfang et al, 1997). An alternate method for the detection of A β is by the enzyme-linked immunoabsorbant assay (ELISA) method (Suzuki et al, 1994), however due to time constraints this method was not pursued. In conclusion, AB10 whilst able to detect APP and synthetic A β , is unable to immunoprecipitate the shorter peptides.

Had A β been detected within the conditioned media from cells expressing the mutant full-length fusion protein and APP₇₇₀, it is likely that there would have been an increase in A β_{42} relative to A β_{40} since ~100 PS1 mutations have been identified to date all of which apparently increase the production of A β_{42} (Selkoe, 1999). Expression of the NTPS1 fusion protein would not be expected to generate A β in transfected cells since previous research has shown that NTF over expression does not increase A β_{42} (Citron et al, 1998) nor is it able to rescue mutant *sel-12* in *C.elegans*.

8.8 Alterations in the ER and Golgi compartments

The decrease or absence of antibody staining of some markers for the cell compartment as illustrated by figures 6.0 and 6.1 was unexpected and may partially reflect toxicity induced by the presence of the fusion protein. It is important to note that reduced antibody staining of the ER and Golgi marker

proteins was not observed in control cells or cells expressing low levels of the fusion proteins, indicating that the fusion protein can be tolerated by the cell, leastways, at low concentrations. The decrease in Colligin staining was most obvious in cells expressing high levels of the fusion proteins where staining was either reduced completely (figure 6.0, row a) or fragmented into vesicle-like structures scattered about the cell (row b). In the latter case these vesicles do not localise with the blob-like aggregate phenotype. Colligin functions as a resident stress protein within the ER thought to participate in the intra cellular processing, folding, assembly and secretion of procollagens (Nagata & Yamada, 1986). Previously it has been demonstrated that Colligin expression is reduced in human fibroblasts under conditions of serum deprivation (Sauk et al, 1990), and in chick embryo fibroblasts transformed by the Rous sarcoma virus (Nagata & Yamata, 1986). In these instances cells are unduly 'stressed' due to either trophic factor withdrawal or infection.

In the case of Cos-7 cells, stress induced by the accumulation of the fusion protein may trigger alterations in the ER so compromising ER integrity as measured by the decrease in Colligin levels. The accumulation of protein within the ER occurs in response to cellular stress events including trophic factor withdrawal, impaired calcium regulation, the inhibition of protein glycosylation, and the reduction of disulphide bonds. Such stresses initiate a series of events referred to as the unfolded protein response (UPR) (Imaizumi et al, 2001) characterised by increased transcription of genes encoding ER-resident chaperones such as GRP78/BiP, GRP94 and PDI. Impairment of the UPR is ultimately linked to apoptosis and therefore cell death.

Another cellular event that may account for the reduction in Golgi antibody staining occurs during cell division. Prior to mitosis cells undergo a series of morphological changes including controlled ER and Golgi fragmentation and vesicle formation so that organelles can be more evenly distributed when the cell divides. Vesicles derived from the Golgi associate with microtubules of the mitotic spindle ensuring an even distribution between the two daughter cells (Lucocuq and Warren, 1987; Warren, 1989; Shima et al, 1998). Golgi fragmentation has also been previously observed as a late step in apoptosis in odontoclasts treated with bisphosphonate (Watanabe et al, 2000). Other studies have shown that Cos-7 cells transfected with mutant growth

hormone results in the accumulation of the hormone within the ER that ultimately leads to Golgi fragmentation (Graves et al, 2001). As a consequence, immunoreactivity for the Golgi markers β -COP, membrin and 58k is completely dispersed or absent altogether. Additionally, the UPR in this study was weakly induced as measured by a two-fold increase in GRP78/Bip mRNA (Graves et al, 2001).

Taken together, these data suggest that the fusion proteins perturb the cellular environment to the extent that some marker proteins to ER and Golgi are severely reduced or dispersed possibly indicating fragmentation of the cell compartment. The knock-on effects of these alterations may then be responsible for induction of the UPR, though a definitive test would be to examine any increase in the levels of Bip mRNA in cells expressing the fusion protein.

8.9 The N-terminal fusion protein sensitizes cells to apoptosis

From the preceding section it is clear that a number of potential factors could be cited to explain the reduced or absent immunoreactivity observed for the ER-Golgi markers in cells expressing the fusion protein. In keeping with other studies, immunoblot data indicate the presence PS caspase cleavage fragments suggesting an apoptotic event associated with the presence of fusion protein (figure 6.11 & 7.2; Kim et al, 1997; Podlisny et al, 1997; Kovacs et al, 1999). Moreover, in a follow-up experiment the truncated fusion protein was found to statistically ($P < 0.05$) increase the sensitivity of cells to STS-induced apoptosis (figure 6.15). To gauge whether the truncated fusion protein was associated with apoptosis, changes in Cos-7 cell morphology were assessed as an end point of apoptosis. Specifically, changes in Golgi morphology were used as an indicator of cell structural integrity by examining mannosidase II antibody staining (figure 6.12). The number of apoptotic cells increased in a time dependent manner following STS treatment and that this increase was greater in transfected cells at all time points compared to the non-transfected, STS-treated cells (figure 6.13).

In the context of AD, PS1 mutations have been demonstrated to increase cellular susceptibility to apoptosis induced by trophic factor withdrawal and

exposure to A β (Zhang et al, 1996; Walsh et al, 2002). Further studies show that the presenilins are involved in the regulation of apoptosis, and that cells expressing PS1 or PS2 FAD mutations die faster than cells expressing wild-type presenilins (many authors). Chronic cellular stress culminates in apoptosis involving nuclear fragmentation, chromatin condensation and shrinkage of cell bodies, however, the images shown in figures 6.0 & 6.1 display intact, albeit, misshapen nuclei in some cells, with no clear sign of nuclear fragmentation. Additionally, not all cells exhibiting the blob-like phenotype show an equal reduction in ER and Golgi antibody staining, suggesting that transfectants may only be vulnerable to high levels of the fusion protein depending on the stage of the cell cycle. In this regard, Janicki et al, demonstrate that over expression of PS1 or PS2 FAD mutants potentiate cell cycle arrest in the G1 phase of the cell cycle in exponentially growing cultures compared to wild type presenilin (Janicki et al, 2000).

A more accurate determination of apoptosis was carried out by assessing the degree of cleavage of the Golgi stacking protein Grasp65 as an early event in apoptosis. Statistically significant differences were observed between the number of STS-treated, Grasp65 negative, transfected NRK cells expressing the fusion protein and the number of STS-treated control cells (figure 6.15). Crucially, there was no statistically significant difference in apoptosis between control-transfected cells and non-transfected control cells indicating that apoptosis was not spontaneously induced due to over expression of the fusion protein (Guo et al, 1997; Kovacs et al, 1999). Whilst immunofluorescent microscopy of NRK cells clearly show Grasp65 cleavage (figure 6.14), immunoblotting (figure 6.16) failed to show the expected Grasp65 cleavage fragments (Lane et al, 2002). In all probability this discrepancy is due to the different experimental approaches (see chapter 6.10).

The earlier observation that certain markers to the ER and Golgi compartments are affected in transfected cells appears to extend to Grasp65. Cells exhibiting the blob phenotype show reduced immunoreactivity or fragmentation of the Golgi (figure 6.14), and decreased immunoblotting of Grasp65 in transfected cells compared to non-transfected cells (figure 6.15). It may therefore follow that less substrate will result in more effective cleavage in response to a given apoptotic stimulus. How this effect is mediated within cells

expressing the fusion protein is unknown, though the blobs may impede trafficking of proteins from the ER to the Golgi or they may physically disrupt cellular organelles, perhaps by arresting cell division once organelles have been disassembled prior to entering mitosis. If true, the cellular effect of the blob phenotype will be independent of PS1 and may therefore represent a more general phenomenon associated with the blob-like aggregates.

Whilst the above explanation that the blob phenotype may account for some of the GRASP65 data, it does not explain the reduction in GRASP65 antibody staining above that seen for control cells. For instance, from 77 non-STS-treated control NRK cells expressing the transgene, 88% exhibited the vesicular/blob phenotype. Only 7% of these cells were in fact, Grasp65 negative. Had the blob phenotype alone been responsible for apoptosis a far greater number of cells should have been affected. However, as demonstrated by immunofluorescence and immunoblotting data, there was an overall reduction in GRASP65 staining within transfected cells compared to non-transfected cells. It should also be noted that HEK293 cells stably expressing the N-terminal and full-length PS1 fusion proteins both display the blob phenotype, suggesting that transgene product numbers are tightly regulated within the cell. If the blob phenotype occurrence is insufficient to account for all cases of apoptosis, then the NTFPS1 fusion protein must be implicated in apoptosis, either by directly affecting caspase activation/GRASP65 cleavage or indirectly by interacting with some other aspect of apoptosis.

The involvement of presenilins in apoptosis was first suggested by studies showing an increased sensitivity in cells to different apoptotic stimuli following PS2 over expression, and reduced sensitivity in the presence of an anti-sense PS2 construct (Vito et al, 1996; Wolozin et al, 1998). Additionally, the presence of apoptotic stimuli induces caspase cleavage of the presenilins proteins. The data on presenilins show PS2 to be pro-apoptotic, in particular the N-terminus bearing the N141I mutation, and PS1 to be anti-apoptotic. In both phenotypes presenilins have been linked to the tumor suppressor p53 activity, which appears to delay apoptosis by down-regulating PS1 expression (Roperch et al, 1998). By contrast, PS2 and N141I-PS2 drastically increases p53 expression and transcriptional activity in various cell systems (Alves da Costa et al, 2002), whereas the C-terminal 103 amino acids of mouse PS2,

referred to as ALG3, rescues a T-cell hybridoma from Fas-induced apoptosis (Vito et al, 1997). Recently it has been demonstrated that CTF-PS2 over expression increases caspase-3 activity and immunoreactivity in STS-treated cells, and PS^{-/-} cells. The latter observation suggests that CTF-PS2 may function independently of the N-terminal, γ -secretase-derived counterpart (Alves da Costa et al, 2003). The data presented herein suggest that the PS1 truncated fusion protein is proapoptotic, though whether this is a direct effect of over expression, the presence of the blob-like aggregates or a PS1NTF-mediated effect is unclear. That the PS1NTF fusion protein does sensitise cells to apoptotic stimuli may be a novel affect since previous reports do not implicate PS1NTF, unlike PS2NTF. Given the absence of data showing a pro-apoptotic PS1NTF effect, it is tempting to associate over expression of the fusion protein as being responsible for apoptosis in the present study.

8.10 Identity of the blob-like aggregates

The presence of the fusion protein results in four clear phenotypes that are independent of the fixation method or the cell line in which they are expressed. Immunoblotting reveals the presence of high weight bands that may correspond to the blob-like aggregate phenotype. To address concerns that the EGFP moiety may contribute to the phenotypes displayed by the fusion protein, a stop-codon was inserted between the end of the PS1 cDNA and the beginning of the EGFP cDNA sequences. The results show that all four stop-constructs when expressed by the cell show near identical phenotypes to those seen in cells expressing the fusion proteins (figure 7.1). In conclusion, the presence of the EGFP tag has no effect on the phenotypes displayed by cells expressing the various fusion proteins. Western analysis of cells expressing the stop-PS1 proteins show a similar immunoblot profile to endogenous staining of PS1 control cells (figure 7.2 b), with the exception that alternative CTF cleavage typical of caspase activity is more prominent in cells transfected with PS1 cDNAs (Kim et al, 1997; Kovacs et al, 1999). However, that the immunoreactivity is approximately equal for all constructs (figure 7.2b, lanes 2-5) and is not just limited to the full-length cDNAs, suggest that over expression of the transgene has a pro-apoptotic effect.

To aid in the identification of the compartment associated with the blob phenotype cells expressing the truncated fusion protein were stained with an array of antibodies to the cell compartment. No clear co-localisation with this phenotype was observed following staining with Colligin, PDI, Ergic53, membrin SNARE, Golgin245, Mannosidase II, β -COP and COPII antibodies. Assuming that the fusion protein is membrane-bound, these data suggest that the blobs accumulate within a unique subcompartment. In a previous study examining the localisation of PS, Kim et al, (2000) have reported the existence of a membrane pool containing PS fragments that similarly do not contain markers of the ER, Golgi, Ergic, COPII vesicles, caveolar membranes, or endocytic vesicles. However, though electron microscopy shows the presence of PS1 immunoreactive compartments, these structures displayed a uniform morphology and were considerably smaller than the blob phenotypes found within the present study (Kim et al, 2000).

As with the earlier observations that the fusion protein affects the distribution of some markers specific to the cell compartment, so the fusion protein alters COP II staining from a peri-nuclear location to a fragmented or diffuse/cytoplasmic distribution (figure 7.8), implying that anterograde vesicular trafficking within the secretory pathway may be disturbed. The alteration in COP II staining from a peri-nuclear to a cytoplasmic phenotype has previously been reported during mitosis. Prior to cell division, protein transport is blocked at ER exit sites as COP II and its binding partner Sec13 shifts from the ER to the cytosol (Gorelick & Shugrue, 2001). Similarly, proteins exiting from the ER in COPII vesicles that cannot achieve their normal configuration accumulate blocking the ER exit sites (Raposo et al, 1995). Whether this observation holds true for the fusion protein or that altered COP II staining in Cos-7 cells is the result of mitotic events is unclear, though in the latter case PS1 over expression potentiates cell cycle arrest in the G1 phase of the cell cycle (Janicki et al, 2000).

An initial consideration in the genesis of the blob phenotype was that they arise as the result of the fusion protein-containing compartment undergoing successive rounds of fusion with each other to generate the blob phenotype. Ordinarily, transmembrane proteins are concentrated at ER exits sites by the presence of COPII. This is further assisted by the presence of di-acidic (DXE)

concentration signals in the cargo protein (Nishimura et al, 1999). A search of the amino acid sequence of PS1 revealed the presence of 5 DXE signals suggesting that PS1 may be concentrated at ER exit sites. The presence of the coat proteins and transmembrane adapters/receptors of the COPII coat is also believed to prevent the fusion of cargo vesicles with each other and with other membrane compartments (Gorelick and Shugrue, 2001). This raises the possibility that the reduced COPII levels (figure 7.8) affects the insulation properties of the coat so allowing the cargo vesicles carrying the fusion protein to fuse together, thereby forming the blob phenotype.

8.11 The fusion protein, aggresomes and the ubiquitin-proteasome system

The lack of co-localisation with markers to the cell compartment prompted an investigation into what mechanism might be responsible for the removal of the blob-like aggregates. The two major pathways for the degradation of damaged or unwanted proteins are carried out by the lysosome and the proteasome. The lysosomes are membrane-bound, acid hydrolase-containing vesicles that deal primarily with extracellular proteins, that are endocytosed by the cell, or cell-surface membrane proteins used in receptor-mediated endocytosis. Antibody staining of lysosomes with LAMP-1 produces a distinctive halo (Chen et al, 1985) quite separate from the blobs suggesting that the lysosomes are not responsible for the degradation of the fusion protein (figure 7.9).

The alternate proteolytic pathway involving the proteasome is known to operate in the removal of PS1 (Kim et al, 1997). Staining with a newly purchased antibody to the 20S subunit failed to resolve any detail within the cell, therefore an anti-ubiquitin antibody that recognises proteins tagged for proteasome destruction was used to stain cells displaying the blob phenotype (figure 7.10). Furthermore, immunoanalysis shows that only those higher weight bands from the membrane fraction show ubiquitin immunoreactivity (figure 7.10, panel d), suggesting that these bands correspond to the blob-like phenotype. The co-localisation of the ubiquitin antibody with the blob-like aggregates indirectly shows that the fusion protein may be targeted for proteasome destruction.

Allied to the breakdown of proteins by the proteasome is the role-played by a novel structure responsible for the containment of excess misfolded protein. Within the present study the description of the blob phenotype as an aggregate was meant purely in the generic sense of the word, however, work carried out by Kopito and colleagues have characterised the existence of a single, stable, juxtannuclear aggregate referred to as an aggresome (Johnston et al, 1998). These structures are a general response by the cell to protein over expression and can be generated artificially by inhibiting the proteasome. Once the degradative capacity of the proteasome is exceeded, polyubiquitinated protein aggregate at the microtubule organising centre (MTOC), and is accompanied by the rearrangement of the intermediate filament protein (IF) vimentin, which forms a containment cage around the aggregated protein core (Johnston et al, 1998).

In the present study, given their high number, the presence of numerous fusion protein blobs and their location within the cell militate against them being aggresomes, since the latter are found as single structures. Nevertheless, previous reports show that PS2 is targeted for degradation by the proteasome (Kim et al, 1997) and that PS1 readily form aggresomes following proteasome inhibition (Johnston et al, 1998). To evaluate whether the NTMPS1-EGFP fusion protein similarly forms aggresomes, cells expressing the fusion protein were treated with the proteasome inhibitors lactacystin or MG132. Aggresome formation was seen in both HEK293 and Cos-7 cells following proteasome inhibition and that these structures were contained by the IF vimentin (figures 7.11, 7.12 & 7.13). Furthermore, proteasome inhibition increased the fluorophore signal in transfected cells and was accompanied by increased ubiquitin immunoreactivity of the high weight aggregates (figure 7.14). Additional antibody staining diagnostic for the presence of aggresomes was also investigated. Antibodies to γ -tubulin, mitochondria and MTOC co-localised with the fusion protein in drug treated cells (figure 7.17).

Although the fusion protein readily forms into an aggresome in response to proteasome inhibition, the blob phenotype persists as a distinctive ring around the aggresome that appears to lie outside the margins of the vimentin cage (figure 7.13). This latter observation suggests that while moderate levels of the fusion protein can be effectively contained within the aggresome, the

blobs remain excluded, perhaps as a reflection of their structure or insolubility. The formation of the aggresomes are dependent on an intact microtubule network as seen following experiments with the microtubule-disruption agent nocodazole (Johnston et al, 1998) and by disruption of the dynactin-dynactin complex by over expression of p50/dynmatin (García-Mata et al, 1999; Johnston et al, 2002). Nocodazole treatment of cells expressing the fusion protein whilst preventing aggresome formation had no effect on the blob phenotype (figure 7.18), which remains dispersed throughout the cell. However, the presence of the blob as a ring surrounding the aggresome indicates the requirement for intact microtubules for transport to this location, but not for their formation.

The lack of antibody staining of the blob phenotype provided no clear indication as to the cellular location/compartiment from which the blobs originated. Although antibody staining data suggest otherwise, the assumption was made that blobs may nonetheless develop according to the scheme: ER/Golgi>Vesicles>Blobs. To address this issue cells were transfected with the truncated cDNA and imaged by fluorescent microscopy over a 6 hour period (figure 7.19). Initially, the fusion protein is limited to the ER after a 3 hour period, however, this quickly changes and by four hours post-transfection, the first signs of the blob phenotype appear as circumnuclear 'swellings' intimately associated with the reticular-nuclear interface. Measurement of the blobs show that they range in size from ~250 nm up to ~3.75 μm (long axis). The first signs of a peri-nuclear phenotype appear after 4 to 5 hours, and by 6 hours cells exhibit the full range of phenotypes.

One possible explanation to account for the genesis of the blob phenotype may involve blobs arising firstly as 'swellings' at the reticular-nuclear interface. Secondly these 'swellings' attain a particular size after which time 'mature' blobs may detach from the nuclear-reticular interface, and scatter as cytoplasmic inclusions (figure 7.20, a-d). Ideally this sequence of events could be verified by recourse to time-lapse fluorescence microscopy using live cells.

In a follow-up experiment, the time intervals post transfection were extended to 58 hours. However, there was no change in number of cells displaying the blob phenotype between each time point, 10 hours after first transfection (data not shown). The proposed sequence of events leading up to

the formation of the blobs i.e. ER/Golgi>vesicles>blobs, does not seem to hold true since the phenotype and their numbers do not change over time. In summary, these data suggest that over expression of the transgene determines the appearance the blob phenotype. The blob phenotype may therefore reflect a controlled attempt by the cell to contain over expression of the fusion protein. In this view the blobs may even be seen as a protective mechanism insulating the cell from high levels of the fusion protein.

8.12 TEM analysis of Cos-7 cells expressing the fusion protein

The data from the preceding section suggest that the blobs arise from the nuclear membrane/ER interface, however, this data falls short of answering the question as to whether or not the blobs are cytoplasmic aggregates or membrane-bounded structures. Close inspection of figure 7.13 (row c, middle panel) as viewed on a high definition cathode-ray screen, reveals the presence of a margin that contrasts sharply with the interior of the blobs, suggesting a membrane-bound structure. This observation was followed-up by analysing the ultrastructure of transfected Cos-7 cells using TEM (figure 7.21, A-O).

TEM revealed the presence of familiar organelles such as numerous mitochondria (A,J,K), lysosomes (A), vacuoles (A) as well as several unexpected features including unusual laminar bodies resembling myelin-like whorls (B-F,L-O), electron dense regions scattered throughout the cell resembling compressed tubules (A), phagosomes (D,F,G), autolysosomes (C) and whole swaths of cytoplasm devoid of any discernable detail (H-M). The latter observation is clearly depicted in L-O, whilst image H shows dense granular remnants surrounded by a vacuole that may show an early event in the removal of the surrounding cytoplasmic contents. Close inspection of the laminar bodies reveals the presence of concentric, electron-dense lines that appear to be enveloped by multiple layers (O). Many of these bodies have a empty inner core which ultimately becomes electron dense. Figures B and C show an unusual arrangement of the ER, which appears to surround the entire region occupied by the laminar bodies. Additionally, patches of the nuclear membrane in the region of the laminar body appear discontinuous or absent altogether (D-G). Interestingly, no clear ER or Golgi structures are visible, which

may explain the earlier data showing a reduction in some cell compartment markers.

8.13 Autophagosomes and multilaminar bodies in transfected cells

In previous TEM studies the aggresome presents as a fine network of closely packed filamentous material that surrounds the centriole (Johnston et al, 1998; García-Mata et al, 1999). However, TEM in the present study show no analogous structures to the aggresome. A prominent feature of transfected cells is the presence of autophagosomes and numerous other structures associated with them, such as lysosomes and myelin-like whorls (figure 7.21). Autophagy is an evolutionary conserved process present within plants, animals and fungi, and is the primary mechanism by which long-lived stable proteins are degraded and is the only mechanism by which entire organelles such as mitochondria and peroxisomes are recycled. Ultimately, autophagosomes by breaking down protein provide amino acids necessary during starvation (Dunn, 1990). The autophagic response is a highly regulated event influenced by several factors including second messengers, purines, growth factors, and adrenergic agonists and kinase/phosphatase activities. One outstanding issue concerning autophagy is the mechanism by which cells sense the starvation signal. Recent studies in yeast suggest that a dedicated signal transduction mechanism may stimulate autophagy directly (Abeliovich et al, 2000)

Autophagy involves dynamic rearrangement of cellular membranes. The sequestering membrane is thought to derive from the ER to form an enveloping vesicle capable of engulfing proteins, organelles and lipids. Initially bounded by a single membrane, the autophagosome fuses with a primary lysosome (also a single membrane bound compartment) to form a double membrane autophagolysosome (Dunn, 1990; Klionsky & Emr, 2000). The presence of autophagosomes and autophagolysosomes constitute autophagic vacuoles. The inner membrane disintegrates and the vacuole contents are digested and recycled to yield amino acids. Control has been partially resolved in yeast where autophagy is under the influence of *apg* genes and mammalian homologues to the *apg* proteins beclin and LC3 have been discovered (Larsen and Sulza, 2002). In yeast many genes have been discovered that appear

necessary for autophagy. In some cases the mammalian homologues have been identified. The process of autophagy has five broadly defined phases with each phases being reflected by several genes: Induction- this involves several kinases such as *Tor2*, a rapamycin-sensitive protein kinase. Conjugation- this operates in a similar fashion to the mammalian ubiquitination conjugation system. *Apg7*, for instance, codes for an E1-like ubiquitin activating enzyme. Size regulation- *Aut2* activity is up-regulated during starvation periods and is responsible for regulating the size of the autophagosome. Docking and fusion- *Vam3* in yeast and *Syntaxin7* in mammals are examples of SNARE components necessary for the trafficking of vacuoles during autophagy. As with cargo transport in mammalian cells, Rab GTPase activity is required to mediate docking and fusion events. Breakdown- several genes encode a series of degradative lipases and proteases and components responsible for acidifying the vacuolar to maintain optimum enzymic activity (Klionsky & Emr, 2000).

The presence of myelin-like whorls (figures 7.21 B-G, L-O) has been previously described in many organisms under a variety of conditions. In the macrophages of rabbit alveolar the number of myelin bodies within a single inclusion varies considerably; many small circular profiles or a single large, membrane whorl may occupy the entire inclusion (Nichols, 1976). Such heterogeneity may be explained by representing different stages of digestion. The presences of so much myelin suggest macrophages ingest large quantities of lipids (Nichols, 1976). Higgins et al, (2001) examining canine tumours of the CNS reported intense ubiquitin staining and autophagosomes containing membrane-bound granules with a dense core and outer halo, empty vesicles comprised of autophagic vacuoles and myelin-like whorls. These single membrane-bound intralysosomal structures are separated by large empty spaces, not unlike those shown on figure 7.21 (L-O). Similarly, the blob-like aggregates are also ubiquitinated and appear to have a dense core and an outer halo.

Membrane whorls can also be induced experimentally following drug treatment. Inhibiting sterol biosynthesis in the parasite *Leishmania amazonensis* induces the formation of inclusion vesicles identified as acidocalcisomes

(Vannier-Santos et al, 1999). Here the ER cisternae form membrane whorls, which enclose large portions of the cytoplasm and some acidocalcisomes. Calcium within these structures may be involved in the stacking of parasite membranes, since it can promote a rapid interaction between multilamellar phospholipid vesicles that resemble myelin whorls. The authors conclude that the enhanced membrane content of the autophagic vacuoles present indicate an altered phospholipid turnover rate in response to sterol biosynthesis inhibition (Vannier-Santos et al, 1999). Just as the ER surrounds the acidocalcisomes, so perhaps the ER encloses the multilaminar bodies as suggested in figure 7.21 (B, C, H). In these images the elongated double unit membrane tubule extends to form a border around the autophagic body, but does not appear to encircle it completely.

Membrane whorls can also form following methamphetamine treatment of neuronal cultures as well as causing neurodegeneration, which typically results in the disappearance of neurites but not cell bodies due to autophagic activity (Larsen & Sulzer, 2002). Xue et al (1999) have also demonstrated the presence of membrane whorls associated with phagosome activity in normal, non-drug-treated sympathetic neurons.

In the present study TEM of Cos-7 cells expressing the fusion protein reveals the presence of numerous autophagic bodies in varying stages of maturity that are also associated with numerous laminar bodies showing similarly heterogeneity. Given these features, it seem likely that the NTFPS1-EGFP fusion protein is able to stimulate autophagy, though whether this is related to over expression or a NTFPS1 mediated effect is unknown. Because autophagy operates under condition of nutrient starvation, it is tempting to believe that some aspect of the fusion protein may some how mimic the starvation conditions within the cell that trigger autophagic response.

8.14 Consequence of fusion protein over expression

The absence of fusion protein blobs from cells expressing moderate levels of the fusion protein suggests that over expression of the transgene is the primary cause of the blob-like aggregates. It may be that a certain level of expression can be tolerated by the proteasome. Any increase above this level of expression or inhibition of the proteasome leads to the formation of aggresomes

(Johnston et al, 1999). In the case of the PS1 fusion protein, the presence of a highly hydrophobic molecule without a stabilizing influence that assists in burying the exposed transmembrane domains i.e. the CTF partner or co-factors such as nicastrin, is more likely to aggregate and conceivably present problems for the cell in how to dispose of it, especially under conditions of over expression. The constant drive of the transgene, which inevitably increases levels of the protein, may overload the proteasome leading to aggresome formation. In all the transfected cells surveyed only a handful show the presence of aggresomes, however, Kopito (2000) warns that a Golgi-like phenotype can easily be mistaken for the presence of an aggresome.

The question arises as to the limiting factors behind aggresome formation. Are they limited to a particular size, perhaps dictated by levels of the fusion protein or IF available to contain them? In the present study the blob-like aggregates are clearly distinct from the aggresome in terms of structure, number and location. Moreover, following proteasome inhibition the blob-like aggregates circle around the aggresome, suggesting that they might be resistant to proteasomal degradation. If correct, then the proteasome is not solely responsible for the breakdown of presenilin aggregates within the cell. In this instance the role of the phagosome may be important. In this context, Gelman et al, (2002) used a cystic fibrosis transmembrane conductance regulator GFP fusion protein (CFTR-GFP), to investigate previous reports that proteasome inhibition is insufficient to account for all instances of CFTR degradation suggesting the action of an ATP-independent proteolytic pathway. However, inhibition of the autophagy had no measurable effect on the breakdown of CFTR-GFP even after proteosomal inhibition indicating that the UPS degradation is the dominant pathway for the disposal of misfolded CFTR-GFP (Gelman et al, 2002). If this observation applies to all transmembrane proteins then presumably PS is similarly affected, however, the presence of phagosome activity in cells expressing the fusion protein argues that this assertion may not hold true, leastways, within the present study.

8.15 Impairment of the ubiquitin proteasome system

One explanation for the presence of the blob-like aggregates may lie in considering the effects this phenotype has on the UPS. The degradation of proteins by the ER relies on the UPS, which relies on ATP hydrolysis for activation of ubiquitin and substrate unfolding. Any disturbance in this system is of crucial importance in the management of protein levels by the cell. The notion that the fusion protein may interfere with the UPS is not without its precedent. Recently the presence of a novel presenilin binding protein (PBP) expressed specifically in the brain has been documented, which in its soluble form, is reduced in AD brains compared to controls. Over expression of PBP or proteasome inhibition generates aggresome formation in Cos-7 cells and neurons (Namekata et al, 2002). From these observations and other reports, that proteasome activity is significantly suppressed in the hippocampus of AD patients, and that mutant ubiquitin in AD can suppress degradation by the proteasome, suggest that impaired proteasome function may be crucial in the pathogenesis of AD (Namekata et al, 2002). This conclusion is based on the association of PBP with NFTs in AD brain, where it modifies the activity of GSK-3 β , one of protein kinases that phosphorylate tau (Takashima et al, 1998). Based on these observations the authors believe that PBP, which may regulate the activity of tau phosphorylation under normal conditions, may accelerate the formation of NFTs once it is sequestered into an aggresome due to impairment of the UPS.

Davies and Murphy, (2002) report the derangement of ER in rat neurons expressing mutant transgene found in Familial Neurohypophyseal Diabetes Insipidus (FNDI). Immunocytochemistry reveals the presence of mutant protein as aggregates within the ER, which are targeted for lysosomal degradation by autophagy. In trying to explain the loss of wild type vasopressin activity in cells expressing the defective FNDI allele, the authors propose that mutant protein accumulating within the ER by thiol retention is likely to be targeted to the UPS, whilst wild type vasopressin traffics normally through the secretory pathway. However, the build up of mutant protein within the ER traps normal protein within aggregates. Under these conditions the UPS is incapable of dealing with the aggregates therefore a rescue attempt is launched by the more general

degradation system of autophagy. In the process the deranged ER is removed and along with it, normal vasopressin thus leading to the disease phenotype (Si-Hoe et al, 2000; Davies & Murphy, 2002). This may also hold true for the fusion proteins. As they accumulate so perhaps the UPS is similarly effected resulting in autophagy as a means of rescuing the 'deranged' ER, hence the decrease or absence of some markers for the ER.

Other data show an increased propensity of mutant rhodopsin to self-associate into toxic high-weight aggregates that impart a robust gain of function directly linked to pathogenesis caused by impairment of the UPS (Illing et al, 2002). Furthermore, expression of mutant CFTR and a CAG repeat-huntingtin fragment likewise caused the near complete inhibition of the UPS (Bence et al, 2001). Also, McNaught et al, (2002) show the presence of numerous discrete ubiquitin protein aggregates in the neurone bodies in Parkinson's disease and 'dementia with Lewy bodies' (DLB). These aggregates are transported to the MTOC where they are sequestered to form Lewy bodies in neurons. They propose that Lewy body formation in PD and DLB is an aggresome-related attempt at protecting neurons from increased levels of potentially toxic proteins. An inability to curb levels of these proteins through regulated degradation could potentially cause the failure of the UPS and aggresome culminating in the aggregation of proteins into Lewy bodies. Again, a compromised UPS may similarly lead to the formation of the blob phenotype. This latter observation then provokes the question as to the role of Lewy bodies. Are they neuroprotective structures induced to shield cells from potential toxicity imparted by rising protein levels in response to a compromised UPS? Could the blobs likewise be an adaptive response to excessive levels of the fusion protein?

Lastly, Harada et al, (2003) show inhibition of the proteasome in cultured cells induces the formation of autophagic vacuoles and lysosomes and ubiquitin-IF inclusions that disrupt the Golgi apparatus. Similarly, Golgi fragmentation has been reported in the neurons of patients with familial amyotrophic lateral sclerosis (FALS) and its animal model. The inhibition of the proteasome induces IF inclusion, accompanied by a loss in the IF network which has the knock-on effect on Golgi organisation, and presumably the passage of materials through the secretory pathway (Harada et al, 2003). From

the above reports in is tempting to speculate that the blobs may indeed disrupt the UPS and that this impairment stimulates the alternate autophagic pathway responsible for the ER and Golgi alterations.

8.16 Formation of the blob-like aggregate phenotype

A possible scenario to account for the blob phenotype may be one in which moderates levels of the fusion protein are initially tolerated by the cell and degraded by the proteasome. However, increases in the level of the fusion protein may then saturate the proteasome leading to the formation of aggresomes. Once the capacity of the aggresome to sequester excessive levels of the fusion protein is reached, perhaps due to size constraints, membrane enwrapping of the ER begins at the nuclear/ER-interface (figure 7.20), leading to the formation of the fusion protein blobs, which ultimately stimulate autophagy. One difficulty with this scenario is that it assumes that the blobs form once the proteasome-aggresome capacity has been exceeded. As mentioned earlier, very few cells appear to show the presence of aggresomes, however, it is possible that their presence may be mistaken for the Golgi apparatus (Kopito, 2000). Furthermore, in stable HEK293 cells expressing the blob phenotype there is no evidence of aggresome formation. In fact data suggest that the blobs are stable, long-lived structures whose presence may be tolerated by the cell (figure 6.9, middle panel), indicating that the cell must be able to deal with these blobs prior to entering mitosis.

A outstanding issue concerning the blobs is the mechanism underlying their formation. Could the fusion protein saturate the membranes of the nuclear /ER-interface until they eventually 'pinch off' as suggested by figure 7.20, or do the blobs form as insoluble protein aggregates giving the appearance of membrane-bound structures? Could the blobs be examples of inclusion bodies or aggregates? Kopito (2000) maintains the necessity to distinguish between aggregates (non-native protein oligomers) and inclusion bodies, which are microscopically distinct cellular regions into which aggregated proteins are sequestered. In FALS, which is characterised by the presence of inclusion bodies, cellular pathology is paralleled by the presence of mutant superoxide dismutase (SOD) aggregates long before such SOD inclusion bodies appear.

This suggests that the toxicity associated with this disease is related to the non-native configuration adopted by SOD and may hold true for other diseases (Illing et al, 2002). The immunoblotting data in the present study are unhelpful in resolving aggregates from inclusion bodies since both outcomes can be represented by the membrane fraction. However, inclusion bodies are usually present in low copy numbers, often only one per cell, whereas the blobs number in the tens.

As the blobs arise from the nuclear/ER interface, it may be that the membrane system at these points becomes saturated as successive levels of the fusion protein build up. If unchecked, such high levels may eventually cause ER enwrapping, resulting in the formation of the multilaminar bodies, and in the process a substantial body of lipid membrane may be lost. Certainly this would explain the decrease in markers for both the ER and Golgi compartments. Presumably smooth ER sites overloaded with the fusion protein may effectively exclude other membrane resident proteins, since the decrease in ER antibody staining is seen only in cells expressing high levels of the fusion protein. The role of the phagosome may be crucial in this respect, since attempts at engulfing the laminar bodies may, in the process, consume healthy ER leaving behind the almost empty vacuole (figure 7.21 L-O). In fact this may explain the small amount of ER and the lack of a discernable Golgi compartment observed following TEM.

A similar mechanism to account for the loss of ER markers has been proposed by Si-Hoe et al, (2000). In this scheme misfolded vasopressin aggregates 'derange' the ER activating the lysosomal-linked autophagic pathway. During autophagocytosis deranged ER is removed and along with it, normal vasopressin, thus leading to the disease phenotype (Si-Hoe et al, 2000). Moreover, studies examining the affect of mutant growth hormone in Cos-7 cells have suggested that misfolded proteins might exert their toxicity by disturbing the ER-to-Golgi trafficking of secretory proteins (Graves et al, 2001).

8.17 Blobs-insoluble aggregates, inclusion bodies or membrane-bound compartments?

One concern regarding transfection experiments is that the transiently expressed membrane proteins tend to overload the secretory pathway, leading to aberrant trafficking and metabolism of the exogenous polypeptide and in many instances, endogenous membrane proteins. Moreover, it has been suggested that PS1 and PS2 are inherently 'sticky' proteins with a propensity to form aggregates (Kovacs et al, 1996; Kim et al, 1997; Thinakaran et al, 1997; Citron et al, 1997). This propensity to aggregate could easily explain the blobs as insoluble cytoplasmic aggregates and may well represent aggresome-related structures, albeit unusual ones in which a vimentin cage is absent (figure 7.12 a & b), though this does not rule out an alternative cage protein. To account for this scheme, the fusion protein must be removed from the membrane to facilitate aggregation within the cytoplasm. Kopito (2000) argues the case for CFTR, which may enter straight into the cytosolic pool, possibly due to failure of, or inefficient translocation. It is well established that the 26S proteasome is able to extract ER-transmembrane proteins from the lipid bilayer (Mayer et al, 1998). One such example is the processing of CFTR within the endoplasmic reticulum by the proteasome.

One other consideration regarding the blobs is that they are examples of inclusion bodies. Kopito (2000) proposes two models to explain inclusion body formation. In the first model protein monomers are directly deposited into a single inclusion body that grows steadily in size as more and more protein aggregate, whilst in the second model, proteins form into small aggregates at the cell periphery, possibly by a nucleation process, before being delivered to a far larger, nascent inclusion body. Certainly the nucleation aspect of the latter model is supported by the present study. Furthermore, a more precise model envisages the requirement of these aggregates to travel along microtubules towards the aggresome, a finding previously demonstrated by Garcia-Mata et al, (1999). A similar observation was made in the present study: In NTFPS1-EGFP expressing cells treated with both nocodazole and the proteasome inhibitor MG132, the blobs remained dispersed throughout the cell, however, MG132 treatment alone results in the blobs encircling the aggresome (figure

7.13 c & d). This result shows that the blobs do not require an intact microtubule system for their formation; however, proteasome inhibition shows a requirement for microtubules to transport the blobs to the MTOC.

In proposing that the blobs are inclusion bodies and not membrane-bound, the fusion protein following 'dislocation' through the ER membrane, must be targeted directly for destruction by the proteasome or else aggregate (Kopito & Sitia, 2000). In both fates the fusion protein will be polyubiquitinated and indeed this is the case for blobs (figure 7.14). A remarkable feature regarding the EGFP moiety, besides its reporter activity, is its ability to maintain fluorescence after being dislocated through the ER membrane. After all, if the blobs are inclusion bodies, how can they fluoresce given that they would ordinarily be 'unwound' (linearised), 'N-terminal' first, before being introduced back into the cytoplasm where they would then, presumably, aggregate due to exposure of the hydrophobic TM stretches. The EGFP moiety requires folding in order to generate fluorescence, so is it conceivable that the fusion protein unfolds all except the EGFP moiety, which remains intact and functional, or that within the aqueous, reducing environment of the cytoplasm EGFP re-assumes its native conformation and the unfolded hydrophobic PS stretches aggregate? Are the blobs therefore composed of partially unfolded PS1 but intact EGFP? Furthermore, could polyubiquitinated EGFP adopt a native conformation following covalent modification by ubiquitin? A parsimonious explanation is that EGFP can tolerate such treatment and that this only goes to show how remarkably robust EGFP is, hence its utility in many cell-based assays.

8.18 Apoptosis and autophagy

Whether the fusion protein blobs are membrane-bound, multilaminar bodies resembling myelin-like whorls, or inclusion bodies formed from aggregates is currently unclear. The evidence suggests that the blobs may stimulate both autophagy and sensitise transfected cells to apoptosis. Autophagy figures prominently in apoptosis and is also responsible for degrading proteins involved in cellular remodeling found during metamorphosis, aging and differentiation. It has been suggested that autophagic (type 2) death is distinct from apoptotic (type 1) death (Clarke, 1990). Morphologically, apoptosis involves nuclear

condensation, DNA fragmentation, organelle swelling, cytoplasmic vacuolization and nuclear envelope disruption, whereas autophagy correlates with autophagosomes, autolysosomes, electron-dense membranous autophagic vacuoles, myelin whorls, multivesicular bodies, as well as engulfment of entire organelles. The latter observations are suggested by the TEM data shown by figure 7.21, however, there is little sign of the morphological changes that accompany type 1 apoptosis. For instance, the TEM data show intact mitochondria (figure 7.21, J, K).

Apoptosis in AD is well established and cleavage of PS1 and PS2 by caspase-3 generates anti-apoptotic CTF (Vito et al, 1997), however, Stadelmann et al, have noted that the frequency of DNA fragmentation is too high to account for the continuous neuronal loss in AD extending over many years. Staining for caspase-3 in AD brain revealed the presence of the activated enzyme within autophagic bodies, referred to as granules of Granulovacuolar Degeneration (GVD) (Stadelmann et al, 1999). The authors conclude that the containment of activated caspase-3 within GVD-autophagic vacuoles serves to counteract apoptosis within the AD brain. Similarly, Tolkovsky and colleagues have demonstrated autophagy can precede apoptosis suggesting that it may have a protective role in programmed cell death (Xue et al, 1999). In section 8.9 the role of the fusion protein was discussed without mention as to whether this was type 1 or type 2 apoptosis. In light of the TEM data showing the absence of classical morphological changes typical of type 1 apoptosis, and the presence of numerous autophagic bodies, it is possible that type 2 apoptosis is responsible for the increased caspase activity seen in control and non-transfected cells (figure 6.11 & 7.2b). Within the present study, the fusion protein sensitizes cells to apoptosis following STS treatment, however, in the absence of proapoptotic stimuli, autophagic activity may be responsible for type 2 apoptosis. This does not mean that autophagic activity is not present under STS conditions. These data suggest that caspase cleavage of PS1 may be associated with type 2 apoptosis and autophagy.

To restate the earlier contention, proteasome action and aggresome formation may be insufficient to deal with excessive levels of the fusion protein leading to the activation of the alternate phagosomal pathway. A difficulty with

this interpretation is the absence of LAMP1 co-localisation with the blob phenotype (figure 7.9), indicating that the lysosomal pathway is insufficient to explain the presence of the blobs. However, if the multilaminar bodies are composed of the fusion protein, then according to the TEM data they may be resistant to lysosomal degradation since a consistent feature observed is the absence of any surrounding detail except for the presence of a residual laminar body eccentrically located within the autophagic vacuole. This is readily seen in figures 7.21 (J, K, N). Barring proteasome degradation of the blob-like aggregates and resistance to lysosomal degradation, how then are the laminar bodies dealt with? One clue may come from figure 7.21 A (inset), which shows the expulsion of an autophagic vacuole, and presumably with it the multilaminar bodies. This raises the possibility that the fusion protein may be detectable within the extracellular medium. In fact, one such study has recently demonstrated such a phenomenon. Benussi et al, (2001) show by immunoblotting the presence of PS CTF and weak membrane NTF in the conditioned media taken from rat neurons and HEK293 cells. Furthermore, this release of PS fragments proposed as 'membrane shedding' increases under apoptotic conditions following STS treatment. Interestingly, caspase inhibition had no effect on the release of CTF, suggesting that the CTFPS1 pool destined for secretion maybe generated by a caspase-independent pathway (Benussi et al, 2001). This membrane shedding may therefore be related to the autophagic pathway.

In the case of HEK293 cells stably expressing the fusion proteins, the presence of the blobs appear to be tolerated by the cells. Whether the proteasome is responsible for their clearance or if they are ejected from the cell by phagocytic activity is unknown. The high number and overall dimensions and morphology argue against the blobs being aggresomes, Lewy bodies or Russell bodies (Kopito & Sitia, 2000), however this does not rule out the possibility that they are in some way related to these structures. Recently, Lelouard et al, (2002) demonstrated the presence of high number, ubiquitinated protein aggregates transiently expressed in dendritic cells. Furthermore, these structures resemble the fusion protein blobs in terms of their gross morphology and biological properties, since they neither induce vimentin cage formation or

localise with the MTOC, nor are they destabilised following nocodazole treatment. The presence of these structures, referred to as dendritic cell aggresome-like induced structures (DALIS) are transient and require continuous protein synthesis. The proteasome degradation of DALIS provides material for MHC class I presentation (Lelouard et al, 2002). Although both DALIS and the fusion protein blobs have clearly different origins, the fact that the proteasome can handle high copy numbers of DALIS may be mirrored to some extent in stable PS1 HEK293 cells exhibiting numerous blobs.

8.19 Summary of main findings

- The putative PS1-NTF 923 antibody does not co-localise with endogenous or exogenous PS1
- PS1-EGFP fusion proteins generated four distinct phenotypes in different cell lines (ER, Golgi, vesicular and blob-like aggregates) that localise to varying degrees with antibodies to the cell compartment
- Immunoblotting of the fusion protein is within the membrane only fraction
- The removal of the EGFP moiety has no effect on the phenotype distribution
- Over expression of the fusion proteins alters or reduces antibody staining of some cell compartment markers
- The N-truncated fusion protein sensitises cells to STS-induced apoptosis
- Caspase cleavage of PS1 may be associated with type 2 apoptosis and autophagy in control and transfected cells
- The fusion protein blob-like phenotype co-localises strongly with ubiquitin
- The blob phenotype does not induce vimentin cage formation, or localise with the MTOC
- The fusion proteins forms aggresomes following inhibition of the proteasome
- In cells over expressing the full-length fusion proteins antibody staining suggest differential regulation of PS NTF and CTF fragments
- The blobs appear to originate from the nuclear-ER interface but do not stain for antibodies to the cell compartment

- The blob phenotype is not destabilised with nocodazole indicating that they do not require microtubules for their formation
- TEM reveals numerous phagosomes and multilaminar bodies that fit the profile seen for the blob-like aggregates in terms of dimension, number and general morphology

Overall, the size and general morphology of the multilaminar bodies as revealed by TEM fit the profile seen for the blob-like aggregates in terms of dimension, number and general morphology. A definitive test for identifying the laminar bodies/vacuoles as the PS1 blobs could ideally be accomplished by immunogold antibody labelling of the EGFP moiety and by cell fractionation experiments aimed at isolating the blobs. The blobs may therefore be membrane-associated structures (multilaminar bodies) that rely on autophagy for their clearance once aggregation of the over-expressed fusion protein has taken place. Kopito (2000) proposes that the aggresome might function as a center for the capture of aggregated protein by the autophagic pathway. Whilst this may hold true under conditions where the proteasome is inhibited, in the present study there was little sign of aggresome formation. Furthermore, the TEM data do not indicate the presence of an aggresome within cells displaying phagosomes (figure 7.21, A). Data presented herein indicate that the blobs form independently of the aggresome and may impair the UPS. A hypothetical scheme to account for the above observation is outlined in figure 8.0.

Unlike aggresomes and inclusion bodies, which are single copy organelles, the numerous blobs may represent novel structures whose function it is to contain excessive protein levels, possibly in response to a comprised UPS, and that their presence stimulates autophagy and/or apoptosis. Alternatively, the blobs are not the multilaminar bodies as seen by TEM, but may instead be a means of safely containing too high a level of expression within the cell, and that they present the fusion protein as manageable packets to the proteasome for degradation. The alteration in the ER and Golgi compartments and the inducement of autophagy would then be considered unrelated phenomena, possibly generated by the over production of the fusion protein that may impact on the UPS.

8.20 Concluding remarks

Increasingly important is the role played by aggregated proteins in the underlying pathology of a human degenerative conditions including Alzheimer's disease, light chain amyloidosis, spongiform encephalopathies, Huntingdon's disease, Parkinson's disease, etc. Recent genetic and biochemical data indicate that impairment of the UPS in these very different disorders may contribute further to the pathogenic mechanism specific to these diseases.

Taken as a whole, much of the evidence presented within this study concerned the effect moderate to high levels of the PS1 fusion proteins had on the general morphology of the cell. Immunofluorescence microscopy, immunoblotting and TEM data show that the blob-like aggregates alter the appearance of the ER and Golgi compartment, which may effect the normal trafficking of materials within the cell. The fusion proteins therefore provide a convenient means for studying the consequence that high levels of protein have on the UPS-aggresome response, apoptosis and phagocytosis within the cell.

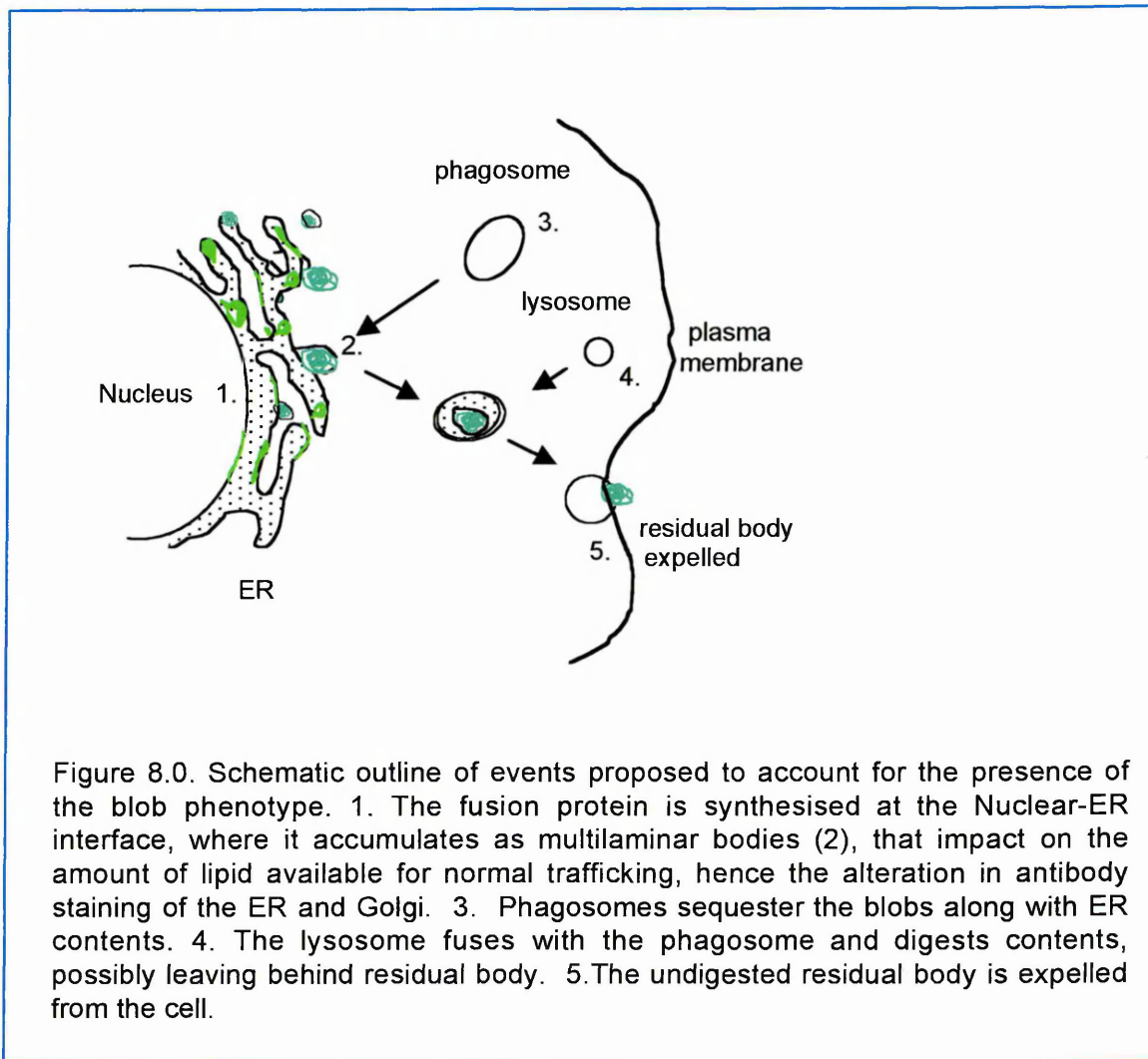


Figure 8.0. Schematic outline of events proposed to account for the presence of the blob phenotype. 1. The fusion protein is synthesised at the Nuclear-ER interface, where it accumulates as multilaminar bodies (2), that impact on the amount of lipid available for normal trafficking, hence the alteration in antibody staining of the ER and Golgi. 3. Phagosomes sequester the blobs along with ER contents. 4. The lysosome fuses with the phagosome and digests contents, possibly leaving behind residual body. 5. The undigested residual body is expelled from the cell.

REFERENCES

- Alves da Costa, C., M. Mattson, K. Ancolio, and F. Checler. 2003. The C-terminal fragment of presenilin 2 triggers p53 mediated staurosporine-induced apoptosis, a function independent of the presenilinase-derived N-terminal counterpart. *J. Biol. Chem.*
- Alves da Costa, C., E. Paitel, M.P. Mattson, R. Amson, A. Telerman, K. Ancolio, and F. Checler. 2002. Wild-type and mutated presenilins 2 trigger p53-dependent apoptosis and down-regulate presenilin 1 expression in HEK293 human cells and in murine neurons. *Proc. Natl. Acad. Sci. USA.* 99:4043-4048.
- Amson, R., J. Lassalle, H. Halley, S. Prieur, F. Lethrosne, J. Roperch, D. Israeli, M. Gendron, C. Duyckaerts, F. Checler, J. Dausset, D. Cohen, M. Oren, and A. Telerman. 2000. Behavioral alterations associated with apoptosis and down-regulation of presenilin 1 in the brains of p53-deficient mice. *Proc. Natl. Acad. Sci. USA.* 97:5346-5350.
- Ankarcrona, M., and K. Hultenby. 2002. Presenilin-1 is located in rat mitochondria. *Biochem. Biophys. Res. Comm.* 295:766-770.
- Arendt, T. 2001. Alzheimer's disease as a disorder of mechanisms underlying structural brain self-organisation. *Neuroscience.* 102:723-765.
- Buxbaum, J., K. Liu, Y. Luo, J. Slack, K. Stocking, J. Peschon, R. Johnson, B. Castner, D. Ceretti, and R. Black. 1998. Evidence that tumour necrosis factor α converting enzyme is involved in regulated α -secretase cleavage of the Alzheimer amyloid protein precursor. *J. Biol. Chem.* 273:27765-27767.
- Bence, N.F., Sampat, R.M., Kopito, R.R. 2001. Impairment of the ubiquitin-proteasome system by protein aggregation. *Science.* 292:1552-5
- Benjannet, S., A. Elagoz, L. Wickham, M. Mamarbachi, J.S. Munzer, A. Basak, C. Lazure, J.A. Cromlish, S. Sisodia, F. Checler, M. Chretien, and N. Seidah. 2001. Post-translational Processing of beta -Secretase (β -Amyloid-converting Enzyme) and Its Ectodomain Shedding. The pro- and transmembrane/cytosolic domains affect its cellular activity amyloid- β production. *J. Biol. Chem.* 276:10879-10887.
- Benussi, L., A. Alberici, M. Mayhaus, U. Langer, R. Ghidoni, F. Mazzoli, F. Nicosia, L. Barbiero, G. Frisoni, and O. Zanetti. 2001. Detection of the Presenilin 1 COOH-Terminal Fragment in the Extracellular Compartment: A Release Enhanced by Apoptosis. *Exp. Cell Res.* 269:256-265.
- Bertram, L., D. Blacker, K. Mullin, D. Keeney, J. Jones, S. Basu, S. Yhu, M. McInnis, R. Go, K. Vekrlis, D. Selkoe, A. Saunders, and R. Tanzi. 2000. Evidence

- for genetic linkage of Alzheimer's Disease to chromosome 10q. *Science*. 290:2302-2303.
- Biere, A.L., Ostaszewski, B. Zhao, H. Gillespie, S. Younkin, S G. Selkoe, DJ.1995. Co-expression of β -amyloid precursor protein (β APP) and apolipoprotein E in cell culture: analysis of β APP processing. *Neurobiol. Dis.* 2:177-187.
- Blacker, D., M. Wilcox, M. Laird, L. Rodes, S. Horvath, R. Go, B. Perry, B.J. Watson, S. Basset, M. McInnis, M. Albert, B. Hyman, and R. Tanzi. 1998. Alpha-2 macroglobulin is genetically associated with Alzheimer's Disease. *Nature Genetics*. 19:357-360.
- Blacker, W., D. Haines, and J. Rodes. 1997. ApoE-4 and age at onset of Alzheimer's disease: the NIMH genetics initiative. *Neurology*. 48:139-147.
- Bottomley, M., M. Batten, R. Lumb, and N. Bulleid. 2001. Quality control in the endoplasmic reticulum: PDI mediates the ER retention of unassembled procollagen C-propeptides. *Current Biology*. 11.
- Braak, H., and E. Braak. 1991. Neuropathological staging of Alzheimer related changes. *Acta. Neuropath.* 82:239-259.
- Bugiani, O., F. Tagliavini, G. Giaccone. 1995. Diffuse senile plaques: amorphous or fibrous. *Am. J. Pathol.* 146:777-778.
- Campbell, E. Pearson, R.C.A., Parkinson, D. (1999). Methods to uncover an antibody epitope in the KPI domain of Alzheimer's amyloid precursor protein for immunohistochemistry in human brain. *J. Neurosci. methods*. 93: 133-38.
- Campion, D. Brice, A. Dumanchin, C. Puel, M. Baulac, M. De la Sayette, V. Hannequin, D. Duyckaerts, C. Michon, A. Martin, C. Moreau, V. Penet, C. Martinez, M. Clerget-Darpoux, F. Agid, Y. Frebourg. 1996. A novel presenilin 1 mutation resulting in familial Alzheimer's disease with an onset age of 29 years. *NeuroReport*. 7(10): 1582-1584.
- Capell, A., J. Grunberg, B. Pesold, A. Diehlmann, M. Citron, R. Nixon, K. Beyreuther, D. Selkoe, and C. Haass. 1998. The proteolytic fragments of the Alzheimer's disease-associated presenilin-1 form heterodimers and occur as a 100–150-kDa molecular mass complex. *J. Biol. Chem.* 273:3205–3211.
- Carlson, G., D. Borchelt, A. Dake, S. Turner, V. Danielson, J. Coffin, C. Eckman, J. Meiners, S. Nilsen, S. Younkin, and K. Hsiao. 1997. Genetic modification of the phenotypes produced by amyloid precursor protein overexpression in transgenic mice. *Human Molecular Genetics*. 6:1951-1959.

- Chalfie, M., Y. Tu, G. Euskirchen, W. Ward, and D. Pasher. 1994. Green fluorescent protein as a marker for gene expression. *Science*. 263:802-805.
- Chan, S., C. Culmsee, N. Haughey, W. Klapper, and M. Mattson. 2002. Presenilin-1 Mutations Sensitize Neurons to DNA Damage-Induced Death by a Mechanism Involving Perturbed Calcium Homeostasis and Activation of Calpains and Caspase-12. *Neurobiology of Disease*. 11:2-19.
- Chapman, P., M. Agnieszka, S. Knevet, and M. Ramsay. 2001. Genes, models and Alzheimer's disease. *Trend in Genetics*. 17:254-261.
- Chen, F., D. Yang, S. Petanceska, A. Yang, A. Tandon, G. Yu, R. Rozmahel, J. Ghiso, M. Nishimura, D. Zhang, T. Kawarai, G. Levesque, J. Mills, L. Levesque, Y. Song, E. Rogaeva, D. Westaway, H. Mount, S. Gandy, P. St George-Hyslop, and P. E. Fraser. 2000. Carboxyl-terminal Fragments of Alzheimer β -Amyloid Precursor Protein Accumulate in Restricted and Unpredicted Intracellular Compartments in Presenilin 1-deficient Cells. *J. Biol.Chem*. 275:36794-36802.
- Chen, J., T. Murphy, M. Willingham, I. Pastan, and J. August. 1985. Identification of two lysosomal membrane glycoproteins. *J. Cell Biol*. 101:85-95.
- Citron, M. Diehl, T S. Capell, A. Haass, C. Teplow, D B; Selkoe, D J. 1996a. Inhibition of β -amyloid protein production in neural cells by the serine protease inhibitor AEBSF. *Neuron*. 17:171-179.
- Citron, M. Westaway, D. Xia, W. Carlson, G. Diehl, T. Levesque, G. Johnson-Wood, K. Lee, M. Seubert, P. Davis *et al.* 1997. Mutant presenilins of Alzheimer's disease increase production of 42-residue amyloid beta-protein in both transfected cells and transgenic mice. *Nature Medicine*. 3:67-72.
- Citron, M., T. Diehl, G. Gordon, A. Biere, P. Seubert, and D. Selkoe. 1996b. Evidence that A β 42 and A β 40 are generated from the β -amyloid precursor protein by different protease activities. *Proc. Natl. Acad. Sci. USA*. 93:13170–13175.
- Citron, M., C. Eckman, T. Diehl, C. Corcoran, B.L. Ostaszewski, W. Xia, G. Levesque, P. Hyslop, S. Younkin, and D. Selkoe. 1998. Additive effects of PS1 and APP mutations on secretion of the 42- residue amyloid beta-protein. *Neurobiology of Disease*. 5:107-116.
- Cook, D., Sung JC, Golde TE, Felsenstein KM, Wojczyk BS, Tanzi RE, Trojanowski JQ, Lee VM, Doms RW. 1996. Expression and analysis of presenilins 1 in human neuronal system: Localisation in cell bodies and dendrites. *Proc. Natl. Acad. Sci. USA*. 93:9223-9228.

Cook, D. Forman MS. Sung JC. Leight S. Kolson DL. Iwatsubo T. Lee VM. Doms RW. 1997. Alzheimer's A β (1-42) is generated in the endoplasmic reticulum/intermediate compartment of NT2N cells. *Nature Medicine*. 3:1021-1023.

Crook, R., Verkkoniemi A., Perez-Tur J., Mehta N., Baker M., Houlden H., Farrer M, Hutton M, Lincoln S., Hardy J., Gwinn K., Somer M., Paetau A., Kalimo H., Ylikoski R., Poyhonen M., Kucera S., Haltia M.1998. A variant of Alzheimer's disease with spastic paraparesis and 'cotton wool' plaques due to deletion of exon 9 of presenilin 1. *Nature Medicine*. 4:452-455.

Cubitt, A., R. Heim, S. Adams, A. Boyd, L. Gross, and R. Tsien. 1995. Understanding, improving and using green fluorescent proteins. *Trends in Biochemical Sciences*. 20:448-455.

Culvenor JG, Maher F, Evin G, Malchiodi-Albedi F, Cappai R, Underwood JR, Davis JB, Karran EH, Roberts GW, Beyreuther K, Masters CL. 1997. Alzheimer's disease-associated presenilin 1 in neuronal cells: evidence for localization to the endoplasmic reticulum-Golgi intermediate compartment. *J. Neurosci. Res*. 49(6):719-31.

Czech, C., Tremp, G., Pradier, L. 2000. Presenilins and Alzheimer's disease: biological function and pathogenic mechanisms. 60:363-384.

Davies, J., and D. Murphy. 2002. Autophagy in hypothalamic neurons of rats expressing a familial neurohypophyseal diabetes insipidus transgene. *J. of Neuroendocrinology*. 14:1-14.

De Jonghe C, Cras P, Vanderstichele H, Cruts M, Vanderhoeven I, Smouts I, Vanmechelen E, Martin JJ, Hendriks L, Van Broeckhoven C. 1999a. Evidence that A β 42 Plasma levels in Presenilin-1 Mutation carriers do not allow for prediction of their clinical phenotype. *Neurobiology of Disease*. 6:280-287.

De Jonghe C, Zehr C, Yager D, Prada CM, Younkin S, Hendriks L, Van Broeckhoven C, Eckman CB. 1998. Flemish and Dutch Mutations in Amyloid β Precursor Protein Have different effects on Amyloid β Secretion. *Neurobiol. of Disease*. 5:281-286.

De Jonghe, C., M. Cruts, E. Rogaeva, C. Tysoe, A. Singleton, H. Vanderstichele, W. Meschino, B. Dermaut, I. Vanderhoven, H. Backhovens, E. Vanmechelen, C. Morris, J. Hardy, D. Rubensztein, P. St George Hyslop, and C. van Broeckhoven. 1999b. Aberrant splicing in the presenilin-1 intron 4 mutation causes presenile Alzheimer's disease by increased Abeta42 secretion. *Hum. Mol. Genetics*. 8:1529-1540.

De Strooper B, Saftig P, Craessaerts K, Vanderstichele H, Guhde G, Annaert W, Von Figura K, Van Leuven F. 1998. Deficiency of presenilin-1 inhibits the normal cleavage of amyloid precursor protein. *Nature*. 391:387-390.

De Strooper, B., M. Buellens, B. Contreras, L. Levesque, K. Craesaerts, B. Cordell, D. Moechars, M. Bollen, P. Fraser, P. St George Hyslop, and F. Van Leuvan. 1997. Phosphorylation, subcellular localisation, and membrane orientation of Alzheimer's disease-associated presenilins. *J. Biol. Chem.* 272:3590-3598.

Dewji, N., D, Chou. S, Singer. 1997. On the spurious endoproteolytic processing of the presenilin proteins in cultured cells and tissues. *Proc. Natl. Acad. Sci. USA.* 94:9926-9931.

Dewji, N., and S. Singer. 1997. Cell surface expression of Alzheimer disease-related presenilin proteins. *Proc. Natl. Acad. Sci. USA.* 94:14031-14036.

Dickson, D. 1997. The pathogenesis of senile plaques. *J. Neuropathol. Exp. Neurol.* 56:321-339.

Doan, A., G. Thinakaran, D. Borchelt, H. Slunt, T. Ratovitsky, M. Podlisney, D. Selkoe, M. Seegar, S. Gandy, D. Price, and S. & Sisodia. 1996. Protein topology of presenilin 1. *Neuron.* 17:1023-1030.

El Khoury, J., S. Hickman, C. Thomas, and e. al. 1996. Scavenger receptor-mediated adhesion of microglia to beta-amyloid fibrils. *Nature.* 382:716-719.

Ertekin-Taner, N., N. Graff-Radford, L. Younkin, C. Eckmann, M. Baker, J. Adamson, J. Ronald, J. Blangero, M. Hutton, and S. Younkin. 2000. Linkage of Plasma A β 42 to a Quantitative Locus on Chromosome 10 in Late-Onset Alzheimer's Disease Pedigrees. *Science.* 290:2303-2304.

Felician, O., and T. Sandson. 1999. The neurobiology and pharmacotherapy of Alzheimer's Disease. *J. Neuropsychiatry Clin. Neurosci.* 11(1):19-31.

Fox, N., and M. Rossor. 2000. Seeing what Alzheimer saw-with magnetic resonance. *Nature Medicine.* 6:20-21.

Francis, R., G. McGrath, J. Zhang, D. Ruddy, M. Sym, M. Apfield, and e. al. 2002. aph-1 and pen-2 are required for Notch pathway signalling, γ -secretase cleavage of β -APP, and presenilin protein accumulation. *Dev. Cell.* 3:85-97.

Gangmin, D., C. Pike, and C. Cotman. 1996. Alzheimer-associated presenilin-2 confers increased sensitivity to apoptosis in PC12 cells. *FEBS Letters.* 397:50-54.

Garcia-Mata, R., Z. Bebok, E. Sorcher, and E. Sztul. 1999. Characterisation and dynamics of aggresome formation by a cytosolic GFP-chimera. *J. of Cell Biol.* 146:1239-1254.

Gelman, M., E. Kannegaard, and R. Kopito. 2002. A principal role for the proteasome in endoplasmic reticulum-associated degradation of misfolded intracellular cystic fibrosis transmembrane conductance regulator. *J. Biol.Chem.* 277:11709-11714.

Georgakopoulos, A., P. Marambaud, S. Efthimiopoulos, J. Shio, W. Cui, H. Li, M. Schutte, R. Gordon, G.R. Holstein, G. Martinelli, P. Mehta, V.J. Friedrich, and Robakis NK.1999. Presenilin-1 forms complexes with the cadherin/catenin cell-cell adhesion system and is recruited to intercellular and synaptic contacts. *Mol. Cell.* 4:1-20.

Glenner, G.A., and C. Wong. 1984. Alzheimer's disease and Down's syndrome: sharing of unique cerebrovascular amyloid fibril protein. *Biochem. Biophys. Res. Commun.* 122:1131-1135.

Goate, A., H. Chartier, M. Mullan, J. Brown, F. Crawford, L. Fidani, L. Giuffra, A. Haynes , N. Irving, L. James, et. al. 1991. Segregation of a missense mutation in the amyloid precursor protein gene with familial Alzheimer's disease. *Nature.* 349:704-706.

Goedert, M. 1996. Tau protein and the neuropathology of Alzheimer's disease. *Ann. N.Y. Acad. Sci.:*121-131.

Golde, T., S. Estus, L. Younkin, D. Selkoe, and S. Younkin. 1992. Processing of the amyloid precursor protein to potentially amyloidogenic derivatives. *Science.* 255:728-730.

Goldgaber, D., M. Lerman, O. McBride, U. Saffiotti, and D. Gadjusek. 1987. Characterisation and chromosomal location of a cDNA encoding brain amyloid of Alzheimer's disease. *Science.* 235:877-880.

Gorelick, F.S. and Shugrue, C. 2001. Exiting the endoplasmic reticulum. *Mol. and Cell. Endo.* 177:13-18.

Graves, T., S. Patel, P. Dannies, and P. Hinkle. 2001. Misfolded growth hormone causes fragmentation of the Golgi apparatus and disrupts endoplasmic reticulum-to-Golgi traffic. *J. of Cell Sci.* 114:3685-3694.

Greenfield, J., J. Tsai, G. Gouras, B. Hai, G. Thinakaran, F. Checler, S. Sisodia, P. Greengard, and H. Xu. 1999. Endoplasmic reticulum and trans-Golgi network generate distinct populations of Alzheimer β amyloid peptides. *Neurobiology.* 96:742-747.

Haass C, Hung AY, Selkoe DJ, Teplow DB.1994. Mutations associated with a locus for familial Alzheimer's disease result in alternative processing of amyloid β -protein precursor. *J. Biol. Chem.* 269:17741-17748.

Haass, C., E. Koo , A. Mellon , A. Hung, and D. Selkoe. 1992. Targeting of cell-surface beta-amyloid precursor protein to lysosomes: Alternative processing into amyloid-bearing fragments. *Nature.* 357:500-503.

Haniu, M., P. Denis, Y. Young, E. Mendiaz, J. Fuller, J. Hui, B. Bennett, S. Kahn, S. Ross, T. Burgess, V. Katta, G. Rogers, R. Vassar, and M. Citron. 2000. Characterization of Alzheimer's beta -Secretase Protein BACE. A pepsin family with unusual properties. *J. Biol. Chem.* 275:21099-10887.

Harada, M., H. Kumemura, M. Omary, T. Kawaguchi, N. Maeyama, S. Hanada, E. Taniguchi, H. Koga, T. Sukanuma, T. Ueno, and M. Sata. 2003. Proteasome inhibition induces inclusion bodies associated with intermediate filaments and fragmentation of the Golgi apparatus. 288(1):60-9 *Exp. Cell Res.*

Harald, S., R. Helmut, G. Melissa, P. Uwe, P. Brigitte, C. Martin, B. Ralf, and H. Christian. 1999. The Biological and Pathological Function of the Presenilin-1 Δ Exon9 Mutation Is Independent of Its Defect to Undergo Proteolytic Processing. *J. Biol. Chem.* 274:7615-7618.

Hardy, J. 1997. Amyloid, the presenilins and Alzheimer's. *Trends in Neuroscience.* 20:154-159.

Hardy, J., and R. Crook. 2001. Presenilin mutations line up along transmembrane α -helices. *Neurosci. Letters.* 306:203-205.

Hardy, J., and D. Selkoe. 2002. The amyloid hypothesis of Alzheimer's disease: Progress and problems on the road to therapeutics. *Science.* 297:353-356.

Hartmann, T., S. Bieger, B. Bruhl, P. Tienari, N. Ida, D. Allsop, G. Roberts , C. Masters, C. Dotti, K. Unsicker , and K. Beyreuther. 1997. Distinct sites of intracellular production for Alzheimer's disease A β 40/42 amyloid peptides. *Nature Medicine.* 3:1016-1020.

Hasegawa, M., R. Crowther, R. Jakes, and M. Goedert. 1997. Alzheimer like changes in microtubule-associated protein Tau induced by sulfated glycosaminoglycans. Inhibition of microtubule binding, stimulation of phosphorylation, and filament assembly depends on the degree of suphatation. *J. Biol. Chem.*272(52):33118-33124.

Hendrie, H.C. 1999. Epidemeology of Demetia and Alzheimer's Disease. *Am. J. of Ger. Psych.* 6:3-18.

Hendriks, L., C. van Duijn, P. Cras, M. Cruts, W. van Hul, F. van Harksamp, M. McInnis, S. Antonarakis, J. Martin, A. Hofman, and C. van Broeckhoven. 1992. Presenile dementia and cerebral haemorrhage linked to mutation at codon 692 of the β -amyloid precursor gene. *Nature Genetics*. 1:218-221.

Higgins, R., R. LeCouteur, K. Vernau, B. Sturges, J. Obradovich, and A. Bollen. 2001. Granular cell tumour of the canine central nervous system: Two cases. *Veterinary Pathology*. 38:620-627.

Ho, L., K. Fukuchi, and S. Younkin. 1996. The alternatively spliced Kunitz protease inhibitor domain alters amyloid beta protein precursor processing and amyloid beta protein production in cultured cells. *J. of Biol.Chem.* 271:30929-30934.

Hof, P., P. Giannakopoulos, J. Vickers, C. Bouras, and J. Morrison. 1995. The morphologic and neurochemical basis of dementia: aging, hierarchical pattern of lesion distribution and vulnerable neuronal phenotype. *Rev. Neurosci.* 6:97-124.

Hong CS, Caromile L, Nomata Y, Mori H, Bredesen DE, Koo EH. 1999. Contrasting role of Presenilin-1 and Presenilin-2 in Neuronal Differentiation *In vitro*. *J. of Neurosci.* 19:637-643.

Hsia, A., E. Masliah, L. McConlogue, G. Yu, G. Tatsuno, K. Hu, D. Kholodenko, R. Malenka, R. Nicoll, and L. Mucke. 1999. Plaque independent disruption of neural circuits in Alzheimer's disease mouse models. *Proc. Natl. Acad. Sci. USA.* 96:3228-3233.

Huse, J., D. Pijak, G. Leslie, V. Lee, and R. Doms. 2000. Maturation and Endosomal Targeting of beta -Site Amyloid Precursor Protein-cleaving Enzyme. The Alzheimer's disease β -secretase. *J. Biol. Chem.* 275:33729-10887.

Hussain, I., D. Powell, D. Howlett, D. Tew, T. Meek, C. Chapman, I. Gloger, K. Murphy, C. D, C. Southan, D. M., D. Ryan, T. Smith, D. Simmons, F. Walsh, C. Dingwall, and G. Christie. 1999b. Identification of a Novel Aspartic Protease (Asp 2) as β -Secretase. *Mol. Cell Neuro.* 14:419-427.

Illing, M., R. Rajan, N. Bence, and R. Kopito. 2002. A rhodopsin mutant linked to autosomal dominant retinitis pigmentosa is prone to aggregate and interacts with the ubiquitin proteasome system. *J. of Biol.Chem.* 277:34150-34160.

Imaizumi, K., K. Miyoshi, T. Katayama, T. Yoneda, M. Taniguchi, T. Kudo, and M. Tohyama. 2001. The unfolded protein response and Alzheimer's disease. *Biochem.et Biophys. Acta.* 1536:85-96.

Janicki, S., S. Stabler, and M. Monteiro. 2000. Familial Alzheimer's disease presenilin-1 mutants potentiate cell cycle arrest. *Neurobiology of Aging*. 21:829-836.

Jarret, J., E. Berger, and P. Lansbury. 1993a. The carboxy terminus of the beta amyloid protein is critical for the seeding of amyloid formation: implications for the pathogenesis of Alzheimer's disease. *Biochemistry*. 32:4693-4697.

Jarret, J., and P.J. Lansbury. 1993b. Seeding 'one-dimensional crystallisation' of amyloid: a pathogenic mechanism in Alzheimer's disease and scrapie? *Cell*. 73:1055-1058.

Jo, D., J. Chang, H. Hong, I. Mook-Jung, and Y. Jung. 2003. Contribution of presenilin/ γ -secretase to caspase-mediated apoptosis. *Biochem. and Biophys. Res. Comm.* 305:62-66.

Johnson-Wood, K., M. Lee, R. Motter, K. Hu, G. Gordon, R. Barbour, K. Khan, M. Gordon, H. Tan, D. Games, I. Lieberburg, D. Schenk, P. Seubert, and L. McConlogue. 1997. Amyloid precursor protein processing and A β 42 deposition in a transgenic mouse model of Alzheimer's disease. *Proc. Natl. Acad. Sci. USA*. 94:1550-1555.

Johnston, J., M. Illing, and R. Kopito. 2002. Cytoplasmic dynein/dynactin mediates the assembly of aggresomes. *Cell Motil. Cytoskeleton*. 53:26-28.

Johnston, J., C. Ward, and R. Kopito. 1998. Aggresomes: A cellular response to misfolded proteins. *J. of Cell Biol.* 143:1883-1898.

Kaether, C., S. Lammich, D. Edbauer, M. Ertl, J. Rietdorf, A. Capell, H. Steiner, and C. Haass. 2002. Presenilin-1 affects trafficking and processing of β APP and is targeted in a complex with nicastrin to the plasma membrane. *J. Cell Biol.* 158:551-561.

Kamal, A., Almenar-QA, J. LeBlanc, E. Roberts, and L. Goldstein. 2001. Kinesin-mediated axonal transport of a membrane compartment containing β -secretase and presenilin-1 requires APP. *Nature*. 414:643-648.

Kang, D., S. Soriano, M. Frosch, C. T, S. Naruse, S. SS, G. Leibowitz, L. F, and E. Koo. 1999. Presenilin 1 facilitates the constitutive turnover of beta-catenin: Differential activity of Alzheimer's disease-linked PS1 mutants in the beta-catenin-signaling pathway. *J. Neurosci.* 19:4229-4237.

Kang, J., H. Lemaire, A. Unterbeck, J. Salbaum, C. Masters, K. Grzeschik, G. Multhaup, K. Beyreuther, and B. Muller-Hill. 1987. The precursor of Alzheimer's disease amyloid A4 protein resembles a cell-surface receptor. *Nature*. 325:733-736.

- Kerr, J., A. Wyllie, and A. Currie. 1972. Apoptosis: a basic biological phenomenon with wide-ranging implications in tissue kinetics. *Br. J. Cancer*. 26:239-257.
- Kim TW, Pettingell WH, Hallmark OG, Moir RD, Wasco W, Tanzi RE. 1997. Endoproteolytic cleavage and proteasomal degradation of presenilin 2 in transfected cells. *J. Biol. Chem*. 272(17):11006-10.
- Kim, SH. Lah, JJ. Thinakaran, G. Levey, A. Sisodia, SS. (2000). Subcellular localisation of presenilins: Association with a unique membrane pool in cultured cells. *Neurobiology of Disease*. 7:99-117.
- Kim, D., L.M. Ingano, and D. Kovacs. 2002. Nectin-1alpha , an Immunoglobulin-like Receptor Involved in the Formation of Synapses, Is a Substrate for Presenilin/gamma -Secretase-like Cleavage. *J. Biol. Chem*. 277:49976-49981.
- Kirschenbaum F, Hsu SC, Cordell B, McCarthy JV. 2001. Glycogen synthase kinase-3beta regulates presenilin 1 C-terminal fragment levels. *J. Biol. Chem*. 276(33):30701-7
- Klausner, R., J. Donaldson, and J. Lippincott-Schwartz. 1992. Brefeldin A: insights into the control of membrane traffic and organelle structure. *J. Cell Biol*. 116:1071-1080.
- Klein, W., Krafft, and C. Finch. 2001. Targeting small A β oligomers: the solution to an Alzheimer's disease conundrum? *Trend in Neurosciences*. 24:219-224.
- Knops J, Suomensaaari S, Lee M, McConlogue L, Seubert P, Sinha S. 1995. Cell-type and amyloid precursor protein-type specific inhibition of A β release by Bafilomycin A1, a selective inhibitor of vacuolar ATPases. *J. Biol. Chem*. 270:2419-2422.
- Koo, E., S. Sisodia, D. Archer, L. Martin, A. Weidemann, K. Beyreuther, C. Masters, P. Fischer, and D. Price. 1990. Precursor of amyloid protein in Alzheimer's disease undergoes fast anterograde axonal transport. *Proc. Acad. Natl. Sci*. 87:1561-1565.
- Kopan, R. 2002. Notch: a membrane-bound transcription factor. *J. of Cell Sci*. 115:1095-1097.
- Kopito, R.R. 2000. Aggresomes, inclusion bodies and protein aggregation. *Trends in Cell Biology*. 10:524-530.
- Kopito, R., and R. Sitia. 2000. Aggresomes and Russell bodies. *J.Euro. Mol. Bio. Org*. 1:225-231.

Kovacs, D., H. Fausett, K. Page, T. Kim, R. Moir, D. Merriam, R. Hollister, O. Hallmark, R. Mancini, K. Felsenstein, B. Hyman, R. Tanzi, and W. Wasco. 1996. Alzheimer-associated presenilins 1 and 2: neuronal expression in brain and localisation to intracellular membranes in mammalian cells. *Nature Medicine*. 2:224-229.

Kovacs, D., R. Mancini, J. Henderson, S. Na, S. Schmidt, T. Kim, and R. Tanzi. 1999. Staurosporine-Induced Activation of Caspase-3 Is Potentiated by Presenilin 1 Familial Alzheimer's Disease Mutations in Human Neuroglioma Cells. *J. Neurochem*. 73:2278-2285.

Kruman, I., and M. Mattson. 1999. Pivotal Role of Mitochondrial Calcium Uptake in Neural Cell Apoptosis and Necrosis. *J. Neurochem*. 72:529-540.

La Voie, M., P. Fraering, B. Ostaszewski, W. Ye, W. Kimberly, M. Wolfe, and D. Selkoe. 2003. Assembly of the γ -secretase complex involves early formation of an intermediate sub-complex of Aph-1 and Nicastrin. *J. Biol. Chem*. 278(39):37213-22.

Lammich, S., E. Kojro, R. Postina, S. Gilbert, R. Pfeiffer, M. Jasionowski, C. Haass, and F. Faherenholz. 1999. Constitutive and regulated α -secretase cleavage of Alzheimer's amyloid precursor protein by a disintegrin metalloprotease. *Proc. Natl, Acad. Sci. USA*. 96:3922-3927.

Lane, JD., Lucocq, J. Pryde, J. Barr, F.A. Woodman, P.G. Allan, V.J. Lowe, M. 2002. Caspase-mediated cleavage of the stacking protein GRASP65 is required for Golgi fragmentation during apoptosis. *J. Cell. Biol*. 156, 3:495-509

Larsen, K., and D. Sulzer. 2002. Autophagy in neurons: a review. *Histology and Histopathology*. 17:1-12.

Law, A., S. Gauthier, and R. Quirion. 2001. Say NO to Alzheimer's disease; the putative links between nitric oxide and dementia of the Alzheimer's type. *Brain Research reviews*. 35:73-96.

Lee, M., H. Slunt, M. LJ, G. Thinakaran, G. Kim, S. Gandy, M. Seeger, E. Koo, D. Price, and S. Sisodia. 1996. Expression of presenilin 1 and 2 (PS1 and PS2) in human and murine tissues. *J. of Neurosci*. 16.

Lee, S., S. Shah, H. Li, C. Yu, W. Han, and G. Yu. 2002. Mammalian APH-1 interacts with presenilin and Nicastrin, and is required for intramembrane proteolysis of APP and Notch. *J. Biol. Chem*. 277:45013-45019.

Lelouard, H., E. Gatti, F. Capello, O. Gresser, V. Camosseto, and P. Pierre. 2002. Transient aggregation of ubiquitinated proteins during dendritic cell maturation. *Nature*. 417:177-182.

Lemere CA, Blusztajn JK, Yamaguchi H, Wisniewski T, Saido TC, Selkoe DJ. 1996. Sequence of deposition of heterogenous amyloid b-peptides and Apo-E in Down's syndrome: implications for initial events in amyloid plaque formation. *Neurobiology. of Disease.* 3:16-32.

Levitan, D., and I. Greenwald. 1995. Facilitation of lin-12-mediated signalling by sel-12, a *Caenorhabditis elegans* S182 Alzheimer's disease gene. *Nature.* 377:351-354.

Levy, E., M. Carman, I. Fernandez-Madrid, M. Power, I. Lieberberg, S. van Duinen, A. Botsgt, W. Luyendijk, and B. Frangione. 1990. Mutation of the Alzheimer's disease amyloid gene in hereditary cerebral haemorrhage, Dutch type. *Science.* 248:1124-1126.

Li, X., and I. Greenwald. 1996. Membrane topology of the *C.elegans* SEL-12 presenilin. *Neuron.* 17:1015-1021.

Li, X., and I. Greenwald. 1998. Additional evidence for an eight transmembrane domain topology for *Caenorhabditis elegans* human presenilins 1. *Proc. Natl. Acad. Sci.* 95:7109-7114.

Li, Y., M. Xu, M. Lai, Q. Huang, J. Castro, J. DiMuzio-Mower, T. Harrison, C. Lellis, A. Nadin, J. Neduvellil, R. Register, M. Sardana, M. Shearman, A. Smith, X. Shi, K. Yin, J. Shafer, and S. Gardell. 2000. Photoactivated γ -secretase inhibitors directed to the active site covalently label presenilin 1. *Nature.* 405:689-693.

Liao, A., R. Nitsch, S. Greenberg, U. Finckh, D. Blacker, M. Albert, D. Redbeck, T. Gomez-Isla, A. Clatworthy, G. Binetti, C. Hock, T. Mueller-Thomsen, U. Mann, K. Zuchowski, U. Beisiegel, H. Staehelin, J. Growdon, R. Tanzi, and B. Hymen. 1998. Genetic association of an α 2-macroglobulin (Val1000Ile) polymorphism and Alzheimer's disease. *Human Mol. Genetics.* 7:1953-1956.

Loetscher, H., U. Deuschle, M. Brockhaus, D. Reinhardt, P. Nelboeck, J. Mous, J. Grunberg, C. Haass, and H. and Jacobsen. 1997. Presenilins are processed by caspase-type proteases. *J.Biol. Chem.* 272:20655-20659.

Loo DT, Copani A, Pike CJ, Whitemore ER, Walencewicz AJ, Cotman CW. 1993. Apoptosis is induced by beta-amyloid in cultured central nervous system neurons. *Proc. Natl. Acad. Sci. USA.* 90:7951-7955.

Lorenzo, A., and B. Yanker. 1994. Beta-amyloid neurotoxicity requires fibril formation and is inhibited by Congo red. *Proc. Natl. Acad. Sci. USA.* 91:12243-12247.

Lowe, S.L., F. Peter, V.N. Subramaniam, S.H. Wong, and W. Hong. 1997. A SNARE involved in protein transport through the Golgi apparatus. *Nature*. 389:881-884.

Lucocuq, J., and G. Warren. 1987. Fragmentation and partitioning of the Golgi apparatus during mitosis in HeLa cells. *J. Euro. Mol. Bio. Org.* 6:3239-3246.

Mah, A., G. Perry, M.A. Smith, M.J. Monteiro, D. Cribbs, L.S. Chen, S.M. Bende, and F.M. LaFerla. 2000. Identification of ubiquilin, a novel presenilin interactor that increases presenilin protein accumulation. 151:847-862.

Mahley, R. 1988. Apolipoprotein E: Cholesterol transport protein with expanding role in cell biology. *Science*. 240:622-630.

Mandelkow, E., and E. Mandelkow. 1998. Tau in Alzheimer's disease. *Trends in Cell Biology*. 8:425-427.

Mann, D., and M. Esiri. 1989. The pattern of acquisition of plaques and tangles in the brain of patients under 50 years of age with Down's syndrome. *J. Neurol. Sci.* 89:167-179.

Marlow, L., R. canet, S. Haugabook, J. Hardy, D. Lahiri, and K. Sambamurti. 2003. APH1, PEN2, and Nicastrin increase A β levels and γ -secretase activity. *Biochem. Biophys. Res. Comm.* 305:502-509.

Masters, C., G. Simms, N. Weinmann, G. Multhaup, B. McDonald, and K. Beyreuther. 1985. Amyloid plaque core protein in Alzheimer disease and Down syndrome. *Proc. Natl. Acad. Sci. USA*. 82:4245-4249.

McNaught, K.S.P., P. Shashidharan, D. Perl, P. Jenner, and C. Olanow. 2002. Aggresome-related biogenesis of Lewy bodies. *Euro. J. of Neurosci.* 16:2136-2148.

Medina, M and Dotti, CG. 2003. RIPPed out by presenilin-dependent γ -secretase. *Cellular Signalling*. 15:829-841.

Mercken, M., H. Takahashi, T. Honda, K. Sato, M. Murayama, Y. Nakazato, K. Noguchi, K. Imahori, and A. & Takashima. 1996. Characterization of human presenilin 1 using N-terminal specific monoclonal antibodies: Evidence that Alzheimer mutations affect proteolytic processing. *FEBS*. 389(3):297-303.

Miguel, M. Dotti, C.G. 2003. RIPPed out by presenilin-dependent γ -secretase. *Cellular Signalling*. 15:829-841.

Myers, A., P. Holmans, H. Marshall, J. Kwon, D. Meyer, D. Ramic, S. Shears, J. Booth, F. DeVrieze, R. Crook, M. Hamshere, R. Abraham, T. N, F. Rice, S. Cartey,

S. Lillystone, P. Kehoe, V. Rudrasingham, J. Williams, M. Owen, J. Hardy, and A. Goate. 2000. Susceptibility locus for Alzheimer's Disease on Chromosome 10. *Science*. 290:2304-2305.

Nagata, K., and K. Yamada. 1986. Phosphorylation and transformation sensitivity of a major collagen-binding protein of fibroblasts. *J. Biol. Chem.* 261:7531-7536.

Nakakamura, N., C. Rabouille, R. Watson, T. Nilsson, N. Hui, P. Slusarewicz, T.E. Kreis, and G. and Warren. 1995. Characterisation of a cis-Golgi matrix protein, GM130. *J. Cell Biol.* 155:543-556.

Namekata, K., N. Nishimura, and H. Kimura. 2002. Presenilin-binding protein forms aggresomes in monkey kidney Cos-7 cells. *J. of Neurochem.* 82:819-827.

Nichols, B. 1976. Normal rabbit alveolar macrophages. *J. of Exp. Med.* 144:906-919.

Nishimura, M., G. Yu, G. Levesque, D.M. Zhang, L. Ruel, F. Chen, P. Milman, E. Holmes, Y. Liang, T. Kawarai, E. Jo, A. Supala, E. Rogaeva, D.M. Xu, C. Janus, L. Levesque, Q. Bi, M. Duthie, R. Rozmahel, K. Mattila, L. Lannfelt, D. Westaway, H.T. Mount, J. Woodgett, and P. St George-Hyslop. 1999a. Presenilin mutations associated with Alzheimer disease cause defective intracellular trafficking of beta-catenin, a component of the presenilin protein complex. *Nature Med.* 5:164-169.

Nishimura, N., S. Bannykh, S. Slabough, J. Matteson, Y. Altschuler, K. Hahn, and W. Balch. 1999b. A di-acidic (DXE) code directs concentration of cargo during export from the endoplasmic reticulum. *J. Biol. Chem.* 274:15937-15946.

Oprins, A., R. Duden, T.E. Kreis, H.J. Geuze, and J.W. Slot. 1993. Beta-COP localizes mainly to the cis-Golgi side in exocrine pancreas. *J. Cell Biol.* 121:49-59.

Pappolla, M., O. RA, and K. KS. 1992. Immunohistochemical evidence of oxidative stress in Alzheimer's disease. *Am. J. Pathol.* 140:621-628.

Parkin ET, Hussain I, Karran EH, Turner AJ, Hooper NM. 1999. Characterization of detergent-insoluble complexes containing the familial Alzheimer's disease-associated presenilins. *J. Neurochem.* 72:1534-1543.

Passer, B.J., L. Pellegrini, P. Vito, J. Ganjei, and L. D'Adamio. 1999. Interaction of Alzheimer's Presenilin-1 and Presenilin-2 with Bcl-XL. A potential role in modulating the threshold of cell death. *J. Biol. Chem.* 274:24007-24013.

Pearson, R., and T. Powell. 1989. The neuroanatomy of Alzheimer's Disease. *Rev. Neurosci.* 2:101-122.

Pereira, C., M. Santos, and C. Oliveira. 1999. Involvement of Oxidative Stress on the Impairment of Energy Metabolism Induced by A β Peptides on PC12 Cells: Protection by Antioxidants. *Neurobiology of Disease*. 6:209-219.

Perry EK, Tomlinson BE, Blessed G, Bergmann K, Gibson PH, Perry RH. 1978. Correlation of abnormalities with senile plaques and mental test scores in senile dementia. *J. of Br. Med.* 2:1457-1459.

Podlisny, M., M. Citron, P. Amarante, R. Sherrington, W. Xia, J. Zhang, T. Diehl, G. Levesque, P. Fraser, C. Haass, E. Koo, M. Seubert, P. St George-Hyslop, D. Teplow, and D. Selkoe. 1997. Presenilin Proteins Undergo Heterogeneous Endoproteolysis between Thr 291 and Ala 299 and Occur as Stable N- and C-Terminal Fragments in Normal and Alzheimer Brain Tissue. *Neurobiology of Disease*. 3:325-337 (313).

Podlisny, M., D. Tolan, and D. Selkoe. 1991. Homology of the amyloid b-protein precursor in monkey and human supports a primate model for β -amyloidosis in Alzheimer's disease. *Am. J. Pathol.* 138:1423-1435.

Poduslo, J.F., G. Curran, B. Sanyal, and D. Selkoe. 1999. Receptor-Mediated Transport of Human Amyloid- β Protein 1-40 and 1-42 at the Blood-Brain Barrier. *Neurobiology of Disease*. 6:190-199.

Pradier L, Carpentier N, Delalonde L, Clavel N, Bock MD, Buee L, Mercken L, Tocque B, Czech C. 1999. Mapping the APP/presenilin (PS) Binding domains: The hydrophilic N-terminus of PS2 is sufficient for interaction with APP and can displace APP/PS1 interaction. *Neurobiology of Disease*. 6:43-55.

Primkoff, P., and D. Myles. 2000. The ADAM gene family, surface proteins with adhesion and protease activity. *Trends in Genetics*. 16:83-87.

Raposo, G., H. van Santen, R. Leijendekker, H. Geuze, and H. Ploegh. 1995. Misfolded major histocompatibility complex class I molecules accumulate in an expanded ER-Golgi intermediate compartment. *J. Cell Biol.* 131:1403-1419.

Rebeck, G., S. Harr, D. Strickland, and B. Hyman. 1995. Multiple, diverse senile plaque-associated proteins are ligands of an apolipoprotein E receptor, the alpha-macroglobulin receptor/low-density lipoprotein receptor-related protein. *Ann. Neurol.* 37:21-217.

Robinson, S., and G. Bishop. 2002. A β as a bioflocculent: implications for the amyloid hypothesis of Alzheimer's disease. *Neurobiology of Aging*. 23:1051-1072.

Rogaev, E., R. Sherrington, E. Rogaeva, G. Levesque, M. Ikeda, Y. Liang, H. Chi, C. Lin, K. Holman, T. Tsuda, and e. al. 1995. Familial Alzheimer's disease in

kindreds with missense mutations in a gene on chromosome 1 related to the Alzheimer's disease type 3 gene. *Nature*. 376:775-778.

Roperch, J., V. Alvaro, S. Prieur, M. Tuynder, M. Nemani, F. Lethrosne, L. Piouffre, M. Gendron, D. Israeli, and J. Dausset. 1998. Inhibition of presenilin 1 expression is promoted by p53 and p21WAF-1 and results in apoptosis and tumor suppression. *Nature Medicine*. 4:835-838.

Roses, A. 1994. Apolipoprotein E affects the rate of Alzheimer's Disease expression: β amyloid burden is a secondary consequence dependent on ApoE4 genotype and duration of disease. *J. Neuropath. Exp. Neurol.* 53:429-437.

Sabbagh, M., D. Galasko, and L. Thal. 1997. β -Amyloid and Treatment Opportunities for Alzheimer's Disease. *Alzheimer's Disease Review*. 2:69-87.

Saido, T. 2003. Chapter 1. Overview- $A\beta$ Metabolism: From Alzheimer's Research to brain Aging Control. *In A β Metabolism and Alzheimer's Disease*. Eureka.com Austin, Texas, USA. Lands Bioscience.

Sambrook, J., E.F. Fritsch, and T. Maniatis. 1989. *Molecular Cloning. A laboratory Manual*. Cold Spring Harbour Laboratory Press.

Santiard-Baron D, Gosset P, Nicole A, Sinet PM, Christen Y, Ceballos-Picot I. 1999. Identification of β -Amyloid-Responsive Genes by RNA Differential Display: Early Induction of a DNA Damage-Inducible Gene, gadd45. *Exp. Neurol.* 158:206-213.

Sauk, J., K. Norris, J. Moehring, R. Foster, and S. MJ. 1990. The expression of colligin/hsp47 after stress in human peridonatal fibroblasts in vitro. *Arch. Oral. Biol.* 35:645-651.

Scales, S., R. Pepperkok, and T. Kreis. 1997. Visualization of ER-to-Golgi transport in living cells reveals a sequential mode of action for COPII and COPI. *Cell*. 90:1137-1148.

Schneider, L. 1999. Cholinergic Deficiency in Alzheimer's Disease. *Am. J. of Ger. Psych.* 6:49-55.

Schwarzman, A., N. Singh, M. Tsiper, L. Gregori, A. Dranovsky, M. Vitek, C. Glabe, P. St. George-Hyslop, and G. D. 1999. Cell Biology Endogenous presenilin 1 redistributes to the surface of lamellipodia upon adhesion of Jurkat cells to a collagen matrix. *Proc. Natl. Acad. Sci. U S A*. 96:7932-7937.

Seemann, J., E. Jokitalo, M. Pypaert, and G. Warren. 2000. Matrix proteins can generate the higher order architecture of the Golgi apparatus. *Nature*. 407:1022-1026.

Selkoe, D., Y. Ihara, and F. Salazar. 1982. Alzheimer's disease: insolubility of partially purified helical filaments in sodium dodecyl sulphate and urea. *Science*. 215:1243-1245.

Selkoe, D., Selkoe DJ, Podlisny MB, Joachim CL, Vickers EA, Lee G, Fritz LC, Oltersdorf T. 1988. β -amyloid precursor protein of Alzheimer's disease occurs as 110-135 kilodalton membrane-associated proteins in neural and nonneural tissues. *Proc. Natl. Acad. Sci. USA*. 85:7341-7345.

Selkoe, D. 1996. Amyloid β -Protein and the Genetics of Alzheimer's Disease. *J. of Biol.Chem.* 271:18295-18298.

Selkoe, D. 1998. The cell biology of the β -amyloid precursor protein and presenilin in Alzheimer's disease. *Trend in Cell Biology*. 8:447-453.

Selkoe, D. 1999. Translating cell biology into therapeutic advances in Alzheimer's disease. *Nature*. 399:A23-A31.

Selkoe, D. (2000).

Seubert P, Vigo-Pelfrey C, Esch F, Lee M, Dovey H, Davis D, Sinha S, Schlossmacher M, Whaley J, Swindlehurst C, et al.1992. Isolation and quantification of soluble Alzheimer's β -peptide from biological fluids. *Nature*. 359:325-327.

Shen, J., R. Bronson, D. Chen, W. Xia, D. Selkoe, and S. Tonegawa. 1997. Skeletal and CNS defects in presenilin-1 deficient mice. *Cell*. 89:629-639.

Sherrington R, Rogaev EI, Liang Y, Rogaeva EA, Levesque G, Ikeda M, Chi H, Lin C, Li G, Holman K, et al. 1995. Cloning of a novel gene bearing missense mutations in early onset familial Alzheimer's disease. *Nature*. 375:754-760.

Shima, D., N. Cabrera-Poch, R. Pepperkok, and G. Warren. 1998. An Ordered Inheritance Strategy for the Golgi Apparatus: Visualisation of Mitotic Disassembly Reveals a Role for the Mitotic spindle. *J. of Cell Biol.* 141:955-966.

Si-Hoe, S., F. De Bree, M. Nijenhuis, J. Davies, L. Howell, H. Tinley, S. Waller, Q. Zeng, R. Zalm, M. Sonnemans, F. Van Leeuwen, J. Burbach, and D. Murphy. 2000. Endoplasmic reticulum derangement in hypothalamic neurons of rats expressing a familial neurohypophyseal diabetes insipidus mutant vasopressin transgene. *The FASEB Journal*. 14:1680-1684.

Siman, R., D. Flood, G. Thinakaran, and R. Neumar. 2001. Endoplasmic Reticulum Stress-induced Cysteine Protease Activation in Cortical Neurons. Effect of an

Alzheimer's disease linked presenilin-1 knock-in mutation. *J. Biol. Chem.* 276:44736-44743.

Sisodia, S. 1992. β -amyloid precursor protein cleavage by a membrane-bound protease. *Proc. Natl Acad. Sci. USA.* 89:6075-6070.

Smith, R., D. Higuchi, and G.J. Broze. 1990. Platelet coagulation factor XIa-inhibitor, a form of Alzheimer amyloid precursor protein. *Science.* 248:1126-1128.

St George Hyslop, P. 2000. Molecular genetics of Alzheimer's Disease. *Soc. of Biol. Psych.* 47:183-196.

Stahl, B., A. Diehlmann, and T. Sodhof. 1999. Direct Interaction of Alzheimer's Disease-related Presenilin-1 with Armadillo Protein p0071. *J. Biol. Chem.* 274:9141-9148.

Steiner, H. Capell, A. Pesold, B. Citron, M. Kloetzel, PM. Selkoe, DJ, Romig, H. Mendla, K. Haass, C. 1998. Expression of Alzheimer's disease-associated presenilin-1 is controlled by proteolytic degradation and complex formation. *J. Biol. Chem.* 273(48) 32322-32331.

Steiner, H., E. Winkler, D. Edbauer, S. Prokop, G. Basset, A. Yamasaki, M. Kostka, and C. Haass. 2002. PEN-2 is an integral component of the γ -secretase complex required for coordinated expression of presenilin and nicastrin. *J. Biol. Chem.* 277:39062-39065.

Steiner, H., E. Winkler, M. Shearman, R. Prywes, and C. Haass. 2001. Endoproteolysis of the ER Stress Transducer ATF6 in the Presence of Functionally Inactive Presenilins. *Neurobiol. of Disease.* 8:717-722.

Strange, P. 1992. Brain biochemistry and Brain Disorders. Oxford University Press. 201-225 pp.

Strittmatter, W., A. Saunders, D. Schmechel, M. Pericak-Vance, J. Enghild, G. Salvensen, and A. Roses. 1993. Apolipoprotein E: high-avidity binding to β -amyloid and increased frequency of type 4 allele in late-onset familial Alzheimer's disease. *Proc.Natl. Acad.Sci.USA.* 90:1977-1981.

Struhl, G., and I. Greenwald. 1999. Presenilin is required for activity and nuclear access of Notch in *Drosophila*. *Nature.* 398(6727):522-5.

Suzuki N, Cheung TT, Cai XD, Odaka A, Otvos L Jr, Eckman C, Golde TE, Younkin SG. 1994. An increased Percentage of Long Amyloid β Protein secreted by Familial Amyloid β Protein Precursor (β APP₇₁₇) Mutants. *Science.* 264:1336-1340.

Takashima, A., M. Murayama, O. Murayama, T. Kohno, T. Honda, K. Yasutake, N. Nihomatsu, M. Mercken, H. Yamaguchi, S. Sugihara, and B. Wolozin. 1998. Presenilin 1 associates with glycogen synthase kinase 3- β and its substrate tau. *Proc. Natl. Acad. Sci. USA.* 95:9637-9641.

Takashima, A., M. Sato, M. Mercken, S. Tanaka, S. Kondo, T. Honda, K. Sato, M. Murayama, K. Noguchi, Y. Nakazato, and H. Takahashi. 1996. Localization of Alzheimer-Associated Presenilin 1 in Transfected COS-7 Cells. *Biochem. and Biophys. Res. Comm.* 227:423-426.

Takasugi, N., T. Tomita, I. Hayashi, M. Tsuruoka, M. Niimura, Y. Takahashi, G. Thinakaran, and T. Iwatsubo. 2003. The role of presenilin cofactors in the γ -secretase complex. *Nature.* 422:438-441.

Takuda, T., T. Fukushima, S. Ikeda, Y. Sekijima, S. Shoji, N. Yanagisawa, and A. Tamoaka. 1997. Plasma levels of amyloid beta proteins A β 1-40 and A β 1-42 (43) are elevated in Down's Syndrome. *Ann. Neurol.* 41:271-273.

Tanzi, R. 1999. A genetic dichotomy model for the inheritance of Alzheimer's disease and common age-related disorders. *The J. of Clin. Invest.* 104:1175-1179.

Tanzi, R.E. 1998. Of calcium, caspases, and cognitive decline. *Nature Medicine.* 4:1127-1128.

Terry, R. 1996. The pathogenesis of Alzheimer's disease: an alternative to the amyloid hypothesis. *J. Neuropath. Exp Neurol.* 55:1023-1025.

Thinakaran, G., D.R. Borchelt, M.K. Lee, H.H. Slunt, L. Spitzer, G. Kim, T. Ratovitsky, F. Davenport, C. Nordstedt, M. Seeger, J. Hardy, A.I. Levey, S.E. Gandy, N.A. Jenkins, N.G. Copeland, D.L. Price, and S.S. Sisodia. 1996. Endoproteolysis of Presenilin 1 and accumulation of processed derivatives in vivo. *Neuron.* 17:181-190.

Thinakaran G, Regard JB, Bouton CM, Harris CL, Price DL, Borchelt DR, Sisodia SS. 1998. Stable association of presenilin derivatives and absence of presenilin interactions with APP. *Neurobiology of Disease.* 4:438-453.

Tokuhiro, K., T. Tomita, H. Iwata, T. Kosaka, T. Saido, K. Maruyama, and T. Iwatsubo. 1998. The Presenilin Mutation (M146V) Linked to Familial Alzheimer's Disease Attenuates the Differentiation of NTera 2 cells. *Biochem. and Biophys. Res. Comm.* 244:751-755.

Tomidokoro, Y., I. Koji, I. Yukifusa, M. Etsuro, K. Mitsuyasu, S. Masami, K. Takeshi, H. Yasuo, K. Shinobu, I. Kunio, I. Masaki, P. St George-Hyslop, H. Shunsaku, O. Koichi, and S. Mikio. 1999. Carboxyl-Terminal Fragments of

- Presenilin-1 Are Closely Related to Cytoskeletal Abnormalities in Alzheimer's Brains. *Biochem. and Biophys. Res. Comm.* 256:512-518.
- Van de Craen, M., C. De Jonghe, I. Van den Brande, W. Declercq, G. Van Gassen, W. Van Criekinge, I. Vanderhoeven, W. Fiers, C. Van Broeckhoven, L. Hendriks, and P. & Vandenaabeele. 1999. Identification of caspases that cleave presenilin-1 and presenilin-2. Five presenilin-1 (PS1) mutations do not alter the sensitivity of PS1 to caspases. *FEBS.* 445:149-154.
- Van Gassen, G., C. De Jonghe, S. Pype, W. Van Criekinge, A. Julliams, I. Vanderhoeven, S. Woodrow, R. Beyaert, D. Huylebroeck, and C. Van Broeckhoven. 1999. Alzheimer's Disease Associated Presenilin 1 Interacts with HC5 and ZETA, Subunits of the Catalytic 20S Proteasome. *Neurobiology of Disease.* 6:376-391.
- Vannier-Santos, M., A. Martiny, U. Lins, J. Urbino, V. Borges, and W. de Souza. 1999. Impairment of sterol biosynthesis leads to phosphorus and calcium accumulation in *Leishmania acidocalcisomes*. *Microbiology.* 145:3213-3220.
- Vassar, R., B. Bennett, S. Babu-Khan, S. Kahn, E. Mendiaz, P. Denis, et. al. 1999. Beta-secretase cleavage of Alzheimer's amyloid precursor protein by the transmembrane aspartic protease BACE. *Science:*735-741.
- Vickers, J., T. Dickson, P. Adlard, H. Saunders, C. King, and G. McCormack. 2000. The cause of neuronal degeneration in Alzheimer's disease. *Prog. in Neurobio.:* 60(2):139-65.
- Vito, P., T. Ghayur, and L. D'Adamio. 1997. Generation of Anti-apoptotic Presenilin-2 Polypeptides by Alternative Transcription, Proteolysis, and Caspase-3 Cleavage. *J. Biol. Chem.* 272:28315-28320.
- Walsh, D., I. Klyubin, J. Fadeeva, W. Cullen, R. Anwyl, M. Wolfe, M. Rowan, and D. Selkoe. 2002. Naturally secreted oligomers of amyloid β protein potently inhibit hippocampal long-term potentiation in vivo. *Nature Medicine.* 416:535-539.
- Walter, J., C. Kaether, H. Steiner, and C. Haass. 2001. The cell biology of Alzheimer's disease: uncovering the secrets of secretases. *Curr. Opin. Neurobiol.* 11:585-590.
- Wang, J., D. Dickson, J. Trojanowski, and V. Lee. 1999. The levels of soluble versus Insoluble Brain AB Distinguishes Alzheimer's Disease from normal and Pathologic aging. *Exp. Neurol.* 158:328-337.
- Ward, R., J. Davis, C. Gray, A. Barton, L. Bresciani, M. Caivano, V. Murphy, K. Duff, M. Hutton, J. Hardy, G. Roberts, and E. Karran. 1996. Presenilin-1 is

- processed into two major cleavage products in neuronal cell lines. *Neurodegeneration*. 5:293–298.
- Warren, G. 1989. Mitosis and Membranes. *Nature*. 342:857-858.
- Watanabe, J., N. Amizuka, T. Noda, and H. Ozawa. 2000. Cytochemical and ultrastructural examination of apoptotic odontoclasts induced by bisphosphonate administration. *Cell. Tissue Res*. 301:375-387.
- Wiltfang, J. Smirnov, A. Schneirstein, B. Kelemen, G. Matthies, U. Wolfgang-Klafki, H. Huther, G. Ruther, E. Kornhuber, J. 1997. Improved electrophoretic separation and immunoblotting of beta-amyloid (A β) peptides 1-40, 1-42, and 1-43. *Electrophoresis*. 18:527-532.
- Wiltfang, J., H. Esselmann, P. Cupers, M. Neumann, H. Kretzschmar, M. Beyermann, D. Schleuder, H. Jahn, E. Ruther, J. Kornhuber, W. Annaert, B. De Strooper, and P. Saftig. 2001. Elevation of beta -Amyloid Peptide 2-42 in Sporadic and Familial Alzheimer's Disease and Its Generation in PS1 Knockout Cells. *J. Biol. Chem*. 276:42645-42657.
- Wolfe, M., W. Xia, C. Moore, D. Leatherwood, B. Ostaszewski, T. Rahmati, I. Donker, and D. Selkoe. 1999a. Petidomimetic probes and molecular modeling Alzheimer's γ -secretase is an intramembrane-cleaving aspartyl protease. *Biochemistry*. 38:4720-4727.
- Wolfe, M., B. Ostaszewski, T. Diehl, W. Kimberly, and D. Selkoe. 1999b. Two transmembrane aspartates in presenilin-1 required for presenilin endoproteolysis and γ -secretase activity. *Nature*. 398:513-517.
- Wolozin, P., P. Alexander, and J. Palacino. 1998. Regulation of apoptosis by Presenilin 1. *Neurobiol. of Aging*. 19:S23-S27.
- Wood, S.A., J.E. Park, and W.J. Brown. 1991. Brefeldin a Causes a Microtubule-mediated Fusion of the trans-Golgi Network and Early Endosomes. *Cell*. 67(3):591-600.
- Wyss-Coray T, Masliah E, Mallory M, McConlogue L, Johnson-Wood K, Lin C, Mucke L. 1997. Amyloidogenic role of cytokine TGF- β 1 in transgenic mice and in Alzheimer's disease. *Nature*. 389:603-606.
- Xia, W., J. Zhang, D. Kholodenko, M. Citron, M. Podlisny, D. Teplow, C. Haass, P. Seubert, E. Koo, and D. Selkoe. 1997a. Enhanced production and oligomerization of the 42-residue amyloid beta-protein by Chinese hamster ovary cells stably expressing mutant presenilins. *J. of Biol.Chem*. 272:7977- 7982.

Xia, W., J. Zhang, R. Perez, E. Koo, and D. Selkoe. 1997b. Interaction between amyloid precursor protein and presenilins in mammalian cells: implications for the pathogenesis of Alzheimer's disease. *Proc. Natl. Acad. Sci. USA*. 94:8208-8213.

Xue, L., G. Fletcher, and A. Tolkovsky. 1999. Autophagy is activated by apoptotic signalling in sympathetic neurons: An alternative mechanism of death execution. *Mol. and Cellular Neurosci.* 14:180-198.

Yamazaki, T., D. Selkoe, and E. Koo. 1995. Trafficking of cell surface β -Amyloid precursor protein: retrograde and transcytotic transport in cultured neurons. *J. Cell Biol.* 129:431-442.

Yan SD, Chen X, Fu J, Chen M, Zhu H, Roher A, Slattery T, Zhao L, Nagashima M, Morser J, Migheli A, Nawroth P, Stern D, Schmidt AM. 1996. RAGE and amyloid-beta peptide neurotoxicity in Alzheimer's disease. *Nature*. 382:685-691.

Yang, J., D. Chandswangbhuvana, T. Theo Shu, A. Henschen, and C. Glabe. 1999. Intracellular Accumulation of Insoluble, Newly Synthesized $A\beta_{n-42}$ in Amyloid Precursor Protein-transfected Cells That Have Been Treated with $A\beta_{1-42}$. *J. Biol. Chem.* 274:20650-20656.

Yanker, B. 1998. Monster plaques: what they tell us about Alzheimer's disease. *Nature Medicine*. 4:394-395.

Yasuda, Y., T. Kudo, T. Katayama, K. Imaizumi, M. Yatera, M. Okochi, H. Yamamori, N. Matsumoto, T. Kida, and A. Fukumori. 2002. FAD-linked presenilin-1 mutants impede translation regulation under ER stress. *Biochem. and Biophys. Res. Comm.* 296:313-318.

Younkin, S. 1995. Evidence That $A\beta_{-42}$ Is the Real Culprit in Alzheimers-Disease. *Annals. of Neurol.* 37:287-288.

Younkin, S.G. 1994. The Amyloid-Beta Protein-Precursor Mutations Linked to Familial Alzheimers-Disease Alter Processing in a Way That Posters Amyloid Deposition. *J. of Exp. Med.* 174:217-223.

Yu, G., F. Chen, G. Levesque, M. Nishimura, D. Zhang, L. Levesque, E. Rogaeva, D. Xu, Y. Liang, M. Duthie, P. St George-Hyslop, and P. Fraser. 1998. The Presenilin 1 Protein Is a Component of a High Molecular Weight Intracellular Complex That Contains β -Catenin. *J. Biol. Chem.* 273:16470-16475.

Yu, G., M. Nishimura, S. Arawaka, D. Levitan, L. Zhang, A. Tandon, Y. Song, E. Rogaeva, F. Chen, T. Kawarai, and et. al. 2000. Nicastrin modulates presenilin-mediated notch/glp-1 signal transduction and β APP processing. *Nature*. 407:48-54.

Zhang, Z., G. Drzeweicki, P. May, R. Rydel, S. Paul, and P. Hyslop. 1996. Inhibition of alpha-macroglobulin/proteinase-mediated degradation of amyloid beta peptide by apolipoprotein E and alpha 1-antichymotrypsin. *Int. J. Exp. Clin. Invest.* 3:156-161.

Zhang, Z., D. Kang, W. Xia, M. Okochi, H. Mori, D. Selkoe, and E. Koo. 1998. Subcellular Distribution and Turnover of Presenilins in Transfected Cells. *J. Biol. Chem.* 273:12436-12442.

Zhou, Y., W. Zhang, R. Easton, J. Ray, P. Lampe, Z. Jiang, A. Brunkan, A. Goate, and E. Johnson. 2002. Presenilin-1 Protects against Neuronal Apoptosis Caused by Its Interacting Protein PAG. *Neurobiology of Disease.* 9:126-138.